Author:
Buffonge, Stanley B

Title:
Identifying matrix metalloproteinases as a therapeutic target to protect the coronary microvascular endothelial glycocalyx in diabetic cardiomyopathy

Identifying matrix metalloproteinases as a therapeutic target to protect the coronary microvascular endothelial glycocalyx in diabetic cardiomyopathy

Stanley Buffonge

A dissertation submitted to the University of Bristol in accordance with the requirements for award of the degree of Doctor of Philosophy in the Faculty of Health Sciences, Bristol Medical School

July 2023

Word count: 46677

Abstract

Introduction:

The coronary microvascular endothelial glycocalyx (EGlx) is a vital regulator of vascular permeability and EGlx damage contributes to the development of diabetic cardiomyopathy. Matrix metalloproteinases 2 and 9 (MMP2/9) have been identified as key enzymes in the degradation of EGlx components, notably syndecan 4, and are upregulated in diabetes. This thesis aimed to investigate if inhibition of MMP2/9 can protect the coronary microvascular EGlx, and improve diastolic function in diabetic cardiomyopathy.

Methods:

Type 1 diabetes was induced in FVB mice by streptozotocin (STZ) injections. Mice were treated with daily injections of the MMP2/9 inhibitor, SB-3CT, for 2 weeks from 7 weeks post STZ. Echocardiography was utilised to assess heart function and lectin staining for the measurement of EGlx depth. Immunolabelling of heart sections for albumin provided an indication of albumin extravasation. A mechanism of EGlx shedding was investigated in vitro in human coronary microvascular endothelial cells treated with tumour necrosis factor α and SB-3CT.

Results:

Diabetic mice developed diastolic dysfunction from 6 weeks post STZ. MMP2/9 inhibition reversed diastolic dysfunction, EGlx thinning and albumin extravasation in diabetic animals. In vitro, TNF-α caused an increase in MMP9 activity and syndecan 4 shedding from human coronary microvascular endothelial cells. Treatment with SB-3CT reduced syndecan 4 shedding.

Conclusion:

This thesis has identified MMPs as a therapeutic target to protect the coronary microvascular EGlx and improve diastolic function in diabetic cardiomyopathy.

Dedication

I dedicate this thesis to my family at large, for the continuous words of support and weekly check-ins.

Specifically, I dedicate this to my mum, for keeping me focused on my path. She has always supported my dreams and encouraged me to persevere through the difficulties and strive towards my goals.

I also dedicate this to my grandma, who has never failed to say a prayer for me. I have felt comforted and reminded that with God, I can do all things.

To Imaan Wright. Thank you!

Acknowledgements

I would like to thank Professor Simon Satchell and Dr Becky Foster, for their guidance from the start to the end of my PhD. They have been a great source of support by providing constructive criticism as well as mentorship ensuring my academic growth. Without them, this would not be possible.

A thank you to Dr Yan Qiu who provided further supervision to this project. I have learnt a vast amount from working alongside her. She has shown me the importance of precision and accuracy ensuring that I am a great scientist.

I would also like to thank Dr Sarah Fawaz for being a great friend and providing me with support in the lab. She encouraged me to be confident in my work and taught me the necessary skills to complete a significant part of this project.

I would like to extend my thanks to the Bristol renal team for being great colleagues as well to those on the BHF programme.

As well as this I would like to thank the Wolfson Imaging Centre at the University of Bristol for training me and supporting me with all my imaging needs.

Lastly, I would like to thank the BHF for providing me with funding to complete this PhD. This has been an amazing opportunity for which I am grateful.

Author's declaration

I declare that the work in this dissertation was carried out in accordance with the requirements of the University's *Regulations and Code of Practice for Research Degree Programmes* and that it has not been submitted for any other academic award. Except where indicated by specific reference in the text, the work is the candidate's own work. Work done in collaboration with, or with the assistance of, others, is indicated as such. Any views expressed in the dissertation are those of the author.

SIGNED: Stanley Buffonge DATE: 14/07/2023

Table of Contents

Table of Figures and tables

Abbreviations

- Endothelial glycocalyx (EGlx)
- Stroke Volume (SV)
- Heart rate (HR)
- Cardiac Output (CO)
- Ejection Fraction (EF)
- Fractional shortening (FS)
- Diabetic cardiomyopathy (DCM)
- Reactive oxygen species (ROS)
- Type 1 diabetes (T1D)
- Type 2 diabetes (T2D)
- Streptozotocin (STZ)
- Matrix metalloproteinase (MMP)
- Heparan sulfate (HS)
- Chondroitin sulfate (CS)
- Syndecan 4 (SDC4)
- Tumor necrosis factor α (TNF- α)
- Glycosaminoglycan (GAG)
- Coronary microvascular endothelial cells (CMVEC)
- Sambucus Nigra Lectin (SNA)
- Lycopersicon Esculentum (tomato) Lectin (LEL)
- Maackia Amurensis Lectin I (MAL-I)
- Rhodamine B Chloride (R18)
- 4',6-diamidino-2-phenylindole (DAPI)
- Wheat germ agglutinin (WGA)
- Atrioventricular (AV)
- Sinoatrial (SA)

But now you also must complete the doing of it; that as there was a readiness to desire it, so there also may be a completion out of what you have (2 Corinthians 8:11)

1 Introduction

1.1 The Heart

1.1.1 The layers of the heart

The heart is a muscular organ composed of three layers known as the epicardium, myocardium, and endocardium (1) enclosed by a fibrous sac known as the fibrous pericardium (Figure 1) (2). The pericardium is divided into the fibrous pericardium and the serous pericardium. As the name suggests, the fibrous pericardium is made up of connective tissue providing support for the heart as well as holding the heart in place. It is fused to the central fibrous area of the diaphragm along with having attachments to the sternum and vertebral column (2). The serous pericardium is further divided into two sub-layers known as the visceral pericardium, which forms the inner layer of the serous pericardium, and the parietal pericardium (2). The parietal layer lines the fibrous pericardium whilst the visceral layer lines the heart itself. The area of the visceral layer that covers the heart excluding the great vessels is also called the epicardium and is composed of connective tissue, fat and mesothelial cells. Nerves and blood vessels that supply the heart are found within the epithelium. The pericardial cavity, found between the visceral and parietal layers of the heart, contains pericardial fluid secreted from the serous layer.

The myocardium is a thick muscular layer found between the epicardium and the endocardium and is made up of striated and uninucleated muscle cells termed cardiomyocytes (3). The endocardium is composed of a single layer of endothelial cells. A sub-

endocardium layer exists between the endocardium and the myocardium (1) and is where specialised cells for electrical conduction are found.

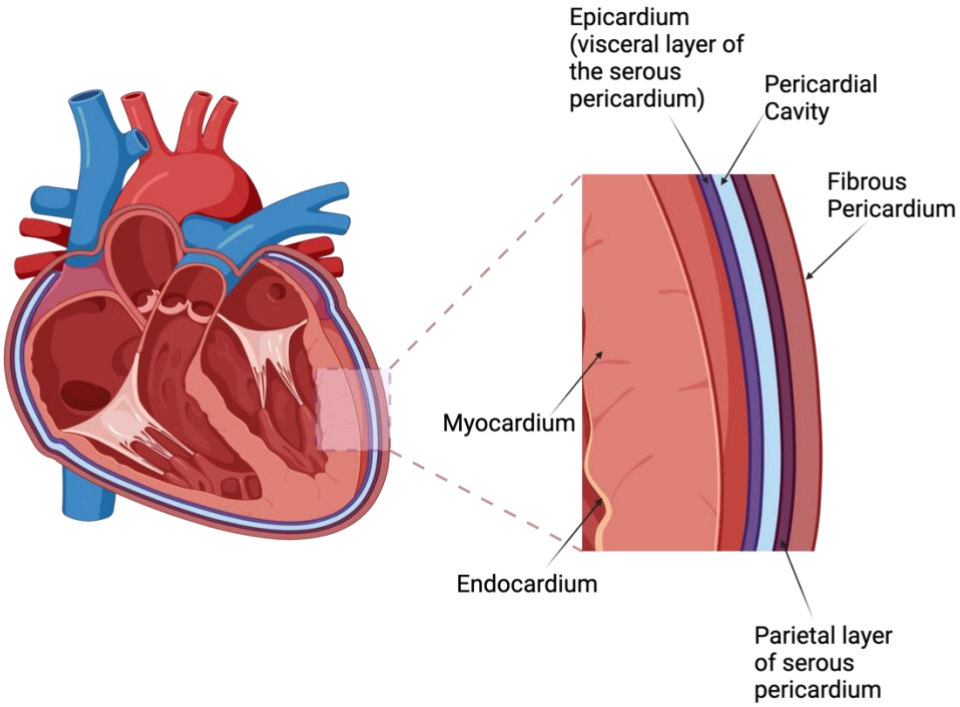

Figure 1. The layers of the heart.

The heart consists of three layers known as the epicardium, myocardium and endocardium and is surrounded by the pericardium. The heart wall and the pericardial membrane share the epicardium. This image was made in Biorender.

1.1.2 Electrical conduction of the heart

The cardiomyocytes house a conduction system creating synchronised contraction of the muscles. The major components of the electrical conduction system are the sinoatrial (SA) node and the atrioventricular (AV) conduction system. The SA node is a discovery by medical student Martin Flack and his mentor Arthur Keith in 1907 (4,5) and is found between the superior vena cava and the right atrium (6). Made from multiple myocytes (7), the SA node can generate an electrical impulse thus providing the heart with an intrinsic heartbeat. There is also a rich supply to the SA node from the autonomic nervous system (ANS) to either increase or decrease heart rate. Bi-atrial contraction occurs as the impulse generated is rapidly spread to the left atrium through muscular connections at the roof of the left atrium.

Once an electrical impulse is generated, it is transferred to the AV node by intra-atrial muscle bundles (6). The AV node, located in the Kotch triangle near the coronary sinus (8), delays the impulse from the atria to the ventricles facilitating in ventricular filling (6). Connecting to the AV node is the bundle of His which transports electrical impulses to its branches, predominantly the Purkinje fibres (9). The Purkinje fibres are specialised cardiomyocytes for electrical conduction that form interweaving networks on the endocardial surface of both ventricles. Therefore, electrical impulses are conducted to the ventricles resulting in ventricular contraction (10).

1.1.3 Excitation contraction coupling of the cardiomyocytes

The normal functioning of cardiac muscle relies on the uptake and release of calcium from the cytoplasm of cardiomyocytes through a process known as excitation-contraction coupling. A key structure necessary for the contraction of cardiomyocytes is the sarcolemma. The sarcolemma contains various ion channels, receptors and transporters and is formed by the cardiomyocyte plasma membrane (11). It invaginates into the cytoplasm of cardiomyocytes forming a network of tubules that pass across the cardiomyocyte. Depolarisation of the sarcolemma via an action potential activates membrane L-type calcium channels resulting in a small influx of calcium ions (Ca^{2+}). Ca^{2+} results in the stimulation of ryanodine receptors (RYR), located at the sarcoplasmic reticulum membrane (SR). The SR releases a larger amount of calcium increasing the intracellular concentration. Ca^{2+} binds to troponin-C on the myofibrils and triggers contraction through actin-myosin engagement. The re-sequestering of calcium into the SR occurs via the SR Ca^{2+} ATPase pump (SERCA2) and calcium is also removed from the cell by the sodium-calcium exchanger (NCX) resulting in relaxation. An alteration in any of the components involved in this process can result in cardiac dysfunction (12–14).

1.1.4 Cardiac cycle

The heart consists of four chambers known as the left and right atrium and the left and right ventricles. The right atrium receives deoxygenated blood from the superior and inferior vena cava as well as the coronary sinus before directing blood to the right ventricle. Blood is then ejected from the right ventricle to the lungs via the pulmonary artery to become oxygenated. The left atrium receives oxygenated blood from the pulmonary veins and pumps blood to the left ventricle. The aim of the left ventricle is to eject the oxygenated blood to the rest of the body via the aorta. Figure 2 portrays the movement of blood through the heart. An important rule to note is that for blood to progress from one area to the next, for example from the right atria to the right ventricle, the pressure must be greater in the upstream region. Both the left and the right-side contract simultaneously and follow the same principles of pressure for blood flow. Therefore, when a chamber is not mentioned specifically as either left or right, the information is relevant to both sides.

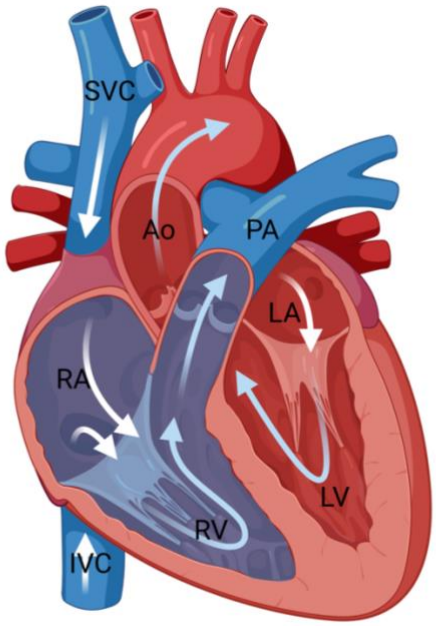

Figure 2. The movement of blood in the heart during diastole and systole.

SVC = superior vena cava; IVC = inferior vena cava; RA = right atrium; RV = right ventricle; PA = pulmonary artery; LA = left atrium; LV = left ventricle; Ao = aorta. The white arrows reflect blood moving into the heart. The blue arrows reflect blood exiting the heart. Blood returns from the lungs to the left atrium via the pulmonary vein. Created with BioRender.com

When explaining the movement of blood throughout the heart, the focus is on the relaxation (diastole) and the contraction (systole) of the ventricular muscles. During mid to late diastole, blood flows into the atria resulting in an increase in atria pressure. Diastole is the relaxation of the ventricles and thus the filling of the atria results in its pressure becoming greater than that of the ventricle (15,16). This leads to the opening of the atrial ventricular (AV) valves

leading to the passive flowing of 70 - 80% of blood from the atria into the ventricles. The firing of the SA node results in the depolarisation of the atria leading to its contraction and thus, the remaining 20% of blood is pumped into the ventricles. The volume of blood within the ventricles at the end of this phase is known as the end-diastolic volume.

The next phase of the cardiac cycle is isovolumetric contraction, a phase which marks the beginning of systole. Depolarisation of the ventricles stimulates contraction which increases ventricular pressure. As the ventricular pressure exceeds that of the atria, the AV valves close. However, at this phase, the pressure is not yet greater than arterial pressure and thus the semilunar (SL) valves, found between the ventricle and the outflow tract, remain closed. This means during this period of contraction, there is no change in blood volume in the ventricle (15,16).

As the ventricles continue to contract the ventricular pressure exceeds arterial pressure resulting in the opening of the SL valves. At this point, known as the mid to late ventricular systole (or ventricular ejection) phase, the pressure is still greater than that of the atria and thus the AV valves remain closed. The majority of the blood volume in the ventricles will exit through the aorta and pulmonary arteries. In fact, a healthy heart will eject more than 60% of its ventricular volume (16). Blood that remains in the ventricle after contraction is known as the end-systolic volume.

Marking the end of systole, the ventricles begin to relax reducing its pressure below that of the aorta and pulmonary trunk and therefore, the semilunar valves close. For a brief moment, all the valves are closed, as the ventricles begin to relax and repolarise. No blood moves between the chambers at this point leading to the term isovolumetric relaxation (16).

1.1.5 Blood supply to the heart muscle

The coronary arteries (which run within the epicardium) exit the ascending aorta by the coronary ostia and directly supply the myocardium with blood (3). These arteries branch into microvascular exchange vessels which are dense at the heart muscle and go on to drain into low-resistance outflow pathways. The venous drainage system of the heart is split into two categories known as the greater and lesser venous system. The greater system drains approximately 70-75% and is composed of the coronary sinus which drains into the right atrium (17,18). The remaining venous flow exits via the besian veins which run in the myocardial layer of the heart. These vessels provide a unique aspect to the heart's circulation as they assist in the drainage of blood from the myocardium by a direct connection to the larger coronary vessels on the epicardial surface (18). The myocardial interstitial space is regarded as a complex three-dimensional space which is vital for the normal functioning of the heart (19). Some fluid that enters the interstitium is drained via the lymphatic vessels (17).

1.1.6 Microcirculation of the heart

The microcirculation of the heart plays a crucial role in the supply of nutrients as well as regulating blood flow to the myocardium. In the heart, arterioles play a critical role in regulating blood flow and therefore, oxygen supply to the myocardium during periods of rest and exercise through dilation and constriction (20). With a lumen size of 30 micrometres or less, arterioles play a major role in slowing down blood flow resulting in a drop in blood pressure. This has led to them being referred to as resistance vessels (20,21).

Capillaries of the heart are composed of a single cell layer of endothelial cells (Figure 3) and are the smallest and most numerous blood vessels with an estimate of 3000 to 4000 per mm^2 of myocardial tissue due to its high oxygen demand (22). The primary function of the capillaries is to exchange materials between the blood and the tissue making them essential to meet the energy demands of the heart (23).

Three types of capillaries exist. The first is continuous capillaries which have a continuous endothelial lining connected by tight junctions limiting the passage of molecules. Tight junctions play an important role in regulating the transport of water, ions and molecules and thus are vital to the barrier formed by endothelial cells (24). A disruption in coronary endothelial tight junctions was found to alter permeability and result in diastolic dysfunction (25). Projecting from the endothelial cells on the luminal side is the endothelial glycocalyx (EGlx), which plays a vital role in the regulation of vascular permeability (26,27). This will be discussed further later on in this chapter. On the basal surface of the endothelial cells, without clear separation, is the basement membrane which separates tissues and provides support to withstand mechanical stress (28).

Fenestrated capillaries contain small pores allowing for the exchange of larger molecules. Capillary supply to the myocardium is largely from continuous capillaries however, fenestrated capillaries have been found to supply the conduction system in the rabbit heart (29). Finally, discontinuous capillaries have large gaps allowing for the passage of larger molecules and are not found within the heart but are found in the liver, spleen and bone marrow (30). Capillaries then drain into venules which transport blood to larger veins as described above.

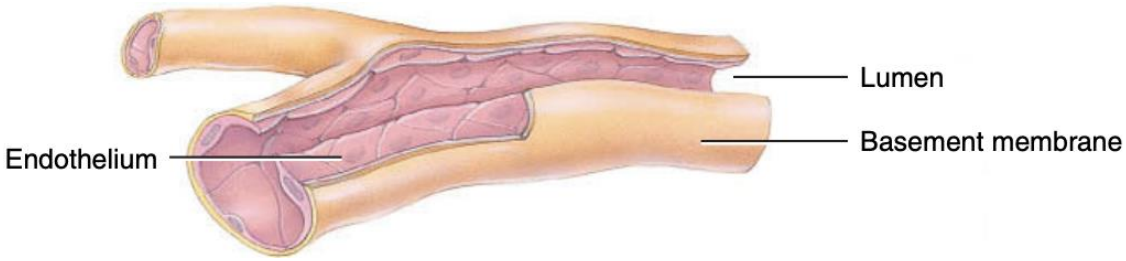

Figure 3. Structure of a capillary.

Capillaries are composed of a single layer of endothelial cells. On the basal surface of the endothelial cells is the basement membrane. Projecting from the endothelial cells on the luminal side is the EGlx (not shown in this image). Image adapted from (31).

1.1.7 Dysfunction of the heart

Dysfunction of the ventricular myocardium can be divided into two categories. The first is related to disorders of systolic ejection and the second is related to disorders of diastolic filling. Systolic dysfunction is a result of reduced effective myocardial contractility. Clinically, the ejection fraction and cardiac output are used to evaluate systolic function. According to the British Heart Foundation and British Society of Echocardiography, a normal ejection fraction is between 55-70% (32). Left ventricular ejection fraction is the stroke volume (SV) as a percentage of end-diastolic volume (33). Cardiac output (CO) is defined as the amount of blood the heart pumps in 1 minute expressed in litres/minute. Logically it is dependent on SV and heart rate (HR) (SV x HR), however, there are three main determinants of CO. Beginning with HR, it is clear that the faster the heart beats the more blood it will pump per minute (33). However, this is only true to an extent; if the heart rate is too fast or slow, then CO will be impaired due to ineffective filling of the ventricle and thus CO will ultimately be reduced (33)

overtime. Thus, it is important to ensure that HR is kept at an optimal level to meet the needs of the body.

Myocardial contractility is both the heart's ability to develop force and generate velocity (34) and this is largely dependent on preload and afterload and other factors such as neurological stimulation and calcium induction. According to the Frank-Sterling law, the more the myocytes are stretched (increased sarcomere length), within physiological parameters, the bigger the tension resulting in a greater contraction (35–37). Therefore, an increase in ventricular diastolic volume (preload) would result in increased myocardial fibre stretching during diastole (35–37). Afterload is the last parameter to be discussed in relation to cardiac output. The heart beats against arterial pressures and thus afterload is the amount of resistance the heart must overcome to eject blood. An increased afterload (increased resistance) means the ventricle will need to work harder to eject blood against the force of the afterload (37,38). Therefore, an inverse relationship is recognised between afterload and cardiac output. Factors such as hypertension and atherosclerosis can increase the afterload making them risk factors for systolic dysfunction.

1.1.7.1 Diastolic dysfunction

The diastolic function of the left ventricle is vital in determining its filling and stroke volume. Diastolic dysfunction is the result of increased left ventricular stiffness leading to increased filling pressures (39) and an impairment of the left ventricular relaxation (14,40–42). Hypertension, age, and left ventricular hypertrophy, are risk factors for diastolic dysfunction. Diastolic dysfunction can have an asymptomatic presence. At this phase dysfunction is

present and the severity is progressing before symptoms of heart failure appear (14,43). This phase is a potential intervention period to prevent heart failure. There are various mechanisms that result in diastolic dysfunction, these include an alteration in the intracellular Ca^{2+} handling (13), an altered microvascular permeability (27) and fibrosis (44). Some of these will be described further later in this chapter when looking specifically at diabetic cardiomyopathy.

1.1.7.2 Heart Failure

Heart failure occurs when the cardiac output is insufficient to meet the metabolic needs of the body. The heart muscle gets progressively weaker until complete pump failure occurs (45). Heart failure can be placed into three main groups depending on the ejection fraction. The first is heart failure with reduced ejection fraction which occurs when the ejection fraction is less than 40%. This typically develops after an index event such as an acute injury to the heart such as myocardial infarction (46). Another category of heart failure is heart failure with mildly reduced ejection fraction (>40% - 49%) which accounts for 25% of patients with heart failure (47). Patients with an ejection fraction of more than 50% but present signs of heart failure are termed to have heart failure with preserved ejection fraction and accounts for 50% of all diagnosis of heart failure (48). The pathophysiological mechanism of heart failure with preserved ejection fraction is complex and remains incompletely understood however it is known that this is associated with diastolic dysfunction (48). Accompanying this criteria of heart failure, is the test for N-terminal pro brain natriutretuic peptide (NT-proBNP). This protein (precursor to BNP) is released from ventricular myocytes in response to increased ventricular wall tension and is increased in patients with heart failure. Testing blood NT-

proBNP levels over BNP levels is preffered due to its longer half life and higher circulating concentrations. Whilst this method is used commonly clinically, it is important to remember that BNP levels are also raised in conditions other than heart failure and therefore it should accompany other methods of diagnosis along with a comprehensive evaluation of the patient's clinical history and symptoms.

1.1.8 Assessing heart function

The increase in medical advancements has led to the development of tools to visualise and better assess heart function. One major technology used both in research and clinically to assess heart structure and function, through the use of ultrasound, is an echocardiogram (echo). Three basic modes are utilised when imaging the heart with echo. The first is two dimensional-imaging which remains the most cost and risk-effective imaging choice in many settings (49). 2D echocardiography produces slices of two-dimensional images with the most common cross-sectional imaging planes utilised being the parasternal long-axis, parasternal short-axis, and the apical view (50). Another mode used is M-mode. M-mode technology was first described in 1953 by Inge Edler (51) and was the primary technology until the development of 2D imaging in 1973 (52). M-mode provides a 1-dimensional view allowing the visualisation of specific structures throughout the cardiac cycle (50,52).

Doppler imaging was developed to estimate blood flow velocity. Pulsed wave Doppler is a technique that allows the localisation of measurements of blood flow velocity and is commonly used to assess ventricular inflow patterns (49,53). Another method of utilising Doppler imaging is colour-flow mapping which has been of great value in assessing blood flow

in a variety of clinical conditions (54). By utilising both velocity and direction of blood flow, a colour pattern can be placed onto a 2D image. Flow towards the transducer appears as red and flow away appears as blue with higher velocities presented in lighter shades (50,54). In practice today, a combination of the three imaging methods is utilised to better understand the heart that is being imaged.

Cardiac magnetic resonance imaging (MRI) is another tool used to image the heart and is known as a gold standard for the assessment of systolic function and tissue characterisation due to its high spatial and temporal resolution in any plane supplying 3D images without the need for an ionising radiation (55,56). Cardiac imaging is constantly evolving leading current MRI technology to provide a wide range of applications for nearly all morphological and functional aspects of cardiac disease (55,56).

As mentioned, certain biomarkers such as B-type natriuretic peptide (BNP) can be used to support the evaluation of heart function. In patients with left ventricular diastolic dysfunction, an increase in plasma BNP levels was found when compared to those with normal heart functioning (57). Similarly, increased plasma BNP levels have been noticed in patients with left ventricular systolic dysfunction (58).

1.1.8.1 Echocardiographic assessment of diastolic function

A commonly used method to assess diastolic function is to measure the transmitral flow parameters. Early blood flow (E) through the mitral valve is passive and is dependent on the pressure gradient between the atrium and the ventricle. Late filling (A) of the ventricle is a result of atrial contraction pumping the remaining blood into the ventricle (39,59). Stiffening of the ventricle in diastolic dysfunction results in reduced E wave velocity due to impaired relaxation and therefore the atria will pump out more blood leading to an increase in the A wave size. A reduced E/A ratio is recognised in patients with diastolic dysfunction.

Another method of assessing diastolic function is the use of the E/e' ratio with e' representing the early ventricular myocardial relaxation (60). When diastolic dysfunction occurs (impaired relaxation) there will be a lowering of e' whilst the E-wave increases with elevated filling pressures. This will result in an increased E/e' ratio. Other methods include an assessment of the isovolumetric relaxation time which is prolonged in patients with impaired LV relaxation but normal filling pressures (39,59). Assessing the mitral E wave deceleration time can provide a further indication of diastolic function as it is influenced by LV pressures following the opening of the mitral valve. Stiffening of the left ventricle will result in a prolonged mitral E wave deceleration time (39,59).

1.2 Diabetic cardiomyopathy

1.2.5 Introduction to Diabetes

Diabetes mellites (DM) is a chronic, metabolic disease affecting millions of people worldwide (61). It is estimated that around 422 million people worldwide have diabetes with 1.6 million deaths being directly attributed to diabetes each year according to the World Health Organisation (62). This is estimated to rise to roughly 642 million people by 2040 (62). Principle characteristics of diabetes include insulin resistance and/or reduced insulin production leading to hyperglycaemia, hyperlipidaemia, and inflammation (63). There are two main classes of diabetes, outlined below, based on the onset and pathogenesis of the disease.

1.2.5.1 Type 1 diabetes

Type 1 diabetes (T1D) is an autoimmune disease, representing 5-10% of all diabetic cases (64) and leads to the destruction of the pancreatic β-cells (65). Clinical symptoms begin to present themselves when roughly 80% of the β-cells have been destroyed (66), leading to insulin deficiency and, therefore, an impairment in the ability to regulate glucose homeostasis (67).

T1D predominantly develops in children and adolescents but is also observed in adults (68,69). The sudden destruction of the β-cells in children and adolescents leads to diabetic ketoacidosis. In adults, this may be prevented for a few years due to producing just enough insulin. However, with the continued damage to the β-cells over time, severe hyperglycaemia develops with ketoacidosis (64). Consequently, those with T1D rely on exogenous insulin for

survival. The interaction between genetic susceptibility and environmental insults results in the complexity of T1D (66).

1.2.5.2 Type 2 diabetes

Type 2 diabetes (T2D), which accounts for 90-95% of diabetic cases (64,68), is one of the most frequent diseases throughout the world (70) and is primarily a result of insulin resistance, a condition in which cells do not respond appropriately to circulating insulin (71), most prevalent in persons over 45 years old. Insulin action and insulin resistance are tightly linked. A decrease in insulin action is initially accompanied by an upregulation of insulin secretion (72), and therefore normoglycemia is maintained for a while (73). The high production of insulin itself stimulates insulin resistance, and therefore hyperinsulinemia is known to be an early indication of T2D. The development of clinically apparent T2D occurs when insulin secretion declines below the point to compensate for insulin resistance (73). Similarly to T1D, T2D results from both genetic and environmental factors, with genetic susceptibility having a more significant role in T2D (66). Other conditions also increase the risk of developing T2D. There is a strong correlation between obesity and T2D, with 60-90% of patients with T2D being obese (73). Therefore, with obesity on the rise, it is no surprise that T2D is increasing in parallel amongst all age groups (74).

1.2.6 What is diabetic cardiomyopathy?

Much can be said of the effect of diabetes on different organs. It is known that diabetes affects many organs, including the nerves, eyes, kidneys, blood vessels and the heart. Diabetic cardiomyopathy (DCM), coined in 1972 due to post-mortem pathological findings (75,76), is clinically characterized by left ventricular hypertrophy (77) and left ventricular diastolic dysfunction (78) in the absence of systolic dysfunction (62). Ultimately, DCM is the progression of diastolic dysfunction to heart failure independent of other cardiovascular factors such as hypertension and coronary artery disease in patients with diabetes (53). Despite this, vascular complications coexist with DCM (78), reflecting the fact that diabetes is multifactorial and complex in nature. It is estimated that 12% of people with diabetes are affected by DCM (78).

Despite this, there is currently a lack of treatments for DCM and drugs used tend to target the different pathological changes that occur in diabetes. Commonly used medications include angiotensin-converting enzyme (ACE) inhibitors (79), oral anti-glycaemic medication (80,81), calcium channel antagonists and insulin-sensitising agents (44). Perhaps the uncertainty of the fundamental cause of DCM has led to reduced available treatments that specifically target alteration in DCM. Therefore, it is vital that research continues to address this clinical need and strive to reveal key therapeutic targets specifically for DCM and further develop the understanding of the mechanisms of DCM.

1.2.7 Mechanisms of diabetic cardiomyopathy

Various molecular changes occur in both T1D and T2D which result in structural and functional alterations in DCM. Whilst this review does not highlight every alteration in DCM, it presents a broad range of molecular and structural changes to demonstrate the complexity of DCM.

1.2.7.1 Molecular alterations in diabetic cardiomyopathy

1.2.7.1.1 Alteration in the substrate utilisation in the heart

The healthy heart utilizes various substrates to best aid its contractility performance (82), a phenomenon termed 'metabolic flexibility' (83). Fatty acids are the primary substrate for energy production in the heart, with further contributions being made from glucose, ketone bodies and lactate depending on the metabolic demands (84). Glucose uptake and utilisation are reduced due to insulin resistance resulting in energy deficiency and cardiac dysfunction (85). Therefore, fatty acid utilization becomes a further dominating source of energy (86). Physiologically, insulin has a fat-sparing effect as it inhibits the breakdown of fat into fatty acids and glycerol. However, the decrease in insulin sensitivity or production in diabetes leads to the lack of lipase suppression and thus a build-up in fatty acids (87,88). A shift in the balance of substrate utilisation to either the predominant use of one is detrimental and can impair cardiac contractility (82). Interest in the fatty acid transporter (CD36) in the heart has risen as it has been shown that altering the favoured substrate uptake by manipulating the recruitment of glucose transporter type 4 (GLUT4) or CD36 led to an improvement in contractile function of the heart (89). The accumulation of lipids and excess fatty acid oxidation leads to lipid toxicity through the induction of reactive oxygen species (ROS) and can cause apoptosis of the cardiac cells (90).

1.2.7.1.2 Impaired calcium handling

During diabetes, effective calcium handling in the heart is reduced. Investigating cardiomyocytes revealed a reduced decay rate in both systolic and diastolic states (91) since less calcium is transported back into the sarcoplasmic reticulum. A significant reduction in the SERCA2a protein is a likely contributor to the impairment in contractility with the restoration of function occurring with overexpression of SERCA2a transgene (92,93). Abnormal insulin signalling also contributes to further alterations in calcium sensitivity. Insulin behaves as a vasodilator mediator through the activation of endothelial nitric oxide synthase (eNOS) from endothelial cells resulting in the production of nitric oxide (NO) (75,94,95). A reduction in endothelial eNOS and therefore NO results in an increased sensitivity to intracellular calcium and reduced sarcoplasmic calcium uptake.

1.2.7.1.3 Increased reactive oxygen species and diabetic cardiomyopathy

Metabolic reactions continuously produce ROS, unstable and highly reactive molecules (96), as a by-product. The majority of ROS production is from the mitochondria, with up to 5% of oxygen consumed during respiration being converted to ROS (97). The dangers of ROS are found in their capacity to interact with proteins, lipids and DNA, which can potentially be mutagenic (98). There is evidence of increased ROS in the diabetic heart as an increase in 8-hydroxydeoxyguanosine, an oxidised derivative of deoxyguanosine, is observed (98). The effect of increased ROS is also observed through the interaction with polyunsaturated fatty acids of cell membranes forming lipid peroxidation. The peroxidation of cell membrane lipids can have detrimental effects, including disruption of the cell membrane permeability (99). The balance between ROS production and antioxidative defence is crucial to prevent damage,

and diabetes is also associated with reduced activation of the heart's antioxidant enzymes, further promoting oxidative stress (100).

1.2.7.1.4 Hyperglycaemia and advanced glycation end products

Hyperglycaemia has several downstream effects which occur as a result of reduced insulin production and/or resistance. Hyperglycaemia increases the levels of advanced glycation end products (AGE) (101), which are formed when proteins or lipids become glycated and oxidised as a result of the interaction with an aldose sugar (102). The formation of AGE can ultimately lead to an alteration in protein structure and function (70) and contribute to oxidative stress when AGE binds to its receptor (98). The effects of AGEs are diverse, with a major action being to reduce endothelial nitric oxide synthase (eNOS) (103) therefore disturbing coronary vasodilation (44). The detrimental effects of AGEs activity are through the ability to cross-link collagen molecules, ultimately limiting their turnover by increasing the resistance to proteolysis (83). A result of this is fibrosis leading to cardiac stiffness and diastolic dysfunction (101). Knockdown of the AGE receptor (RAGE) has been shown to protect left ventricular functionality (104).

1.2.7.1.5 Inflammation and diabetic cardiomyopathy

It is recognised that hyperglycaemia also induces pro-inflammatory cytokines such as TNF-α, IL-1b, and IL-6, all of which contribute to the various mechanisms of diabetes, such as an alteration of insulin sensitivity (105,106). Whilst inflammation itself begins as an adaptive protective response to short-term stress, the persistent stress of hyperglycaemia quickly turns this maladaptive with an increase in M1 macrophages (pro-inflammatory) and a decrease in M2 anti-inflammatory macrophages (83). There is also a link between inflammation and fibrosis, with inflammatory inhibitors reducing heart fibrosis in diabetic mice (107).

1.2.7.2 Structural alterations in diabetic cardiomyopathy

1.2.7.2.1 Ventricular Hypertrophy

Ventricular hypertrophy is a standard morphological change observed in DCM. In T2D, an increase in left ventricular (LV) wall thickness is prominent and a predictor of cardiovascular complications, particularly in those under 65 years of age (108). When in a hypertrophied state, the left ventricular wall increases in stiffness (109), disrupting the wall's elasticity when relaxed. The use of echocardiography in diabetic patients reveals an increase in left ventricular posterior and septal wall thickness (83). Concentric remodelling is the primary remodelling seen in DCM. Still, there is a debate as to whether this can be solely linked to diabetes as the geometry of the left ventricle is altered by various factors, including ethnicity, obesity and hypertension (110). Despite this, in a study assessing the association between diabetes and left ventricular hypertrophy in a multi-ethnic population, it was observed that

diabetes mellites were associated with an increased ventricular mass independent of cofounders (111).

1.2.7.2.2 Fibrosis

Fibrosis results from an increase in collagen deposition (83), mainly types I and III (100). The excessive production of extracellular matrix proteins leads to cardiac stiffness and, thus, cardiac dysfunction (44) and is commonly observed in diabetic patients. This is due to an upregulation of profibrotic factors found in the diabetic heart (83), such as those mentioned above, as well as a decrease in the activity of certain matrix metalloproteinases (MMPs) from specific cardiac cell types such as myocytes that would normally degrade the collagen (112,113). An examination of biopsy samples found that diastolic stiffness was associated with fibrosis when left ventricular ejection fraction was reduced (114). Therefore, fibrosis appears to be accompanied by late-stage and developed DCM when the ejection fraction is reduced.

1.2.7.2.3 The endothelial glycocalyx and diabetic cardiomyopathy

To the best of my knowledge, in heart failure randomized clinical trials, the evaluation of myocardial oedema has not yet been evaluated as an endopoint and therefore its specific contribution to heart failure in a human disease has not fully been revealed. This also means that the effects of most drugs on myocardial fluid balance remains unknown. However myocardial oedema has been identified in patients with heart failure through which release of myocardial oedema correlated with improved cardiac function (115). The use of cardiac magnetic resonance has shown that in patients with dialated cardiomyopathy there was an increased myocardial water content which increased as the disease progressed (116). The accumulation of interstitial oedema results in a rise in interstitial pressures leading to stiffness of the myocardium (17). In fact, increasing the permeability of myocardial microvessels, leads to oedema and has been shown to directly cause diastolic dysfunction in the absence of fibrosis or inflammation providing a direct link between increased permeability, oedema and heart dysfunction in animla models (25). Therefore oedema appears to play a role in the development of cardiac dysfunction and should thus be studied further.

A vital regulator of vascular permeabilty and therefore oedema is the endothelial glycocalyx (EGlx) which is a gel-like layer that lines the luminal side of vascular endothelial cells. The heart is extremely sensitive to changes in microvascular permeability, with a slight increase in interstitial fluid compromising heart function (17). During diabetes, there is a reduction in EGlx depth and coverage of the microvessels such as in the kidney and retina (117,118). We

have recently shown that the coronary microvascular EGlx is damaged in diabetes and is associated with oedema (27). Therefore, the EGlx may potentially be a therapeutic target of protection to improve vascular permeability and cardiac performance during DCM.

Despite the knowledge of the importance of the EGlx in regulating vascular permeability, it has been severely understudied in the heart. Several molecular alterations in DCM described above such as inflammation and ROS result in the activation of enzymes that cause damage to the EGlx such as matrix metalloproteinases and heparanase thus the EGlx is largely targeted as a result of diabetes. We will explore the structure (as shown in Figure 5) and function of the EGlx in greater depth in section 1.3. The mechanisms of DCM discussed above are summarised in Figure 4.

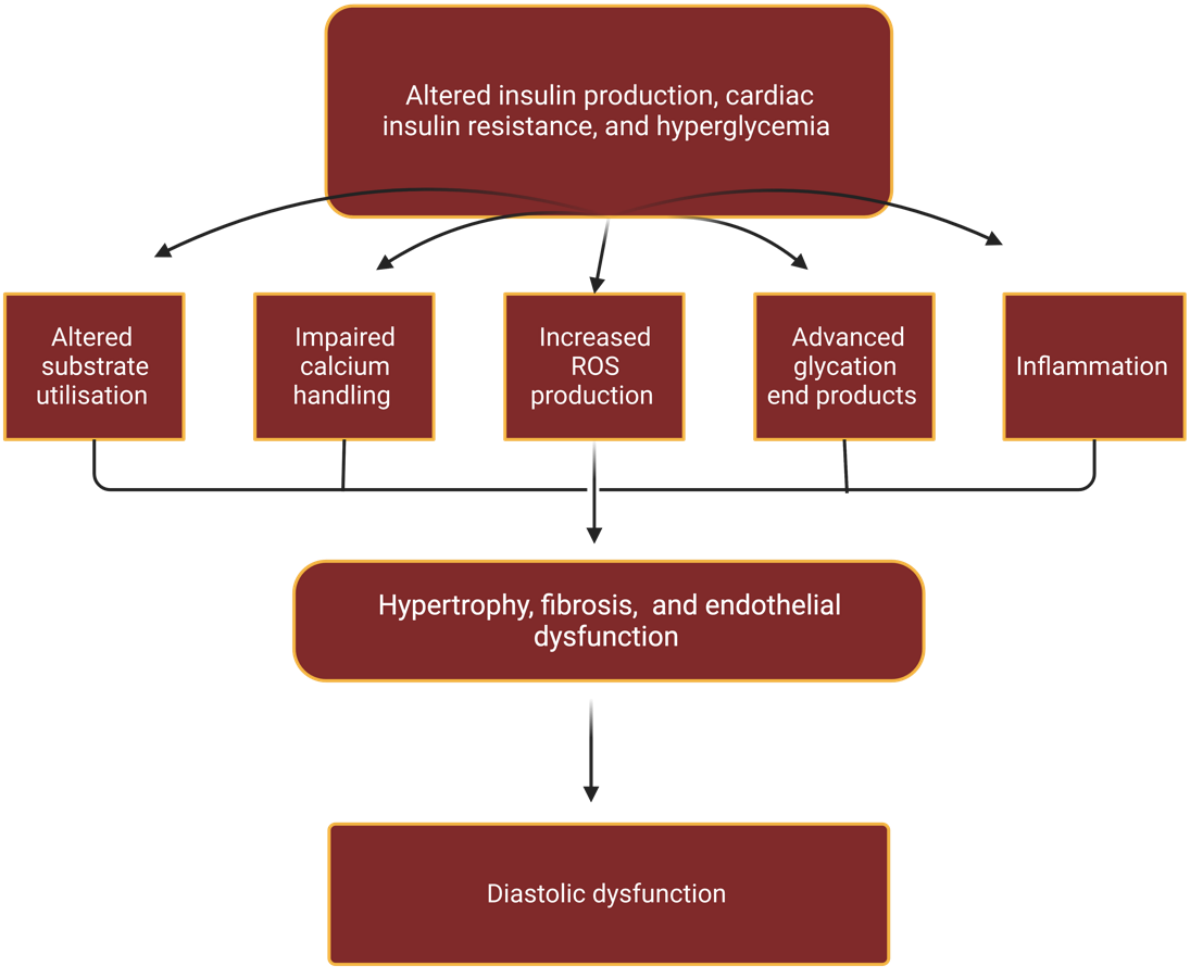

Figure 4. Mechanisms of diabetic cardiomyopathy.

The molecular alterations such as altered substrate utilisation and impaired calcium handling, result in structural alterations leading to diastolic dysfunction. Created with BioRender.com

1.2.8 Rodent models of diabetic cardiomyopathy

Various models exist that allow a better understanding of the mechanisms of DCM, and choosing the correct model is essential to test the desired question accurately. Rodent models are the most commonly used model of diabetes and have proven helpful in studying DCM, with 99% of the genes of the mouse genome having a homologue in humans (119). Also, rodents are resistant to developing atherosclerosis, making them a suitable model for investigating DCM (120). There are observable similarities in the phenotype of DCM in T1D and T2D diabetes. However, there are still significant differences, primarily in the onset of diabetes. There may also be differences molecularly, such as a greater increase in mitochondrial reactive oxygen species (ROS) production seen in T2D models compared to T1D models (120).

1.2.8.1 Type 1 models

Models of T1D involve the damage of the β-cells of the pancreas. This can occur in various ways, such as the generation of an autoimmune model or chemically induced damage of the β-cells.

1.2.8.1.1 Chemically induced (streptozotocin)

The streptozotocin (STZ) rodent model is the most commonly used model of T1D. STZ is an antibiotic that leads to the destruction of the pancreatic β-cells (121). Hyperglycaemia is induced with a single low dose of STZ (122). Most studies utilise a repeated single low dose of STZ (20-50 mg/kg per day) over five consecutive days and conduct investigations 7-9 weeks post-injections, with some studies extending when pathophysiological functioning is well established (122). In rats induced with STZ, distinct fibrosis is observed in heart tissue sections 12 weeks after STZ injection. This was evidenced by an increase in collagen I and α-SMA mRNA (84), which is used as a marker for activated fibrogenic cells (123). The fibrotic phenotypic changes observed in the STZ-induced rat resemble that of human patients with DCM which also show an increase in collagen I mRNA expression and α-SMA (124). However, the appearance of cardiac fibrosis in the STZ model appears to vary by species and strain as some studies also show no differences in collagen content when examined early after STZ injection. (122). In fact, in an STZ mouse model, no change in collagen content was found in the hearts of diabetic mice compared to controls 9 weeks post STZ (27). On the other hand, a different study using the same strain of mice found an increase in collagen content 4 weeks post-STZ (125). It is important to recognise that both of these studies used a slightly different dose of STZ for the induction of diabetes for 5 days (50mg/kg and 55mg/kg respectively). Therefore,

the disease progression may not only be strain-dependent but also STZ dose-dependent providing an additional explanation for variability between different studies.

As mentioned, DCM is first identified as diastolic dysfunction, which is indicated by a reduced E/A ratio. This can be recorded as early as four weeks post induction of diabetes in FVB mice (125). Similarly to what is seen in humans, diastolic dysfunction occurs before systolic dysfunction (126). Therefore, it is clear that the STZ mouse model is suitable to examine cardiac functional changes linked to DCM.

There is an increase in blood glucose levels in the STZ diabetic model, which is more pronounced in male mice than in female mice (126). The rise in blood glucose is maintained throughout the duration of the experiment and is accompanied by reduced body weight and increased food consumption (127) due to the lack of insulin production. Increased ROS in the STZ rodent model is accompanied by reduced superoxide dismutase (128), which generally protects against oxidative stress (129). There is also an increase in inflammatory markers with IL-6 (128) and TNF-α (130) being commonly measured in the STZ rodent model of DCM. It is clear that some aspects of the pathophysiology of DCM in the rodent model mirror that seen in human patients, and therefore conclusions drawn from the studies provide information relevant to human DCM. However, there appears to be a lack of studies showing the long-term effects of DCM on the heart in the STZ model, which may be due to the reduced life span of the rodents. Nevertheless, the use of STZ has proven to be effective in producing a T1D model of DCM.

1.2.8.1.2 Non-Obese diabetic mouse

Another T1D rodent model of DCM is the spontaneous autoimmune model, with the most commonly used being the non-obese diabetic (NOD) mouse (131). The NOD mouse was the first strain shown to present spontaneous autoimmune diabetes and develop T1D when leukocytes infiltrate the pancreatic islets and has been instrumental in deciphering the complex mechanisms of T1D (132). As a result, the mice develop insulitis and β-cell failure (119,133). These NOD mice show increased blood glucose within the first four weeks of age (133). This is the prediabetic phase of the model in which overt diabetes occurs at around 10-14 weeks of age when 90% of the pancreatic insulin is lost (131). Two months after diagnosis of diabetes, NOD mice peak in lipid production producing cardiac lipotoxicity, which, as described, is a prominent feature of DCM (134). A reduction in contractile function is also observed after 2-3 months of diagnosis (134), with decreased systolic pressures and increased left ventricular end-diastolic pressures recognised (135). NOD mice also present with an increase in heart-to-body weight ratio, with an observable decrease in body weight five weeks after diabetes diagnosis (134,135). Thus, various mechanisms contributing to human DCM can be studied in the NOD mouse model.

1.2.8.1.3 Akita mouse

Another model used is the Akita mouse model. In these mice, a spontaneous mutation occurs in the insulin 2 gene, altering the insulin protein folding. It also results in endoplasmic reticulum stress leading to β-cell failure (119). In this model, mice develop severe hyperglycaemia, hyperinsulinemia, and polydipsia at 3-4 weeks of age (136). At 3 and 6 months of age, progressive diastolic dysfunction with preserved systolic function is exhibited. Similarly to NOD mice, there is also evidence of lipotoxicity in the Akita model (137,138). A prominent observation is the structural remodelling of the heart observed in the Akita mouse. When compared to the controls, an increase in fibrosis is recognised and also an increase in β-myosin heavy chain, which is used as a molecular marker for hypertrophy (138).

Other rodent models exist for T1D, such as the OVE26 mouse, which causes damage to the pancreatic β-cells through overexpression of calmodulin in the β-cells (119). It is important for models to aim to adequately encapsulate the development of T1D including its autoimmune contribution as immunosuppression has been shown to be beneficial in preserving β-cells in patients with TID (132).

1.2.8.2 Type 2 models

1.2.8.2.1 High-fat diet model

It is common for studies to utilise dietary treatments to induce T2D. In many cases, T2D is accompanied by obesity and insulin resistance. Therefore, the utilisation of dietary treatments in rodents produces models which represent not only T2D, but also obesity.

The high-fat diet has proven to be effective in stimulating cardiac damage. When mice were given a high fat and sugar diet of 35.5% fat and 36.5% carbohydrate, after 8 months, they were not only diabetic but also developed diastolic dysfunction with the preservation of systolic function compared to mice on a normal diet (119,139). These mice also present with left ventricular hypertrophy and a significant increase in cardiac fibrosis (119,139). As mentioned, these are marked features of DCM. In fact, a high-fat diet in mice can cause insulin resistance within two weeks. As a result, these mice have increased myocardial fatty acids and impaired glucose utilization (140).

1.2.8.2.2 Ob/ob mouse model

Monogenic models are commonly used to induce obesity and diabetes, with the most used being a model with defective leptin signalling. However, the problem with this is that human T2D and obesity are rarely caused by a single mutation (141). Despite this, these models are suitable for investigating potential treatments and studying the mechanisms of T2D. In the ob/ob mouse model, mice fail to produce leptin, resulting in uncontrolled food intake. The mice develop severe hyperglycaemia by 15 weeks of age (142), depending on mouse strain. Accompanying hyperglycaemia is hyperinsulinemia, therefore, suggesting insulin resistance. As the ob/ob mouse model is also an obesity model, there is no surprise that there is an

increase in the supply of fatty acids. However, insulin resistance makes the heart unable to modulate its substrate use, and thus it becomes metabolically inefficient (143). Despite these conditions, the hearts of ob/ob mice are still able to retain their function and do not show diastolic dysfunction (143,144). Therefore, they cannot fully encapsulate the main hallmarks of DCM and may not be the best model to utilize for investigations. The db/db mouse model is more commonly used for investigations of heart function.

1.2.8.2.3 db/db mouse model

Whilst these mice still develop obesity like ob/ob mice, due to a leptin receptor mutation, diabetes develops more rapidly and with greater severity (141) and diastolic dysfunction is recognised in db/db mice. Recently, we have shown that the coronary microvascular EGlx is damaged in these mice, resulting in interstitial oedema (27). Along with this, various molecular and structural changes found in the human pathology also occur in the db/db model, such as increased fibrosis, left ventricular mass, cardiac inflammation and oxidative stress (145,146). Therefore, the db/db mouse model may prove helpful in developing therapeutics and understanding the molecular mechanisms of DCM.

1.2.8.2.4 Zucker diabetic fatty rat model

The Zucker diabetic fatty rat model (ZDF) is a popular model of T2D as they develop obesity and insulin resistance at a young age. As the rats age, they progressively develop hyperglycaemia (147). Zucker diabetic fatty rats show an increase in left ventricular hypertrophy and lipid accumulation, reflecting the switch to lipid-dominant substrate usage of the diabetic heart, leading to an increase in ROS and therefore increasing cell death (90,119,148,149). However, whilst many molecular mechanisms can be investigated in this model, it is difficult to establish diastolic dysfunction (90,148). Further development in the ZDF rat model was made by breeding ZDF rats with obese-prone Sprague Dawley rats, thus creating the Zucker diabetic Sprague Dawley rat. At 34 weeks of age, diastolic dysfunction is identified in these mice, indicated by a reduced E/A ratio (150).

Evidently, various models can be used to investigate DCM. The STZ mouse model presents a suitable model of DCM being able to encapsulate the various alterations observed. There are still mechanisms to be explored in the various animal models to better understand the pathophysiology of DCM and aid in the development of treatments. An example of an understudied area in animal models is the EGlx and its role in heart function. The EGlx is complex in structure and function and therefore requires dedicated study to elucidate its role within the heart.

1.3 The Glycocalyx

1.3.5 History of the glycocalyx

Every cell in the human body contains an extracellular negatively charged coat known as the glycocalyx (151) which translates to mean sweet husk (152). Despite this, the glycocalyx was severely understudied and this was due to the belief that it simply provided a protective layer around the cell surface ignoring its role in the functioning of the cell (151). Whilst the term 'glycocalyx' was proposed by Bennett (1963) (153), the concept of the glycocalyx was introduced as early as the 1940s and described as a thin non-cellular layer found on the inner lining of the endothelial cells (154) which was associated with the absorption of blood protein. Danielli, through his study of perfused hind legs, indirectly proposed an adsorbed protein layer and suggested that changes in permeability were a result of changes in this layer (155). Visualisation of the glycocalyx became possible through electron microscopy of different cells from different species and was first presented by Yamada (1955) who identified the presence of structures projecting irregularly from the cell membrane of mouse gall bladder epithelium (156). Since then, numerous works have been conducted identifying the structures of the glycocalyx and its physiological purpose. Fawcett, through his literature review, highlighted that the surface coating of cells consisted of glycoproteins and pointed to its potential role in absorption supporting previous work (157).

As the glycocalyx is studied further using various techniques to explore its complexity in structure and function, its role in physiology and pathophysiology is constantly being revealed.

1.3.6 Structure of the endothelial glycocalyx

The EGlx is a brush-like layer which lines the luminal side of the vascular endothelial cells (158). It is a multi-component layer, as shown in Figure 5, and is largely composed of proteoglycans (PG) as well as glycoproteins and adsorbed plasma components (159). Proteoglycans are the primary backbone of the EGlx and consist of a core protein attached to one or more negatively charged glycosaminoglycan (GAG) side chains (160).

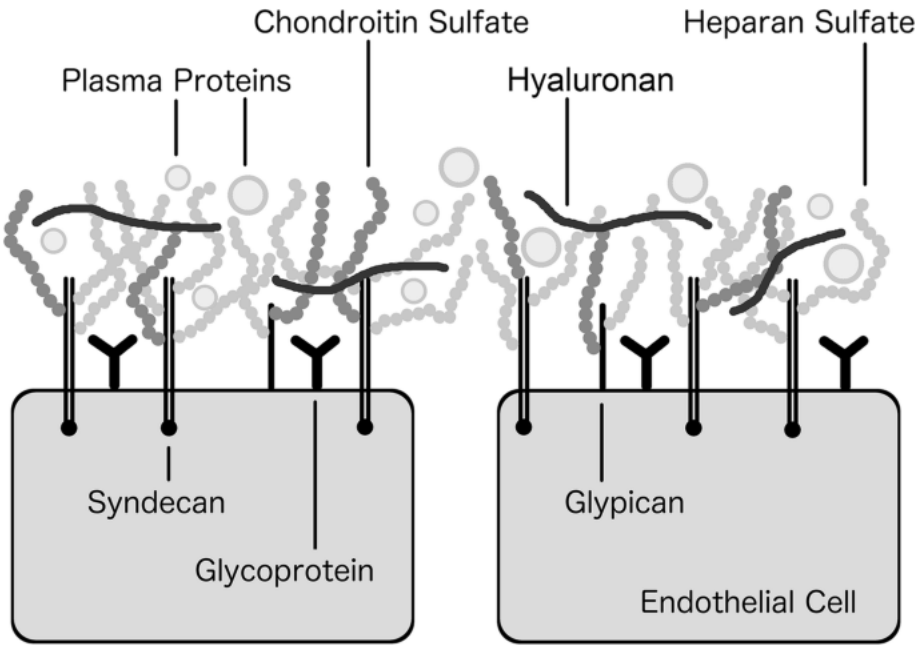

Figure 5. Structure of the EGlx.

The different components of the EGlx are shown projecting from the endothelial cell. The EGlx lines the luminal side of vascular endothelial cells and is composed of proteoglycans, which are made up of a core protein such as syndecan, with glycosaminoglycan side chains such as heparan sulfate. Other structures include glycoproteins and adsorbed plasma proteins. This image was taken from (161).

1.3.6.1 Proteoglycans: Core proteins

Syndecans are transmembrane core proteins with a molecular weight of 19-35 kDa and consist of four family members (162). Their structure consists of an ectodomain, a single transmembrane domain and a short cytoplasmic domain which is conserved across species (163). Diversity is seen in their ectodomains (163) with the possibility of up to five GAG insertions (164). Syndecan 1, 2 and 4 have three insertion sites close to their N-terminus with syndecan 1 having two additional sites close to the membrane reserved for chondroitin sulfate (CS) (165). Syndecan proteins, therefore, have the largest attachment possibilities when compared to the accompanying core proteins of the EGlx. Both heparan sulfate (HS) and CS are linked to syndecan through serine residues on the core protein with HS is the most common GAG of the EGlx (166).

Another major core protein of the EGlx is glypican (57-69 kDa) which has 6 subtypes (162) all of which share the same structural property for the insertion site of HS at the last 50 amino acids in the C terminus (167) placing HS chains towards the plasma membrane. Only glypican 1 is found on endothelial cells (165). Unlike syndecans, glypicans are associated with the membrane through a glycosylphosphatidylinositol anchor (162) which attaches to the glypican by the hydrophobic domain at the C-terminus (167). Whilst syndecan and glypican are the primary core proteins of the EGlx, other core proteins exist which are secreted after the attachment and modification of GAGs. These include perlecan, decorins, versican, mimecans and biglycans (160).

1.3.6.2 Proteoglycans: Glycosaminoglycans

As previously mentioned, GAGs are long polysaccharide chains of which many are modified through sulfation (166,168). The biosynthesis of GAGs begins in the cytoplasm with the synthesis of precursor sugars, uridine diphosphatase (UDP)-derived activated sugars. Once this occurs, the UDP sugars are translocated into the Golgi apparatus through an antitransporter transmembrane transporter (169). The addition of some GAGs to core proteins occurs post-translation within the Golgi apparatus through O-linked glycosylation, or both O and N-linked glycosylation in the case of keratan sulfate (166). It is also within the Golgi apparatus that modifications and sulfations occure for sulphated GAGs. The sulfated GAGs (with the exception of keratan sulfate) are covalently linked to the core proteins described above. The structure of GAGs extends into the lumen of vessels and has a net negative charge as a result of its numerous sulfate groups.

Contrary to the synthesis of the other GAGs, the synthesis of hyaluronan occurs at the plasma membrane by three hyaluronan synthase isoenzymes (HAS1,2 and 3). These enzymes utilse the UDP sugars as substrtaes (166,169). Hyaluronan (HA) is currently the only GAG that is not sulfated and not attached to a core protein (170) but interacts with CD44, a type 1 transmembrane glycoprotein (169,171).

The main GAG of the EGlx is HS which is a linear polysaccharide of repeating hexuronic acid and D-glucosamine disaccharides (172,173) and makes up 50% of the GAGs in the EGlx (170). Other sulfated GAGs include CS which is the second most common sulfated GAG and dermatan sulfate (170) (162). Both HS and CS chains vary in length with an average molecular weight of 50kDa (174).

1.3.7 Functions of the endothelial glycocalyx

1.3.7.1 The glycocalyx and inflammation

The EGlx plays an anti-inflammatory role in an unstimulated state preventing leukocyte adhesion. The interactions between leukocytes and endothelial cells require adhesion molecules and these are masked by the EGlx (175,176). Therefore, damage to the EGlx allows leukocytes in circulation to adhere easily to endothelial cells stimulating the progression of inflammation. Also, when the EGlx is damaged, cleaved components such as syndecans may be able to initiate a signalling cascade elsewhere (177).

On the other hand, specific components of the EGlx can participate in inflammation. It is known that HS acts as a ligand for L-selectin, a cell adhesion molecule expressed on most leukocytes, regulating the rolling of leukocytes (177). Therefore, an increase in specific components of the EGlx such as HS may be more harmful than beneficial.

1.3.7.2 The glycocalyx and mechanotransduction

As fluid moves across a cell surface, it creates a force. That dragging force is what is known as shear stress. Shear stress plays a critical role in the homeostasis of vascular endothelial cells. Through the regulation of vascular tone by inducing the release of substances such as nitric oxide and prostacyclin, shear stress has an athero-protective effect, with atherosclerosis developing at sites of turbulent flow (178,179). The EGlx is the first sensor of shear stress triggering the relay of forces through a cascade of signalling molecules (179). The process of how the EGlx translates information on shear stress is not yet understood. Perhaps understanding which specific components of the EGlx are important for shear stress will aid in understanding the mechanisms in which the EGlx acts as a mechanotranducer. In endothelial cells, shear stress appears to upregulate the synthesis of hyaluronan and results in a thicker EGlx. Therefore, there appears to be a need for the EGlx in response to the shear stress (180,181). A study utilising atomic force microscopy to investigate the EGlx demonstrated that glypican-1 and HS are important in mediating shear-induced NO production (180,181). The importance of the EGlx in protective signalling as a result of shear stress should not be ignored and research should continue to unravel the mechanisms of signalling from the EGlx. It is known that diabetes results in damage to the EGlx and ultimately has an impact on vascular tone. In fact, after 6 days of treatment with high glucose, a loss of HS was found in bovine aortic endothelial cells and this was associated with lower activation of eNOS after exposure to shear (181).

1.3.7.3 The glycocalyx as a sodium buffer

The GAGs of the EGlx provide a negative charge attracting positively charged ions as well as some plasma proteins. Sodium is a positively charged ion and thus is attracted to the negatively charged EGlx making the EGlx a sodium buffer (182–184). The ability of the EGlx to act as a sodium buffer is largely dependent on the number of GAGs, as well as their charge density (183). The EGlx is able to reversibly store sodium initiating a first-line barrier against sodium overload for endothelial cells. Thus, under normal physiology, the EGlx acts as a buffer to normal sodium levels without the saturation of their negative charges (182). The negative charges of the EGlx results in the repelling of erythrocytes preventing friction. If sodium levels increase in the blood and the negative charges of the EGlx become saturated this can result in friction between the EGlx and the erythrocytes resulting in endothelial damage (182). Salt overload results in the stiffening of the endothelium by converting endothelial cells into a sodium-absorbing state (185). Thus, there is potentially a link between salt, the EGlx and hypertension and perhaps protection of the EGlx should be investigated more as a target for hypertension.

1.3.7.4 Microvascular permeability and the endothelial glycocalyx

In 1864, Starling proposed that fluid filtration across the microvasculature was a result of two opposing forces, hydrostatic (leading to water leaving the capillary to the interstitial space) and oncotic (resulting in water returning into the capillary). From the ideas generated, net fluid movement between plasma and tissues was represented by the following equation (186,187):

$Jv = K [(Pc-Pi) – (\Pi p-\Pi i) = K (\Delta P - \Delta \Pi)$

- JV = fluid filtration or absorption
- K = Microvascular filtration coefficient
- Pc = Microvascular hydrostatic pressure
- Pi = interstitial fluid hydrostatic pressure
- Πp = Microvascular plasma oncotic pressure
- Πi = Interstitial fluid oncotic pressure
- ΔP, $\Delta \Pi$ = Hydrostatic and oncotic pressure differences across the microvascular wall

However, this equation implies that microvascular walls are impermeable to plasma proteins which is not the case. The reflection coefficient has been added to the equation to indicate the fraction of osmotic pressure that can be measured across a leaky membrane to that solute (187):

$Jv = K (\Delta P - \sigma \Delta \Pi)$

With σ representing the osmotic reflection coefficient to a solute.

Starling's affirmation was based on his work in which injected saline solution into the hindlimb of dogs could be absorbed directly into the blood whilst the injection of plasma into the tissues could not be absorbed (188). From reviewing his work, he concluded that the role of the lymphatics was to drain any excess fluid remaining in the tissues. Whilst that was believed to be true for many years, it is now understood and accepted that tissue fluid balance depends heavily on other components of the vasculature. With the consistent revolutions within microvascular biology, the starling's principle has been revised to accompany the more recent additions to vascular permeability including the EGlx, endothelial basement membrane, the extracellular matrix and, lymphatic function (31). However, although the principle has been revised, this does not mean that it is incorrect. The idea of fluid movement based on forces still stands as the basis and should not be ignored.

Both continuous and fenestrated capillaries utilise the EGlx as an important permeability barrier (189). By interacting with plasma proteins such as albumin through binding, an oncotic pressure difference occurs beneath the EGlx layer (26) thus contributing directly to the oncotic gradient for fluid movement back into the capillary. To date, much research on the EGlx in relation to permeability has been focused on the glomerular microvasculature (117,118,190). Perhaps this is due to the clinical importance of albuminuria noticed in diseased states such as diabetes. However, in organs such as the heart, there is not much research into the EGlx despite the importance of regulating permeability within these organs. Whilst it is clear that the EGlx plays a role in regulating vascular permeability, it is uncertain which specific components are key. Charged EGlx components such as sialic acids seem to be important for the EGlx to function as a regulator of permeability. In rats, a disruption to EGlx sialic acids by neuraminidase resulted in increased microvascular albumin permeability (191).

1.3.8 Visualising the glycocalyx

In 1966 the EGlx was visualised for the first time by Rambourg et all who used silver methenamine to detect proteoglycans on the surface of endothelial cells in mice (192). That same year the EGlx was labelled using ruthenium red, which binds to acidic mucopolysaccharides, and imaged using transmission electron microscopy which resulted in an underestimated EGlx thickness (20nm) (193). The reason for this is due to the delicacy of the EGlx being easily disturbed or dehydrated during vessel handling. This has led to difficulties in the estimation of EGlx depth. Today the use of a cation such as Alcian blue in combination with a fixative such as glutaraldehyde has been most frequently used to visualise the EGlx (190,191,194). However, although the value for EGlx depth is measured closer to that predicted, it is still less than what is expected and is most likely due to the reason of dehydration for electron microscopy.

Another method now used is lectin staining. This method allows the visualisation of the EGlx using fluorescent probes and confocal microscopy. Lectins are proteins that bind specific carbohydrate structures (195). Different lectins allow a better understanding of the composition of the EGlx due to the binding of different epitopes within the EGlx. By co-staining with a membrane marker, the EGlx can be identified on the luminal side of vascular endothelial cells (117).

Whilst there are difficulties in the accuracy of the visualisation of the EGlx, the development of methods to investigate the EGlx has allowed research to elucidate its unique structure and to understand more of its role in physiology and its alteration under pathophysiological conditions.

1.3.5 Modulation of the glycocalyx

The role of the EGlx in various physiological processes such as vascular permeability has been highlighted. It is because of its diverse actions in physiology, that damage to the EGlx is detrimental to health. Degradation of the EGlx occurs by several enzymes which are increased in various pathological conditions. These include but are not limited to, hyaluronidase, heparanase, neuraminidase, and matrix metalloproteinases.

1.3.5.1 Hyaluronidase

The degradation of HA is mainly dependent on hyaluronidase with hyaluronidase 1 (HYAL1) and 2 (HYAL2) being the predominant hyaluronidases in mammalian tissue (196,197). HYAL2 is found at the cell surface attached to the cell membrane by a glycosylphosphatidylinositol anchor and cleaves HA into smaller fragments of approximately 20-kDa (196,197). HYAL1 is in abundance within endothelial cells through endocytosis from the bloodstream (198) and is activated at a pH 4 (199). It is assumed that small fragments of HA are internalised to lysosomes and endosomes allowing HYAL1 to further degrade the HA fragments. Interestingly, it has been shown that HYAL1 deficiency in TID mice resulted in an increased EGlx thickness and HA content (200). However, there is still much to be revealed about the mechanism by which HA is shed from the EGlx. Despite this, it is clear that hyaluronidase plays an important role in the modulation of the EGlx.

1.3.5.2 Heparanase

The only enzyme to degrade heparan sulfate is heparanase (HPSE), generating fragments between 5-7kDa (201). Heparanase is synthesised as a 65 kDa inactive precursor before proteolytic cleavage in the lysosome resulting in 8 kDa and 50 kDa protein subunits. These subunits heterodimerize to form the active enzyme. This is then released from the lysosome or late inclusion body to the outside of the cell (197,202). There is a strong link between the upregulation of HPSE in diabetes and inflammation and this has been demonstrated in several studies (201,203–205).

1.3.5.3 Neuraminidase

Neuraminidase 1 (NEU1) cleaves terminal sialic acid residues which are expressed on cell-surface proteoglycans and glycolipids (206,207). Patients with T2D have been shown to have an increase in circulating neuraminidase and this was associated with an impairment in endothelial function (208). In a mouse model of T2D, inhibition of neuraminidase with a neuraminidase inhibitor (Zanamivir) protected the EGlx from damage highlighting neuraminidase as a key player in EGlx shedding (208).

1.3.5.4 Matrix metalloproteinases (MMPs) and the shedding of the EGlx

An important contributor to EGlx damage are MMPs, first described in 1949 (209,210). MMPs are a family of zinc-containing enzymes and are produced by a variety of cell types including endothelial cells (211,212). The secretion of MMPs occurs as inactive pro-enzymes and so MMPs remain inactive until proteolytic cleavage (211). There are various roles for MMPs but most commonly they are known to be involved in tissue remodelling. Evidence shows that MMPs, specifically MMP2 and 9, can modify the EGlx through the cleavage of syndecans (118). In normal physiology, there is tight regulation of the production of MMPs and their endogenous inhibitors, tissue inhibitors of metalloproteinases (TIMPS). In regard to the EGlx, tight regulation of MMPs allows effective turnover of EGlx components through shedding and repair. However, in many disease states, such as diabetes, there is an alteration in MMP activity and inhibition of MMP2 and 9 has shown to be beneficial in protecting the EGlx in diseases such as diabetic kidney disease (118). Proinflammatory cytokines which are a part of the profile of diabetes, lead to the upregulation of MMP9 resulting in the cleavage of core proteins such as SDC4 in glomerular endothelial cells (213–215). Evidently, MMPs play a crucial role in the shedding of the EGlx and their upregulation in diseases such as diabetes, points to them as therapeutic targets for protecting the EGlx. In this thesis, we will focus on the role of MMP2 and 9 in the shedding of the coronary microvascular EGlx. Therefore, we will further elaborate on the structure, function, and regulation of MMPs in the next section.

1.4 Matrix metalloproteinases

1.4.1 What are Matrix Metalloproteinases?

MMPs, first described in 1949 (209,210), are a family of 24 zinc-containing enzymes involved in the remodelling of several proteins, of which 23 are found in humans and are produced by a variety of cell types including endothelial cells (211,212). In 1962, the first official MMP was isolated and termed as a collagenase (MMP-1) involved in the degradation of the extracellular matrix (ECM) in the tadpole tail (216). Since then, the study of the structure and function of MMPs has consistently been investigated and their extensive involvement in physiology and disease has been revealed. The family of MMPs can be subdivided into 5 categories based on their actions and sequence homology. These groups are known as; collagenases (MMP1, 8, 13, 18), gelatinases (MMP2 and 9), matrilysins (MMP7 and 26), stromelysins (MMP3, 10, 11) and membrane-type MMPs (MMP14, 15, 16, 17, 24, 25) (217,218). Most MMPs, apart from MT-MMPs (membrane-type MMPs), are secreted as zymogens in the extracellular space (218).

1.4.2 The general structure of matrix metalloproteinases

Whilst there are differences in the substrates of the proteolytic enzymes, there are general structures conserved across MMPs (Figure 6). All MMPs have a **pre-domain** (N-terminal signal sequence) which directs their synthesis to the endoplasmic reticulum before it is removed (219). Typically, secreted MMPs consist of **a pro-domain** of about 80 amino acids long (220). Within the pro-domain, with the exception of MMP23, is a conserved free cysteine residue commonly called the “cysteine switch” (221,222). This cysteine-thiol residue interacts with

the zinc ion in the active site of the enzyme preventing substrate binding and cleavage (221). Therefore, MMPs are secreted in a latent, zymogen form due to the shielding of the catalytic site by the prodomain (223). Activation requires the removal, allosteric reformation or, chemical modification of the prodomain.

The **catalytic domain** is highly conserved and is composed of 3 α-helixes and 5 β-sheets connected by 8 loops with 4 of the β-sheets running parallel and 1 running antiparallel (224). This domain has a shape of a sphere with a diameter of roughly 40Å (224). At the catalytic centre is a zinc ion (Zn^{2+}) which is bound in place by 3 histidine residues (209,225). The gelatinases (MMP2 and 9) show unique structural components in that within their catalytic domain, in close vicinity to their active site, are three **fibronectin type II-like repeats** (FN2) (225) allowing them not only to bind to gelatine but also to collagen and laminin (226). Within the catalytic motif is a glutamate residue that activates a water molecule bound to zinc supplying the nucleophile that cleaves peptide bonds (227).

Connecting the catalytic domain to the hemopexin-like domain is the proline-rich **linker region**. This region is variable in length, from 8 to 72 amino acid (225) allowing interdomain flexibility. Mutations in this region may restrict movement between the catalytic domain and the hemopexin-like domain and thus reduce the activity of the MMP (220).

The **hemopexin-like domain** is vital for substrate specificity and consists of about 200 amino acids (224). Despite this, MMP7, 23 and 26 don't have this domain (209). Studies consistently reveal the importance of this domain in enhancing specificity in MMP binding to its substrate (228). It is also important for the binding of molecules to MMPs including various inhibitors (229). In pro-MMP9, this domain is able to bind to TIMPS particularly 1 and 3 via the COOH terminal (230).

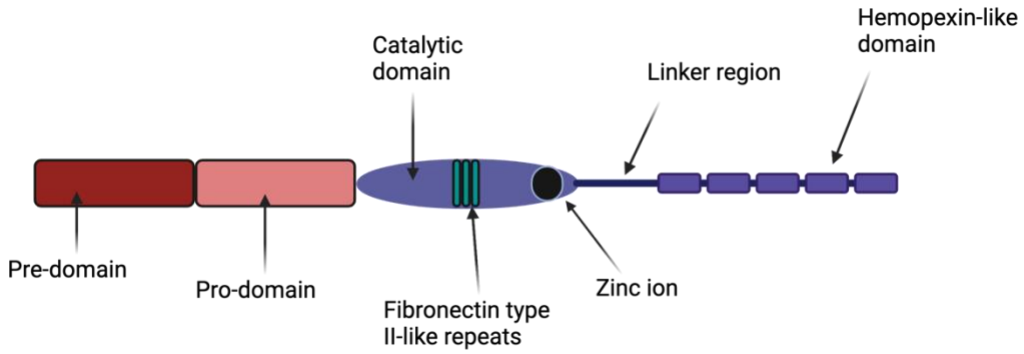

Figure 6.The general structure of matrix metalloproteinases.

The structure shown in the illustration is conserved between MMPs. Fibronectin type II-like repeats are found within the catalytic region of gelatinases specifically. Created with BioRender.com

1.4.3 Regulation of MMP expression and activity

1.4.3.1 Transcriptional regulation of MMPs

The primary regulation of MMP gene expression occurs at the transcriptional level (221,231,232). Several MMPs are co-expressed as a result of stimuli and this is due to the shared cis-elements found within their promotor sequences (221,231). On the other hand, some functionally similar MMPs such as the gelatinases, have distinct promoter regions.

There are several key transcription factors involved in the regulation of MMP genes and these include activator protein 1 (AP-1) which is regulated by various cytokines and growth factors (233,234), and nuclear factor kappa-light-chain-enhancer of activated B cells (NF-KB) which is upregulated as a result of inflammatory stimuli such as IL-1a and TNF-a (235,236). Other transcription regulators common amongst MMPs include members of the signal transducer and activator of transcription (STAT) family (232,237) and polyomavirus enhancer activator 3 (PEA3) (238,239). The differences observed within the promotor regions of MMPs, allow a

further categorization of the MMPs into three groups. Members in group 1 contain a TATA box, a DNA sequence which indicates where a genetic sequence can be read and decoded, in the -30bp region and this is accompanied by AP-1 adjacent to the TATA box, at -70bp (218,240). MMPs that fall within this group are MMP1, 3, 7, 9, 10, 12, 13, 19 and 26 (218). Those within group 2 (MMP8, 11 and 21) contain the TATA box in the absence of an AP-1 binding site and require the binding of other transcription factors. Members of group 3 (MMP2, 14, and 28) are constitutively expressed and, unlike groups 1 and 2, neither contains a TATA box or AP-1 binding site. The expression of MMPs within this group is mainly determined by the specific protein 1 (Sp-1) transcription factor. Whilst growth factors and cytokines may significantly upregulate MMPs within groups 1 and 2, the effect is reduced on MMPs within group 3 and a subtle, if any, induction of their expression is recognised (218,232,240).

Post-translational regulation of MMPs is key to its function. MMPs require cleavage of the pro-domain for complete activation. There are several mechanisms by which MMPs can be activated. Below we will focus on MMP2 and 9 due to the particular interest in their involvement in EGlx shedding.

1.4.3.2 Human MMP2

MMP2 is a 72 KDa protein ubiquitously expressed in its pro form and is cleaved to an active 67 kDa protein. Unlike MMP9, the majority of pro-inflammatory stimuli fail to increase the expression level of MMP2 due to the lack of transcription factor binding sites for pro-inflammatory cytokines (241). MMP2 has been implicated in various diseases such as atherosclerosis (242), cancer (243), myocardial infarction (112), and diabetes (244). It appears crucial to maintain MMP2 expression and activity in homeostasis. Physiologically, MMP2 can cleave various matrix proteins such as fibronectin, elastin and collagen due to the cysteine-rich inserts within its catalytic domain (245,246). In the heart reduced MMP2 activity as a result of diabetes has been shown to increase fibrosis and stiffening of the left ventricle leading to diastolic and systolic dysfunction (112) thus, highlighting the importance of MMP2 in both physiology and pathophysiology.

A confirmational change in the pro-domain of MMP zymogens is necessary for activation. This is accomplished in three ways: 1) direct proteolytic cleavage of the prodomain; 2) allosteric reconfirmation of the prodomain; and 3) chemical modification of the cystine residue by reactive oxygen species and non-physiological agents (219,221,247). MMP2 is activated upon release from the cell although research is beginning to identify potential intracellular activation mechanisms for various MMPs (248).

A well-known mechanism of MMP2 activation occurs via MMP14 and TIMP2 at the cell surface as shown in Figure 7. MMP14 attached to the cell surface is first inhibited by the N-terminal of TIMP2. The C-terminal domain of the now-bound TIMP2 behaves as a receptor for pro-MMP2 binding to its hemopexin domain. This results in the positioning of MMP2 at the cell surface allowing an adjacent, uninhibited MMP14 to initially cleave the pro-domain of MMP2 resulting in an activated enzyme. However, this is not yet the mature activated form of MMP2 as further cleavage of the pro-domain is required which occurs by another MMP2 molecule (219,248). Therefore, to maintain stable activation and inhibition of MMP2, the ratio of TIMP2 to MMP2 is crucial as well as the other enzymes necessary for its activation such as MMP14.

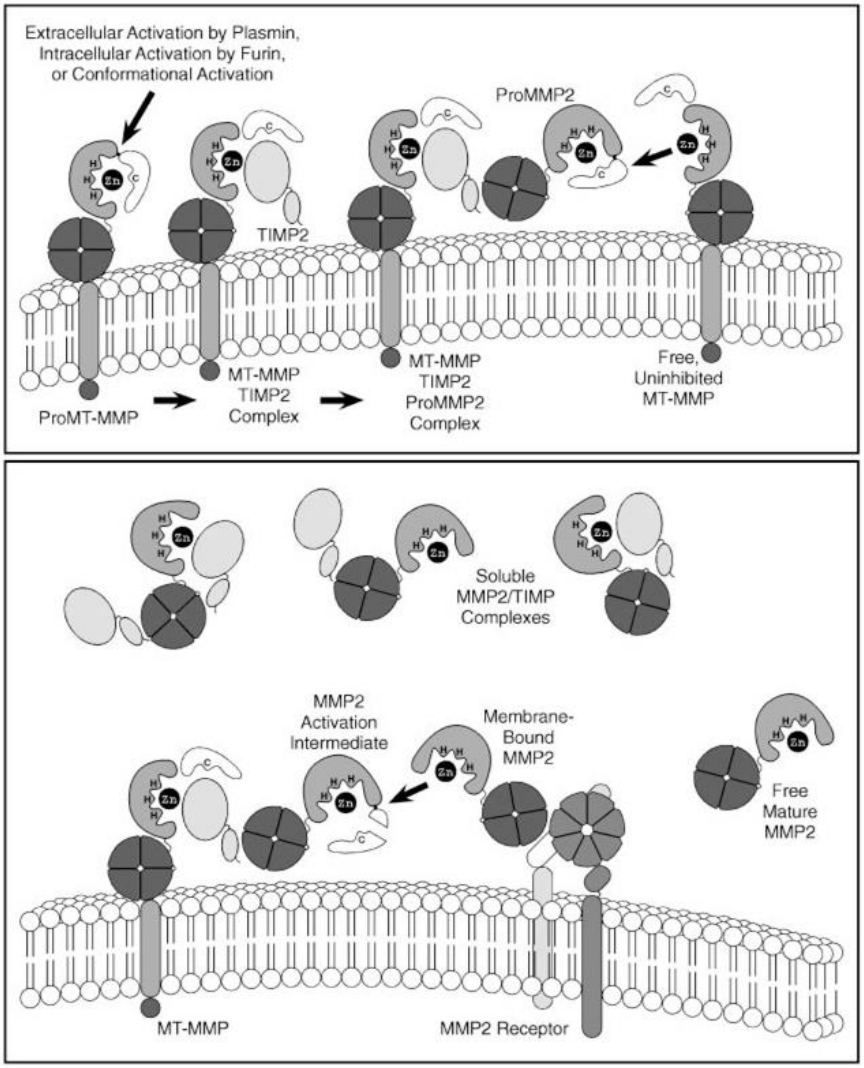

Figure 7. Activation of MMP2 by TIMP2 and MMP14.

Activation of MMP2 by TIMP2 and MMP14 occurs at the cell membrane. Activated MMP14 is inhibited my TIMP2 which also binds to ProMMP2 forming a trimolecular complex. Pro-MMP2 is partially activated by MMP14 with the remaining portion of the pro-peptide being removed by a mature MMP2 molecule leading to the mature and fully active MMP2 enzyme. This image was taken from (219).

1.4.3.3 Human MMP9

The pro form of MMP9 has a molecular weight of 92 kDa whilst once cleaved and activated the molecular weight is 88 kDa in humans. From examining the crystal structure, it was revealed that the catalytic domain consists of 2 zinc ions and 5 calcium ions (249) and as a zinc-dependent endopeptidase, the zinc ions are necessary for catalytic activity (250). Like MMP2, MMP9 has been implicated in several diseases including cancer (250), diabetes (251) and atherosclerosis (252). Physiologically MMP9 is crucial for cleaving the extracellular matrix due to its fibronectin-like domain. Pro-MMP9 is bound to TIMP1 via the hemopexin-like domain of MMP9 and the COOH-terminal domain of TIMP1 before being secreted from the cell (230).

Several proteases can cleave the pro-domain of MMP9 resulting in its activation. These include MMP2, 3, cathepsin G and plasmin, of which MMP3 is said to be the most potent activator for MMP9 (230,253–256). Not only is MMP3 a key protease in directly cleaving the pro-domain of MMP9, but in macrophages, it has been shown to upregulate the protein expression of MMP9 (257). As research continues to study the complexity of MMP9, a greater understanding of its role in physiology and disease is being developed.

1.4.4 Factors that increase MMP activity

Diabetes is a complex multifactorial disease that results in various cellular and molecular changes including, increased cytokines, ROS, and hyperglycaemia to name a few. Many of these changes can cause an alteration in MMP activity.

1.4.4.1 Reactive oxygen species

It is well understood that an increase in oxidative stress contributes to the damage observed in several diseases including diabetes (258). Whilst increased oxidative stress can lead to the apoptosis of cells and damage organs such as the heart (258), ROS can also regulate MMPs from transcriptional regulation to pro-enzyme activation (259). Specifically, mitochondrial-associated ROS is important for the regulation of MMP9 and is proposed to stimulate the induction of NF-kB expression. As elevated ROS results in an increase in MMP expression, it is no surprise that the utilization of antioxidants would alleviate this increase. Indeed, the use of tempol, an intracellular antioxidant (260), has proven to be effective in reducing MMP9 mRNA expression through the reduction of NF-kB (261). Whilst ROS can indirectly cause an upregulation of MMPs, it may also cause direct activation. Due to the ability to reversibly react with thiol groups, a prominent feature of the pro-domain ensuring the latent state of MMPs, an oxidative attack can occur in the thiol group disrupting the coordination with the zinc ion in the catalytic region and thus the enzyme can become partially or fully active (223).

1.4.4.2 Inflammation

In many diseases, MMPs play a crucial role in progressing the inflammatory response by activating cytokines such as TNF-α and TGF-β (262). On the other hand, pro-inflammatory cytokines modulate the secretion of MMPs and thus a vicious cycle occurs. Pro-inflammatory cytokines upregulate MMP expression through the increase in the transcription factors. TNF-α and IL-1B has shown to upregulate several MMP expressions and activities including MMP1, 3, 9, 11, 13, and 14 in human cells (213,262–266). As mentioned, activation of the NF-kB pathway induces the expression of some MMPs such as MMP9 and this mechanism is employed by proinflammatory cytokines. In fact, blocking NF-kB or interfering with its activation pathways prevents cytokine-induced MMP upregulation (263,266).

1.4.4.5 Hyperglycaemia

There is a positive association in patients with blood glucose levels and MMP activity (267). This is probably because hyperglycaemia can result in various downstream effects such as increased inflammation and increased ROS, which have been highlighted to increase MMP activity. In vitro, it has been demonstrated that high glucose in cell culture is able to induce MMP expression, particularly MMP1, 2, and 9 (267,268). In cell culture, the use of the antioxidants such as polyethene glycol–superoxide dismutase can significantly reduce the enhanced MMP activity observed when treated with high glucose (269). This, therefore, suggests that oxidative stress resulting from chronic high blood glucose is a downstream driving mechanism utilized to stimulate MMP activity.

1.4.5 Inhibition of matrix metalloproteinases

1.4.5.1 Tissue inhibitors of metalloproteinases

As the name suggests, tissue inhibitors of metalloproteinases (TIMP), are endogenous inhibitors of metalloproteinases. Four isoforms of TIMPS have been identified (TIMP1, 2, 3 and 4) which act as inhibitors of MMPs through a non-covalent interaction with Zn^{2+} (218,270). Despite varying efficacy, all TIMPs can inhibit all MMPs. Due to being natural inhibitors of MMPs a tight balance is kept between the levels of MMPs and TIMPS in normal physiology. All four TIMPS have been identified in the heart with TIMP1 and 2 being best characterized (271). The expression of TIMP1 occurs in response to proinflammatory cytokines. In fact, TIMP1 is recognized as a cytokine modulator of cell functions (272,273). TIMP2 appears to be expressed in the majority of heart cells (271) and is crucial in protecting the heart from cardiac dysfunction and pathological remodelling both dependently and independently of its MMP inhibitory properties (274,275). In knockout mouse models of TIMP3, there is an upregulation of MMP9 protein levels and this is associated with compromised cardiac contractile function (271). Unlike TIMP1, 2, and 3, the mechanism of action of TIMP4 is unclear. Alone TIMP4 may not have many effects however, when co-expressed with TIMP2, it can reduce pro-MMP2 activation by MMP14 (276).

1.5.1.2 Chemical inhibitors

The development of MMP inhibitors has become a crucial part of scientific research. Currently, there are various inhibitors, some of which are broad acting whilst others are specific to certain MMPs. Whilst drug discoveries have shown great potential, not many have progressed due to failures at clinical trials mainly because of their lack of specificity leading to various side effects. A specific targeting approach has become crucial as whilst some MMPs have a detrimental function when overexpressed, some also act protectively in physiology. An example of this is MMP8 which is crucial in wound healing. This, therefore, limits the use of broad-spectrum inhibitors (277–279). There is a serious concern for MMP2 and 9 as they appear to be in greater concentrations in pathological states and have been implicated in many cardiovascular diseases such as severe cardiac remodelling, EGlx damage, atherosclerosis and DCM (27,118,213,280,281). Mechanistic inhibitors are molecules that are inactive until activated through enzymatic catalysis to become a molecule that inhibits the enzyme usually through covalent modification at the active site (282). Mechanistic inhibitors for MMP2 and 9 have proven effective due to their high potency with a prime example being SB-3CT.

SB-3CT

SB-3CT, identified in 2000, is the first known selective slow binding and mechanistic inhibitor for gelatinases causing a conformational change to the inhibitor-enzyme complex (283). The slow binding component of its inhibition reflects that of TIMP1 and TIMP2 (284). Unlike broad-spectrum MMP inhibitors, which act by chelating the zinc ion in the active site, the deprotonation (removal of a proton) of SB-3CT results in the generation of a thiolate which coordinates with the zinc ion forming a tight binding inhibition (283). This leads to irreversible inhibition of the protease (285) through a stable Zn^{2+} thiolate complex (286). In fact, the reconstruction that occurs places the enzyme in structural similarity to the proenzymes (287). The specificity of SB-3CT is due to the biphenyl moiety fitting in the S1' deep hydrophobic pocket of the gelatinases (283), a region adjacent to the zinc-binding site which shows clear variability among MMPs (288). Inhibition of MMP2 and 9 with SB-3CT occurs in the nanomolar concentrations (Ki = 14 ± 4 nm and Ki = 600 ± 200 nm respectively) (289). Metabolism of SB-3CT in vivo results in a more potent inhibitor (p-hydroxy SB-3CT) with a better inhibitory activity (Kis = 6 and 160 nM for MMP2 and MMP9 respectively) (290). This daughter molecule also acts as a slow-binding inhibitor of MMP14 (283). Figure 8 illustrates the structure of SB-3CT and its mechanism of inhibition.

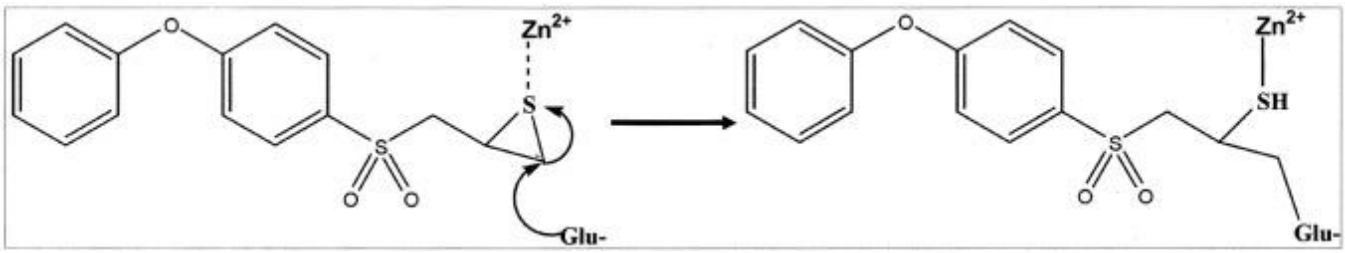

Figure 8: Structure of SB-3CT.

The opening of the thiirane ring from the nucleophilic attack of the glutamate found in the active site of the enzymes, results in a stable irreversible bond between the sulfur and the zinc ion. This figure was adapted from (285).

MMP2/9 inhibitor I

Another MMP2 and 9 specific inhibitor is (2R)-2-[(4-Biphenylylsulfonyl)amino]-3-phenylpropionic Acid (MMP2/9 inhibitor I) which acts by binding directly to the zinc ion at the active site resulting in inhibition of the MMPs (291). Previously, this inhibitor has been used to protect the glomerular EGlx in a mouse model of diabetic kidney disease through the inhibition of MMP9 activity (118). Therefore, there may be potential to protect the EGlx of other organs such as the heart in diabetes.

Tetracyclines

Independent of their antimicrobial actions, tetracyclines can inhibit MMP activity; doxycycline is the most potent inhibitor (292). At sub-antimicrobial doses, tetracyclines can chelate the zinc ion of the active site, altering the activity of MMPs (293,294). Research shows that doxycycline is a broad-spectrum inhibitor with the ability to reduce the expression and activity of both MMP2 and 9 (295).

Other variable nonspecific inhibitors exist such as Batimastat which reached clinical trials but failed to demonstrate a survival benefit and had low solubility and oral bioavailability (296).

The development of MMP inhibitors has increased vastly as scientists continue to reveal more about the characteristics of MMPs. With their diverse presence in many diseases, identifying selective and effective MMP inhibitors is crucial. Therefore, this should be a primary focus as researchers continue to reveal the complexity of MMPs.

1.5 Rational, hypothesis, and aims

1.5.1 Summary of introduction

DCM is a leading cause of death amongst diabetic patients and is defined as the progression of diastolic dysfunction to heart failure independently of other cardiovascular factors such as hypertension and coronary artery disease in patients with diabetes (77). Microvascular damage is a recognised characteristic of DCM, and this is associated with altered permeability. The heart is extremely sensitive to changes in microvascular permeability with a slight increase in interstitial fluid compromising heart function (17). A major regulator of microvascular permeability is the EGlx. Evidence suggests that MMPs can modify the EGlx (118). In normal physiology, there is tight regulation of the production of MMPs and their inhibitors, tissue inhibitors of metalloproteinases (TIMPS). However, in diabetes, there is an alteration in MMP production. Previously it has been shown that there is an upregulation of MMPs particularly 2 and 9 during diabetes which results in the shedding of the EGlx. Protecting the EGlx by inhibition of these MMPs has shown to be beneficial for conditions such as diabetic kidney disease (118) and thus may be beneficial in DCM.

1.5.2 Hypothesis

Taking together all that has been outlined, there are clear gaps in the knowledge of the mechanisms of DCM and identifying therapeutic targets is crucial for the development of treatments for DCM.

Four main factors provide the rationale for this thesis.

1. MMPs are upregulated as a result of diabetes.
2. MMPs cause shedding of the EGlx.
3. The EGlx is important for microvascular permeability homeostasis in the heart.
4. An alteration in coronary microvascular permeability can lead to diastolic dysfunction.

The hypothesis for this thesis is:

Matrix metalloproteinases cause shedding of the coronary microvascular endothelial glycocalyx in diabetic cardiomyopathy and therefore, inhibition of MMP2 and 9 will protect the coronary microvascular endothelial glycocalyx and improve diastolic function.

1.5.3 Aims

The project has three primary main aims:

1. ***Investigate whether MMP activity is increased in DCM and if MMP2/9 inhibitor I protects the coronary microvascular EGlx in DCM (Chapter 3).***

Members of the group showed, prior to my arrival, that the coronary microvascular EGlx is damaged in a mouse model of DCM (27) (NB although much of the animal work described in this paper was conducted by prior to my arrival, I performed the in vitro work described below in aim 2 and in chapter 4. The MMP activity of the heart shown in Chapter 3 also formed part of the paper). Also, previous research shows in a mouse model of diabetic kidney disease, that the inhibition of MMP2 and 9 with MMP2/9 inhibitor I protected the glomerular EGlx (118). Based upon this, aim 1 will be tested through:

a. Examining if diastolic function is protected when treated with MMP2/9 inhibitor I in a mouse model of DCM. The mouse model used in this study will be the same one used previously in our group which shows diastolic dysfunction in the absence of systolic dysfunction at 9 weeks post STZ (27).
b. Examine if MMP inhibition protects the coronary microvascular EGlx depth. Mice hearts from this study will be sectioned and lectin immunofluorescence will be utilised to investigate the EGlx. The peak-to-peak method used previously in our group (117,118) will be adopted to assess EGlx depth in the heart. This will be the first time EGlx has been assessed using this method on

coronary microvessels. I will test several lectins to identify suitable lectins that can be used to investigate the coronary microvascular EGlx.

c. An assessment of MMP2 and 9 activity to determine any changes in DCM and if the inhibitor was successful in inhibiting the MMPs. This will be done using commercially available activity assay kits. The MMP activity will be assessed in the heart, plasma and urine of mice within this study.

2. ***Identify if TNF-α causes an upregulation in MMP activity and SDC4 shedding from coronary microvascular endothelial cells (CMVEC) in vitro. Within this, I aim to investigate if SB-3CT prevents SDC4 shedding from CMVEC. Further to this, I aim to determine if the EGlx contributes to CMVEC barrier function.***

A relationship has previously been established between TNF-α and SDC4 shedding from glomerular endothelial cells (213). TNF-α is also a common inflammatory cytokine upregulated in diabetes and is known to upregulate MMP activity specifically MMP9 (213,257,263,297–299).

a. To investigate the effect of TNF-α alters SDC4 expression, CMVEC will be treated with TNF-α and SDC4 mRNA and protein expression will be examined. Cells will also be treated with SB-3CT to examine if inhibition of MMP2 and 9 protects the EGlx.

b. To determine if TNF-α results in an upregulation in MMP activity, MMP2 and 9 activity will be assessed in the conditioned media using a commercially available activity assay.

c. The role of the EGlx in contributing to CMVEC barrier properties will be assessed using a transwell assay. The EGlx will be removed using a combination of enzymes and the effect of stripping the EGlx on albumin leak across the CMVEC monolayer will be assessed.

3. Investigate whether the inhibition of MMP2 and 9 with SB-3CT protects the coronary microvascular EGlx and restores diastolic function in a mouse model of DCM.

To determine the therapeutic role of MMP inhibition, SB-3CT will be used in the mouse model of DCM used previously within the group. In this model, diastolic dysfunction occurs in the absence of systolic dysfunction, and this is also clinically recognised in humans. It is also recognised in this model that the EGlx is damaged and therefore this aim follows on from the previous aim, adding therapeutic value to the use of SB-3CT to inhibit MMPs in DCM.

a. To ensure diabetic mice develop diastolic dysfunction prior to MMP inhibition with SB-3CT, echocardiography will be done. Some diabetic mice will be treated with a daily dose of SB-3CT for 2 weeks and echocardiography will be utilised to determine if MMP inhibition restores diastolic function.
b. To determine if the coronary microvascular EGlx is protected by treatment with SB-3CT mouse hearts will be fixed and sectioned following which I will utilise lectin staining, confocal microscopy and the peak-to-peak method of analysis to assess EGlx depth.
c. To investigate if SB-3CT successfully inhibits MMP2 and 9, an MMP2 and 9 activity assay will be used to quantify MMP activity in the mouse hearts and plasma.

d. As the EGlx contributes to the regulation of endothelial protein permeability, to assess if increased albumin extravasation occurs in the hearts of diabetic mice and if protection is found from MMP inhibition, I will conduct albumin immunofluorescence on the mouse heart section.

2 Materials and Methods

2.1 Materials

All general reagents, unless stated otherwise were purchased from Sigma-Aldrich Co, Dorset, United Kingdom.

2.2 In vitro methods:

2.2.1 Cell culture

2.2.1.1 ciCMVEC culture

Human conditionally immortalised coronary microvascular endothelial cells (ciCMVEC), shown in Figure 9, were established as described previously (27), using a similar approach as that described for glomerular endothelial cells (213,300). In brief, primary CMVEC were transduced with temperature-sensitive simian virus 40 large tumour antigen (tsSV40LT) and telomerase using retroviral vectors allowing the proliferation of the cells at 33 °C (without telomere shortening). ciCMVEC were cultured in endothelial growth medium 2 microvascular (EGM2-MV; Lonza, Basel, Switzerland) with the addition of the supplied growth factors and 5% fetal calf serum. Vascular endothelial growth factor (VEGF) and Gentamicin Sulfate-Amphotericin (GA-1000) were excluded from the media.

Stock cells were grown and maintained in T75 tissue culture flasks containing 10 ml of media. The cells were grown in humidified incubators at 33 °C in the presence of 5% CO2 until they were at 80% confluency. The media was replaced with fresh media every 2-3 days.

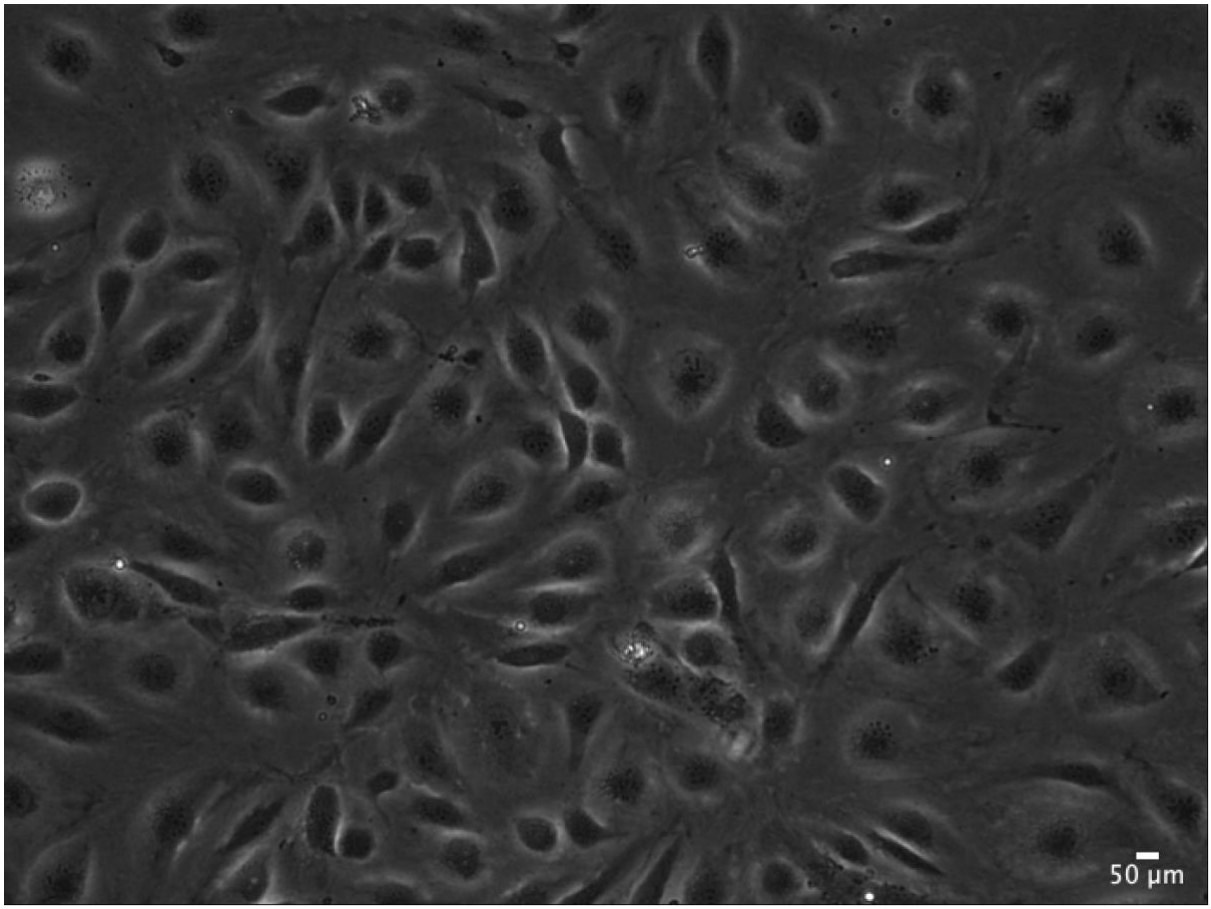

Figure 9. Human ciCMVEC prior to being thermoswitched

Human ciCMVEC were grown at 33℃ before being thermoswitched to 37℃ to allow the cells to become quiescent.

2.2.1.2 Cell passaging

Inactivation of the virus at 37 °C, allowed the cells to become quiescent. Once at 80% confluency, the cells were either 'thermoswitched' to 37 °C for 3-5 days to allow cells to terminally differentiate; reseeded into desired tissue culture dishes for experiments; or frozen for later use.

To passage cells, the media was aspirated, and the cells were washed with sterile phosphate-buffered saline solution (PBS) to remove any residual media. Trypsin-EDTA (0.25%) was then added to the flask to cover the cell's surface. Excess trypsin was aspirated immediately before placing the cells back into the 33 °C incubator for 3 minutes. To confirm the detachment of cells from the plate surface, light

microscopy was used, and the flask was gently tapped on the sides to detach any cells still adhered to the flask. To neutralise trypsin, as well as resuspend the cells, 4 ml of new culture medium was added to the flask. For each T7S plate that was being seeded, 1 ml of the cell suspension was added and topped up with 9 ml of media. Each time a cell was detached and reseeded increased the passage number by 1. The cells were then returned to the 33 °C incubator to continue growing.

2.2.1.3 Counting cells

If a specific number of cells was to be seeded, the cells were counted manually following the detailed protocol from Abcam (https://www.abcam.com/protocols/counting-cells-using-a-haemocytometer) using a glass hemocytometer. The hemocytometer was cleaned with alcohol each time before use. Only cells that sat within a square were counted (examples of squares are shown in Figure 10). The number of cells to be seeded was then calculated from the total number of cells in suspension and seeded accordingly in the desired plate.

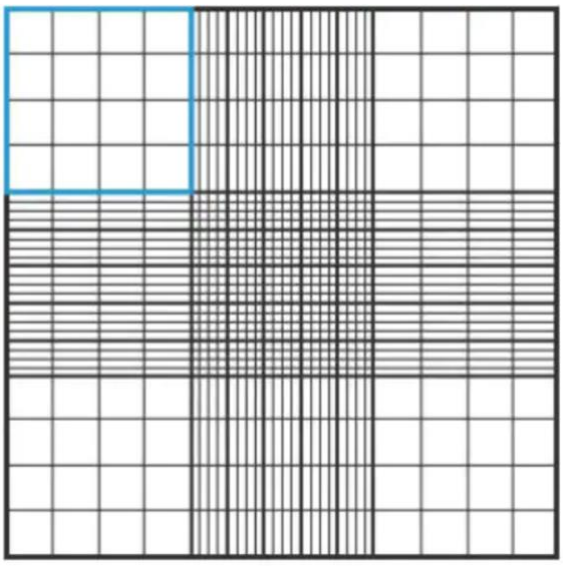

Figure 10.Hemocytometer gridlines.

The 4 sets of 16 squares (highlighted in blue) were used to count the cells. Only cells that sat within a square were counted. This image was taken from Abcam.

2.2.1.4 Freezing and thawing ciCMVEC

Cryopreservation of the cells was necessary to avoid excessive ageing of the cells and to preserve the cell line. A freezing solution was made containing 10% dimethyl sulphoxide (DMSO), 45% foetal bovine serum (FBS), and 45% complete media. This was then added to a 1.8 ml cryovial containing resuspended cells (as described above) to a 1:1 ratio. To allow slow freezing, the cryovials were wrapped in tissue and placed at -80 °C for short-term storage. For long-term storage (more than a month) the cells were transferred to liquid nitrogen.

To thaw the cells for use, the cells were warmed by hand swiftly before being transferred to a T75 flask containing 8.2 ml of media and placed into the 33 °C incubator. After 24 hours, the media was aspirated and replaced with fresh media to remove traces of DMSO. Cells were then cultured normally as previously described.

2.2.2 Treatments of ciCMVEC

2.2.2.1 Treatment with TNF-α and SB-3CT

To investigate the effects of TNF-α on the eGlx as well its effect on MMP regulation, ciCMVEC were seeded in 6 well plates. After reaching 80% confluency, the cells were thermoswitched for 3-5 days before being placed into the experimental conditions. Cells were placed in serum-free media to reduce interferer proteins, 1 hour before treatment with 10 ng/ml of Recombinant Human TNF-α Protein (R&D systems, 210-TA-005), as this concentration has been used previously in several studies investigating the effect of high dose of TNF-α (213,301), or vehicle (PBS) for 6 hours unless stated otherwise. To investigate the effects of MMP inhibition on the eGlx, some cells were treated with 10 μM of SB-3CT (MedChemExpress, HY-12354) whilst the others were treated with the vehicle for the

inhibitor (DMSO), 2 hours prior to TNF-α treatment and remaining for the duration of TNF-α treatment.

2.2.2.2 Treatment with MMP2 and MMP9

To directly investigate the effect of either MMP2 or MMP9 on the EGlx, ciCMVEC were treated with 3 ng/ml of either MMP2 or 9 in serum-free media for 1 hour. Prior to incubation, recombinant human pro-MMP2 (Anaspec, AS-72224) or recombinant human pro-MMP9 (Anaspec, AS-72017) was activated with 1mM of 4−aminophenylmercuric acetate (APMA) at 37 degrees for 2 hours as this temperature has been shown to increase MMP activity physiologically (302–304). APMA activates MMPs by disrupting the cysteine switch therefore exposing the enzyme's active site (305) and so some cells were also treated with APMA alone to act as a vehicle control.

2.2.3 Knockdown of MMP9 expression in ciCMVEC

RNA interference is a tool commonly used in research to specifically study the function of a gene of interest. Short hairpin RNAs (shRNA) are a form of RNA interference that can be transfected into cells by viral vectors or as plasmid vectors (306). shRNA is capable of DNA integration and following transcription, it is transferred to the cytosol where it is processed to small interfering RNA (siRNA) (306). siRNA then binds to the target mRNA causing sequence-specific degradation of the target mRNA through various enzymes (306,307).

To specifically investigate the role of MMP9 on EGlx shedding, MMP9 expression was knocked down in ciCMVEC using MMP9 shRNA lentiviral particles (Santa Cruz Biotechnology, sc-29400-V). Control cells were infected with lentiviral particles containing a scrambled shRNA sequence (Santa Cruz Biotechnology, sc-108080). ciCMVEC were seeded in 6 well plates and the media was replaced with complete media containing polybrene at 5 μg/ml. Polybrene enhances virus attachment to the cell surface by neutralising charge interactions (308). Some cells were then infected with either 15 μl of

MMP9 shRNA lentiviral particles or lentiviral particles with a negative scrambled shRNA sequence. The cells were then incubated overnight at 33 °C. As polybrene is toxic, the media was changed the next day to complete media without polybrene and placed back into the 33°C incubator for 2 days. To select stable clones, the cells were incubated with puromycin dihydrochloride at a concentration of 0.8 μg/ml in normal media. Puromycin is toxic to both prokaryotic and eukaryotic cells (309). The lentivirus contains a puromycin-resistant gene and so successfully infected cells will be resistant to puromycin. The media was replaced every 2 days with fresh puromycin until resistant colonies were identified. The concentration of puromycin used was determined appropriate for this cell line by other members of the lab group who had conducted a kill curve. The cells were then passaged into T25 flasks to grow before being further passaged into T75 flasks to generate a stock of cells.

Once successful cell lines had been generated, the cells were seeded in 6 well plates at a density of 0.3×10^6 and treatment with TNF-α was carried out as described above.

2.2.4 RNA extraction and qPCR analysis

2.2.4.1 RNA extraction and quantification

To investigate gene expression, RNA was extracted from cultured cells using Quiagen RNeasy mini kit (Qiagen, 74104). The cells were washed with PBS on ice then monolayers were lysed directly from the 6 well plates by the addition of 300 μl of buffer RLT (supplied by the manufacturer). The lysate was collected and centrifuged at maximum speed for 3 minutes after which the supernatant was removed by pipetting and used for the remaining steps. Once RNA was extracted, if the samples were not being used immediately, they were stored at -80 °C. The concentration of RNA was measured as well as the quality determined, using a nanodrop system (Thermo Scientific, Waltham, USA). The A260/280 was used to determine the quality of the RNA with a ratio between 1.8 and 2 being deemed acceptable suggesting minimal protein or phenol in the samples. The A260/230 ratio

was used to determine the presence of other purified contaminants in the samples with a ratio of more than 1.6 being deemed acceptable.

2.2.4.2 cDNA synthesis

The conversion of RNA to cDNA was done using a high-capacity RNA to cDNA kit (Thermo Fisher Scientific, 4387406). From the calculated concentration of RNA, 1µg of RNA was converted to cDNA by the following reaction mix:

Component	**Amount needed for reverse transcription reaction**
2X RT Buffer Mix	10.0 µL
20X RT Enzyme Mix	1.0 µL
RNA sample	up to 9 µL
Nuclease-free H2O	Top up to 20 µL
Total per reaction	20.0 µL

Table 1. Components needed for cDNA conversion.

The tubes were then placed into the thermocycler at 37 °C for 60 minutes and the reaction was stopped by heating to 95 °C for 5 minutes as this denatured the enzyme. The samples were then cooled to 4°C. The samples were stored at -20 °C or used directly for real-time PCR.

2.2.4.3 Quantitative polymerase chain reaction (qPCR)

qPCR is commonly used to quantitate changes in gene expression and is a sensitive and reproducible technique (310). Sybr green is used as a fluorescent reporter molecule which when bound to double-stranded DNA, emits a fluorescence. Therefore, the more double-stranded DNA present, the more Sybr green will be bound increasing the fluorescent signal (311). Each primer pair, shown in Table 2, was diluted to 100-pmol/μl with DEPC water (Thermo Fisher Scientific, AM9915G) as per the guidance of Eurofins genomics. From this, the working stock primer solution was prepared to 10 μM. A master mix was made using 5.5μl of Fast Sybr Green (Thermo Fisher Scientific, 4385612), 0.8μl of primer mix and 2.7μl of DEPC water making a total of 9μl per well in a 96 well plate (Sarstedt, 72.1981.202). 1μl of cDNA (diluted 1:5) was added to each well of testing making a final total of 10μl per well. The negative controls received 1μl of DEPC water. All samples were done in triplicates and the mRNA expression was quantified using a Real-Time PCR system (Applied Biosystem) using the fast Sybr Green settings. Melt curve analysis was performed to confirm the specificity of the primers as well as further show the purity of the samples. Primer sets should have 1 melting point at a certain temperature to show the specificity of the primer to the gene of interest. As well as this, no melting point should be present in the negative control to ensure no primer dimers were being formed. Figure 11 shows an example of melt curves generated from a qPCR run. Samples were normalised to the housekeeping gene, glyceraldehyde-3-phosphate dehydrogenase (GAPDH), and the $2^{-\Delta\Delta CT}$ method of quantification was used to calculate fold change (below).

Human Primer	Forward sequence	Reverse sequence	Designed or previously published
GAPDH	AAGGTGAAGGTCGGAGTCAAC	GGGGTCATTGATGGCAACAAT	(312)
SDC4	CCTCCTAGAAGGCCGATACTT	AGGGCCGATCATGGAGTCTT	(213)
MMP2	GAGACCATGCGGAAGCCAAGATG	GGTGTGTAACCAATGATCCTGTATGT	Designed and optimised previously
MMP9	GCTCACCTTCACTCGCGTG	CGCGACACCAAACTGGATG	(313)
Heparanase	TACCTTCATTGCACAAACACTG	ACTTGGTGACATTATGGAGGTT	(314)

Table 2. Primers used to investigate mRNA expression.

All primers were synthesised by Eurofins genomics.

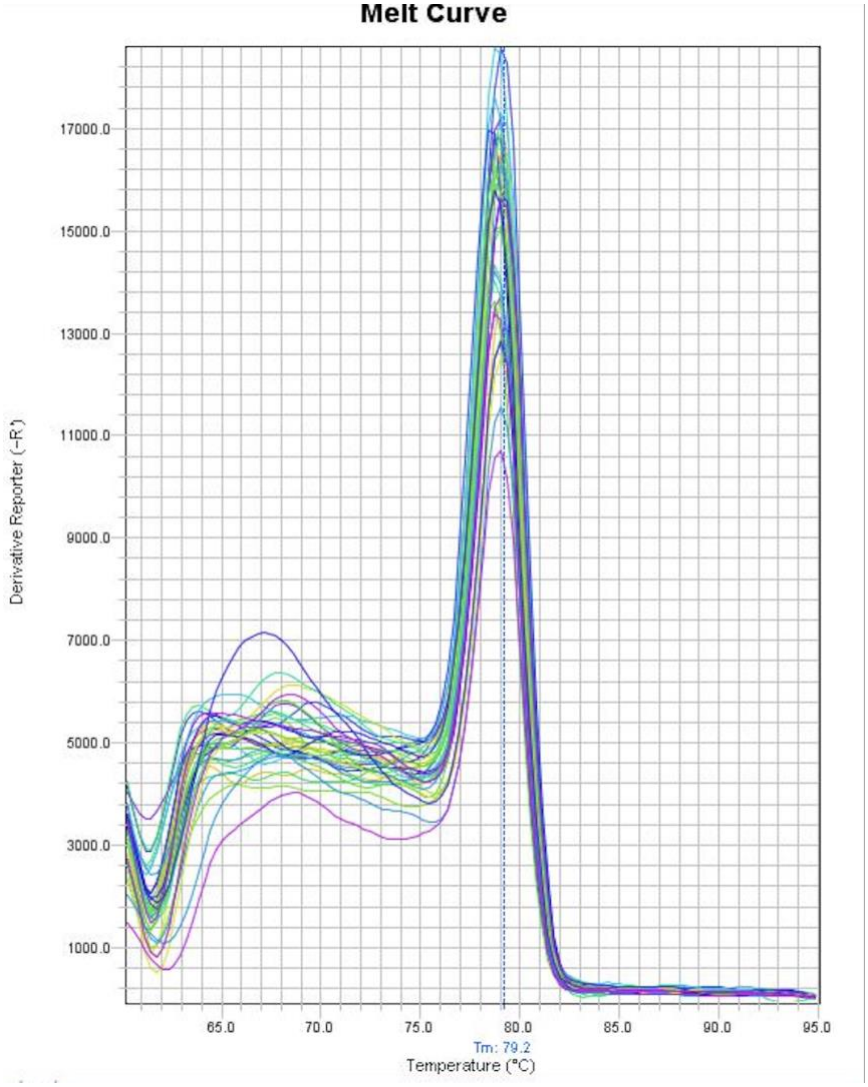

Figure 11. Melt curve from qPCR.

Melt curve analysis was performed to confirm the specificity of the primers as well as further show the purity of the samples. Primer sets would have 1 melting point if specific to the gene of intertest.

2.2.4.4 Analysis of qPCR

Prior to analysis, the data for each sample was assessed to determine if it could be included in the analysis. The criteria for the inclusion of data were:

- Consistency between the cycle threshold (CT) values for each sample as they were run in triplicates. Any clear outlier would be emitted.
- A single product on the melt curve analysis

The data was exported to an Excel spreadsheet and a manual analysis of the fold change was done. As samples were run in triplicates, the means of the cycle threshold values (CT values) were first calculated before being normalised to the matched housekeeping gene result, GAPDH (ΔCT). This was then further normalised to the control condition of the samples run in the qPCR (ΔΔCT). From this, the $2^{-\Delta\Delta CT}$ was calculated to provide the fold change of the gene of interest relative to the untreated control which was taken as 1.

2.2.5 Syndecan 4 Enzyme-linked immunosorbent assay (ELISA)

A human syndecan 4 (SDC4) ELISA (Human Syndecan-4 DuoSet ELISA , R&D Systems, DY2918) was conducted to quantify SDC4 concentration in the conditioned media of ciCMVEC. The media was collected from the cells and spun down at 800X g for 3 minutes to remove all cellular debris and the supernatant was removed and stored at -20 °C until use. A 96-well microplate was coated overnight with human SDC4 capture antibody before being washed three times with 300 μl of wash buffer (0.05% tween 20 in PBS, pH 7.2-7.4) using a multichannel pipette. The cells were then blocked by adding 300 μl with reagent diluent (1% BSA in PBS, pH 7.2-7.4) for 1 hour at room temperature to reduce the non-specific binding of the antibody before being washed another three times with wash buffer. To conduct the assay procedure, 100 μl of standard (in reagent diluent) and the samples were plated in triplicates. The plate was covered with an adhesive strip and incubated for 2 hours at

room temperature before being washed three times with wash buffer. During this time, SDC4 in the samples and standards binds to the capture antibody. 100 μl of the detection antibody (diluted in reagent diluent) was then added to each well. The plate was covered and incubated at room temperature for 2 hours before being washed again 3 times. The detection antibody binds to SDC4 attached to the capture antibody. 100 μl of the working dilution of streptavidin-HRP was then added to each well for 20 minutes in the dark at room temperature. The streptavidin binds to biotinylated antibodies (the detection antibody) and the HRP provides enzyme activity for detection using an appropriate substrate. The plate was then washed 3 times with wash buffer before the addition of 100 μl of substrate solution (1:1 mixture of colour reagent A and colour reagent B, R&D Systems, DY999) for 20 minutes at room temperature. To stop the reaction, 50 μl of stop solution (R&D Systems, DY994) was added, and the plate was gently tapped to ensure mixing. The plate was read immediately using a microplate reader set to 450 nm with a wavelength correction of 540 nm. The standard curve was then plotted (Figure 12) and the concentration of SDC4 in the samples was calculated by interpolation of the standard curve using Prism version 9 (GraphPad Software).

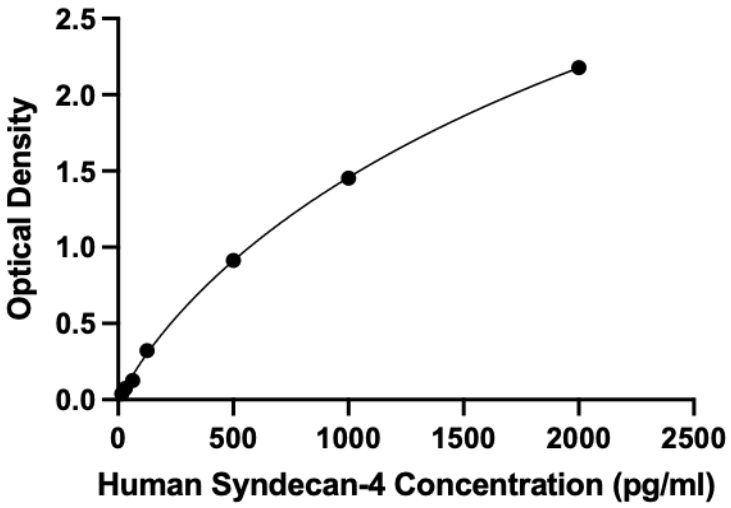

Figure 12. SDC4 standard curve from SDC4 ELISA.

SDC4 concentration in each sample was interpolated from the standard curve.

2.2.6 Shed sulphated GAG assay

An Alcian blue colorimetric assay was used to quantify the number of sulphated GAGs shed into the cultured media from the surface of ciCMVEC as previously done (118). The assay is based on the interaction between the sulphated polymers (GAGs) which are negatively charged and the tetravalent cationic Alcian blue (positively charged). The assay was carried out at a low Ph to neutralise all carboxylic and phosphoric acid groups and at an ionic strength that can prevent interactions other than that between Alcian blue and sulphated GAGs.

The media harvested was centrifuged at 800X g for 3 minutes to remove cellular debris. The supernatant was added to a freshly prepared solution of Alcian blue (0.4%) in sodium acetate (0.5 M), magnesium chloride hexahydrate (30 mM), and sulphuric acid (2.8%). Standards were prepared using chondroitin sulfate (CS) and absorbance at 490 nm was measured using a plate reader after 15 minutes incubation. The linear relation between GAG mass and decreased absorption of 490 nm by Alcian blue solution was used to quantify supernatant GAG content, referenced to known concentrations (0 to 125µg/ml) of CS.

2.2.7 Immunofluorescence

2.2.7.1 Immunofluorescence for SDC4

ciCMVEC were grown on autoclaved glass coverslips in 6 well plates treated with TNF-α and SB-3CT as described above and washed with PBS after the treatments. Fixation of the cells occurred for 10 minutes with 4% paraformaldehyde (PFA) in PBS at room temperature and again the cells were washed with PBS three times for 5 minutes each. Subsequently, the cells were incubated with 1% BSA in PBS (blocking buffer) for 1 hour at room temperature to prevent non-specific binding of the antibodies. The cells were then incubated with the SDC4 primary antibody (Bio-Techne, AF2918-SP) (10 μg/ml in blocking buffer) for 1 hour at room temperature. After three washes with PBS for 5 minutes each, the cells were incubated with the Anti Goat IgG/Alexa Fluor 488 Secondary antibody (Fisher Scientific Ltd, 15930877) (1:500 in blocking buffer) for 1 hour at room temperature and the washes were repeated. To label the nucleus, the cells were incubated with 4',6-diamidino-2-phenylindole (DAPI, 1:1000 in PBS) (Thermo Fisher Scientific, D1306) for 2 minutes at room temperature before being washed three times with PBS for 5 minutes each. After being washed the cells were mounted with vectashield antifade mounting medium (BioServ UK Limited) inverted onto a microscope slide. Images were captured using confocal microscopy at the Wolfson Bioimaging Facility at the University of Bristol. The laser intensity was set for the green channel (SDC4) and was kept the same for all samples imaged. All samples were imaged using the same lens and resolution. For each sample, 3 images were taken at random areas and total fluorescent intensity was determined using Fiji Image J (a Java-based image processing programme) (315) and normalised to the DAPI to correct for cell number.

2.2.8 Quantifying MMP2 and 9 activity

The activity of MMP2 (Anaspec, AS-72224) and MMP9 (Anaspec, AS-72017) in the conditioned media from ciCMVEC was investigated following the manufacturer's instructions. At the end of cell treatments, the media was collected and centrifuged for 10 minutes at 1000X g, 4 °C before being stored at -80 °C until use. Media was only thawed once as MMP activity is significantly reduced with each freeze-thaw cycle. MMP standard was made by diluting 10 μg/mL of human recombinant MMP2 or 9 in dilution buffer (from the kit) to a concentration of 200 ng/mL. From this six 2-fold serial dilutions were done in MMP dilution buffer. Following this, 100 μl of the samples and standards were plated in triplicates in 96 well plates, either precoated with monoclonal anti-human MMP2 or monoclonal anti-human MMP9 antibody (supplied by the manufacturer). As well as this, a blank control which contained the MMP dilution buffer without MMP2 or 9 was plated. The plate was covered with an adhesive strip (supplied by the manufacturer) to prevent evaporation and incubated on a plate shaker at 100 rpm for 1 hour at room temperature. After incubation, the well was washed by adding 200 μl of wash buffer to each well and removing it by inverting the plate. This process was repeated three more times for a total of 4 washes. After the final wash, the plate was blotted against some tissue to ensure all the wash buffer was removed from the well. The standards were zymogens and thus required activation. Therefore, 100 μl of 1mM APMA (diluted in assay buffer supplied by the manufacturer) was used to activate all MMPs in the standards only. The plate was covered with an adhesive strip and incubated at 37 °C for 2 hours.

After incubation, the plate was washed four times as described above with wash buffer. To measure MMP activity, 100 μl of the substrate for either MMP2 or 9 was added to all wells including the standards. The substrate contained a fluorophore which when digested by the MMPs resulted in a fluorescent signal that could be detected by a plate reader. Therefore, the more MMPs bound to the monoclonal antibodies of each well, the greater the amount of digested substrate resulting in greater fluorescence intensity. The plate was covered with an adhesive strip and incubated at room

temperature in the dark for 1 hour. Fluorescence intensity was then measured at excitation/emission = 490 nm/520 nm.

To analyse the data, the mean fluorescence intensity was taken for the triplicates. Any clear outlier was removed. The standard curve was then plotted as relative fluorescence units versus the concentration of MMP (Figure 13) and the standard curve was interpolated in prism to determine the MMP activity in the samples.

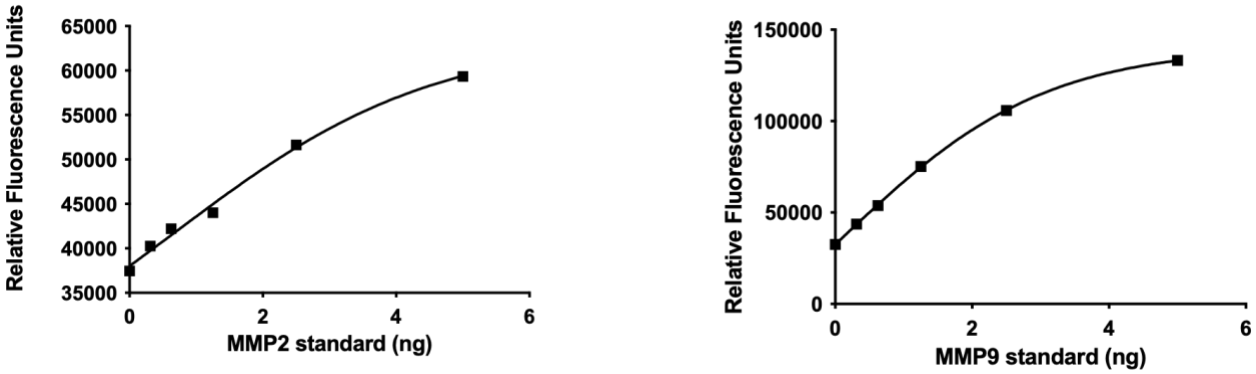

Figure 13. MMP2 and 9 standard curve.

MMP2 and 9 activities were calculated by interpolating the standard curve.

2.2.9 Measurement of transendothelial protein passage

To investigate if the EGlx is important for ciCMVEC barrier function the EGlx was stripped using a combination of enzymes and a transwells assay was conducted. The cells were seeded at a density of 37,500 cell/cm^2 in 500 μl of media onto the inserts (Corning, 10565482) and 500 μl of media was placed into the well. The transwell inserts contain a polyester membrane with a pore size of 0.4 μm making them permeable to substances such as albumin. By ensuring a monolayer of endothelial cells was formed on the cell surface prior to treatments ensured that whatever was measured was a result of an alteration in the endothelial cells and not due to albumin moving freely across the pores.

To conduct treatments, the cells were first serum starved for 2 hours. To do this, the media in the well was first aspirated followed by the aspiration of the media in the inserts. 500 μl of serum-free media was then added to the insert first and then to the well. The media was added on the side of the inserts to not disturb the cell monolayer. After 2 hours, 70 μl of media was removed from the inserts and 50 μl of media was removed from the wells. The insert media was then replaced with 20 μl of the enzyme treatment containing heparanase III (1U/ml, 0.02%BSA/serum-free media) + hyaluronidase (4.5 U/ml, 0.02%BSA/serum-free media) + chondroitinase (100 mU/ml, 0.02%BSA/serum-free media) to strip the EGlx or vehicle and 50 μl of 1mg/ml of Alexa Fluor 488 conjugated BSA (ThermoFisher, A13100) in SFM. Each condition was done in triplicates. The media in the wells were replaced with 50 μl of 1 mg/ml of unlabelled BSA. After 1, 2 and 3 hours of incubation at 37^{o}C, 100 μl was removed from the wells for measurement and replaced with 100 μl of media containing unlabelled BSA (100 μg/ml). To determine the amount of BSA that crossed the cell monolayer, 100 μl of the media collected after each hour was plated in a 96-well plate. The standards were made up by making up a solution of 100 μg/ml of Alexa Fluor 488 conjugated BSA in 100 μg/ml of non-conjugated BSA in SFM. 10 two-fold serial dilutions were done as well as a blank control containing 100 μg/ml of non-conjugated BSA in SFM. The plate was read using a plate reader at an emission of 488 and sample concentration was calculated by interpolating the standard curve (Figure 14) in Prism.

At the end of the experiments, the media was removed from the wells and the inserts, and the cells were stained with Alexa Flour 488-WGA to identify any changes in the EGlx as a result of enzyme treatment. In brief, the cells were rinsed once with room-temperature PBS before being fixed with 4% PFA for 15 minutes at room temperature. The cells were then washed with PBS three times for 5 minutes each. To stain the EGlx, the cells were then incubated with Alexa Flour 488-WGA in PBS (5 μg/ml) in the dark for 1 hour at room temperature after which they were washed once with PBS for

5 minutes. To counterstain the nuclei the cells were incubated with DAPI in PBS (1:1000) at room temperature for 2 minutes before being washed 3 times with PBS for 5 minutes each time. The membrane of the insert was then gently cut out of the insert and placed onto a coverslip. The coverslip was then inverted onto a microscope slide with vectashield (BioServ UK Limited) applied to prevent rapid photobleaching of the fluorescent probe.

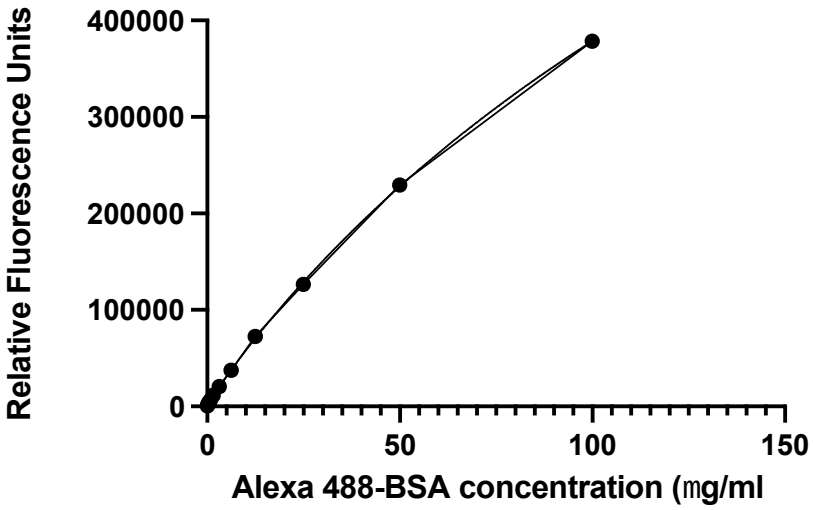

Figure 14. Standard curve for the transwells assay.

The standard curve was interpolated in prism to calculate the concentration of BSA within the samples.

To investigate if MMP inhibition protects endothelial barrier function in response to TNF-α, the cells were seeded and grown to a confluent monolayer on the inserts as described above. Treatment with SB-3CT and TNF-α occurred as detailed in 2.2.2.

2.3 In vivo methods:

2.3.1 Animals

I obtained a personal license for all work involving live animals (PIL No.: I76844178). All animal work carried out in this project was conducted in accordance with the Home Office Guidance at the University of Bristol and the Animal (Scientific Procedure) Act 1986 on Dr. Rebecca Foster's project license (PPL No.: P855B71B4). All animals used in this project were FVB mice (Chapter 3: TG 287 SATOJ, The Jackson Laboratory, US; Chapter 5: FVB/NCrl, Charles River, UK).

2.3.1.1 Type 1 diabetes model

Type 1 diabetes was induced in male FVB mice by injection of streptozotocin (Sigma Aldrich, WXBD4533V) (STZ; 50 mg/kg body weight per day, i.p. for 5 consecutive days) as done previously (118). STZ was dissolved in 0.1M of sodium citrate buffer, pH 4.5. Control animals received injections of the vehicle (citric acid buffer). The buffer was made from the following recipe:

- 1.47 g sodium citrate dissolved in 30ml dH2O (distilled water)
- pH to 4.5 using a citric acid solution
- top up to 50ml using dH2O
- filter sterilise for use.

All animals were fasted for 4–6 hours before the administration of STZ. Hyperglycaemia was confirmed by blood glucose levels of more than 16mmol/L on two consecutive days two weeks post STZ.

2.3.1.2 Assessment of blood glucose

To assess blood glucose the tail vein of the mice was pricked with a sharp needle and a drop of blood was placed on the glucose strip. Blood glucose was assessed with a glucometer (ACCU-CHEK Aviva, Roche, UK) at 2, 6, and 9 weeks post STZ.

2.3.1.3 Measurement of mouse body weights

Electric scales were used to measure mouse body weight weekly. The scales were first zeroed with the weight bucket before the mouse was placed into the bucket and the weight recorded.

2.3.2 MMP inhibitor treatment

To determine the impact of MMP inhibition on the protection of the coronary microvascular eGlx and heart function, mice were injected intraperitoneally with an MMP2 and 9 specific inhibitor for either 14 or 21 days from 7 weeks post STZ. Details on the specific inhibitor used, the length of time the inhibitors were given as well as the age of the mice, can be found within specific chapters (Chapters 3 and 5).

2.3.3 Assessment of heart function

An assessment of heart function was made using a high-frequency, high-resolution echocardiography system (Vevo 3100, Visual Sonics, Toronto, Canada). Each mouse was first anesthetised in the induction box at 4% isoflurane before being transferred to the preheated platform (37.9°C). Each paw was taped onto an electrode of the platform to allow heart rate monitoring. Mice were maintained on isoflurane at 1-3% whilst heart function was being assessed. All assessments were done within 30 minutes of the mouse being under anaesthesia. Prior to

imaging, mouse fur around the area being imaged was removed using hair removal cream. Once the fur was removed, a clean cotton pad was damped in water and used to wipe away any cream remaining. This was important to prevent the irritation of the skin. Pre-warmed electrode gel was then applied to the desired area and images were collected.

To assess diastolic function, pulsed wave Doppler and tissue Doppler was utilised. The apical four-chamber view was used to visualise the left ventricle and left atria (with the mitral valve in between appearing as a bright line). This was then combined with colour Doppler to visually indicate the velocity of blood across the mitral valve allowing the identification of the area with the highest blood flow. The sample volume gate was then placed at the point of highest velocity (as indicated by aliasing) and the angle was adjusted to the angle of flow from the left atria to the left ventricle. Pulsed wave Doppler was used to generate the E/A ratio. Tissue Doppler was used to determine the velocity of the mitral valve. The tissue Doppler sample volume gate was placed at the mitral annulus and opened wide. The angle was then placed to point at the apex. Using Tissue Doppler allowed the calculation of E/e'. All diastolic parameters were captured at a heart rate of 380±20 beats per minute.

To determine systolic function, the heart was first imaged in the parasternal long-axis view (Figure 15). Characteristics of the parasternal long axis included:

- A clear presence of the aorta and apex on the same horizontal plane.
- An aorta and apex form a horizontal line together on the screen.
- Visible right ventricle outflow tract.

Once satisfied with the image on the screen, an M-mode image could then be taken.

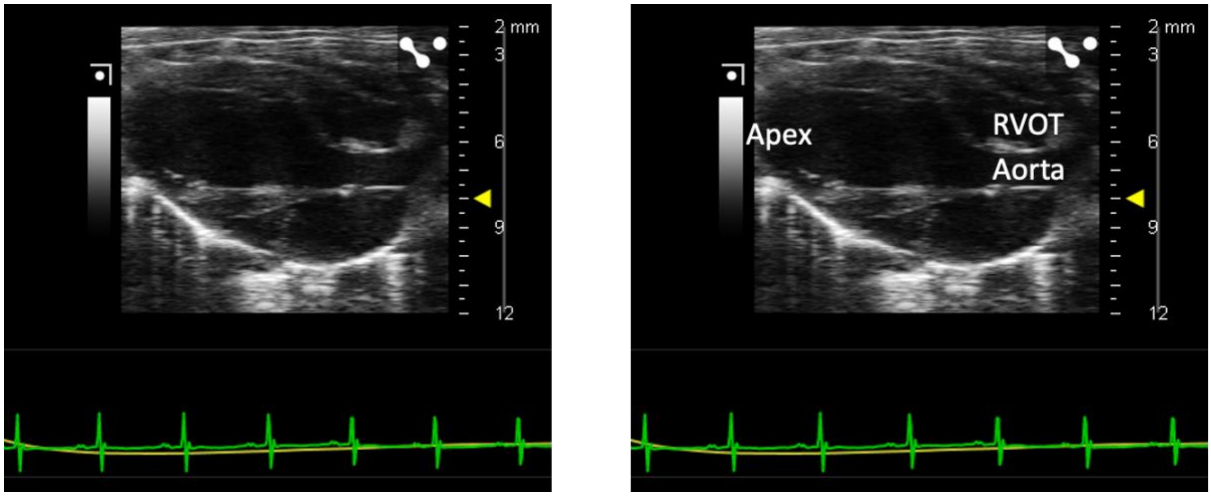

Figure 15. Representation of images captured in parasternal long axis.

The image on the right is a duplicate of the image on the left with specific areas labelled. RVOT = right ventricle outflow tract.

2.3.4 Analysis of echocardiography images

Analysis of samples was done using the Vevo lab software.

2.3.4.1 M-mode analysis

Using the tool 'LV trace', points were placed starting at the anterior endocardial border at full systole and full diastole along the wall border. This was repeated for the posterior endocardial border as shown in Figure 16. This calculated key systolic parameters including, ejection fraction, cardiac output, stroke volume abd fractional shortening. If LV mass was being assessed, points were then placed along the epicardial border that match up with the points of the endocardial border.

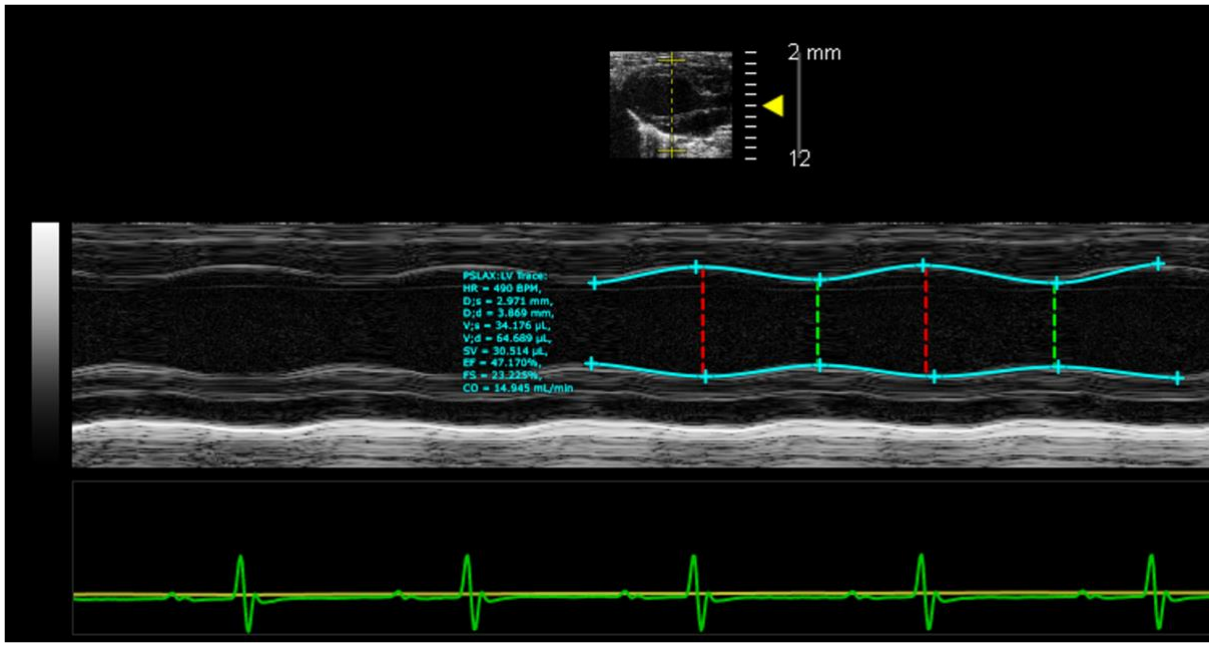

Figure 16. Representation of images captured in M-mode.

The anterior and posterior endocardium is traced using the tool LV-trace. Cardiac output, stroke volume, ejection fraction and fractional shortening were calculated to provide an indication of systolic function.

2.3.4.1 Pulsed wave Doppler analysis

To investigate the E/A ratio, mitral valve flow was selected in Vevo lab. Using the 'MV E' option a point was placed at the apex of the E peak. A point was then placed on the apex of the A peak using the 'MV A' option. This generated a max velocity measurement for both the E and A peaks in mm/s. Four E peaks and A peaks were determined per sample. Each A peak was selected from its corresponding E peak (Figure 17).

To calculate Isovolumetric relaxation time (IVRT) a point was placed at the end of the aortic ejection and at the start of the E wave. This was measured in ms.

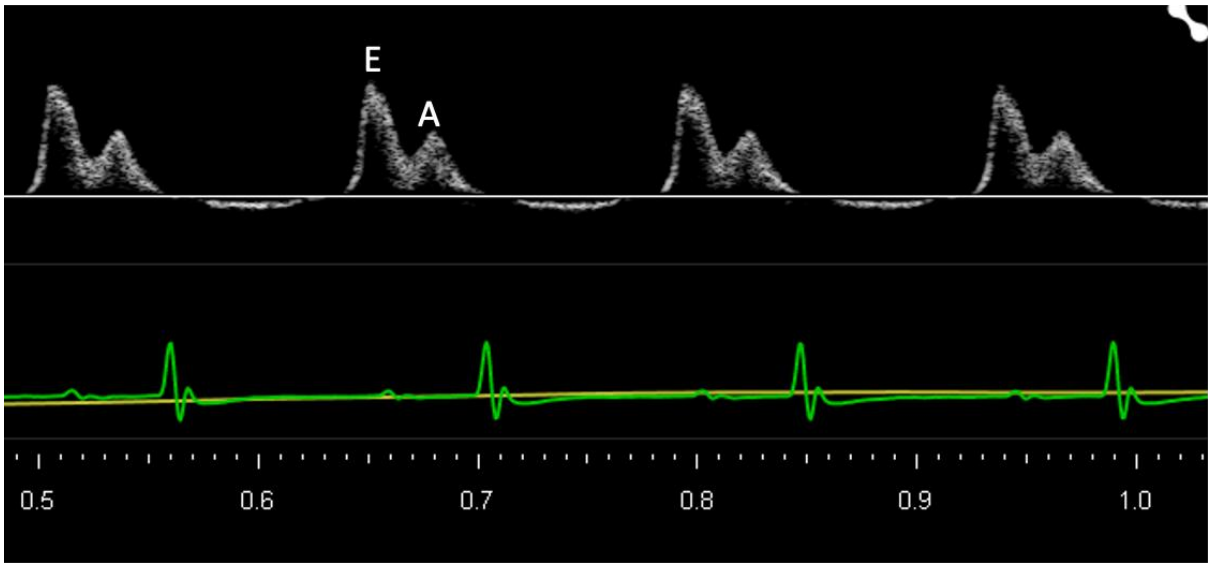

Figure 17. Representative image of E and A peaks.

Mitral valve flow was assessed using pulsed wave Doppler.

2.3.4.3 Tissue Doppler analysis

Using the tool ‘E’’ under ‘MV flow’ a point was placed at the peak of the E’ wave. This was then repeated for the A’ wave using tool ‘A’’. Four corresponding E’ and A’ were calculated per sample (Figure 18).

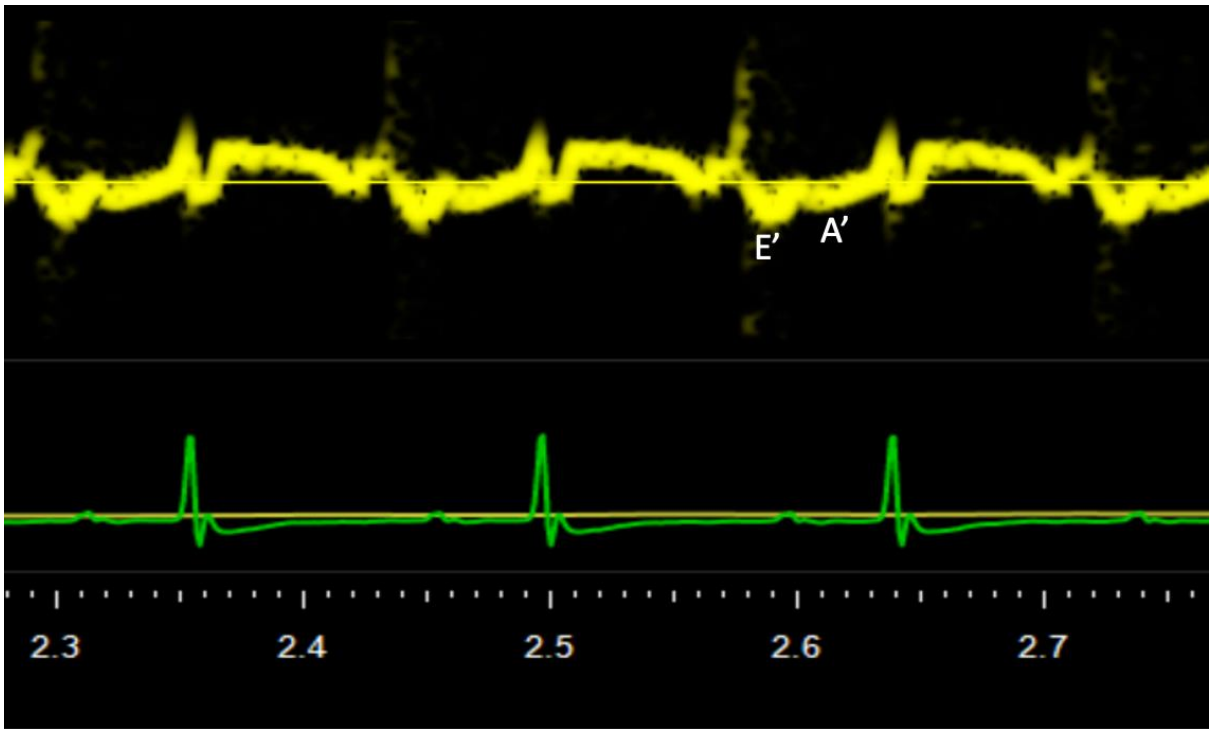

Figure 18. Representative images of E' and A' peaks.

The image was collected using tissue Doppler.

2.3.4 Collection of samples

2.3.4.1 Heart tissue collection

At the end of the study, mice were first perfused through the heart with 2.5 ml of 0.1 M cadmium chloride ($CdCl_2$) in 0.05M trizma base to stop the heart at diastole followed by PBS as done previously (27). In brief, whilst under anaesthesia, the abdominal cavity of the mice was opened followed by the thoracic cavity of the mice to expose the heart. Using a clipper, the sternum was pulled back and the apex of the left ventricle was quickly cannulated with the needle through which perfusion would occur. The tap to allow the flow of the perfusate through the needle was turned on and the pressure of the perfusion pump was kept at 100-110 mmHg. When the heart expanded as a result of cadmium chloride, the right atrium was snipped, and blood was collected (see below). Immediately after cadmium chloride perfusion, the hearts were perfused with 5-10 ml of heparinised PBS (1 IU/μl of heparin in PBS, pH 7.4).

Once clear discolouration of the heart was observed due to the lack of red blood cells, the perfusion was stopped and the heart was taken. The heart was then cut into 2 parts transversely and the bottom half was fixed overnight in 4% PFA in PBS before being transferred to 70% ethanol until they were sectioned. The top half was quickly frozen in liquid nitrogen and then stored at -80 °C.

2.3.4.2 Blood collection and plasma extraction

1.5 ml Eppendorf tubes were coated with 25 μl of heparin (764 USP units/ml). After perfusing with $CdCl_2$, the right atrium was cut when the heart expanded. Blood was collected using a 1ml pipette immediately as it flowed out of the heart and gently released into the precoated Eppendorf tubes. Following collection, the blood was centrifuged at 800X g at 4 °C for 5 minutes to extract plasma. The supernatant was gently extracted and placed into new Eppendorf tubes.

2.3.4.3 Urine collection

Urine was collected directly from the bladder whilst the mice were under anaesthesia by placing a needle into the bladder and withdrawing the urine. The samples were swiftly frozen in liquid nitrogen.

2.4 Ex vivo methods:

2.4.1 Quantification of the endothelial glycocalyx through lectin-based immunofluorescence

PFA-fixed mouse heart tissue was paraffin-embedded and sectioned at a thickness of 5 μm, by the University of Bristol Histology unit. To determine the EGlx depth, the tissue was first dewaxed in xylene for 20 minutes followed by rehydration of the tissue in graded ethanol (100%, 90%, and 50%). The sections were then washed 3 times for 5 minutes with PBS and a hydrophobic pen was used to create a water-repellent barrier around the section. Each section was blocked with 50 μl of blocking solution (1% BSA in PBS containing 0.5% tween-20) for 1 hour at room temperature before being washed with 0.5% tween in PBS (PBX) 3 times for 5 minutes each. For endogenous biotin blocking, the sections were then incubated with streptavidin (BioServ UK Limited , ZJ0912) by placing one drop on each section and incubating for 15 mins at room temperature. Following this, the sections were washed once with PBX and then incubated with biotin (BioServ UK Limited, ZJ0912) by placing one drop on each section for 15 minutes at room temperature. After another set of washes with PBX (2x), the sections were incubated with either Sambucus Nigra Lectin (SNA, Vector Laboratories , ZF0207) (1:50), Biotinylated Maackia Amurensis Lectin I (MAL I, Vector Laboratories, ZF0118) (1:100), or Biotinylated Lycopersicon Esculentum (tomato) Lectin (LEL, Vector Laboratories, ZE0321) (1:100) in 1% BSA in PBX at pH 6.8 for 1 hour at room temperature. This was followed by 4 washes in PBX before being incubated with the secondary antibody streptavidin-488 (Thermo Fisher Scientific, 2273715) (1:500 in 1%BSA/0.5%PBX Ph 6.8) for 1 hour at room temperature. For nuclear and

membrane staining, sections were washed twice in PBX followed by 2 more washes with PBS. The sections were then incubated with DAPI (1:1000 in PBS) for 2 minutes at room temperature to counterstain the nucleus before being washed twice in PBS. To stain the membrane, sections were incubated with Octadecyl Rhodamine B Chloride (R18, Invitrogen, 2061441) (1:1000 in PBS) for 10 minutes at room temperature. No washes occurred after this incubation, but the sections were briefly rinsed by dipping them into a Coplin jar filled with PBS.

2.4.1.1 Confocal imaging

The University of Bristol Wolfson Bioimaging Facility was used for confocal imaging. Slides were imaged using a 63X oil immersion lens for EGlx analysis and at a pixel resolution of 2048 x 2048.

2.4.1.2 Analysis of the lectin-stained images

All images were analysed with Fiji image analysis software (315). As lectins are able to bind to GAGs in the basement membrane, extracellular matrix and as well as the glycocalyx on cells other than endothelial cells, it was important to ensure that the glycocalyx being measured was endothelial. To do this, a line was drawn from the centre of the selected vessel to the outside of the membrane. Fluorescent plot profiles were then generated for the green channel (glycocalyx, AF488) and the red channel (membrane) and the distance between the two peaks was regarded as the EGlx depth. To be classified as a round vessel for analysis, the ratio of shortest and longest diameter length had to be between 0.8 and 1 μm. If the vessel was classified as circular and the membrane staining was specific to the vessel and not surrounding areas, then that vessel was classified as suitable for analysis.

The process of analysis was automated using a MACRO. For the MACRO to generate a line across the vessel, a dot was placed in the centre of the vessel and the shortest and longest diameter of the

vessel was determined using the line tool in Fiji. 360 plot profiles were taken around the vessel on both the red and green channels and a Gaussian distribution was applied to the plot profiles. The distance between the Gaussian peak on the green channel and the Gaussian peak on the red channel at each matched point was taken as the EGlx depth. The mean was subsequently determined from 360 lines per capillary loop and 15 loops per heart. Data were excluded with a standard deviation of more than 7.5 and/or a signal-to-noise ratio of less than 15. Further details on the MACRO can be found at (117).

2.4.2 Assessing MMP activity in the heart, plasma and urine

The activity of MMP2 and 9 from the heart, plasma and urine of mice was investigated using MMP activity assays following the manufacturer's instructions and detailed in 2.2.8. Urine MMP activity was normalised to creatinine which was measured by Langford Vets Diagnostic Laboratories at the University of Bristol.

Frozen hearts were homogenized on the day of testing in assay buffer (from the kit) containing 0.1% Triton-X 100 before being centrifuged for 15 minutes. The lysate was collected and used immediately to determine MMP activity as a further freeze-thaw cycle would interfere with MMP activity. The heart tissue MMP activity was normalised to the total protein. The determination of total protein was calculated using a BCA protein assay kit (Thermo Scientific, WF327082) following the manufacturer's instructions.

The BCA assay combines the reduction of (copper) Cu^{+2} to Cu^{+1} by protein in an alkaline medium with a sensitive and selective colorimetric detection of Cu^{+1} using a reagent containing bicinchoninic acid (BCA). The purple-coloured reaction product of this assay is formed by the chelation of two molecules of BCA with one cuprous ion exhibiting a strong absorbance at 562 nm.

In brief 25 μl of standards and samples were plated into a 96-well microplate. 200 μl of the working reagent was then added to each well and the plate was mixed thoroughly on a plate shaker for 30 seconds. The plate was then incubated at 37°C for 30 minutes before being cooled to room temperature and the absorbance was read at 562 nm using a plate reader. For analysis, the blank standard absorbance measurement was subtracted from all samples and standard absorbance measurement and a standard curve was plotted (Figure 19). The concentration of protein within the samples was determined by interpolating the standard curve.

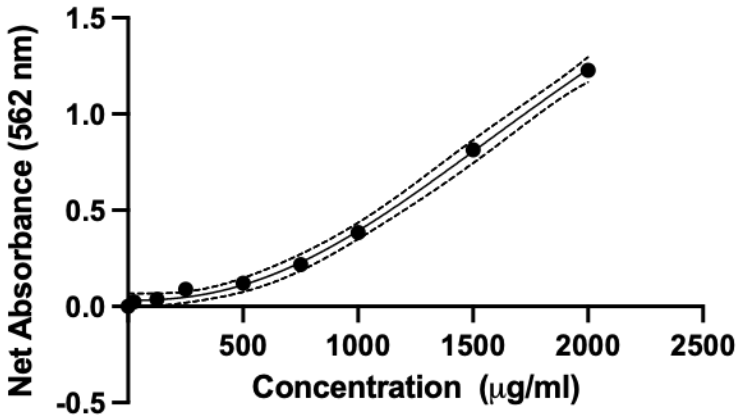

Figure 19. Standard curve from the BCA assay.

The standard curve was used to interpolate the protein concentration in the heart lysates.

2.4.3 Albumin immunofluorescence

To investigate albumin leak in the heart tissue, tissue sections were deparaffinised and rehydrated in graded ethanol as described in 2.4.1. The tissue was blocked with 0.3% Triton-X, and 3% BSA in PBS solution for 30 minutes. After blocking, the sections were incubated with goat anti-mouse albumin antibody (Bethyl Laboratories, A90-134A-17) (1:200) in the blocking buffer for 1 hour at room temperature. The sections were washed 3 times for 5 minutes each in 0.3% Triton-X in PBS before being incubated with donkey anti-goat Alexa Fluor 488 (Fisher Scientific Ltd, 15930877) (1:200) in the blocking buffer for 1 hour at room temperature. Images were taken using confocal microscopy as described in 2.4.1.1. The laser intensity for albumin (green) was set and kept the same for all samples being imaged.

2.4.3.1 Albumin immunofluorescence analysis

All images were analysed on Fiji Image J analysis software. The 'analyse' tool was used to obtain the area of the image and the integrated density. Three background fluorescent values were obtained by drawing a small circle using the freehand tool in the area of the background. Using the 'analyse' tool, generated the fluorescent intensity for the circled background. Corrected total fluorescence was calculated using the following equation:

CTCF = Integrated density – (area of the region of interest x mean fluorescence of background means)

2.5 Statistics

All statistical analyses were performed with Prism version 9 (GraphPad Software). If p values were $\geq$ 0.05 for a given data set, then it was considered not statistically significant. The data was first assessed for normal distribution using the Shapiro-Wilk test. For normally distributed data with two groups, statistical significance was determined using an unpaired t-test. Non-normally distributed data were assessed using a Mann-Whitney test. For data with more than two groups, normally distributed data were assessed using ANOVA followed by Tukey's to compare the means of each group with that of every other group. Non-normally distributed data was assessed using the Kruskal-Wallis test followed by Dunn's multiple comparison test. To determine if there was any significant correlation between data sets, the Pearson r test was conducted. All data are presented graphically as the mean $\pm$ standard error of the mean.

Chapter 3: MMP activity is increased in diabetic cardiomyopathy

---

Prior to my arrival within the group, Dr Yan Qiu conducted experiments showing that the endothelial glycocalyx (EGlx) was damaged in diabetic cardiomyopathy (DCM) in both a type 1 and type 2 mouse model. In that experiment, she showed that angiopoietin 1 restored the EGlx, reduced cardiac interstitial oedema, and improved diastolic function (27). This showed that the EGlx is a target of protection in DCM. A previous publication from our group showed that inhibition of MMP2 and 9 with MMP2/9 inhibitor I protected the glomerular EGlx in diabetic kidney disease (118). Therefore, I aimed to apply this to DCM to protect the coronary microvascular EGlx.

Part of the work presented in the chapter has contributed to the following publication:

*Qiu Y, **Buffonge S**, Ramnath R, Jenner S, Fawaz S, Arkill KP, et al. Endothelial glycocalyx is damaged in diabetic cardiomyopathy: angiopoietin 1 restores glycocalyx and improves diastolic function in mice. Diabetologia*

3.1 Introduction

DCM is clinically characterized by diastolic dysfunction and left ventricular hypertrophy (77) and has an estimated prevalence of 14.5% and 35% in those with type 1 and 2 diabetes respectively (316,317). With diabetes on the rise in the general population, DCM presents as a public health concern. Despite this, there is currently no specific treatment for DCM; thus, understanding its mechanisms is extremely important. Contributing to the pathophysiology of DCM is microvascular dysfunction with increased permeability of the microvessels of the heart resulting in interstitial oedema (27). The increase in interstitial pressure as a result of oedema results in the stiffening of the left ventricle, leading to diastolic dysfunction (17).

An important regulator of vascular permeability and endothelial barrier function is the EGlx which lines the luminal side of vascular endothelial cells (26,166,189,196,198). Despite the importance of the EGlx in regulating permeability, there is a lack of research investigating its role in the heart.

MMP2 and 9 are known to be upregulated as a result of diabetes and it has been shown that these enzymes can cause shedding of the EGlx (27,117,118,213). Previous studies have shown that inhibition of MMP2 and 9 with MMP2/9 inhibitor I, has proven beneficial to protect the glomerular EGlx in diabetic kidney disease (118).

Therefore, there are serval objectives that will be tackled within this chapter:

1. Reinforce that the coronary microvascular EGlx is damaged in a mouse model of DCM.
2. Identify if MMP activity is increased in a mouse model of DCM.
3. Examine if MMP2 and 9 inhibition with MMP2/9 inhibitor I can protect the coronary microvascular EGlx in DCM and improve diastolic function.

3.2 Methods

Any methods described within this section are specific to this chapter. Methods not described here but used to generate results shown in this chapter are described in ***Chapter 2: Materials and Methods***.

**Note: All in vivo work conducted within this chapter was conducted by Dr Yan Qiu prior to my arrival in the group. Analysis of heart function was also carried out by Dr Yan Qiu. All other ex vivo work and analysis within this chapter were carried out by me unless stated otherwise.*

3.2.1 Type 1 DCM mouse model

7-week-old FVB mice (TG 287 SATOJ, The Jackson Laboratory, US) were injected with STZ to induce diabetes as described in 2.3.1. All mice that did not receive STZ were injected with citric acid buffer as vehicle control. Blood glucose was monitored weekly to confirm hyperglycaemia and only mice that remained hyperglycaemic throughout the duration of the study were used.

3.2.2 Treatment with MMP2/9 inhibitor I

At 7 weeks post STZ administration, some mice were given daily i.p. injections, for 3 weeks, of the MMP2 and 9 inhibitor, biphenylylsulfonylamino-3-phenylpropionic acid (MMP2/9 inhibitor I) (Merck, 444241, Middlesex, UK) at 5mg/kg). All other mice received daily injections of the vehicle (0.05% DMSO in PBS) as illustrated in Figure 20. The inhibitor has been utilised previously in a diabetic mouse model of kidney disease and has proven to be successful at the concentration used (118,318).

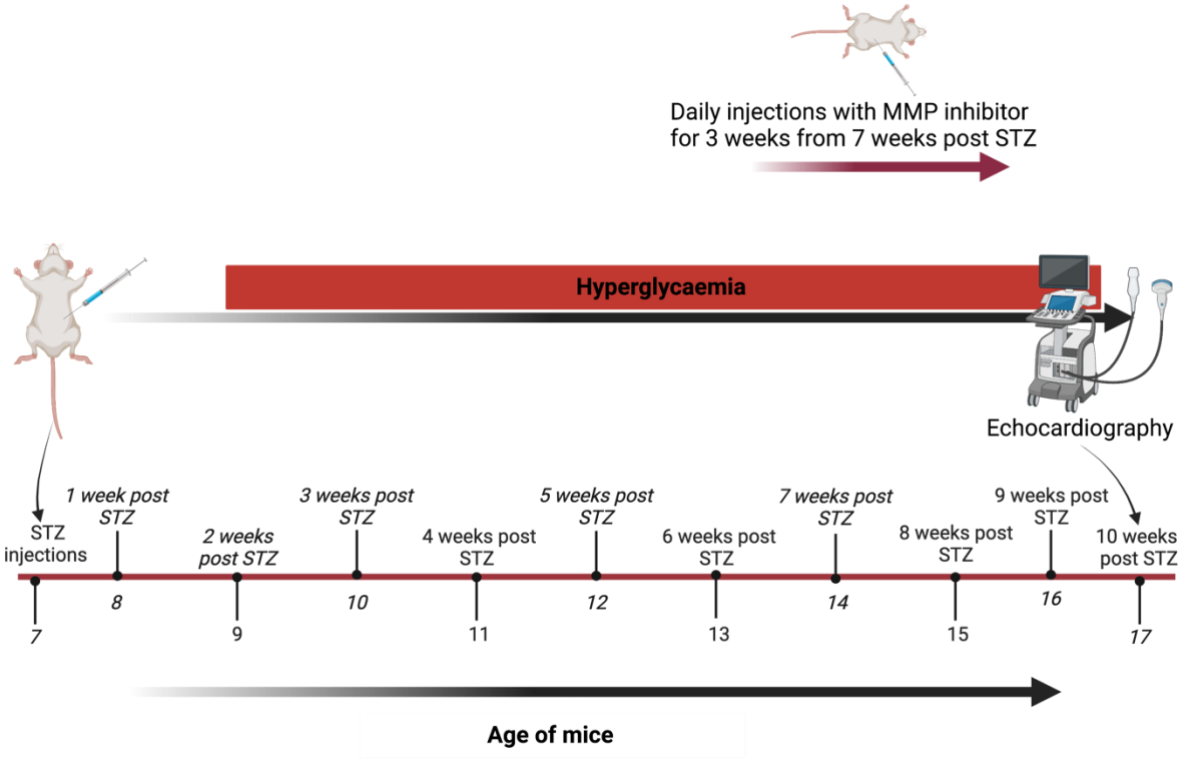

Figure 20. Illustration of the timeline of animal experiments in this chapter.

Initially, mice were randomized to receive either STZ or the vehicle. From 7 weeks post STZ mice were randomised again to receive either MMP2/9 inhibitor I or vehicle for 3 weeks. Echocardiography was conducted to assess heart function from 10 weeks post STZ after which the mice were culled. The image was made on Biorender.com

3.3 Results

3.3.1 Diabetic mice have diastolic dysfunction 10 weeks post STZ

To confirm diastolic dysfunction in diabetic mice, echocardiography was utilised. The E/A ratio as well as the E/E' ratio was used to assess the diastolic function of the left ventricle as both parameters are used clinically to assess diastolic function in humans. The methods for how the E/A and E/E' ratio was determined is detailed in 2.3.3. The E/A ratio reflects left ventricular filling properties in both early diastole (E) and late diastole (A). Increased left ventricular filling pressure will result in a reduced E peak velocity and an increased A peak velocity leading to a reduced E/A ratio (59,319,320). This parameter to assess diastolic function is used commonly in mouse models (27,125). However, it is important to combine this parameter with other measurements. The E/E' is a measure of the early diastolic velocity of mitral inflow to early diastolic velocity of mitral annular motion (E') providing an indication of left ventricular filling pressures. In patients, the E/E' ratio has been shown to be a good predictor of left ventricular function but should not be used in isolation from other assessments (321). With this parameter, diastolic dysfunction is indicated by an increase in E/E' ratio.

In this study, a reduced E/A ratio was found in diabetic mice compared to controls (Figure 21. A). This was accompanied by an increased E/E' in diabetic mice when compared to the controls (Figure 21. B). No significant difference was observed in the E/A and E/E' ratio between the diabetic mice and diabetic mice treated with MMP2/9 inhibitor I (MMPI).

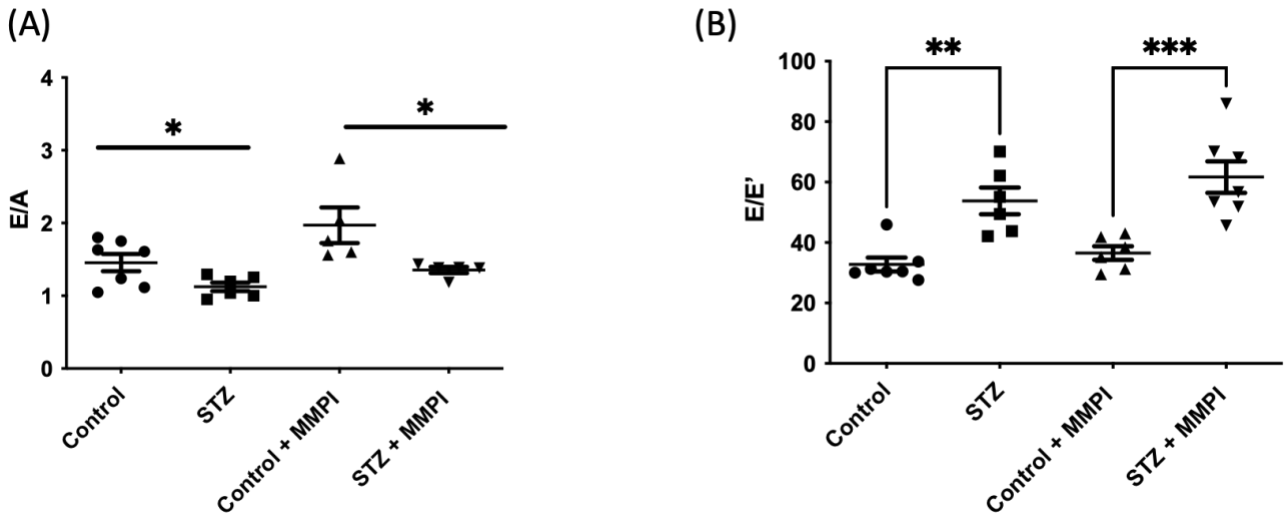

Figure 21. Diabetic mice have diastolic dysfunction 10 weeks post STZ.

All mice underwent echocardiography at 10 weeks post STZ. ***(A)*** *Reduced E/A ratio in STZ mice when compared to controls (n=7 for Controls, 6 for STZ, 5 for Control + MMPI, and 5 for STZ + MMPI; *p<0.05; One-way ANOVA).* ***(B)*** *Increased E/E' ratio in STZ mice compared to controls (n=7 for Controls, 6 for STZ, 6 for Control + MMPI, and 7 for STZ + MMPI; Control vs STZ: **p<0.01; Control + MMPI vs STZ + MMPI: ***p<0.001; One-way ANOVA). No significant difference was found in the E/A and E/E' ratio of mice treated with STZ + MMPI when compared to the STZ alone group. Echocardiography was conducted and analysed by Dr Yan Qiu.*

3.3.2 The Coronary microvascular EGlx is reduced in DCM and MMP2/9 inhibitor I do not protect the EGlx

3.3.2.1 Identifying suitable lectins to investigate the EGlx

To investigate the coronary microvascular EGlx, mouse heart sections were stained with lectins and the peak-to-peak method was utilised to provide an indication of EGlx depth. As mentioned, lectins bind carbohydrate structures and these are distributed within the EGlx (322). By utilising a membrane marker, the EGlx can be identified on the luminal side of the vessels (117,118). When a line is drawn from within the vessel across the vessel membrane, fluorescent intensity plot profiles

could be generated. The plot profile reflects the fluorescent intensity of the specific channel of interest along the distance of the line drawn. To assess EGlx depth, the distance between the peak fluorescent intensity for the lectin staining (the EGlx, AF488) and the peak fluorescent intensity for the R18 staining (the membrane), provides an indication of EGlx depth. Three lectins were tested to identify a suitable lectin for this mouse strain (LEL, SNA, and MAL-I) as they have been used previously to examine the EGlx of both mouse and human endothelial cells (27,117,118,322). To confirm the specificity of the lectin to the EGlx, along with the quality of staining, 4 lines were drawn across 5 randomly selected vessels. To determine the quality of staining, clear fluorescent peaks should have easily been identified from the red and green channels when a line was drawn across the vessel. A clear peak was determined as one which did not plateau, but after a peak, the fluorescent intensity reduced back or close to the intensity of the start of that plot profile. If a green peak appeared to the left of the red peak, then this was classified as the EGlx and deemed acceptable to assess using the macro. Further details of the use of the macro and analysis of lectin staining are found in 2.4.

Successful staining was found with all three lectins used (Figure 22. A-C) and the fluorescent plot profiles show a green peak to the left of the red peak indicating that there is staining of the coronary microvascular EGlx without interference from basement membrane lectin binding. All lectins were used going forward to continue their assessment within the heart and determine the depth of the EGlx with the macro.

(A.I)

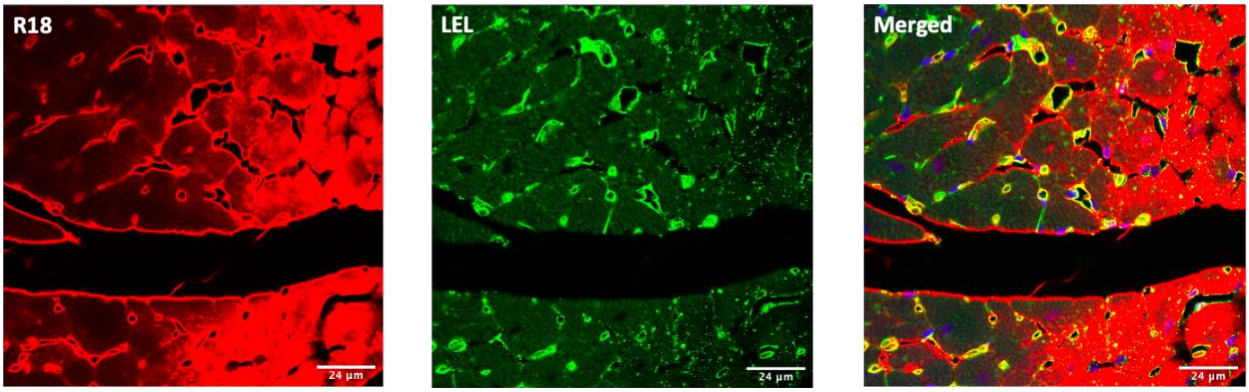
R18
LEL
Merged
24 µm
24 µm
24 µm

(A.II)

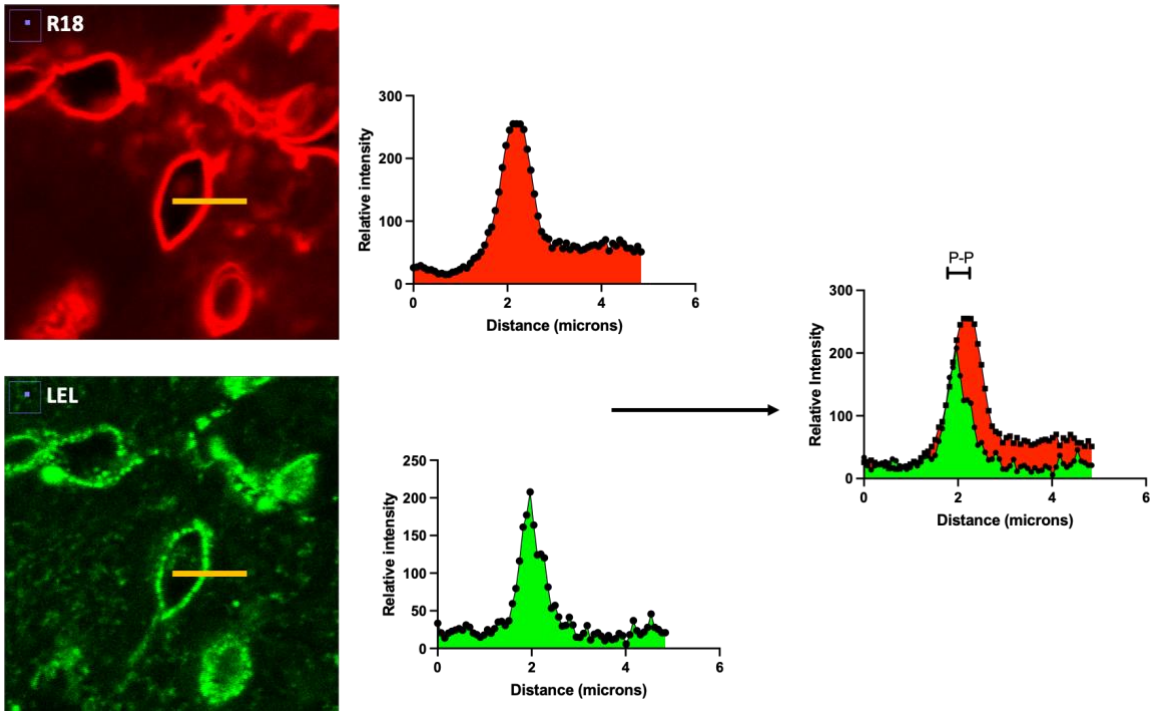
R18
LEL
Relative intensity
Distance (microns)
Relative intensity
Distance (microns)
P-P
Relative Intensity
Distance (microns)

(B.I)

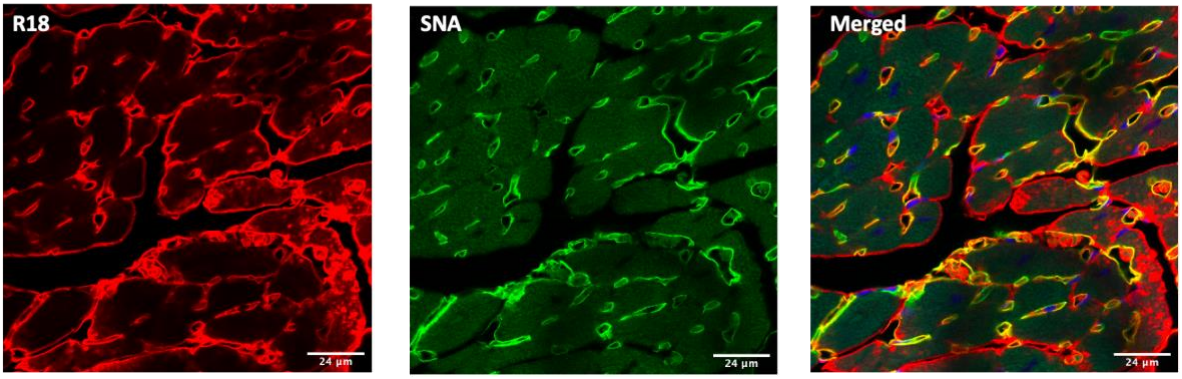
R18
SNA
Merged
24 µm
24 µm
24 µm

(B.II)

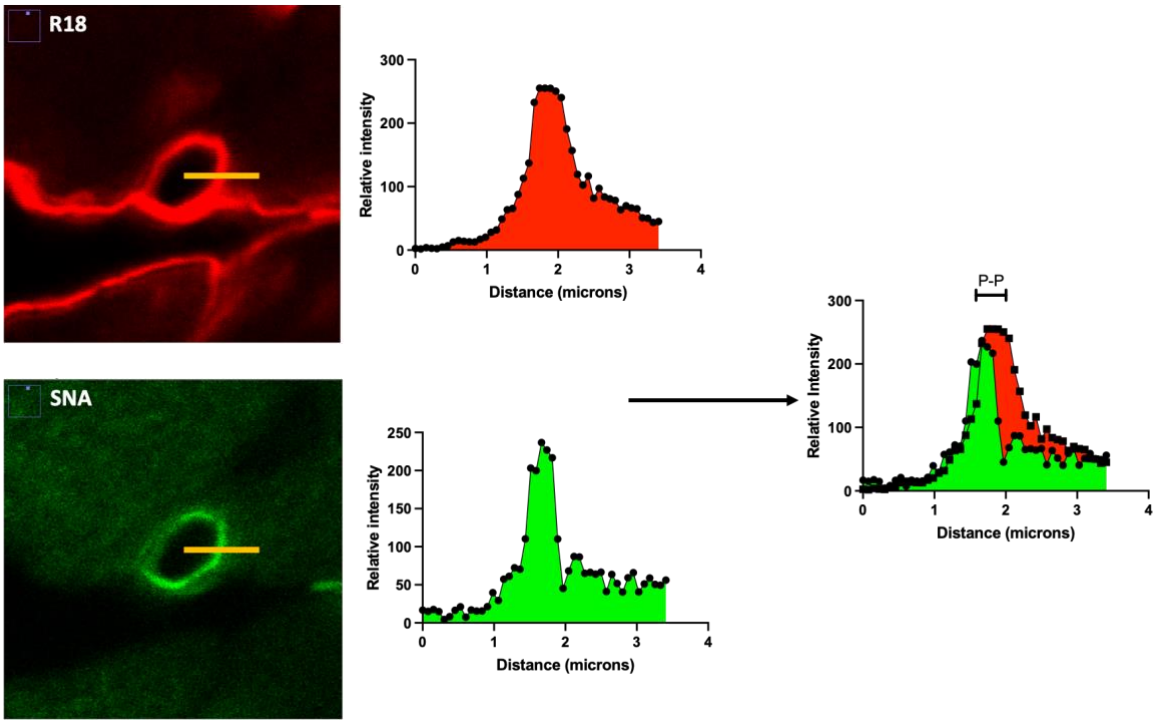
R18
SNA
Relative intensity
Distance (microns)
Relative intensity
Distance (microns)
P-P
Relative Intensity
Distance (microns)

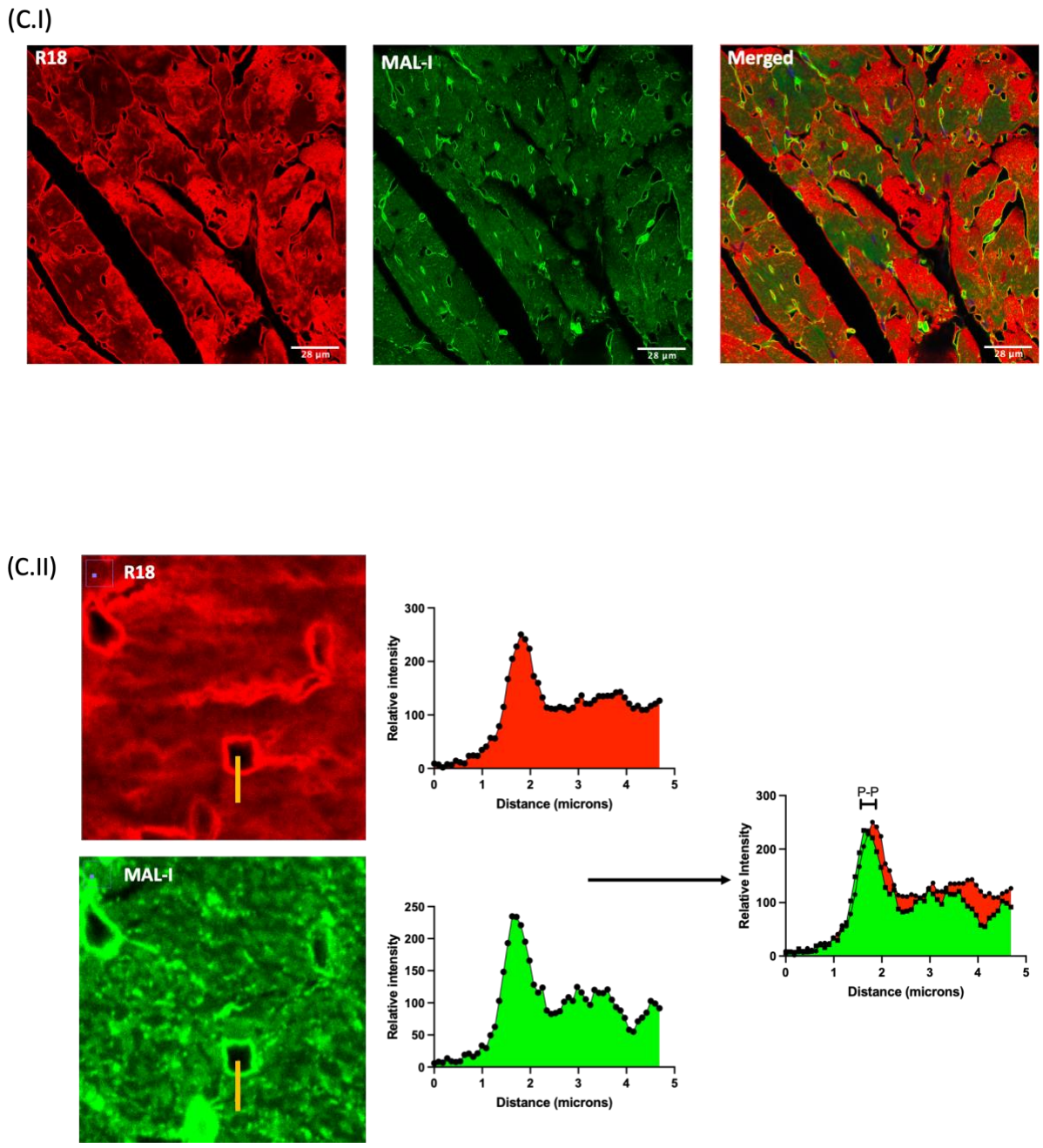

Figure 22. Identifying suitable lectins to investigate the coronary microvascular EGlx.

Three lectins were tested to determine their ability to bind to the EGlx. ***(A.I, B.I, and C.I)*** *Mouse heart tissue stained with R18 and the chosen lectin (A.I = LEL; B.I = SNA; C.I = MAL-I). The merged images show the overlay of DAPI (blue), R18 (red) and the lectin (green).* ***(A.II, B.II, and C.II)*** *Image of a vessel with a linear region of interest manually drawn from the centre of the vessel to the outside of the membrane. The fluorescent profiles for representative images are also shown. The green peak is the lectin, and the red peak is the R18. The distance between the two peaks (P-P) is an indication of EGlx depth (A.II = LEL; B.II = SNA, C.II = MAL-I).*

3.3.2.2 The coronary microvascular EGlx depth is reduced in DCM and MMP2/9 inhibitor I does not protect the EGlx

A macro was used to automate the analysis of EGlx depth and conduct more measurements of a single vessel in a shorter amount of time. Briefly, a macro was developed to take multiple measurements (360) in a preselected capillary loop and generate fluorescence intensity profiles for the lectin components of the coronary microvascular EGlx and the endothelial cell membrane label. Gaussian curves were then applied to the raw intensity data of each plot for peak-to-peak measurements (Figure 23. A). The mean was subsequently determined from 360 lines per capillary loop and 15 loops per heart. Data were excluded with a standard deviation of more than 7.5 and/or a signal-to-noise ratio of less than 15. Further details on how EGlx depth was assessed and the use of the macro are detailed in 2.4.1.2.

With all three lectins, a reduction in EGlx depth was found in diabetic mice when compared to the controls (Figure 23. B). No significant difference in EGlx depth was found between diabetic mice and diabetic mice treated with MMP2/9 inhibitor I (MMPI). Different coronary microvascular EGlx depths were also recognised between lectins.

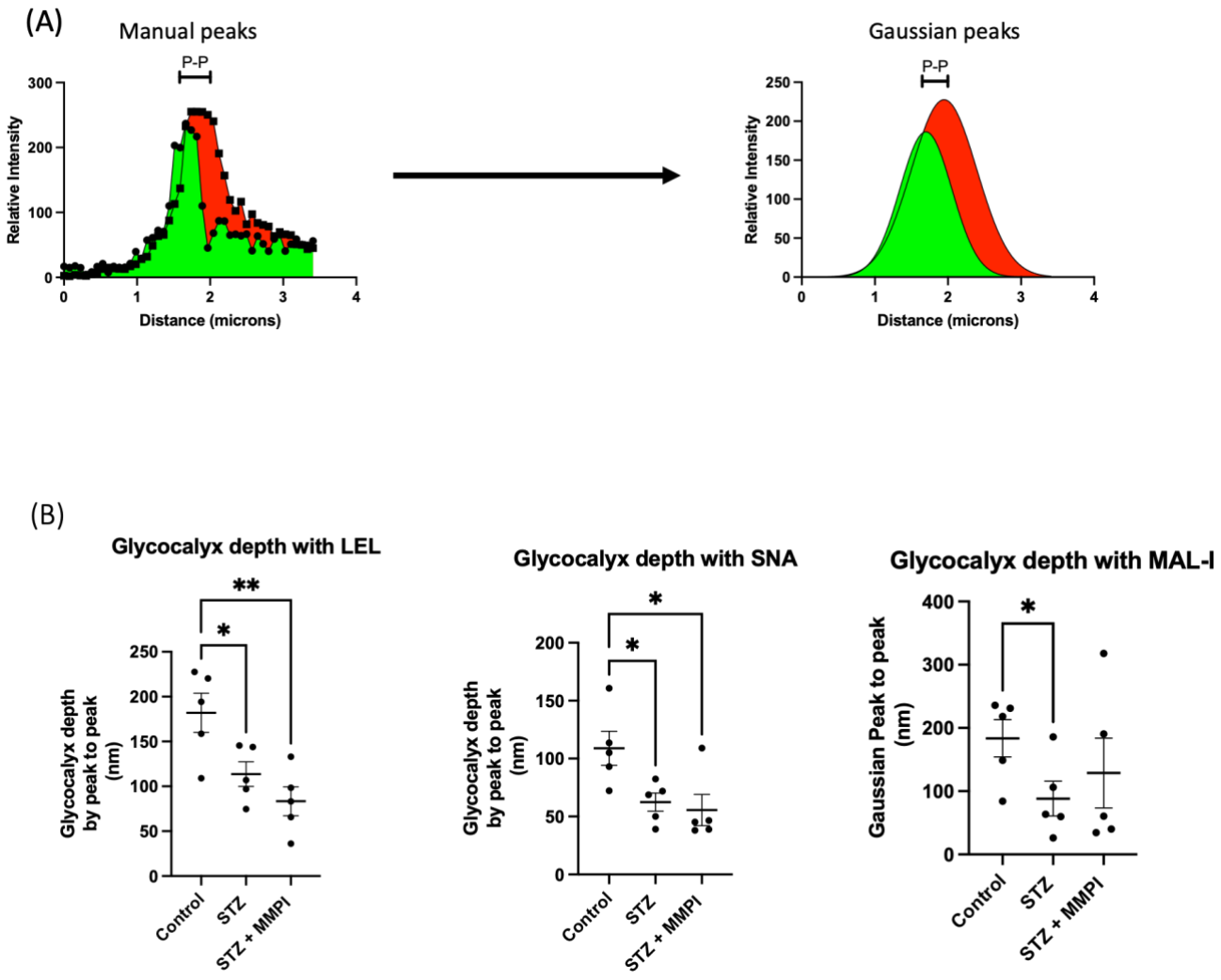

Figure 23. The coronary microvascular EGlx depth is reduced in mice with DCM and MMP2/9 inhibitor I does not protect the EGlx.

The analysis of EGlx depth was automated using a macro. ***(A)*** *An example of a Gaussian curve applied to the raw fluorescent peak plot profiles.* ***(B)*** *A reduction in EGlx depth using all three lectins was found in the STZ mice when compared to the controls (n=5 for all groups with all three lectins; LEL: *p<0.05; One-way ANOVA; SNA: *P < 0.05; One-way ANOVA; MAL-I: *p < 0.05; One-way ANOVA). No significant difference in EGlx depth between STZ and STZ + MMPI mice with all lectins. Different depths is recognised between lectins. A significant reduction in depth was found in the STZ + MMPI group when compared to the control mice with both SNA and LEL lectin (LEL: **P < 0.01; One-way ANOVA; SNA: *P < 0.05; One-way ANOVA;).*

3.3.3 There is a correlation between coronary microvascular EGlx depth and diastolic function

The relationship between EGlx depth and diastolic function was assessed (Figure 24). The EGlx depth for the mouse was matched to its E/E' diastolic measurement from 9 weeks post STZ. The E/E' ratio was used to represent diastolic function in this correlation due to the greater difference observed between the control and diabetic mice. A significant negative correlation was found with all lectins between EGlx depth and E/E' ratio suggesting an increased EGlx depth is associated with better diastolic function.

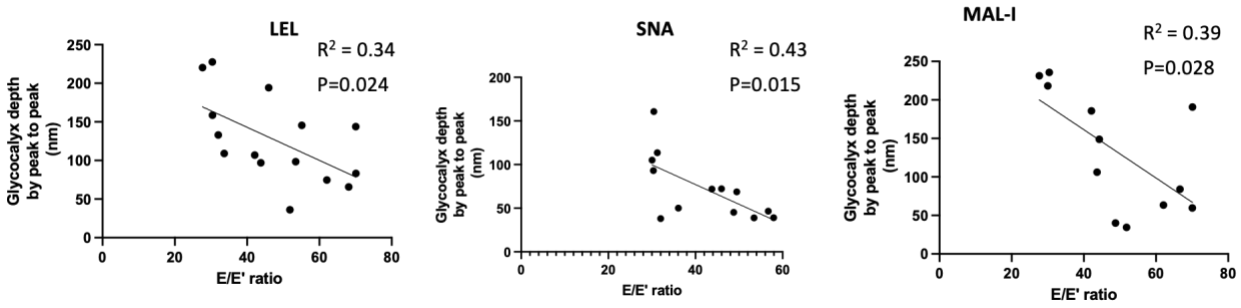

Figure 24. There is a correlation between coronary microvascular EGlx depth and diastolic function.

*A negative correlation between EGlx depth and diastolic function was found with all lectins used (LEL: n=15; *p < 0.05; R^2 = 0.34; Pearson r; SNA: n =13; *p < 0.05; R^2 = 0.43 Pearson r; MAL-I: n=10; **p = 0.0027; R^2 = 0.7; Pearson r).*

3.3.4 There is an increase in MMP activity in DCM

Frozen mouse hearts were lysed and used to assess MMP2 and 9 activity. To get an indication of circulating MMP activity, plasma and urine was also assessed. Whilst no significant increase in MMP2 activity was found in the heart tissue of diabetic mice when compared to the controls, there was a trend towards an increase in activity (Figure 25. A). No significant difference in MMP2 activity was observed in the urine between the controls and diabetic mice. However, a clear reduction in MMP2 activity was noticed in the urine of control mice treated with MMP2/9 inhibitor I when compared to the untreated control mice (Figure 25. B). This trend was also noticed between diabetic mice and diabetic mice treated with the inhibitor.

As expected, an increase in MMP9 activity was found in the heart (Figure 25. A), urine (Figure 25. B) and plasma (Figure 25. C) of diabetic mice when compared to the controls. However, no significant difference in MMP9 activity was observed in the heart and urine of diabetic mice treated with MMP2/9 inhibitor I when compared to diabetic mice treated with the vehicle. A significant reduction in MMP9 activity was observed in the plasma when treated with the inhibitor.

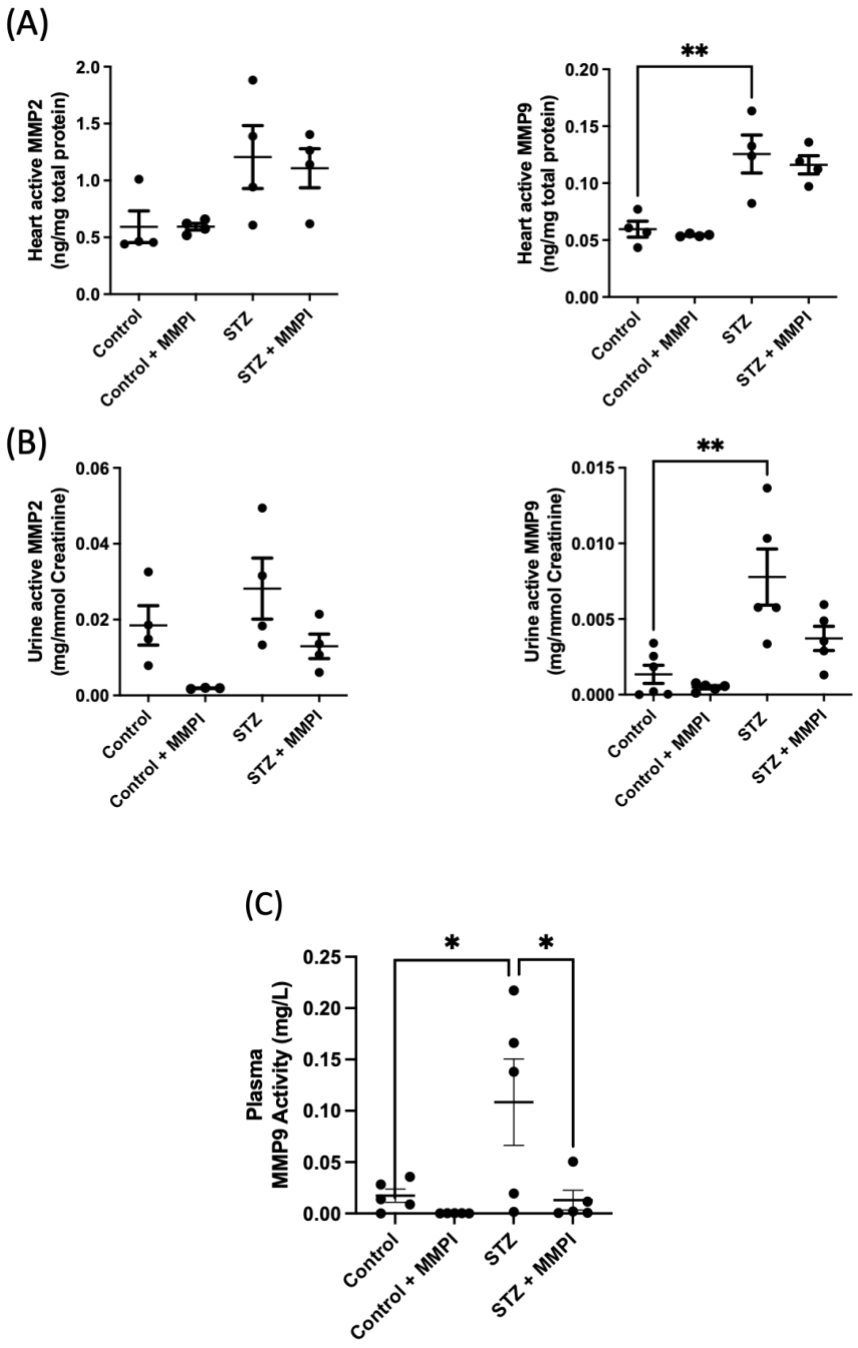

Figure 25. There is an increase in MMP activity in DCM.

MMP2 and 9 activity were assessed in the heart, urine, and plasma of mice. ***(A)*** *MMP2 and 9 activity in the heart (MMP9 activity: n=4 for all groups; control vs STZ; **p < 0.01; One-way ANOVA;). Whilst not significant, a trend towards an increase in MMP2 activity was recognised in STZ mice compared to controls. No significant difference in MMP2 or 9 activity was found between STZ and STZ + MMPI. These resulted contributed to the following paper (27).* ***(B)*** *Urine MMP2 and 9 activity. No significant upregulation in MMP2 activity was found*

*in the urine of STZ mice when compared to controls. An increase in MMP9 activity was found in the urine of STZ mice when compared to the controls (n=6 for all groups; *p < 0.05; One-way ANOVA). Treatment with the inhibitor did not reduce MMP9 activity in diabetic mice.* ***(C)*** *Significant increase in MMP9 activity in the plasma of STZ mice when compared with the controls. This activity was reduced when treated with the MMP inhibitor (n=5 for all groups; *p < 0.05; One-way ANOVA)*

4.3.5 There is a correlation between heart MMP9 activity and diastolic function

An analysis to assess the relationship between MMP activity and diastolic function was conducted. A positive correlation was found between the MMP9 activity in the heart tissue and the E/E' ratio (Figure 26. A) suggesting an increase in MMP9 activity is associated with a reduction in diastolic function. No correlation was found between heart MMP2 (Figure 26. A) activity and diastolic function. No correlation was found between diastolic function and urine MMP2 and 9 activity (Figure 26. B) as well as plasma MMP9 activity (Figure 26. C).

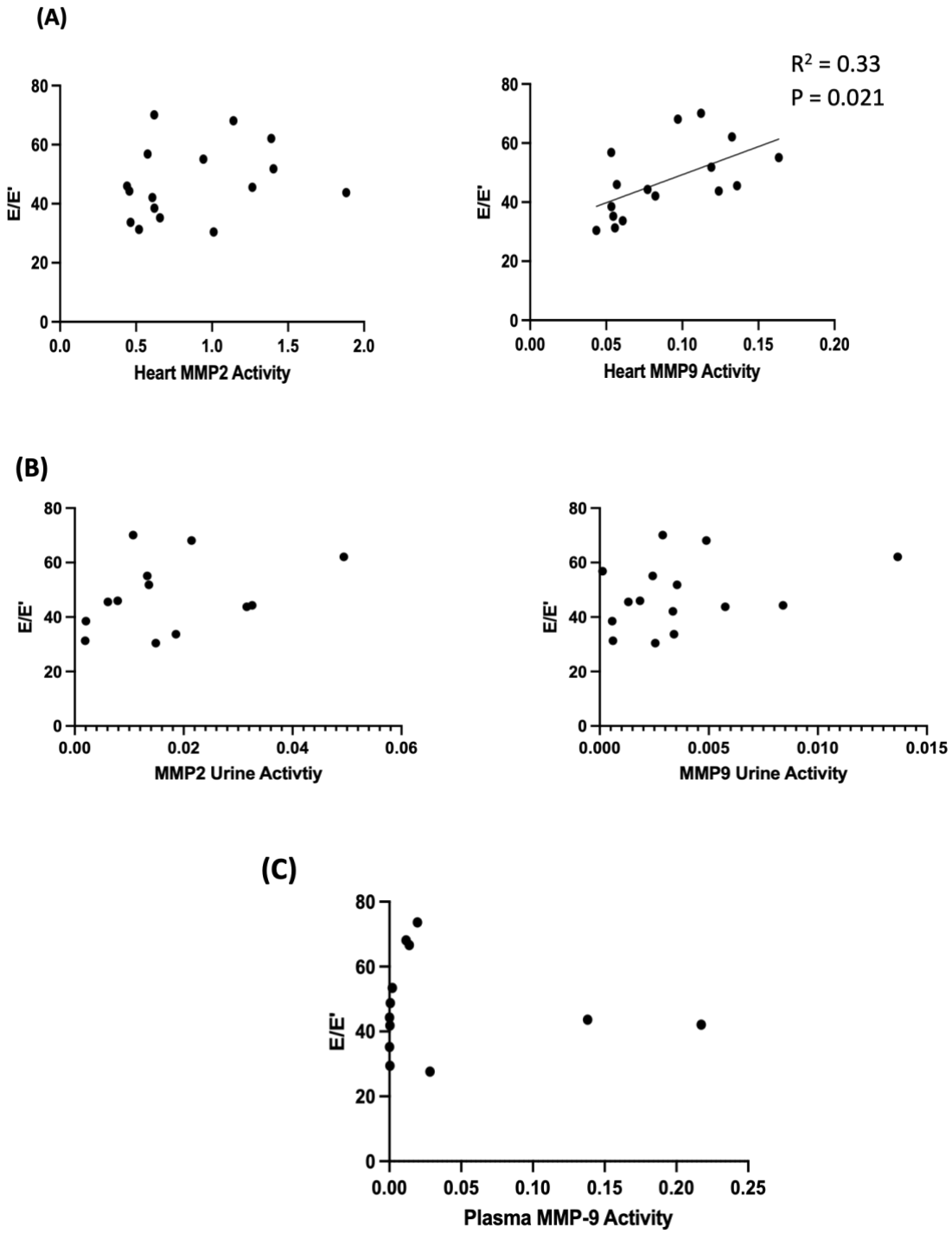

Figure 26. Correlation between MMP9 activity and diastolic function.

*A significant positive correlation was found between MMP9 activity and the E/E' ratio assessment of diastolic function (n=16; *P < 0.05; R^2 = 0.33; Pearson r). No significant relationship was found between heart MMP2 activity and diastolic function. No correlation was also found between diastolic function and MMP2 and 9 activity. As well as this no correlation was observed between plasma MMP9 activity and diastolic function.*

3.4 Discussion

In this chapter, I aimed to identify if there was an increase in MMP activity in DCM and if inhibition of MMP2 and 9 with MMP2/9 inhibitor I can protect the coronary microvascular EGlx and restore diastolic function. Using the STZ diabetic mouse model, we have shown that at 10 weeks post STZ, diabetic mice have diastolic dysfunction indicated by a reduced E/A ratio and increased E/E'. This reinforces what we have shown previously in the STZ mouse model of DCM (27), therefore, showing that the results are reproducible in our hands. We have also reinforced in this chapter that there is reduced coronary microvascular EGlx depth, and this has been shown by the peak-to-peak method to analyse lectin staining. To the best of my knowledge, this study is the first to utilise this method to investigate the coronary microvascular EGlx depth. We can be confident that diabetes does lead to damage to the coronary microvascular EGlx as this has now been shown through several methods of analysis and imaging in the same mouse model (27). As well as this, this study shows that the EGlx depth negatively correlates with the E/E' ratio suggesting that a thicker EGlx depth is associated with better diastolic function. Regarding MMP activity, I have shown that there is an increase in MMP activity in DCM. Specifically, MMP9 is increased in the heart, plasma and urine of diabetic mice. To my surprise, the inhibitor did not inhibit MMP activity in the heart and urine of diabetic mice but did reduce MMP9 activity in the plasma. Treatment with MMP2/9 inhibitor I also did not improve diastolic function in diabetic mice or protect the coronary microvascular EGlx.

3.4.1 The STZ model to study DCM

In this study, diastolic dysfunction was observed at 10 weeks post STZ. Literature shows that defined diastolic dysfunction is recognised at 8 weeks post-STZ (125,323) and therefore, the results of this chapter fall in line with current literature which indicates that at the time point used in this experiment (10 weeks), mice should have already developed defined diastolic dysfunction. It may be beneficial to assess the progression of diastolic dysfunction to understand how heart function alters in DCM over time. As well as this, understanding the progression of DCM can help to identify potential markers of disease and therefore will allow early intervention and the prevention of further damage. However, this may prove difficult with this model. The use of the STZ mouse model is beneficial in the fact that it is reproducible and relatively low cost, however, a major limitation is that the health of the mice declines swiftly making it difficult to examine early changes in diabetes. Therefore, other models may need to be considered when trying to investigate heart changes over time in DCM.

In the early phase of the human pathology of DCM, diastolic dysfunction is the only functional abnormality recognised with systolic dysfunction supervening in later stages (324). We have previously shown in this same model, that mice develop diastolic dysfunction in the absence of systolic dysfunction at 10 weeks post-STZ (27) and other studies show diastolic dysfunction with preserved ejection fraction at later time points (325,326). Therefore, we have demonstrated that this is a relevant DCM model in our hands.

The use of echocardiography to assess diastolic function is frequently used clinically with early studies showing a decreased ratio of peak early to peak late filling velocities with pulsed wave Doppler in diabetic patients (327,328). The early filling of the ventricle is a passive process and is due to the pressure difference between the ventricle and the atria. Increased ventricular pressures will result in a reduced E wave velocity as less blood will be transported from the left atria to the left ventricle during early filling. The reduced early filling will result in more blood left in the atria at the end of the early filling phase. This will result in the atria pumping out more blood in the late filling phase, therefore increasing the peak A velocity wave. Overall, this results in a reduced E/A ratio (329,330). The E/A ratio itself has its limitations and should not be used on its own to assess diastolic function. A major limitation of the E/A ratio is that it is unable to distinguish between normal filling patterns and pseudo-normal filling patterns. As a compensatory response for increased left ventricular filling pressures, the left atrial pressure may rise ultimately leading to an increased E wave velocity as a greater pressure difference between the atria and the ventricle is established again (329,330). This will cause the E/A ratio to appear normal even though the diastolic function is still impaired. Therefore, other assessments must be done with the E/A ratio to confirm diastolic function. In this study, the E/E' ratio was also used and was found to be increased in diabetic mice suggesting diastolic dysfunction. In diabetic patients, an increase in E/E' is recognised and is associated with the subsequent development of heart failure (331). Therefore, we can be confident that the assessment of heart function done within this chapter provides a suitable evaluation of diastolic function that is replicated in humans.

3.4.2 Lectin staining to investigate glycocalyx depth

Methods for investigating the EGlx have greatly evolved. The use of lectins allows the direct visualisation of the EGlx by binding to disaccharide moieties on the GAG side. In this study, LEL, SNA and MAL-I were used to detect the EGlx. SNA and MAL-I were chosen as prior to my arrival, Dr Yan Qiu showed that they bound mainly to the EGlx in the mouse heart. LEL was also chosen as it has been used previously to investigate the EGlx in the kidneys and so I wanted to know if it could be used in the heart also (332). Whilst a similar trend was observed with all three lectins, it is evident that their binding properties are different. This could be based upon the distribution of their epitopes within the EGlx in that some lectins such as LEL bind to terminal components of GAGs whilst others do not and thus the measurement of depth with the peak-to-peak method would vary. A wide variety of α-2-6-sialic acids is tolerated by SNA which make up a vital part of the periphery of the EGlx (333). Interestingly, SNA predominantly binds to α-2-6-sialylated LacNAc. With the clear specificity of this lectin to the EGlx, based on the staining, it is possible that α-2-6-sialylated LacNAc is distributed within the coronary microvascular EGlx, however, this is unknown. Sialic acids have been identified to be critical regulators of microvascular permeability and thus there is a potential link between the reduction in SNA binding to the EGlx and altered permeability in diabetes (191). LEL binds to N-acetylglucosamine (GlcNAc) as well as N-Acetyllactosamine (LacNAc) (334). Whilst GlcNAc is known to make up structures such as heparan sulfate, the distribution of LacNAc within the EGlx is not completely understood (335). However, it has been revealed that GAGs such as chondroitin sulfate may contain the LacNAc binding site for some lectins (336). Therefore the depth observed may be a result of a broad variation in epitopes available for LEL and highlights the importance of understanding the biochemical structure of the EGlx to better understand its alterations in disease. MAL-I has similar binding properties to SNA binding to glycans with sialic acids in α-2-3-linkages to galactose (322) as well as 6-O sulfations on GlcNAc.

The use of lectins can provide a basis for further understanding the chemical structure of the EGlx. However, individually, the lectins may not accurately reflect changes in EGlx depth as it may just be the specific epitope for the lectin of interest that is altered rather than a general disruption in the EGlx. Perhaps the use of a combination of lectins together would better reflect the EGlx depth however, this is still to be investigated. Despite this, the individual use of lectins is beneficial in understanding the unique signature of the EGlx.

It is known that GAGs are distributed in areas other than the EGlx such as the basement membrane, and connective tissues (337). However, we provide confidence in the measurement of the EGlx by utilising the peak-to-peak method. As the EGlx is on the luminal side of vascular endothelial cells, only the fluorescent peak that occurred to the left of the membrane peak was taken to reflect the EGlx. This is the first time this method has been used in the heart to quantify EGlx depth with lectins and proves advantageous over the previous method used, by assessing lectin fluorescent intensity (27). Carbohydrate structures are also found at the basement membrane in which lectins can also bind (338). Due to this, the use of the fluorescent intensity method to determine EGlx depth in the heart, as done previously, does not discriminate between the lectins that are bound specifically to the EGlx and the lectins bound to other structures. This is overcome with the peak-to-peak method as this method measures the anatomical distance between the peak endothelial plasma membrane signal and the peak glycocalyx-bound lectin signal thereby only focusing on the EGlx. Therefore, I can be confident in the changes observed in EGlx depth as a result of diabetes. By manually conducting the quality control step of assessing the fluorescent plot profiles, I demonstrated that all lectins used in this chapter could be used to visualise aspects of the EGlx in this mouse model of DCM. However, it is not clear exactly what the lectins are binding to in the EGlx and what is altered. The differences in lectin binding may suggest an wide disruption in the EGlx as a result of diabetes and may suggest that the structure of the EGlx is far more complex than what is understood.

The EGlx depth observed with this method appears to be substantially higher than that observed with EM in the same strain, sex, and age of mice (27). This may be due to the dehydration that is required for EM which alters the EGlx structure. Therefore, as this is not required for confocal microscopy, a better indication of the EGlx depth can be gained from lectin staining. On the other hand, confocal microscopy has optical limitations, making it difficult to demonstrate the geometrical characteristics of the EGlx (339).

3.4.3 The coronary microvascular EGlx is reduced in DCM

We have shown a reduction in coronary microvascular EGlx depth in the diabetic group when compared to the controls. This is expected and is supported by the present literature suggesting that diabetes results in a reduction in EGlx depth making it a key characteristic of diabetes (27,117,118,340,341). Earlier studies on the heart found that the myocardial capillary EGlx in rats played a key role in regulating vascular permeability and its degradation instantly resulted in myocardial oedema (342). Our group has also shown in a mouse model of DCM that diabetes reduces the coronary microvascular EGlx depth resulting in altered microvascular permeability leading to oedema and ultimately diastolic dysfunction (27). The EGlx also plays a role in other aspects of microvascular physiology other than permeability, such as regulating microvascular flow (343) which is important for oxygen delivery and metabolite clearance. Therefore, the reduction of EGlx depth in the heart may ultimately result in several insults to the myocardium impairing cardiac function.

The relationship between EGlx depth and diastolic function is shown with a significant negative correlation between EGlx depth and the E/E' ratio. This, therefore, suggests that a reduced EGlx depth is associated with diastolic dysfunction in DCM and thus, efforts to protect the coronary microvascular EGlx are vital. It is interesting to note however the strength of the correlations. A

weak/moderate correlation was found with all lectins although this could be influenced by various factors. The heart tissue was stored in ethanol for a year before my arrival and so the EGlx could have been damaged during this process as ethanol causes dehydration of the EGlx (344). Therefore, it is important to interpret correlation with caution as it does not suggest causation.

3.4.4 Increased MMP activity in DCM

An increase in MMP9 activity was found in the heart tissue, urine, and plasma of diabetic mice when compared to the controls suggesting both a systemic and local increase in MMP activity. There are various alterations in diabetes that result in an increase in MMP activity such as increased ROS (345,346) and inflammation (266) and others have previously identified an increase in MMP9 activity in both human and animal models of diabetes (27,117,118,347,348). MMP9 causes the shedding of SDC4 from glomerular endothelial cells (213), and Dr Yan Qiu has shown a reduction in the colocalization of SDC4 with coronary microvascular endothelial cells in the hearts of diabetic mice (27). It can therefore be inferred that the increase in MMP9 activity found in the heart may cause the shedding of SDC4 and be a mechanism of the EGlx damage observed in this chapter. This is a mechanism that we will explore further in the next chapter.

Whilst we see a trend towards an increase in MMP2 activity in the heart, we do not see this increase in the urine. However, although the results were not statistically significant this may be because of insufficient n to show an effect with this assay in the heart samples. Therefore, increasing the n may reveal that the trend observed in the heart is significant. Perhaps the potential increase in MMP2 activity in the heart is due to its intracellular actions (349). Whilst it was believed that MMPs simply act extracellularly, research is consistently revealing the intracellular role of MMPs and these actions have been found within the cardiomyocytes for MMP2. Indeed, it has been shown that MMP2 is

able to cleave troponin I intracellularly and may impact myocyte contractile ability (350). Active MMP2 has also been found in the nucleus of cardiac myocytes of which the biological role remains unclear (351). Along with this, oxidative stress has been shown to induce an intracellular isoform of MMP2 which further enhances the inflammatory cascade (352). Therefore, it may be that the increased trend in active MMP2 found in the heart is a result of its intracellular and extracellular actions and may be why this trend is not recognised in the urine.

The urine provides an indication of the active MMPs excreted from the body, however, a better reflection of circulating MMPs would be from the blood or plasma. Unfortunately, we were unable to investigate MMP2 activity in the plasma due to the lack of commercially available kits at the time. Due to many active MMPs being released in the circulating blood to act extracellularly, the plasma may be more sensitive than urine for the detection of MMP activity. Therefore, we cannot rule out the role of MMP2 in the shedding of the EGlx from the results of this chapter.

3.4.5 Treatment with the MMP inhibitor did not protect the coronary microvascular EGlx

When looking at the activity in the heart tissue, no significant difference was found in both MMP2 and 9 activities between diabetic mice and diabetic mice treated with the inhibitor. This suggests that the inhibitor is not effective at inhibiting heart MMPs.

A similar trend to that of the heart was observed for urine MMP9 activity. However, it seems that there may have been some inhibition of MMP2 activity. Whilst not significant, perhaps with an increase in n, this would prove to be significant. Whilst no significant increase in MMP2 activity was found in the urine of diabetic mice, the reduction in its activity in mice treated with the inhibitor shows that the inhibitor is active and working. This was reinforced by the assessment of plasma

MMP9 activity which was reduced close to control levels when diabetic mice were treated with the inhibitor.

This has raised various questions due to the fact that MMP cleavage of the EGlx is extracellular (353), yet we see no protection of the EGlx when diabetic mice were treated with the inhibitor. As it has been shown that protecting the coronary microvascular EGlx improves diastolic dysfunction in DCM (27), the lack of coronary microvascular EGlx protection in this study seems to be the main reason why we observe no improvement in diastolic function in diabetic mice treated with the inhibitor. The question now arises as to why MMP inhibition did not protect the EGlx. The positive correlation between heart MMP9 activity and the E/E' ratio suggests that an increase in MMP9 activity in the heart is associated with reduced diastolic function. Thus, it appears that inhibition of the heart MMP activity may be more important than just inhibiting circulating MMPs. However, the reasons for this remain unclear.

There are several ideas that can be speculated in an attempt to explain why MMP inhibition did not protect the EGlx. The first is that the inhibitor is not cell permeable (according to the manufacturer) sparking the idea that the inhibition of intracellular MMPs is important to protect the EGlx. As mentioned above, the intracellular activity of MMP2 and 9 has been found in the cardiomyocytes and localisation to the nucleus has been identified (351,354). It may be possible that MMPs participate in the gene regulation of other enzymes involved in the shedding of the EGlx. Indeed, literature shows that active nuclear MMP9 is able to facilitate in the proteolysis of histone H3 tails, which may cause open chromatin structures increasing DNA accessibility for transcription factors (355,356). In fact, the literature suggests that there is coregulation of heparanase and MMP9 with increased heparanase expression and activity being linked with increased MMP9 activity (357–359). If nuclear MMP9 does enhance the expression and activity of heparanase, then this would explain

why inhibition of intracellular MMPs is important as this would reduce the expression of heparanase which also cleaves the components of the EGlx (heparan sulfate). Research should continue to investigate the role of MMPs in pathology as well as physiology to further understand their targets of action both intracellularly and extracellularly.

Another reason why no protection of the EGlx was observed when diabetic mice were treated with the inhibitor is that other circulating enzymes that cause the shedding of specific components of the EGlx may have also been increased. Whilst diabetes causes an upregulation in MMP activity, it has also been shown there is an increase in other enzymes such as heparanase (360), hyaluronidase (200), and neuraminidase (361), all of which cause damage to the EGlx. Whilst MMP2 and 9 are said to cleave syndecans, lectins bind to GAG residues and so whilst inhibition of MMPs may protect the core protein, there may be a lack of protection of the GAGs resulting in reduced EGlx depth.

On the other hand, the inhibitor used in this study has been used previously at the same dose and shown to protect the glomerular EGlx when visualised with EM (118). Whilst the kidney varies in many ways to the heart, the idea of circulating MMPs causing the shedding of the EGlx places the data from this chapter in conflict with that of the previous study (118). However, there are variations that may lead to the differences observed. As mentioned, the STZ mouse declines rapidly in health and an extra week of diabetes could be the difference between the severity of sickness the mouse experiences. This mean that each week of diabetes for the STZ mouse could result in significant changes in organ structure and function. The endpoint of this study is a week longer than that of the previous study described (118). Therefore, damage to the EGlx could be more severe and more difficult to recover. It could also be a time point which results in a compensatory increase of other enzymes that cause damage to the EGlx. Therefore, there may be an optimal treatment window after which the effect of the inhibition is reduced, and this may have been missed in this study.

3.5 Conclusion

We have shown that MMP9 activity is increased in DCM as well as reinforced that the coronary microvascular EGlx is damaged in DCM. We have also shown that MMP2/9 inhibitor I is not be suitable to protect the coronary microvascular EGlx in DCM but have revealed that inhibition of MMP activity of the heart is important. Therefore, we cannot rule out the idea that inhibition of MMPs can protect the coronary microvascular EGlx. The use of another inhibitor, one which is able to inhibit MMPs of the heart may be more suitable to protect the EGlx.

Going forward, we will use a different inhibitor to assess its protection on the coronary microvascular EGlx, considering the points discussed in this chapter.

Chapter 4: TNF-α results in the MMP-mediated shedding of SDC4

From the previous chapter, I confirmed that the coronary microvascular endothelial glycocalyx (EGlx) depth is reduced in diabetic cardiomyopathy (DCM) and that the EGlx positively correlates with diastolic function. I have also shown that there is an increase in MMP activity, specifically MMP9 activity in DCM and this is associated with reduced EGlx depth and diastolic dysfunction. It has previously been shown in glomerular endothelial cells that tumour necrosis factor-α (TNF-α) increases MMP2 and 9 activity, leading to syndecan 4 (SDC4) shedding from the glomerular EGlx (213). This revealed a mechanism through which the EGlx could be damaged in diabetes as diabetes is known as a chronic inflammatory disease. Knowing this, I aimed to identify if this same mechanism of EGlx damage occurs in coronary microvascular endothelial cells (CMVEC). I also demonstrated in the previous chapter that the inhibitor used (MMP2/9 inhibitor I) was unsuitable for protecting the coronary microvascular suggesting a reason as to why no improvement in diastolic function was found when diabetic mice were treated with the inhibitor. It appeared that the inhibition of heart MMP activity was important to protect the coronary microvascular EGlx. Therefore, as this did not occur with the MMP2/9 inhibitor I, I decided to investigate the use of another MMP2 and 9 specific inhibitor, SB-3CT, to examine its potential in protecting the coronary microvascular EGlx. I started this investigation in vitro rather than in vivo to provide confidence in the use of the inhibitor before moving to live animals and therefore reduce the number of animals used in this thesis.

Part of the work presented in the chapter (Fig.42-43) has contributed to the following publication:

*Qiu Y, **Buffonge S**, Ramnath R, Jenner S, Fawaz S, Arkill KP, et al. Endothelial glycocalyx is damaged in diabetic cardiomyopathy: angiopoietin 1 restores glycocalyx and improves diastolic function in mice. Diabetologia*

4.1 Introduction

Coronary microvascular EGlx damage has previously been associated with interstitial oedema and cardiac dysfunction in animal models (27,362) and so protecting the EGlx is vital. Syndecans are transmembrane core proteins which are 19-35 kDa and consist of four family members (162). They are the most abundant core proteins of the proteoglycan family within the EGlx (166). SDC4 is a common core protein of the EGlx (363) and recently we have demonstrated that mice with DCM have a reduction of SDC4 at the endothelial cells of coronary microvessels (27). Studies show that the upregulation of MMP2 and 9 observed in diabetes contributes to the damage of the EGlx (27,117,118,213,364,365) through the cleavage of the SDC4 ectodomain (118,213).

As discussed in the general introduction, serum proinflammatory cytokines such as TNF-α are elevated as a result of diabetes (366). TNF-α plays a key role in the upregulation of MMP gene expression (235,236) and a relationship has been established between elevated TNF-α and the increased shedding of EGlx components (367). In fact, it has been shown that TNF-α induces SDC4 shedding from glomerular endothelial cells through MMP9 upregulation (213). Therefore, a similar mechanism of SDC4 shedding may occur from CMVEC.

SB-3CT, identified in 2000, is the first known selective slow binding and mechanistic inhibitor for gelatinases, causing a conformational change to the inhibitor-enzyme complex (283). Unlike broad-spectrum MMP inhibitors, which act by chelating the zinc ion in the active site, the deprotonation of SB-3CT results in the generation of a thiolate (283). Through the thiirane sulfur, the inhibitor coordinates with the zinc ion of MMP2 and 9 activating the thiirane ring for nucleophilic attack by

the conserved glutamate in the active site. This leads to the irreversible inhibition of the protease (285) through a stable Zn^{2+} thiolate complex (286). Figure 27 illustrates the mechanism of SB-3CT inhibition of MMP2 and 9.

Knowing the potential benefit of SB-3CT in inhibiting MMP2 and 9, it is reasonable to assess its ability to protect the coronary microvascular EGlx as both MMPs are known to cause shedding of the EGlx.

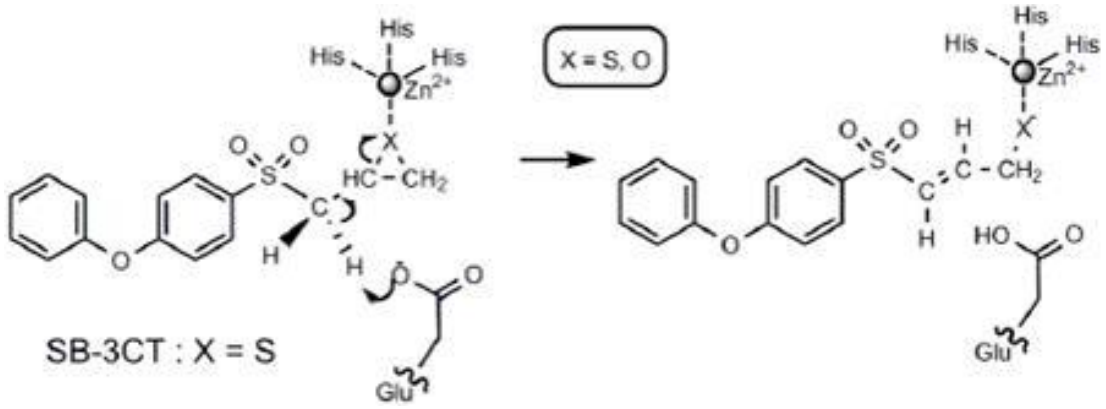

Figure 27. The mechanism of MMP2 and 9 inhibition by SB-3CT.

The deprotonation of SB-3CT by a conserved glutamate in the MMPs causes the opening of the thiirane resulting in the inhibition of the protease through a Zn^{2+} *thiolate complex. This image was taken from* (368).

4.2 Objectives

Based upon the knowledge presented above, throughout this chapter, my objectives are to examine if TNF-α causes the upregulation of MMP2 and 9 resulting in SDC4 shedding from CMVEC. As well as this, I am to investigate if the inhibition of MMP2 and 9 with SB-3CT can prevent SDC4 shedding thereby protecting the coronary microvascular EGlx. I would also like to identify if the EGlx is important for CMVEC barrier function.

4.3 Methods

All methods done within this chapter are detailed in ***Chapter 2: Materials and Methods***.

4.4 Results

4.4.1 TNF-α causes an upregulation in SDC4 mRNA expression in CMVEC

It has previously been shown in glomerular endothelial cells that 10 ng/ml of TNF-α induced SDC4 mRNA upregulation (213). Whilst not confirmed, this is believed to be due to a feedback mechanism as a result of the shedding of SDC4. Therefore, the effect of TNF-α on the expression of SDC4 mRNA in CMVEC was investigated using the same concentration. Conditionally immortalised coronary microvascular endothelial cells (ciCMVEC) were first treated with TNF-α for varying times to identify a suitable length of treatment for further studies. In the previous study (213), glomerular endothelial cells were treated with TNF-α for 1-2 hours which appeared to be enough to cause SDC4 shedding. However, studies have shown in other cell types, an increase in MMP9 expression as a result of TNF-α from 4 hours which peaked at 6 hours (298). Therefore, I decided to explore time points of 1 hour, 2 hours, 4 hours, and 6 hours (Figure 28). The results show that TNF-α caused a 3-fold increase in SDC4 mRNA expression at 1 hour although not significant with a One-way ANOVA. A

significant increase in SDC4 mRNA expression was recognised from 2 hours of TNF-α treatment with a 6.9-fold change in mRNA expression. This continued to increase at 4 hours of TNF-α treatment leading to a 9.3-fold change with the highest increase in SDC4 mRNA expression being recognised at 6 hours (fold change of 11.9).

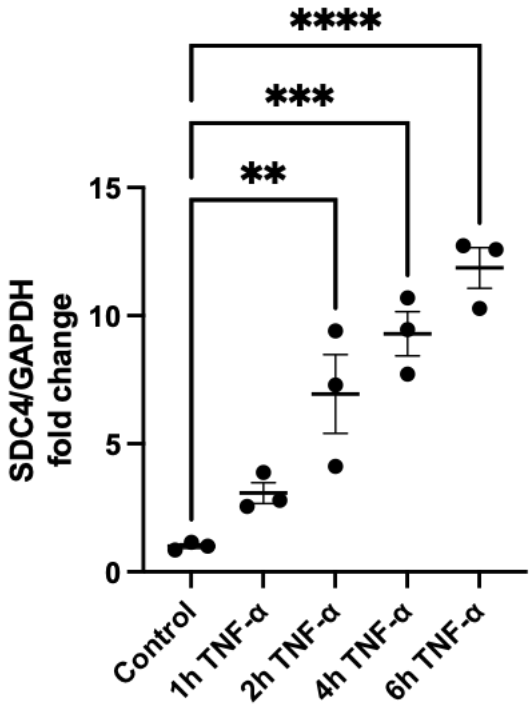

Figure 28. TNF-α causes an upregulation in SDC4 mRNA expression in CMVEC.

*Cells were treated with 10 ng/ml of TNF-α for either 1, 2, 4 or 6 hours. An increase in SDC4 expression was found at all time points with significance occurring from 2 hours of TNF-α treatment (n=3 for all conditions; 2 hours: **p < 0.01; 4 hours: ***p < 0.001; 6 hours: ****p < 0.0001; One-way ANOVA).*

4.4.2 TNF-α causes an upregulation in MMP9 mRNA expression in CMVEC

Based upon previous literature suggesting that TNF-α causes a peak in MMP9 expression at 6 hours (298) as well as 6 hours of TNF-α treatment showing the greatest increase in SDC4 mRNA expression, I decided to continue with this time point for further investigations. ciCMVEC were treated with 10 ng/ml of TNF-α for 6 hours and an assessment of MMP2 and 9 mRNA expression was done. No significant upregulation in MMP2 mRNA expression was found whilst, as expected, MMP9 mRNA expression was significantly upregulated by 1.9-fold (Figure 29).

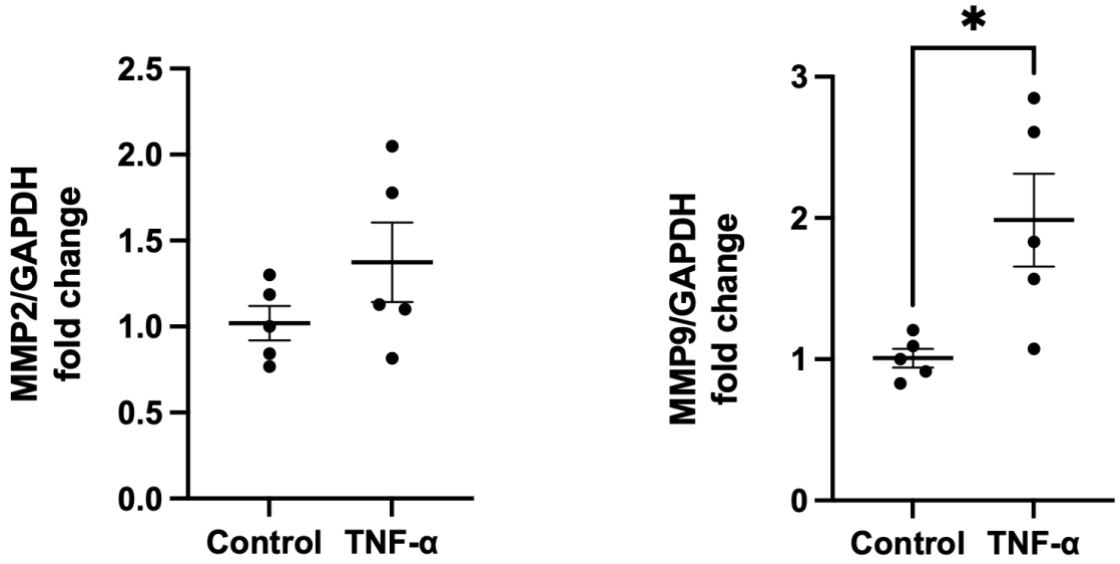

Figure 29. TNF-α causes an upregulation in MMP9 mRNA expression in CMVEC.

*The cells were treated with 10 ng/ml of TNF-α for 6 hours. No significant difference in MMP2 mRNA expression was observed. An increase in MMP9 mRNA expression was found as a result of TNF-α (n=5; *p < 0.05; unpaired t-test).*

4.4.3 TNF-α increases in MMP9 activity in CMVEC

As MMPs need to be activated to cleave the desired substrates, I assessed MMP2 and 9 activity in the conditioned media of the ciCMVEC. I also wanted to confirm the ability of SB-3CT to inhibit MMP2 and 9. ciCMVEC were pre-incubated with 10 μM of SB-3CT for 2 hours prior to TNF-α treatment for 6 hours (and remaining for the duration of treatment). The pre-treatment of ciCMVEC with the inhibitor was to replicate that done previously in glomerular endothelial cells and proved to be effective at reducing MMP activity (213).

No significant difference in MMP2 activity was found in the conditioned media of cells treated with TNF-α when compared to the controls. SB-3CT reduced the MMP2 activity of cells treated with TNF-α below that of the controls. An increase in MMP9 activity was found in the conditioned media of cells treated with TNF-α when compared to the controls. As expected, SB-3CT inhibited the TNF-α induced increase in MMP9 activity (Figure 30).

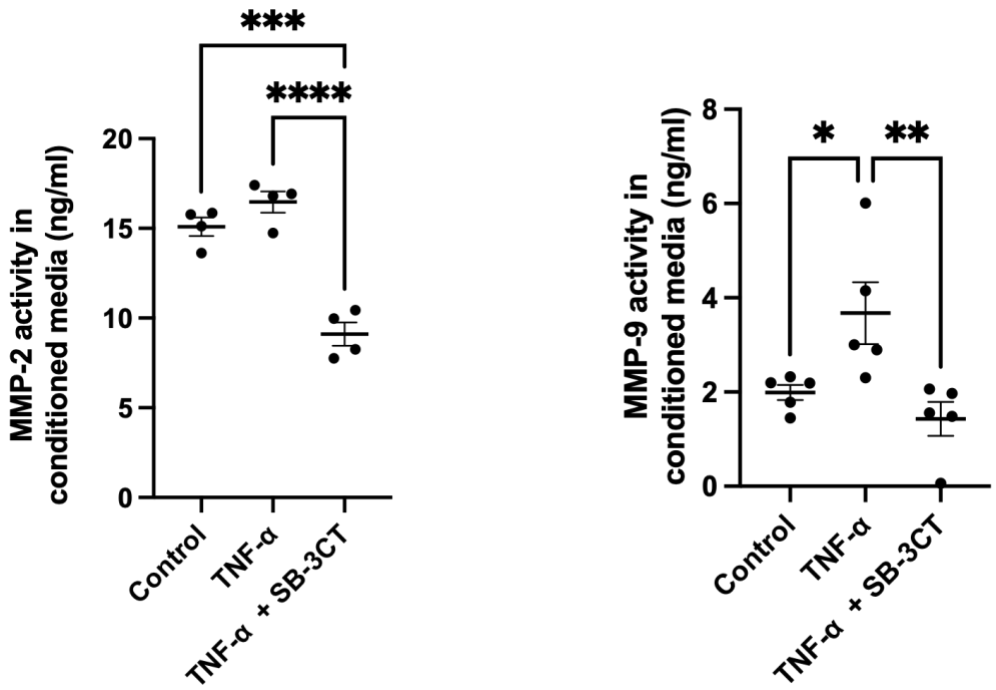

Figure 30. TNF-α increases MMP9 activity from CMVEC.

*Cells were preincubated with SB-3CT (10μM) before being treated with TNF-α for 6 hours. MMP2 and 9 activities were assessed in the conditioned media. No significant difference in MMP2 activity was found between the controls and cells treated with TNF-α. A reduction in MMP2 activity was found in cells treated with SB-3CT (n=4 for all groups; control vs TNF-α + SB-3CT: ***p < 0.001; TNF-α vs TNF-α + SB-3CT: ****p < 0.0001; One-way ANOVA). An increase in MMP9 activity was observed in cells treated with TNF-α and this was reduced when treated with SB-3CT (n=5 for all groups; control vs TNF-α: *p < 0.05; TNF-α vs TNF-α + SB-3CT: **p < 0.01; One-way ANOVA).*

4.4.4 MMP2 and 9 inhibition reduces TNF-α induced SDC4 mRNA upregulation

As mentioned, MMP2 and 9 can cleave SDC4 from endothelial cells (213) and the shedding of SDC4 may stimulate an upregulation in SDC4 mRNA expression potentially through a feedback mechanism. Due to this, I investigated the effect of MMP inhibition on SDC4 mRNA expression. As described, ciCMVEC were pre-incubated with SB-3CT before incubation with TNF-α. As expected, TNF-α caused an increase in SDC4 mRNA expression. This upregulation was reduced when treated with SB-3CT suggesting MMPs play a role in SDC4 mRNA regulation (Figure 31).

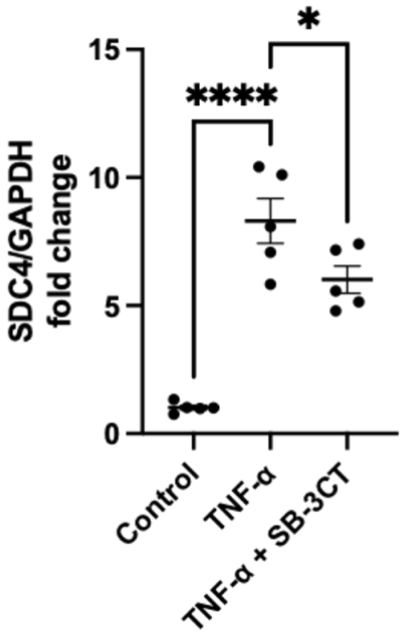

Figure 31. MMP2 and 9 inhibition reduces TNF-α induced SDC4 mRNA upregulation.

*ciCMVEC were preincubated with SB-3CT for 2 hours before being treated with TNF-α for 6 hours. TNF-α caused the upregulation in SDC4 mRNA expression when compared to the controls. This was reduced when treated with SB-3CT (n=5 for all groups; control vs TNF-α: ****p < 0.0001; TNF-α vs TNF-α + SB-3CT: *p < 0.05; One-way ANOVA).*

4.4.5 MMP2 and 9 inhibition prevents SDC4 shedding into the conditioned media

Whilst an upregulation in SDC4 mRNA expression may indicate shedding that alone does not confirm that SDC4 is being shed. Cleaved fragments of SDC4 should be released from the cell surface into the conditioned media. Therefore, a SDC4 ELISA was used to quantify the SDC4 concentration in the conditioned media (Figure 32). When ciCMVEC were treated with TNF-α, an increase in SDC4 concentration was observed in the conditioned media when compared to the controls. This was reduced when treated with SB-3CT suggesting less shedding of SDC4 from the cells.

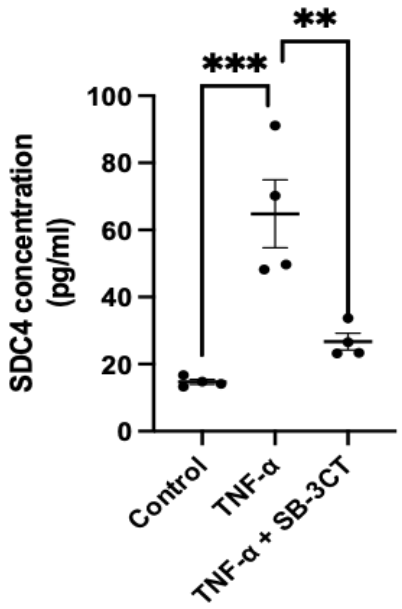

Figure 32. Inhibition of MMP2 and 9 prevents SDC4 shedding into the conditioned media.

*An ELISA was conducted to quantify SDC4 concentration in the conditioned media. An increase in SDC4 concentration was found in the conditioned media of cells treated with TNF-α when compared to the controls. This was reduced when treated with SB-3CT (n=4 for all groups; control vs TNF-α: ***p < 0.001; TNF-α vs TNF-α + SB-3CT: **p < 0.01).*

4.4.6 Inhibition of MMP2 and 9 reduces SDC4 shedding from the cell surface

To confirm the shedding of SDC4 directly from the ciCMVEC, immunofluorescence for SDC4 was conducted. The total fluorescence was determined and normalised to the DAPI number (nuclear staining). As expected, TNF-α resulted in a reduction of SDC4 cell expression suggesting more shedding. Cell SDC4 expression was protected when treated with SB-3CT (Figure 33).

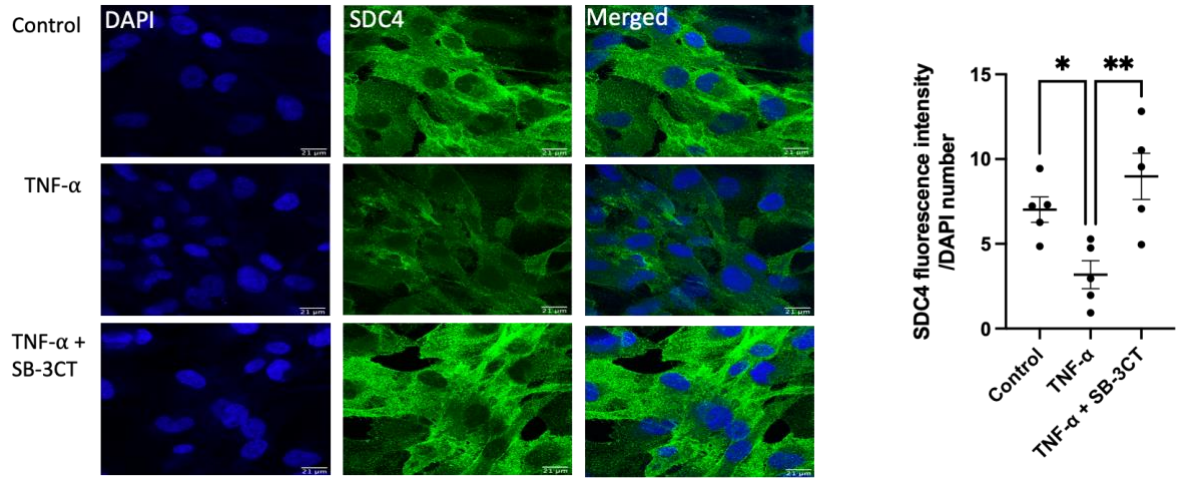

Figure 33. Inhibition of MMP2 and 9 reduces SDC4 shedding from the cell surface.

*Immunofluorescence for SDC4 was carried out on ciCMVEC and the fluorescent intensity for SDC4 was normalised to the number of nuclei indicated by DAPI counterstaining. A significant reduction in SDC4 cell expression was found in the TNF-α group compared to the controls. SDC4 cell expression was protected when treated with SB-3CT (n=5 for all groups; control vs TNF-α: *p < 0.05; TNF-α vs TNF-α + SB-3CT; **p < 0.01; One-way ANOVA).*

4.4.7 MMP2 and 9 inhibition prevents GAG shedding into the conditioned media

Attached to SDC4 are glycosaminoglycans (GAG). Therefore, it would be expected that increased SDC4 shedding into the conditioned media would be accompanied by increased GAG shedding from the EGlx. To confirm this, an Alcian blue assay was conducted on the conditioned media. As expected, treatment of ciCMVEC with TNF-α resulted in a significant increase in GAG concentration in the conditioned media from a mean of 18.27 μg in the controls to 27.7 μg in the TNF-α treated group. This was significantly reduced when treated with SB-3CT to a mean of 13.77 μg (Figure 34).

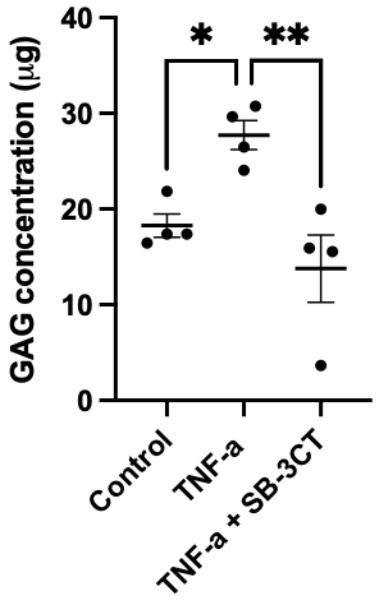

Figure 34. Inhibition of MMP2 and 9 prevents GAG shedding into the conditioned media.

*An Alcian blue assay was conducted on the conditioned media to determine GAG concentration. A significant increase in GAG concentration in the conditioned media was observed in the TNF-α group when compared to the control. Inhibition of MMP2 and 9 with SB-3CT reduced GAG concentration in the conditioned media (n=4 for all groups; control vs TNF-α: *p < 0.05; TNF-α vs TNF-α + SB-3CT: **p < 0.01; One-way ANOVA).*

4.4.8 MMP9 shRNA successfully reduced MMP9 mRNA expression

As an increase in MMP9 activity was found as a result of TNF-α, I decided to specifically investigate the role of MMP9 on SDC4 shedding from ciCMVEC. To do this, shRNA lentiviral particles were used to knock down the expression of MMP9 in ciCMVEC. To confirm the reduction in MMP9 expression, qPCR was conducted. A successful knockdown in the MMP9 mRNA expression by 50% was found between the scrambled control and the shRNA MMP9 treated cells (Figure 35). No significant difference was found between the untreated control and the scrambled control suggesting the scrambled shRNA had no impact on MMP9 expression.

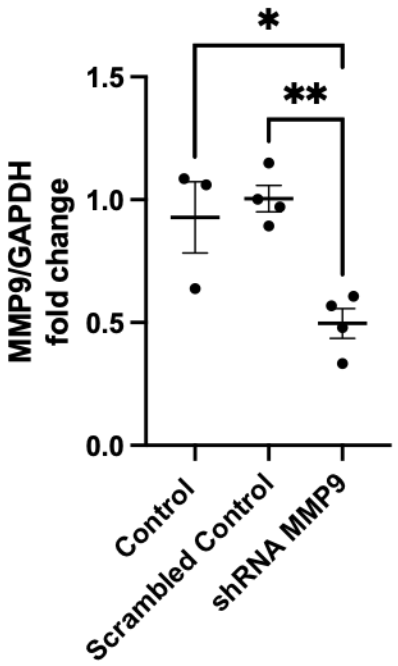

Figure 35. shRNA MMP9 lentiviral particles successfully reduced MMP9 mRNA expression.

*Cells treated with shRNA MMP9 showed reduced MMP9 mRNA expression when compared to the scrambled control. This was also significant when compared to the non-treated control. No difference was recognised between the untreated control and the scrambled control (n=3 for controls, and 4 for the scrambled control and shRNA MMP9; Control vs shRNA MMP9: *p < 0.05; Scrambled Control vs shRNA MMP9: **p < 0.01; One-way ANOVA).*

4.4.9 Knockdown of MMP9 expression reduces TNF-α-induced SDC4 mRNA upregulation

My next task was to determine if the knockdown of MMP9 expression would reduce TNF-α-induced SDC4 shedding from ciCMVEC. As shown in Figure 30, inhibition of MMP2 and 9 with SB-3CT reduced SDC4 mRNA upregulation by TNF-α. Therefore, it is expected that reduced MMP9 expression would also reduce the TNF-α-induced SDC4 mRNA upregulation. As expected, scrambled control cells treated with TNF-α had an increase in SDC4 mRNA expression (4.5-fold) when compared to the controls. Knockdown of MMP9 expression reduced the TNF-α-induced upregulation in SDC4 mRNA to 3.6-fold (Figure 36). No difference was found between the scrambled control and cells infected with shRNA MMP9 alone.

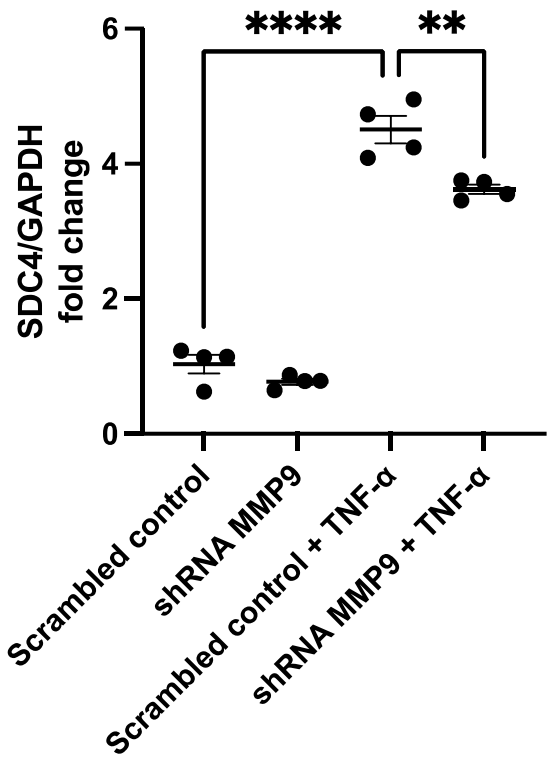

Figure 36. Knockdown of MMP9 expression reduced SDC4 mRNA upregulation from TNF-α. *ciCMVEC were treated with 10 ng/ml of TNF-α for 6 hours. An increase in SDC4 mRNA expression was found between the scrambled control and scrambled control + TNF-α. This was reduced in cells with reduced MMP9 expression (n=4 for all groups; scrambled control vs scrambled control + TNF-α: ****p < 0.0001; scrambled control + TNF-α vs shRNA MMP9 + TNF-α: **p < 0.01; One-way ANOVA).*

4.4.10 Knockdown of MMP9 expression reduces TNF-α induced SDC4 shedding

To further examine the role of MMP9 on SDC4 shedding from ciCMVEC, a SDC4 ELISA was conducted on the conditioned media to quantify SDC4 concentration. As expected, an increase in SDC4 concentration was found in the conditioned media of scrambled control cells treated with TNF-α. This upregulation was decreased as a result of a reduced MMP9 expression (Figure 37).

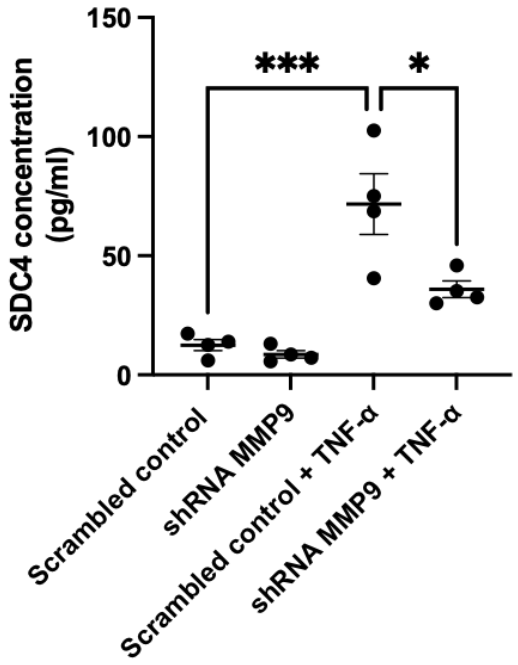

Figure 37. Knockdown of MMP9 expression reduced TNF-α induced SDC4 shedding.

*Cells were treated with TNF-α and a SDC4 ELISA was used to quantify SDC4 concentration in the conditioned media. An increase in SDC4 concentration in the conditioned media was found when cells were treated with TNF-α. This was reduced with a knockdown in MMP9 expression (n=4 for all groups; scrambled control vs scrambled control + TNF-α: ***p < 0.001; scrambled control + TNF-α vs shRNA MMP9 + TNF-α: *p < 0.05; One-way ANOVA).*

4.4.11 MMP9 causes an upregulation in SDC4 mRNA expression

The effect of MMP2 and 9 on SDC4 mRNA expression was further investigated. ciCMVEC were treated with 3 ng/ml of either MMP2 or 9 for 1 hour. Prior to incubation with ciCMVEC, the MMPs were pre-activated with 1 mM of 4−aminophenylmercuric acetate (APMA). As APMA activates all MMPs, some cells were treated with APMA to act as a vehicle control. The results show that APMA leads to an increase in SDC4 mRNA expression when compared to the controls. No significant difference in SDC4 mRNA expression was observed when cells were treated with active MMP2 when compared to the APMA alone treated cells. Treatment of ciCMVEC with active MMP9 upregulated SDC4 mRNA expression when compared to the APMA alone treated cells (Figure 38).

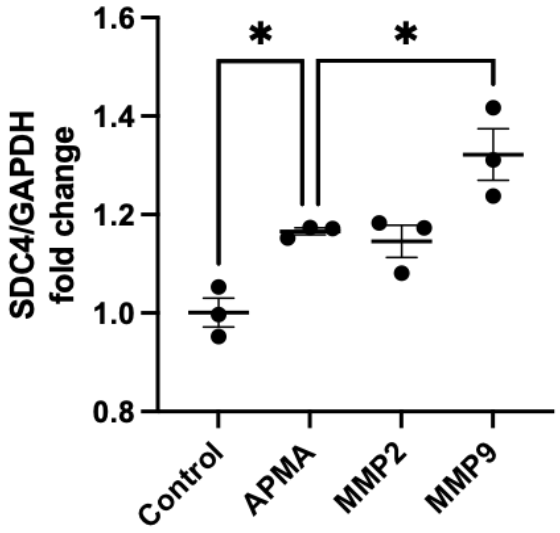

Figure 38. MMP9 causes an upregulation in SDC4 mRNA expression.

*ciCMVEC were treated with either active MMP2 or 9 for 1 hour. As a vehicle control, cells were incubated with APMA (n=3 for all groups; control vs APMA: *p < 0.05; APMA vs MMP9: *p < 0.05; One-way ANOVA).*

4.4.12 Treatment with MMP2 and 9 causes an increase in GAG shedding

Following the incubation of ciCMVEC with active MMP2 or 9 for 1 hour, the conditioned media was taken and an Alcian blue assay was conducted to assess the GAG concentration in the conditioned media. To my surprise, despite no effect of active MMP2 on SDC4 mRNA expression, both MMP2 and MMP9 resulted in an increase in GAG concentration in the conditioned media when compared to the cells treated with APMA alone. No significant difference was found between the APMA alone treated cells when compared to the untreated cells although there was a trend towards an increase to a lesser extent (Figure 39).

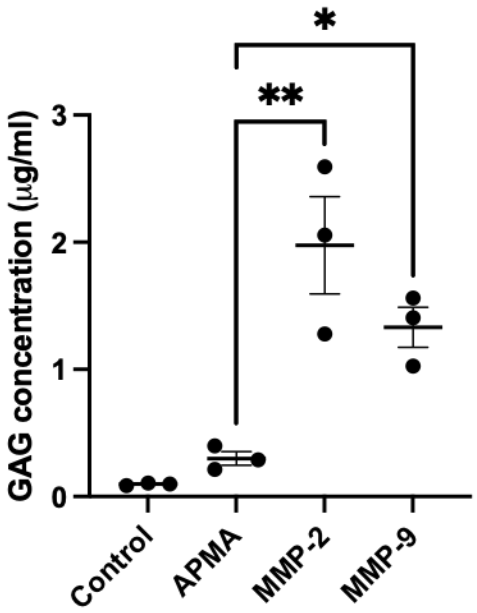

Figure 39. Treatment with MMP2 and 9 causes an increase in GAG shedding.

*An Alcian blue assay was conducted to assess the GAG concentration of the conditioned media after treatment with active MMP2 and 9. An increase in GAG concentration was found after treatment with MMP2 and 9 when compared to the AMPA-alone treated cells (n=3 for all groups; AMPA vs MMP2: **p < 0.01; AMPA vs MMP9; *p < 0.05; One-way ANOVA).*

4.4.13 Knockdown of MMP9 expression reduces heparanase mRNA expression

Heparanase cleaves heparan sulfate side chains from the EGlx and literature has shown a co-regulation of MMP2 and 9 with heparanase, with an increase in heparanase expression and activity being related to an increase in MMP activity (369–371). Based on this, I decided to examine the potential link between MMP9 and heparanase expression in CMVEC. Interestingly the knockdown of MMP9 expression resulted in reduced heparanase mRNA expression also (Figure 40).

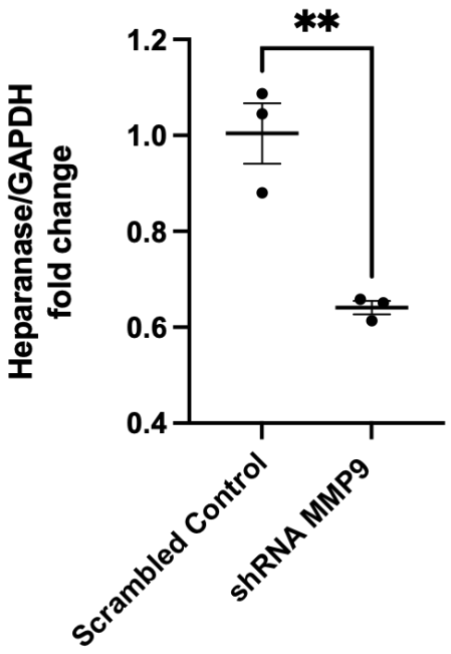

Figure 40. Knockdown of MMP9 expression reduces heparanase mRNA expression.

*The relation between MMP9 expression and heparanase expression was examined. Knockdown of MMP9 expression led to a reduction in heparanase mRNA expression when compared to the controls (n=3 for both groups; **p < 0.01; unpaired t-test).*

4.4.14 MMP9 upregulates heparanase mRNA expression

To further assess the relationship between MMPs and heparanase, the mRNA expression of heparanase was examined after ciCMVEC were treated with active MMP2 and 9. No difference was found between the AMPA-alone treated cells and the untreated controls. As shown in Figure 41, an increased trend in heparanase mRNA expression was found when treated with MMP2 compared to the AMPA control with an average 1.45-fold increase. Treatment with MMP9 significantly upregulated heparanase mRNA expression with an average 1.83-fold increase.

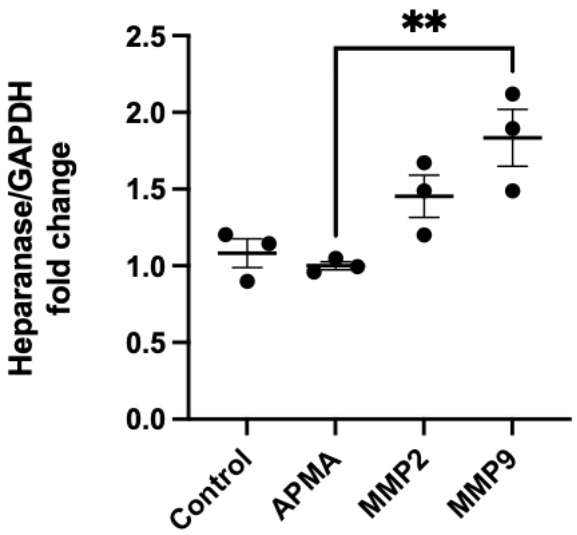

Figure 41. MMP9 upregulates heparanase mRNA expression.

*ciCMVEC were treated with either MMP2 or MMP9 to examine the effect on heparanase mRNA expression. A significant increase in heparanase mRNA expression was found after treatment with MMP9 when compared to the AMPA control (n=3 for all groups; **p < 0.01; One-way ANOVA)*

4.4.15 The coronary microvascular EGlx is important for endothelial barrier function

As mentioned in the introduction, the EGlx regulates vascular permeability. However, to the best of my knowledge, whether the EGlx contributes to CMVEC barrier properties was not yet investigated. Therefore, I wanted to establish if this was the case and also investigate if inhibition of MMP2 and 9 can aid in the protection of endothelial barrier function.

The EGlx plays a role in maintaining endothelial barrier properties and regulating the permeability of albumin across the cell monolayer (27,362). However, to the best of my knowledge, this was not examined in CMVEC until now. To investigate the importance of the EGlx for CMVEC barrier function, the EGlx was stripped using a combination of enzymes (heparanase 1U/ml + hyaluronidase 4.5 U/ml + chondroitinase 100 mU/ml). A transendothelial permeability assay to measure Alexa Fluor 488-BSA passage across the cell monolayer was done over a 3-hour time period. An increase in albumin leak across the cell monolayer was found after 2 hours of treatment with a greater increase in albumin leak being found at 3 hours of enzyme treatment (Figure 42).

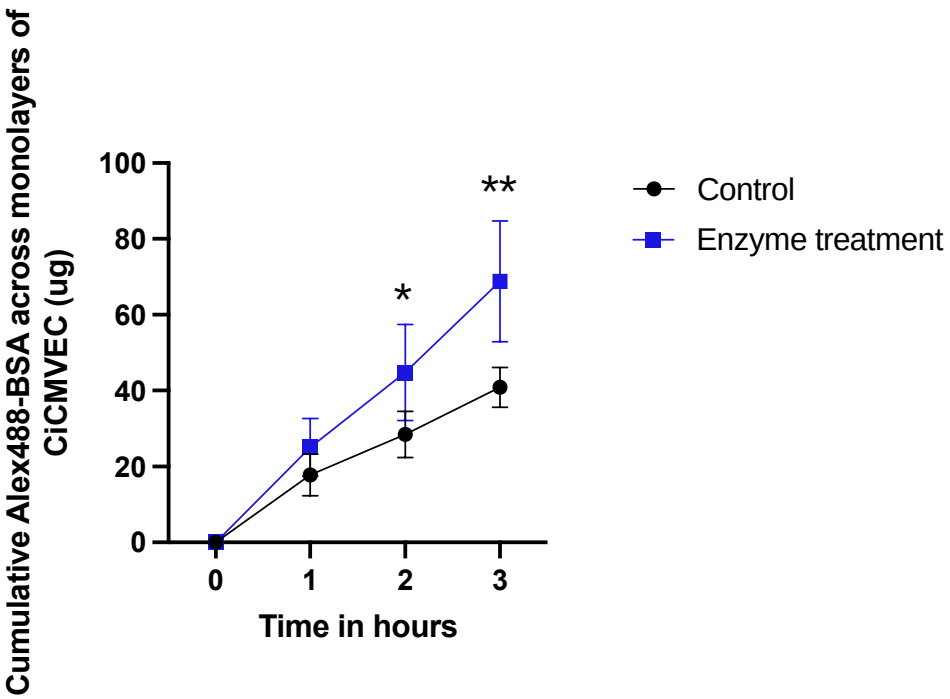

Figure 42. The coronary microvascular EGlx plays is important for endothelial barrier function.

*ciCMVEC were cultured until a confluent monolayer was formed before being subject to enzyme treatment (heparanase 1U/ml + hyaluronidase 4.5 U/ml + chondroitinase 100 mU/ml). Enzymatic treatment enhanced BSA passage across the cell monolayer from 2 hours, further increasing at 3 hours (n=3 both groups; 2 hours: *p < 0.05; 3 hours: **p < 0.01; Two-way ANOVA). This data is published in* (27).

4.4.15.1 Treatment with a combination of GAG enzymes reduced the EGlx

To confirm that treatment with the combination of enzymes as described above caused a reduction in the EGlx, ciCMVEC on inserts were stained with WGA to visualise the EGlx. As shown in Figure 43, treatment with enzymes caused reduced WGA staining suggesting a reduction in the EGlx.

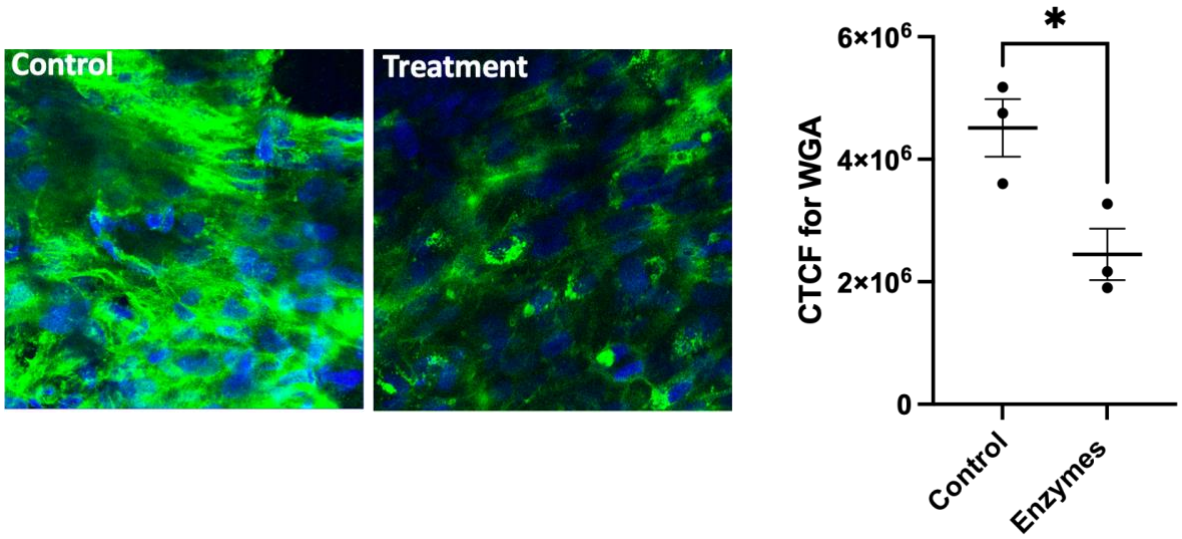

Figure 43. Treatment with a combination of EGlx shedding enzymes reduced the EGlx.

*After treatment with enzymes, ciCMVEC were stained with WGA (green) to provide an indication of the EGlx on the cell surface. Co-staining of the nuclei was done with DAPI (blue). The corrected total cell fluorescence (CTCF) method was used to calculate total WGA fluorescence intensity. Enzymatic treatment caused a reduction in WGA staining indicating a reduced coronary microvascular EGlx (n=3 for all groups; *p < 0.05; paired t-test). This data is published in* (27).

4.4.16 MMP2 and 9 inhibition protects CMVEC barrier function

Having confirmed that the EGlx contributes to CMVEC barrier function, the impact of TNF-α and MMP inhibition was investigated. ciCMVEC were preincubated with SB-3CT for 2 hours before treatment with TNF-α for 6 hours. An increased BSA passage across the cell monolayer was recognised at 6 hours of TNF-α treatment. This increase was reduced when ciCMVEC were treated with SB-3CT (Figure 44).

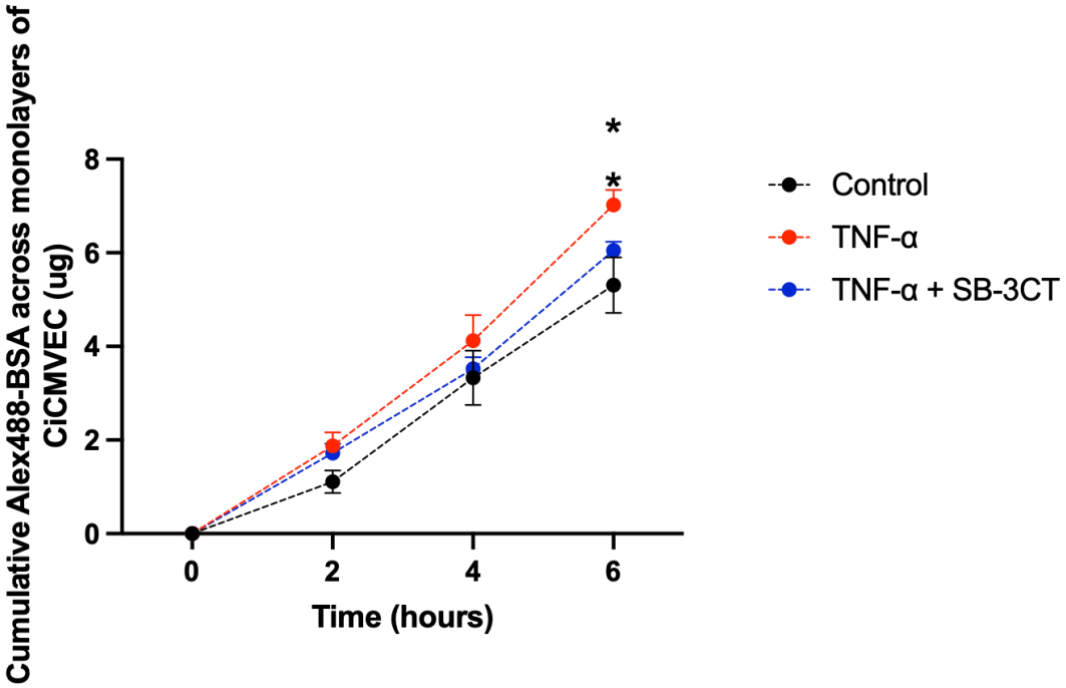

Figure 44. MMP2 and 9 inhibition protects the CMVEC barrier function.

*ciCMVEC were preincubated with SB-3CT before being treated with TNF-α for 6 hours. An increase in BSA passage across the cell monolayer was recognised at 6 hours of TNF-α treatment. This was reduced when treated with SB-3CT (n=3 for all groups; control vs TNF-α: *p < 0.05; TNF-α vs TNF-α + SB-3CT: *P < 0.05; Two-way ANOVA)*

4.5 Discussion

This chapter aimed to investigate if TNF-α causes the shedding of SDC4 from CMVEC through the upregulation of MMP activity. I also aimed to investigate if MMP2 and 9 inhibition with SB-3CT protects the EGlx of CMVEC. Indeed, I have shown that TNF-α causes the shedding of SDC4 by the upregulation of MMP9 activity. Inhibition of MMP2 and 9 with SB-3CT prevents SDC4 shedding from CMVEC. Along with this, the EGlx has been highlighted as important for CMVEC barrier function providing an insight into its functional role within the heart.

4.5.1 The use of TNF-α for investigations

TNF-α is a common proinflammatory cytokine that is increased in diabetic conditions and contributes to several pathological alterations noticed in DCM (125,130). In fact, increased plasma TNF-α has been associated with left ventricular diastolic dysfunction in human patients (372), a characteristic also recognised in animal models of DCM (125). Along with this, TNF-α has been implicated previously to cause damage to the EGlx through the MMP9 mediated shedding of SDC4 in glomerular endothelial cells (213). Therefore I investigated whether this same mechanism of damage to the EGlx occurs at CMVEC. Whilst it may have been more suitable to use a medium with a combination of substances such as high glucose, TNF-α, and insulin, to better reflect the human diabetic state, focusing on specific elements of diabetes allows a better understanding of how each contributes to the pathophysiology. This is important for the development of treatments as it reveals individual therapeutic targets.

4.5.2 TNF-α upregulates MMP9 activity and expression

In this study, there was no upregulation in MMP2 mRNA expression or activity. It appears that MMP2 may not be directly upregulated as a result of TNF-α stimulation and this has been recognised in other endothelial cells such as human cerebral microvascular endothelial cell (297). The lack of MMP2 upregulation as a result of TNF-α is likely due to its transcription regulation sites. The lack of AP-1 results in a reduced effect of cytokines and growth factors on the induction of MMP2 expression (218,232,240).

From this study, it is clear that TNF-α results in an upregulation of MMP9 mRNA expression and activity which supports several studies (213,297–299). MMP9 has been implicated in several cardiovascular complications and higher levels of circulating MMP9 were found in patients with diabetes compared to non-diabetic patients (347).

Inhibition of MMP2 and 9 with SB-3CT occurs in the nanomolar concentrations (Ki = 14 ± 4 nm and Ki = 600 ± 200 nm respectively) (289) and therefore the concentration used in this study is effective. Despite no significant increase in MMP2 activity as a result of TNF-α, treatment with SB-3CT was able to reduce MMP2 activity below that of the controls. Whilst this shows that the inhibitor is effective and working, physiologically reducing MMP2 activity below that of basal levels may have negative effects. In fact, it has been shown in an STZ rat model of DCM that the lack of increase in MMP2 activity may contribute to other pathological mechanisms recognised in DCM such as fibrosis (112). To note, the baseline values for MMP2 activity are high when compared to MMP9. Unlike MMP9, MMP2 is constitutively expressed and a high expression and activity have been shown in endothelial cells (373). Therefore, this was not surprising to observe when assessing the CMVEC MMP activity. Treatment with SB-3CT also successfully inhibited MMP9 activity in the conditioned

media supporting the concentration used in this study. Thus, conclusions drawn from this study can be said to be a result of MMP2 and 9 inhibition. However, the specific contribution of each MMP cannot be deciphered with the use of SB-3CT. In this study, we have started to tease out the contribution of the individual MMPs to the shedding of the EGlx which will be discussed later.

4.5.3 TNF-α upregulates SDC4 mRNA expression

TNF-α upregulated SDC4 mRNA expression in a time-dependent manner. This has also been observed previously in glomerular endothelial cells (213), cardiac fibroblasts, and myocytes (374). TNF-α can upregulate SDC4 mRNA expression independently of MMP activity through transcriptional factors such as NF-kB (375). In a study examining the molecular mechanisms of SDC4 upregulation by TNF-α, it was found that deletion of the NF-kB binding sites on the SDC4 gene significantly reduced the effects of TNF-α (376). Whilst the increased SDC4 mRNA expression tells us that TNF-α is active and having an effect, taken on its own, it does not necessarily mean that this is a result of MMP cleavage of SDC4. However, in this study inhibition of MMP2 and 9 with the inhibitor caused a reduction in the upregulation of SDC4 mRNA when treated with TNF-α. Therefore, it is clear that MMP activity has some role in the regulation of SDC4 mRNA expression.

This study has confirmed the relationship between active MMP9 and SDC4 mRNA expression. When ciCMVEC were treated with active MMP9, SDC4 mRNA expression was increased. This was further confirmed with a knockdown of MMP9 expression, which reduced the upregulation of SDC4 mRNA expression as a result of TNF-α. Therefore, a direct link has now been established between MMP9 and SDC4 mRNA expression. This reflects

previous work in glomerular endothelial cells which also shows that a reduction in MMP9 mRNA expression reduces TNF-α induced SDC4 mRNA upregulation (213). I believe that the MMP9 shedding of SDC4 ectodomains further enhances SDC4 mRNA upregulation by TNF-α. However, whether MMP9 directly induces an effect on SDC4 mRNA expression or if it is a feedback mechanism in response to shedding is yet to be explored.

4.5.4 Inhibition of MMP2 and 9 reduces SDC4 and GAG shedding

To the best of my knowledge, until now there has not been research into the effect of TNF-α on the coronary microvascular EGlx. In this study SDC4 was chosen as a core protein of interest as a direct relationship has previously been established between TNF-α and SDC4 shedding from endothelial cells (213,376). To confirm the shedding of SDC4, I first used an ELISA to assess SDC4 concentration in the conditioned media. It is expected that increased shedding will result in an increased SDC4 concentration in the conditioned media as SDC4 accumulates. This was confirmed as a result of TNF-α and reduced when treated with SB-3CT.

Further support for SDC4 shedding as a result of TNF-α was demonstrated with immunofluorescence. A clear reduction in SDC4 cell surface expression was observed when treated with TNF-α and this was protected when treated with SB-3CT. As CMVEC were pre-incubated with SB-3CT 2 hours prior to TNF-α, this is a preventative protocol. Therefore, it is clear that the inhibition of MMP2 and 9 is protective for the EGlx.

SDC4 cleavage occurs at the ectodomain it has been previously demonstrated that when the ectodomain is cleaved by MMPs, the GAGs are still attached (213). Therefore, it is expected

that the more SDC4 is shed, the more GAGs will also be shed. This is exactly what I have shown with an increase in GAG concentration in the conditioned media being observed as a result of TNF-α. TNF-α can also induce other sheddases such as heparanase (370), which cleave GAG residues. However, the specificity of SB-3CT to MMP2 and 9 provides confidence that the reduction in GAGs found in the conditioned media when treated with the inhibitor is the result of MMP2 and 9 inhibition.

Whilst I would expect to see a reduction in GAG shedding as a result of MMP inhibition, I would not expect to see complete protection from only inhibiting the MMPs. To my surprise, a reduction in GAG shedding back to the levels of the controls was found when treated with SB-3CT. This has led to several speculations. Perhaps there was no upregulation of enzymes that cleave GAGs, or maybe MMP2 and 9 are regulators of EGlx shedding enzymes. I will discuss this further below.

4.5.5 MMP9 is a major sheddase of SDC4

I have shown that MMP9 plays a significant role in shedding SDC4 from CMVEC. As discussed earlier, no increase in MMP2 activity was recognised as a result of TNF-α however, MMP9 mRNA expression and activity were upregulated. This led to further investigations on the role of MMP9 specifically. Examining the SDC4 concentration in the conditioned media showed that when MMP9 expression was knocked down, a protective effect on SDC4 was found to a similar degree as treatment with SB-3CT. MMP9 has been shown to cleave syndecan from various cell types and therefore the results fall in line with the present literature (213,377–379). Whilst I have focused on SDC4 in this chapter, it is important to note that other members of the syndecan family exist in the EGlx such as SDC1. In fact,

it has been shown that MMP9 causes SDC1 shedding from lung EGlx in mice which resulted in tight junction damage and increased permeability and pulmonary oedema (380). Perhaps this is a mechanism of increased permeability that also occurs in the heart as a result of increased MMP9 activity.

However, whilst MMP9 is highlighted as a contributor to EGlx damage, the role of MMP2 cannot be eliminated. Whilst we see no increase in MMP2 activity as a result of TNF-α, the activity of MMP2 is clearly reduced as a result of SB-3CT, which may still supply some protection to the EGlx. No impact on SDC4 mRNA expression was found when CMVEC were treated with active MMP2 suggesting MMP2 may not have a direct role on SDC4 shedding. However, to my surprise, treatment of CMVEC increased GAG shedding. As mentioned earlier, whether the MMPs directly regulate SDC4 mRNA expression or if it is feedback from shedding is not known and as an ELISA or immunofluorescence was not done for SDC4, it cannot be claimed that MMP2 did not cause SDC4 shedding. However, it can be said that MMP2 results in an increase in GAG shedding but the reasons for this remain unknown. Maybe it is due to a cross-regulation with other enzymes such as heparanase as discussed in the previous chapter. Whilst this remains to be explored further, we can be confident in the role of MMP9 in SDC4 shedding based on previous literature and the evidence presented in this chapter.

It is important to recognise that treatment of CMVEC with APMA alone caused an upregulation in SDC4 mRNA expression when compared to the untreated control. As mentioned APMA activates all endogenous MMPs (304) and therefore any latent MMPs including MMP9 would become activated and cause shedding of the EGlx. Others have shown that APMA can cause the shedding of SDC4 from chondrocyte cells by increasing MMP2 and 9 activity (377). This would also explain the slight increase in GAG concentration found within the conditioned media CMVEC treated with APMA

alone. This in itself reinforces that an alteration in MMP activity from physiological levels can cause damage to the EGlx.

4.5.6 There is co-regulation between MMP2 and 9, and heparanase

Although I did not conduct an investigation on the effect of TNF-α on heparanase activity, the literature suggests that TNF-α does upregulate heparanase mRNA expression (370). However, as mentioned, inhibition of MMP2 and 9 was effective at reducing GAG shedding back to the level of the controls suggesting a potential influence of MMP inhibition on other enzymes. This led me to investigate the cross-talk between MMPs and heparanase mRNA expression. I found that reduced MMP9 mRNA expression led to reduced heparanase mRNA expression. This was further supported when cells were treated with MMP9 in which an increase in heparanase mRNA expression was observed. Clearly, there appears to be crosstalk between MMP9 and heparanase which may explain the large positive effect observed when CMVEC were treated with SB-3CT. This is not the first time cross-regulation has been shown. Myeloma cells infected with heparanase shRNA showed reduced MMP9 expression (371). As well as this, the relationship between heparanase and MMP9 has also been established in the heart. Heparanase is largely produced in endothelial cells of the heart and previous research suggests that in diabetes, latent heparanase produced by endothelial cells can be uptaken by cardiomyocytes and activated in the myocyte lysosome. This activated heparanase can enter the nucleus and upregulate the gene expression of MMP9 (381). Ultimately, the co-regulation of both heparanase and MMP9 means that the EGlx could be severely damaged in many ways at the same time. However, it also means that targeting either heparanase or MMP9 may be able to reduce the damage by both. Therefore, there appears to be a direct link between MMP9 and heparanase which research should continue to unravel.

Whilst not significant, a clear trend in the increase in heparanase mRNA expression was observed when cells were treated with MMP2. However, the study is underpowered and increasing the n may prove the results to be significant. An increase in heparanase expression and potential activity would explain why GAG shedding is observed in the absence of SDC4 regulation when CMVEC were treated with active MMP2. Similarly, research also shows co-regulation of heparanase and MMP2 (357) and therefore it may be that whilst we don't see an increase in MMP2 activity as a result of TNF-α, inhibition by SB-3CT still offered some beneficial effects potentially by reducing heparanase. Therefore, MMP2 may not play a direct role in the damage of the coronary microvascular EGlx but may enhance its damage through the regulation of other EGlx degrading enzymes.

4.5.7 The EGlx is vital for endothelial barrier function

To investigate if the EGlx contributes to CMVEC barrier function, I utilised the transwell assay. The transwell assay is a widely used in vitro technique to evaluate the permeability of cellular barriers, such as endothelial monolayers (382–384). The popularity of the use of the transwell assay in vitro is based on its ability to mimic the physiological barrier found in vivo providing a realistic representation of cellular permeability in vitro. However, as with many in vitro assays, the absence of certain physiological cues, such as shear stress or the interaction with other cell types may affect the behaviour of the cell monolayer in the Transwell assay. This can lead to differences in permeability witnessed in vitro compared to in vivo situations. Despite this, the transwell assay proves to be a suitable model to investigate the movement of protein across the cell monolayer in vitro but should be supported further by in vivo studies.

We have shown that the EGlx is crucial for CMVEC barrier function. Stripping of the EGlx resulted in increased albumin leak across the cell monolayer. The increased leak of albumin is indicative of increased permeability which in the heart has detrimental effects. In fact, in rat myocardial capillaries, it was observed that degradation of the EGlx resulted in hyperosmolarity leading to oedema of the heart (385). This was further supported by our group in a mouse model of DCM, showing that reduced coronary microvascular EGlx results in increased microvascular permeability, leading to interstitial oedema and diastolic dysfunction (27). Therefore, the results of this chapter not only fall in line with current literature but highlight a direct functional role of the EGlx for CMVEC.

Stripping of the EGlx using a combination of enzymes did not alter the monolayer cell-cell junctions which remained intact as shown by VE-cadherin staining (27). Therefore, this chapter provides direct evidence that EGlx disruption is enough to increase protein permeability across the monolayer of CMVEC.

The GAGs provide a negative charge to the EGlx which may be vital for its ability to regulate permeability. It has been found that neutralisation of the negative charges can increase the vascular permeability (386). However, whilst it is clear that the EGlx contributes to the CMVEC barrier properties, specifically how it regulates permeability is not completely understood. Therefore, research should continue to unravel the EGlx ability in regulating permeability.

4.5.8 SB-3CT reduced albumin leak across the endothelial cell monolayer

TNF-α caused an increase in albumin leak across the CMVEC monolayer. TNF-α itself can alter the protein and mRNA content of tight junction proteins such as claudin-5, therefore, impacting endothelial barrier properties (387,388). Despite this, a reduction in albumin leak was noticed when treated with SB-3CT. Thus, a link has been established between MMP2 and 9 activity and CVMEC permeability. Previous research has identified a relationship between MMP9 and vascular permeability highlighting the beneficial effect of SB-3CT both in vivo and in vitro. In a mouse vascular permeability model, SB-3CT was able to restore the vascular permeability of cells overexpressing MMP9 (389). This was also confirmed in vitro in which MMP9 increased endothelial permeability and this effect was diminished with SB-3CT (390). Knowing the suggested impact of MMP9 on the EGlx, whilst it may not have been directly mentioned in the study outlined above, it is likely that its overexpression resulted in damage to the EGlx contributing to the alteration in permeability. Therefore, future work should focus on examining the role of the EGlx when investigating permeability and also investigate the role of MMPs in pathologies where an increased vascular permeability is recognized.

4.6 Conclusion

This study has identified a new mechanism of damage to the coronary microvascular EGlx through MMP9-mediated SDC4 shedding as a result of TNF-α. The EGlx is a vital regulator of vascular permeability and in conditions such as DCM, an alteration in permeability can alter the interstitial pressure ultimately leading to diastolic dysfunction. Therefore, the protection of the coronary microvascular EGlx is extremely important. This study directly shows that MMP9 is a target to protect the coronary microvascular EGlx and thus, research should continue to identify and develop MMP-specific inhibitors. Importantly, we have also shown that SB-3CT is effective in preventing EGlx damage. It is therefore necessary to assess the use of SB-3CT in protecting the coronary microvascular EGlx in an animal model of DCM to apply translatability to its use. This will allow us to completely identify MMPs as a therapeutic target to protect the coronary microvascular EGlx and diastolic function in DCM. This will be explored in the next chapter.

Chapter 5: Inhibition of MMPs protects the glycocalyx and diastolic function in a mouse model of diabetic cardiomyopathy

5.1 Introduction

In Chapter 3, the STZ mouse model of type 1 diabetes was used to investigate diabetic cardiomyopathy (DCM) and showed that MMP9 activity was increased in DCM. It was also found that whilst MMP2/9 inhibitor I was able to inhibit plasma MMP9, it was unable to inhibit the MMP activity of the heart. No protection of the EGlx was found when diabetic mice were treated with MMP2/9 inhibitor I as well as no protection of diastolic function. From this, it was determined that inhibition of heart MMP activity was important and so further investigations occurred using a different MMP2 and 9 inhibitor, SB-3CT. In Chapter 4, I investigated the ability of SB-3CT to protect the EGlx and found that SB-3CT was able to prevent TNF-α induced MMP9 shedding of SDC4 in vitro. However, this alone does not prove that SB-3CT can protect the EGlx in DCM.

To arrive at this conclusion, in vivo, testing of SB-3CT is necessary to apply therapeutic value to its use. SB-3CT has been used in several preclinical studies providing confidence in its use. In a type 2 diabetic mouse model through a high-fat diet and STZ injections, an increase in MMP9 protein expression activity was observed. In these mice, SB-3CT was shown to reduce collagen shedding in the skin through the inhibition of MMP9 activity (391). SB-3CT has also been used in a rat model of traumatic brain injury. With its ability to cross the blood-brain barrier, SB-3CT significantly reduced MMP9 protein expression and activity of the brain preventing neuronal apoptosis (392). As mentioned, the inhibition of MMP activity in the heart was not achieved with the previous inhibitor.

From my in vitro data in the previous chapter, as well as literature showing the ability of SB-3CT to inhibit organ MMP activity (392), I found it suitable to investigate the use of SB-3CT to inhibit heart MMP activity in DCM. Therefore, this study aims to identify if SB-3CT can be used to inhibit MMP activity, protect the coronary microvascular EGlx, and restore diastolic function in a mouse model of DCM.

5.1.1 Objectives

Throughout this chapter, there are several questions to be explored.

1. Does SB-3CT inhibit MMP2 and 9 activity in a mouse model of DCM?
2. Does SB-3CT protect the coronary microvascular EGlx?
3. Does inhibition of MMP2 and 9 with SB-3CT restore diastolic function in a mouse model of DCM?

5.2 Methods

Any methods described within this section are specific to this chapter. Methods not described here but used to generate results shown in this chapter are described in ***Chapter 2: Materials and Methods****. I conducted all the work presented in this chapter.*

5.2.1 Type 1 DCM mouse model

Six weeks old FVB mice (FVB/NCrl, Charles River, UK) were injected with multiple doses of STZ to induce diabetes as described in 2.3.1. Mice that did not receive STZ were divided into mice that received either citric acid buffer as vehicle control or did not receive any injection during this time. This was to determine if the citric acid buffer affected heart function. If not, vehicle injection would no longer be necessary and the procedure could be refined for the animals.

5.3.2 Assessing blood glucose and body weight

A baseline blood glucose reading was taken before STZ and blood glucose was monitored at 2, 6, and 9 weeks post STZ. The body weight of mice was recorded weekly until culling.

5.3.3 Treatment with SB-3CT

Two attempts were made to investigate the effect of SB-3CT in DCM.

1. From 7 weeks post STZ, mice were treated with SB-3CT (25mg/kg in 10% DMSO, 90% and corn oil) daily for 3 weeks. The concentration used has been used by others previously and was successful in inhibiting the MMPs (283,393). STZ and control mice were randomly divided to either receive the inhibitor or not leading to four final experimental groups: control, control + SB-3CT, STZ, and STZ + SB-3CT. All mice in the control and STZ groups received the vehicle alone daily.

After two weeks of daily SB-3CT injections, the study ended early due to severe adverse effects. Three of the four diabetic mice receiving the vehicle died as a result of a build-up of abdominal fluid. When an autopsy was conducted, it was noticed that there was a lot more abdominal fluid than normal which was also very oily suggesting a lack of absorption of the corn oil. One control mouse receiving the vehicle also died for the same reason. Another control mouse receiving the inhibitor had to be culled due to an immediate effect after the injection in which the mouse was breathing slowly, dragging its hindlimbs and had puffed-up fur showing clear signs of discomfort. After culling, it was found that the mouse was developing fibrosis around the lungs and the heart. From this point, the study had to end immediately. Culling the remaining mice also revealed a buildup of abdominal fluid. Whilst I was unable to gain any results from this study, it revealed that corn oil may not be a suitable vehicle for long-term injections and therefore has proven useful in informing changes that will enhance the well-being of the animals.

I would also like to add that injections with corn oil are a difficult process due to its viscosity. As it is thick, it is not only difficult to withdraw into the needle for injections, but releasing it is also a slow process requiring steady pressure. This means that the investigator must hold the animal in restraint for a longer period whilst giving the injection. This becomes very distressing for the animals. I suggest

that when given the option to use an alternative vehicle for a compound, it is considered for long-term injections before the use of corn oil.

Modifications were made to the protocol including changes to the vehicle, the length of time the inhibitor was injected, and the concentration of the drug injected as detailed below. The vehicle was changed to another option suggested by the manufacturer. I also lowered the dose of the inhibitor to 10mg/kg to reduce the volume that was to be injected based on previous studies (394,395). As well as this, I decided to shorten the daily injections of SB-3CT to 2 weeks instead of 3 weeks to increase the likelihood of mice surviving to the end of the study. This modified protocol proved more successful in ensuring the mice reached the endpoint of the study as no adverse effects occurred to any of the mice in the modified study.

2. From 7 weeks post STZ, mice were treated with SB-3CT (10mg/kg in 10% DMSO, 40% PEG-300, 5% tween and 45% saline) daily for 2 weeks. STZ mice were randomly divided to either receive the inhibitor or not leading to three final experimental groups: control, STZ, and STZ+ SB-3CT. All mice in the control and STZ groups received the vehicle alone daily. Unfortunately, I was unable to have a control + SB-3CT group due to a shortage in the inhibitor. Therefore, to ensure that there was enough inhibitor for the three main groups, the control + SB-3CT group was omitted.

5.3.4 Echocardiography

Echocardiography was used to assess systolic and diastolic function at 2, 6, and 9 weeks post STZ.

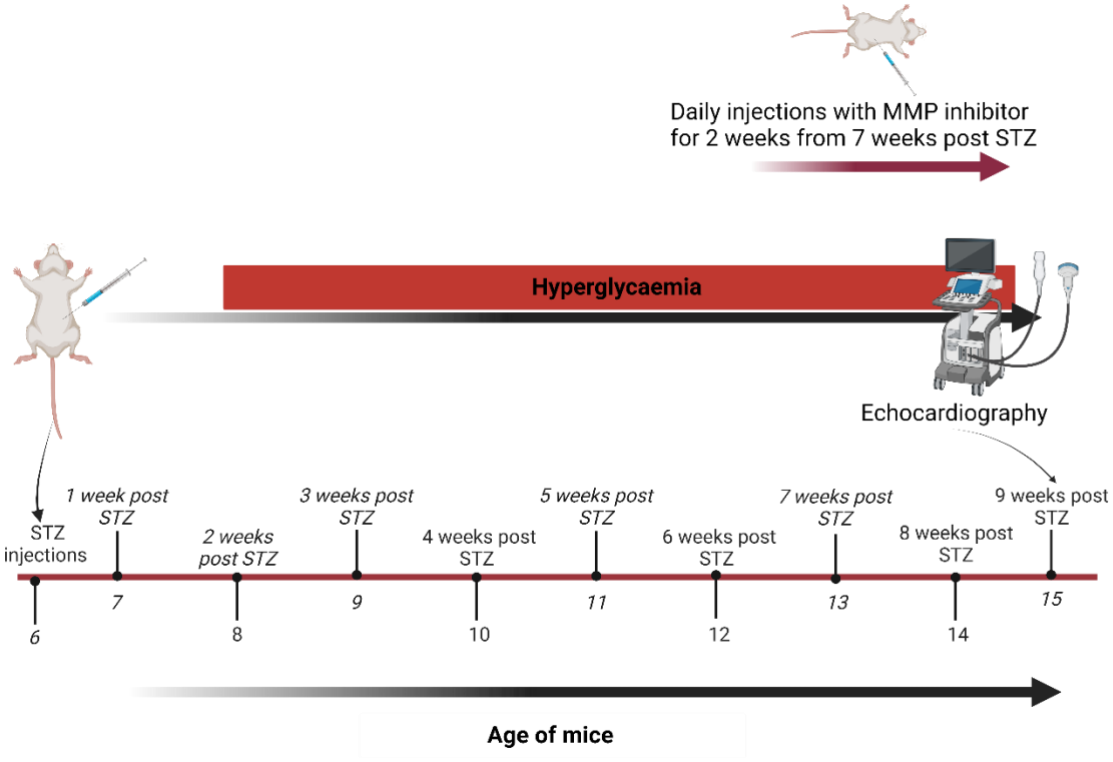

Figure 45. Illustration of the timeline of animal experiments in this chapter.

Initially, mice were randomized to receive either STZ or the vehicle. From 7 weeks post STZ, diabetic mice were randomised again to receive either SB-3CT daily for 2 weeks or the vehicle. Echocardiography was conducted to assess heart function at 2, 6 and 9 weeks post STZ after which the mice were culled. This image was created on Biorender.com

5.3 Results

5.3.1 FVB mice develop hyperglycaemia 2 weeks post STZ

To determine if the mice developed diabetes, blood glucose was assessed after 2 weeks post STZ. Hyperglycaemia was confirmed by blood glucose levels of more than 16mmol/L on two consecutive days as done in previous studies (27,117,118). All mice injected with STZ developed hyperglycaemia by 2 weeks after injections and remained hyperglycaemic for the duration of the study (Figure 46 A). No significant difference in blood glucose was found between the citric acid control and the untreated mice and therefore they were combined to form one control group (Figure 46 B).

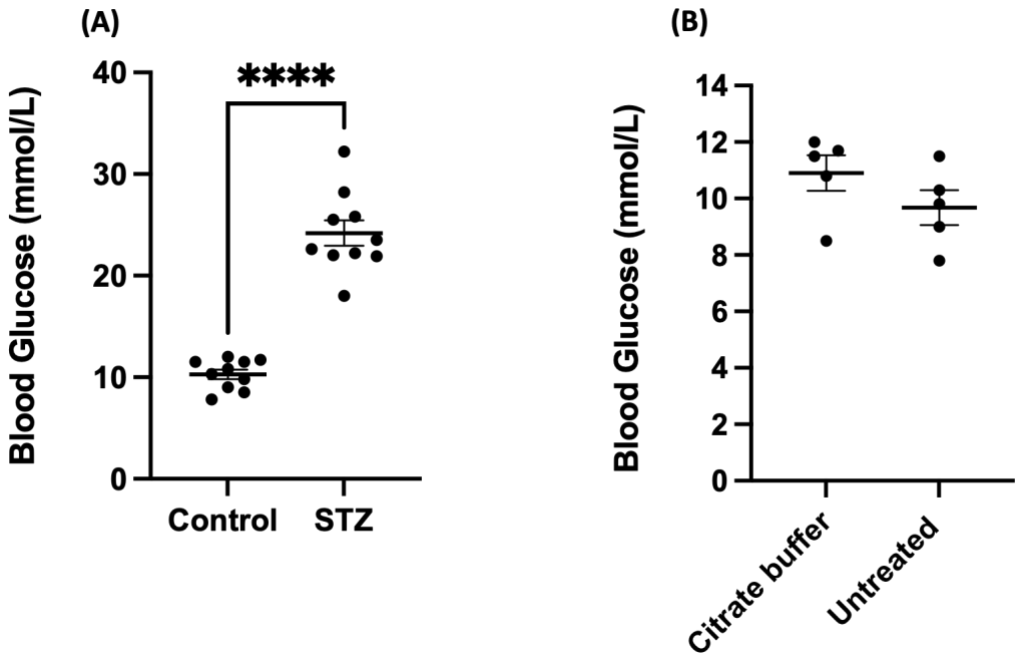

Figure 46. FVB mice develop hyperglycaemia 2 weeks post STZ.

Blood from the tail vein was used to assess blood glucose at 2 weeks post STZ. ***(A)*** *An increase in blood glucose was recognised in all mice injected with STZ when compared to the controls (n=10 for all groups; ****p < 0.0001; Unpaired t-test).* ***(B)*** *No significant difference in blood glucose between control mice treated with citrate buffer vs control mice that did not receive citrate buffer (n=5 for both groups; p = 0.205; Unpaired t-test).*

5.3.2 STZ mice have a reduced body weight

To monitor mouse health, the body weight was measured weekly. All mouse body weight increased over time however, diabetic mice had a significantly lower body weight than control mice from 1 week post STZ and this remained lower than the controls for the duration of the study (Figure 47).

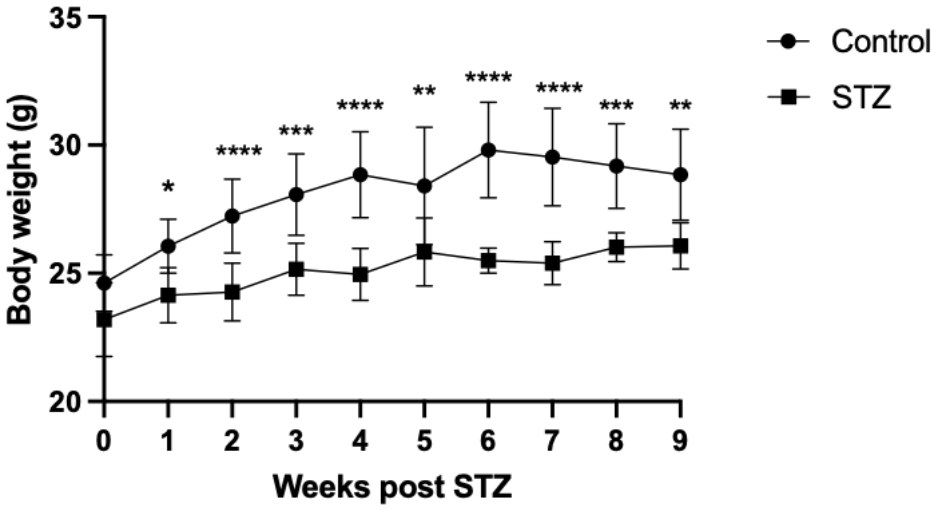

Figure 47. STZ mice have reduced body weight.

*The body weight of the mice was monitored weekly for the duration of the study (n=10 for controls for all weeks, 10 for STZ mice from baseline to 6 weeks post STZ, and 5 for STZ mice from weeks 7-9 post STZ; 1 week post STZ: *p < 0.05; 2, 4, 6, and 7 weeks post-STZ: ****p < 0.0001; 3- and 8 weeks post STZ: ***p < 0.001; 6- and 9-weeks post STZ: **p < 0.01; Two-way ANOVA).*

5.4.3 Heart function 2 weeks post STZ

5.4.3.1 No difference in diastolic function was observed at 2 weeks post STZ

Heart function was assessed by echocardiography, 2 weeks post STZ to assess if the development of diabetes immediately impacted heart function. The E/A and E/E' ratio was used to provide an indication of diastolic function. As expected, no difference was found in both the E/A and E/E' ratio 2 weeks post STZ in diabetic mice compared to the controls (Figure 48 A-B). No difference was found in the E/A ratio and E/E' in mice treated with the citric acid buffer control and untreated mice (Figure 48 C-D) and thus the mice were merged as one control group for the rest of the study.

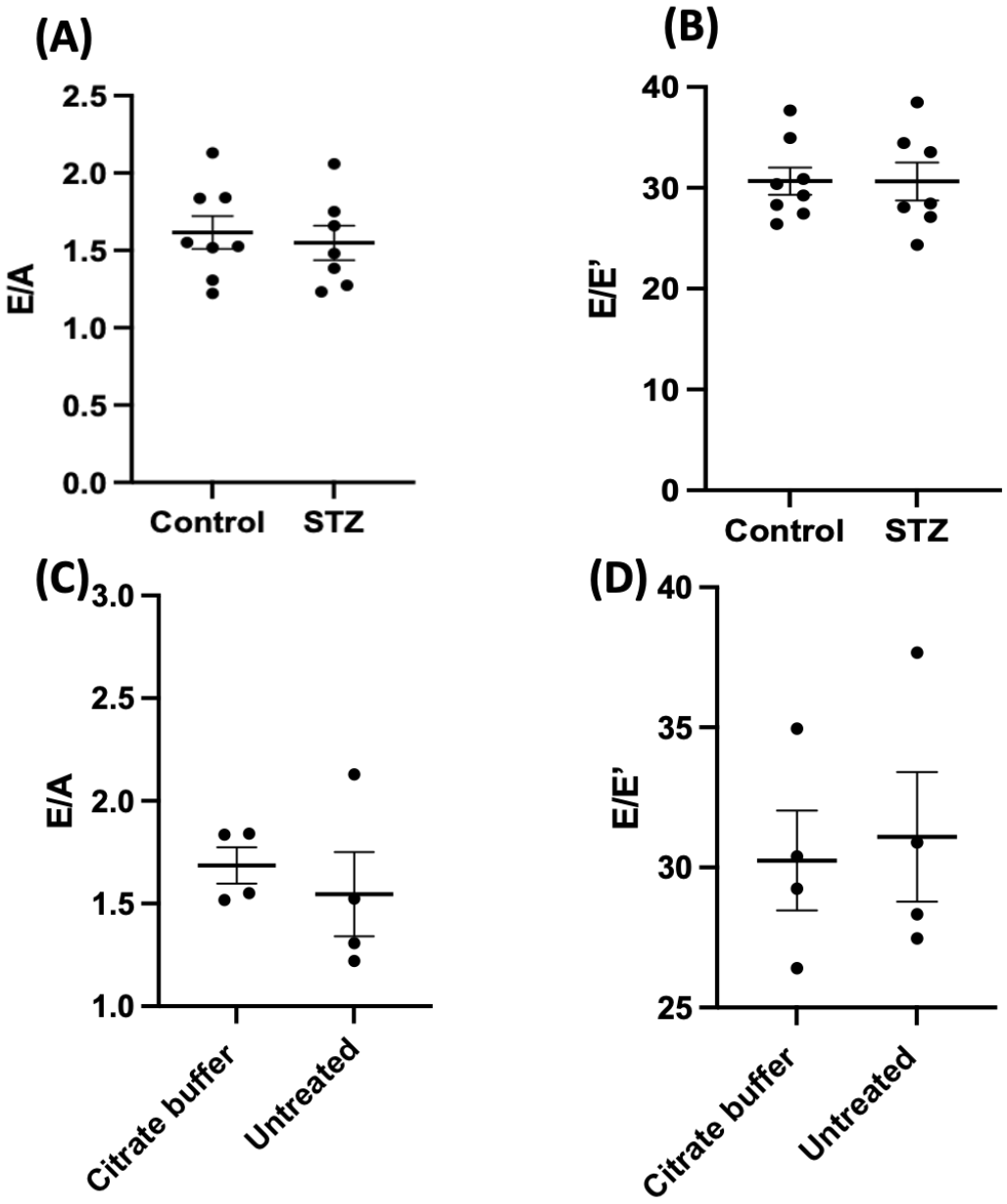

Figure 48. No difference in diastolic function was observed at 2 weeks post STZ.

Echocardiography was conducted to assess the diastolic function of mice. ***(A-B)*** *No difference in the E/A and E/E' ratio was observed between the control group and the STZ mice (n=8 for controls and 7 for STZ mice; E/A: p = 0.67; E/E': p = 0.99; unpaired t-test).* ***(C-D)*** *No difference in diastolic function between control mice injected with citrate buffer and the untreated mice (n=4 for both groups; E/A: p = 0.55; E/E': p = 0.78; unpaired t-test)*

5.4.3.2 No difference in systolic function was observed at 2 weeks post STZ

To provide an indication of systolic function, the cardiac output (CO) and ejection fraction (EF) of the mice were assessed. No significant difference in CO and EF was found between the control and diabetic mice (Figure 49 A-B). No significant difference was also found between mice injected with citric acid buffer and the untreated controls (Figure 49 C-D).

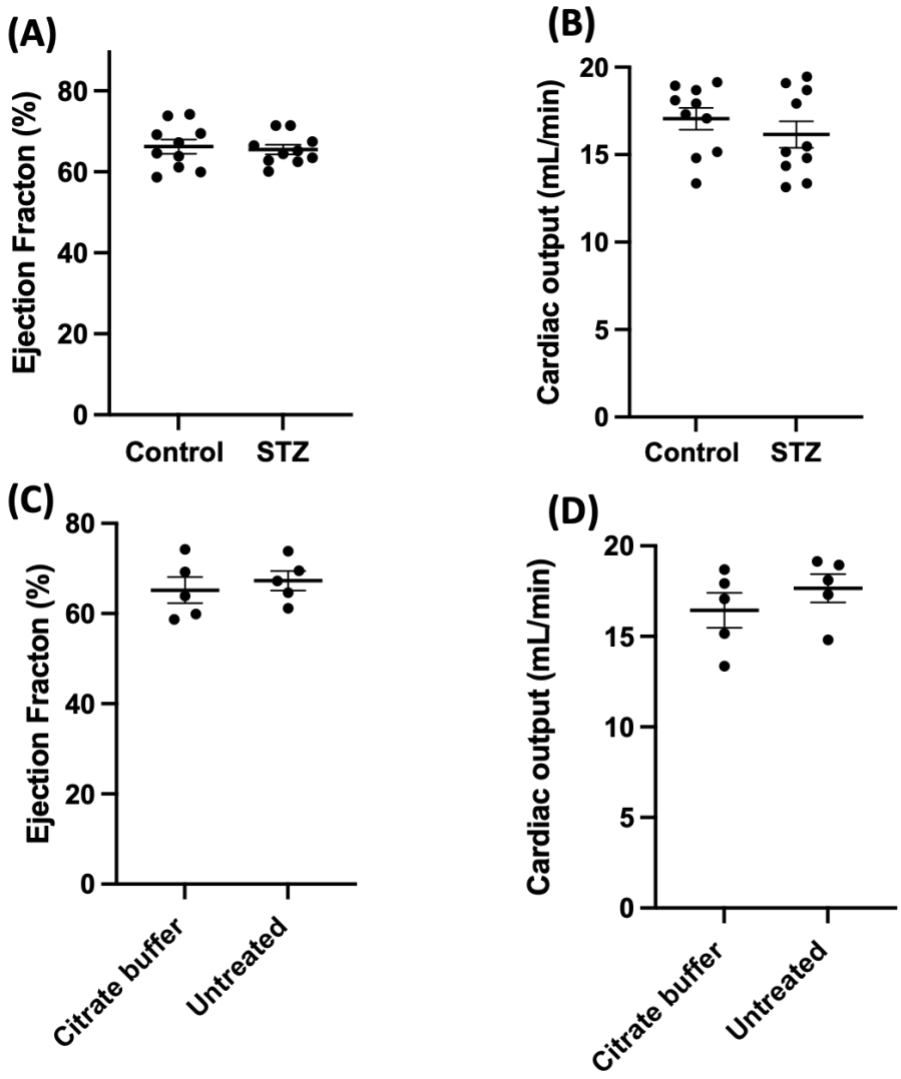

Figure 49. No difference in systolic function was observed at 2 weeks post STZ.

*Echocardiography was utilised to assess the ejection fraction and cardiac output of the mice. (**A-B**) EF and CO in mice treated with STZ compared to controls (n=10 for both groups; EF: p = 0.74; CO: p = 0.37; unpaired t-test). (**C-D**) EF and CO of control mice treated with citrate buffer and control mice that did not receive citrate buffer (n=5 for both groups; EF: p = 0.582; CO: p = 0.357).*

5.4.4 Heart function at 6 weeks post-STZ

5.4.4.1 STZ mice develop diastolic dysfunction 6 weeks post STZ

We have previously seen in this model of DCM that mice begin to develop diastolic dysfunction from 6 weeks post STZ. Therefore, to identify if any changes in heart function occurred as a result of diabetes, echocardiography was done at 6 weeks post STZ.

The E/A ratio, E/E' ratio, isovolumetric relation time (IVRT), and E'/A' were used as parameters to provide an indication of diastolic function. Some parameters are difficult to accurately capture due to inaccuracies in the echocardiographic procedure such as the positioning of the probe. Thus, it is important to measure as many parameters as possible to give a better diagnosis of diastolic function. Therefore as we expect diastolic dysfunction at this time point, I decided to include the additional assessment of IVRT and E'/A'. When compared to controls, diabetic mice showed a reduced E/A ratio and an increased E/E' ratio. Furthermore, an increased IVRT was found in diabetic mice as well as a reduced E'/A' ratio. All measurements indicate diastolic dysfunction in diabetic mice (Figure 50 A-F).

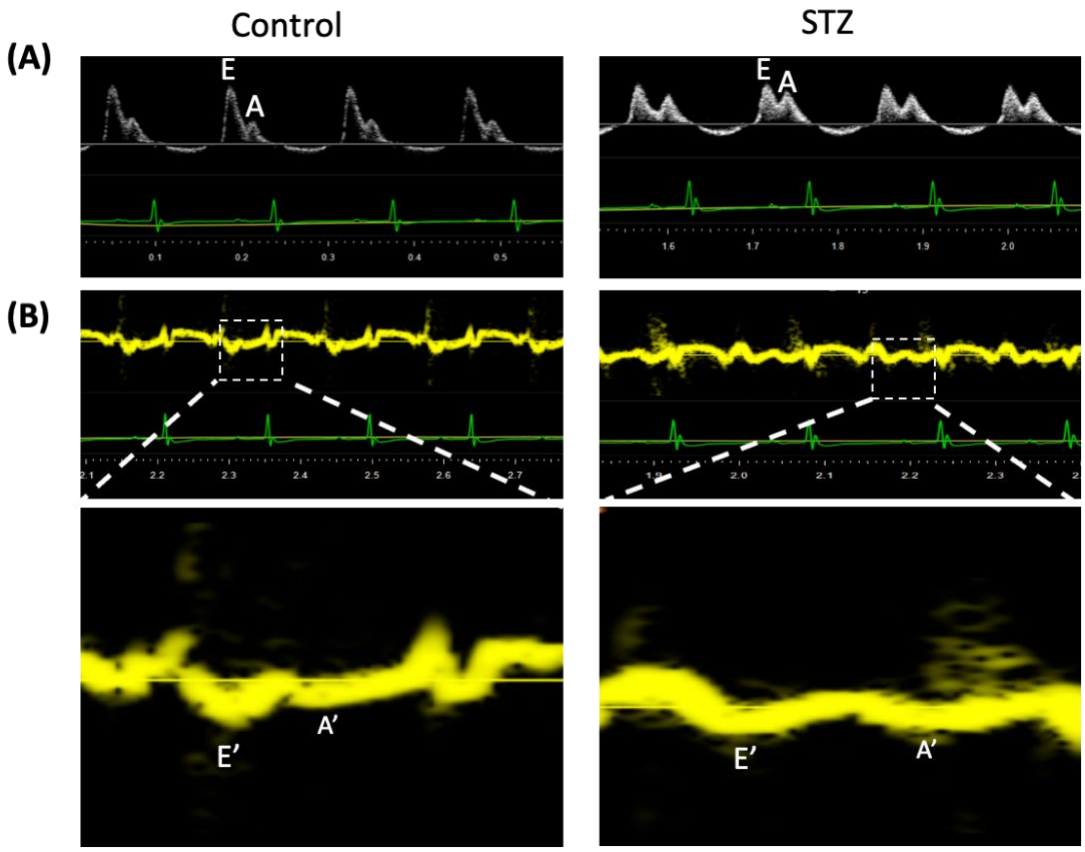
Control
STZ
(A)
E
A
E
A
(B)
A'
E'
E'
A'

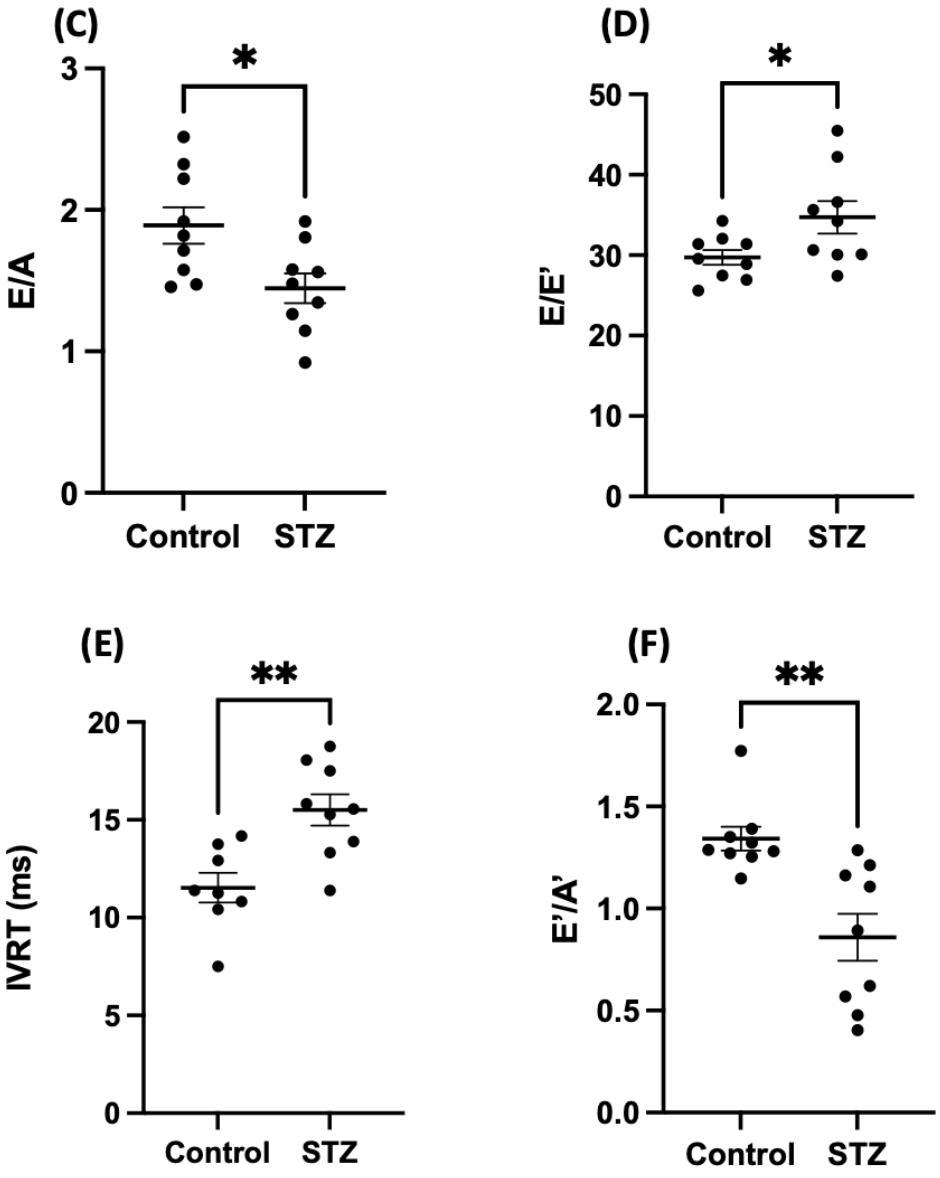

Figure 50. STZ mice develop diastolic dysfunction 6 weeks post STZ.

The E/A, E/E', IVRT and E'/A' were used as parameters to assess diastolic function. ***(A)*** *Representative pulsed wave Doppler images.* ***(B)*** *Representative tissue Doppler images.* ***(C)*** *Reduced E/A ratio in STZ mice (n=9 for control and STZ; *p < 0.05; unpaired t-test).* ***(D)*** *Increased E/E' ratio in STZ mice (n=9 for control and STZ; *p < 0.05; unpaired t-test).* ***(E)*** *Increased IVRT in STZ mice (n=9 for control and STZ; **p < 0.01; unpaired t-test).* ***(F)*** *Reduced E'/A' in STZ mice (n=9 for control and STZs; **p < 0.01; Mann-Whitney test).*

5.4.4.1 There is no change in systolic function at 6 weeks post STZ

To assess systolic function, CO, EF and fractional shortening (FS) were used as parameters. FS is another conventional method used to assess systolic function (396) and refers to the fraction that the left ventricle shortens during the systole. This assessment was added as an extra parameter at this point to further strengthen the confidence in the results of cardiac function. As expected, no significant difference in cardiac output (Figure 51 A), ejection fraction (Figure 51 B), and fractional shortening (Figure 51 C) were found 6 weeks post STZ between control mice and STZ mice.

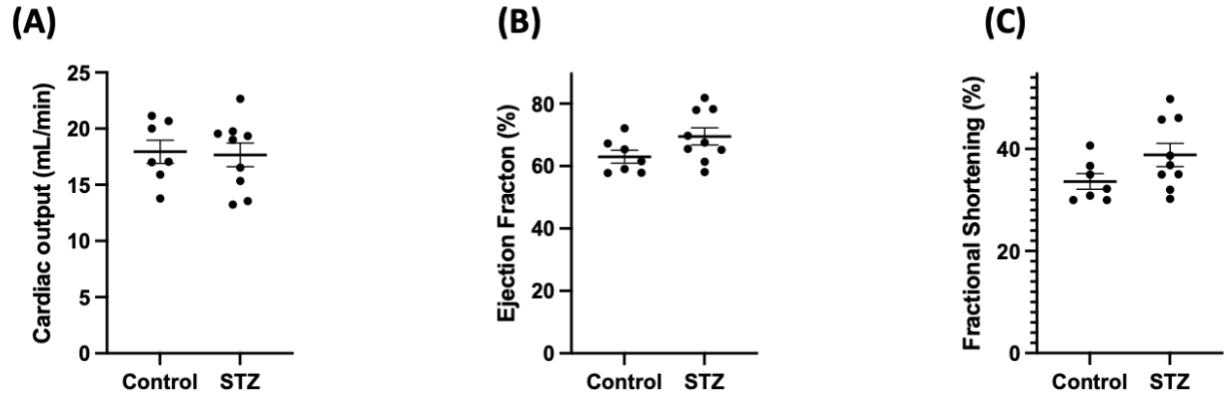

Figure 51.There is no change in systolic function 6 weeks post STZ.

An assessment of systolic function was performed using M-mode. No significant difference in any systolic parameters was recorded between the controls and diabetic mice (n= 7 for control and 9 for STZ for all parameters; CO: p = 0.86; EF: p = 0.091; FS: p = 0.098; unpaired t-test)

5.4.5 Heart function at 9 weeks post-STZ

5.4.5.1 MMP2 and 9 inhibition improves diastolic function in diabetic mice

Echocardiography was carried out at 9 weeks post STZ to assess systolic and diastolic function. To determine if MMP inhibition improves diastolic function, from 7 weeks post STZ, some diabetic mice were treated with SB-3CT daily for 2 weeks. Diastolic dysfunction, indicated by a reduced E/A ratio, increased isovolumetric relaxation time (IVRT) and reduced E'/A', was observed in diabetic mice. When treated with SB-3CT, diastolic function was improved as shown by an increased E/A ratio, reduced IVRT and increased E'/A'. No difference was found in the E/E' ratio between all groups (Figure 52 A-E).

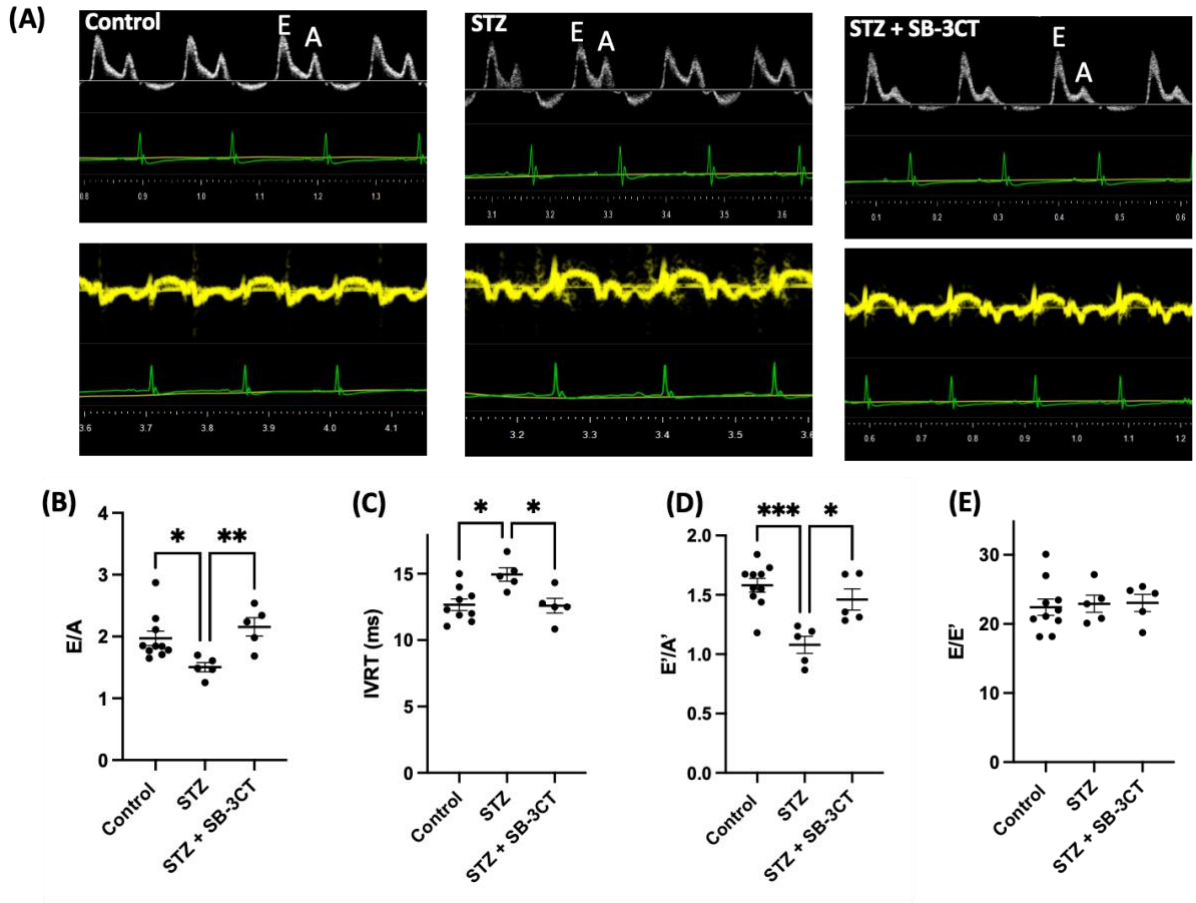

Figure 52. MMP2 and 9 inhibition improves diastolic function in diabetic mice.

Echocardiography was used to assess diastolic function through pulsed wave Doppler and tissue Doppler. ***(A)*** *Representative pulse wave and tissue Doppler images.* ***(B)*** *E/A ratio was determined by pulsed wave Doppler (n=10 for control, 5 for STZ and 5 for STZ + SB-3CT; control vs STZ: *p < 0.05; STZ vs STZ + SB-3CT: **p < 0.01; Kruskal-Wallis test).* ***(C)*** *IVRT determined from pulsed wave Doppler (n=9 for control, 5 for diabetes and 5 for STZ + SB-3CT; control vs STZ: *p < 0.05; STZ vs STZ + SB-3CT: *p < 0.05; One-way ANOVA).* ***(D)*** *E'/A' ratio determined by tissue Doppler (n=10 for control, 5 for STZ and 5 for STZ + SB-3CT; Control vs STZ: ***p < 0.001; STZ vs STZ + SB-3CT: *p < 0.05; One-way ANOVA).* ***(E)*** *No significant difference in E/E' ratio between all groups (n=10 for control, 5 for STZ and 5 for STZ + SB-3CT; control vs STZ: p = 0.96; STZ vs STZ + SB-3CT: p = 0.99; One-way ANOVA).*

5.4.5.2 Diabetic mice do not develop systolic dysfunction 9 weeks post-STZ

M-mode was utilised to assess the systolic function of the heart 9 weeks post-STZ. No significant difference in CO, EF, and FS was found at 9 weeks post STZ in diabetic mice when compared to controls. Similarly, treatment with SB-3CT did not alter systolic function (Figure 53 A-C).

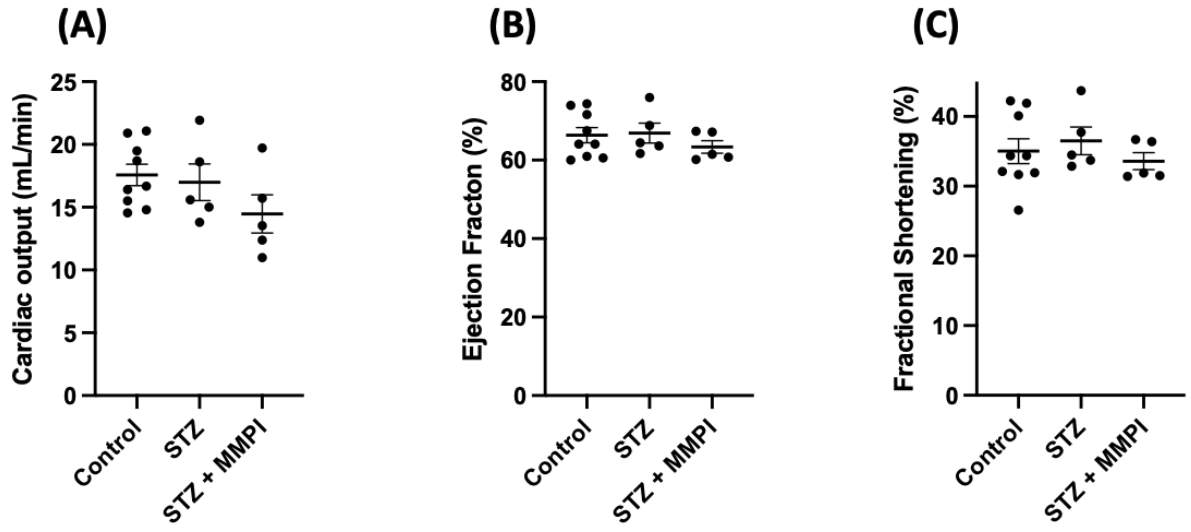

Figure 53. There is no change in systolic function 9 weeks post STZ.

An assessment of systolic function was performed using M-mode. ***(A)*** *Cardiac output of mice.* ***(B)*** *Ejection fraction of mice.* ***(C)*** *Fractional shortening of mice. No significant difference in any systolic parameters was recorded between all groups (n= 9 for control, 5 for STZ and 5 for STZ + SB-3CT; CO: control vs STZ, p = 0.93, STZ vs STZ + SB-3CT, p = 0.4; EF: control vs STZ, p = 0.98, STZ vs STZ + SB-3CT, p = 0.58; FS: control vs STZ p = 0.83, STZ vs STZ + SB-3CT, p = 0.58; One-way ANOVA).*

5.4.6 SB-3CT does not alter blood glucose

To ensure any differences found in this study were a result of MMP inhibition and not a reduction in blood glucose in diabetes, blood glucose levels were assessed at 9 weeks post STZ. As expected, diabetic mice remained hyperglycaemic, and no significant difference in blood glucose levels was found between diabetic mice and diabetic mice treated with SB-3CT (Figure 54).

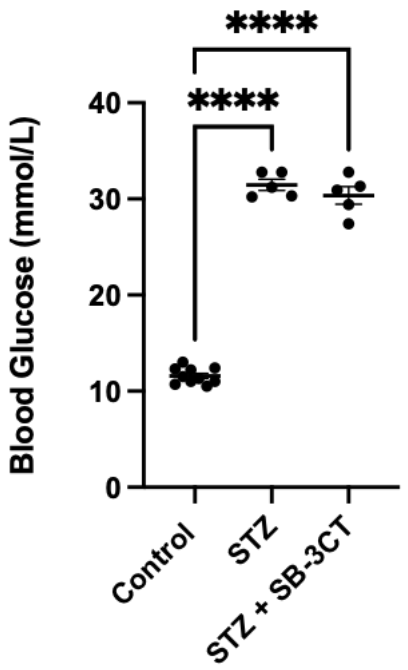

Figure 54. SB-3CT does not alter blood glucose.

*Blood glucose was measured via the tail vein. Diabetic mice had increased blood glucose which was not altered with SB-3CT (n=10 for controls, 5 for STZ and 5 for STZ + SB-3CT; control vs STZ: **** p < 0.0001; control vs STZ + SB-3CT: ****0.0001; STZ vs STZ + SB-3CT: p = 0.4).*

5.4.7 MMP2 and 9 inhibition protects the coronary microvascular EGlx in DCM

To determine EGlx depth, Sambucus Nigra lectin (SNA) was used to bind to the EGlx on paraffin-embedded heart tissue. In Chapter 3 I showed that this lectin was suitable to investigate the EGlx of the heart microvessels in FVB mice, and so I continued using this lectin in this Chapter. This was accompanied by R18 to stain the membrane, allowing the identification of the EGlx on the luminal side of the vessels (Fig 55 A.ii). A measure of EGlx depth was provided using the fluorescent profile peak-to-peak analysis as described in Chapter 2 and shown in Chapter 3. The results show that the EGlx depth was reduced in diabetic mice and this was restored when treated with SB-3CT (Figure 55 B-C). A positive correlation was also found between EGlx depth and E/A ratio (Figure 55 D) indicating that a thicker EGlx is correlated with better diastolic function.

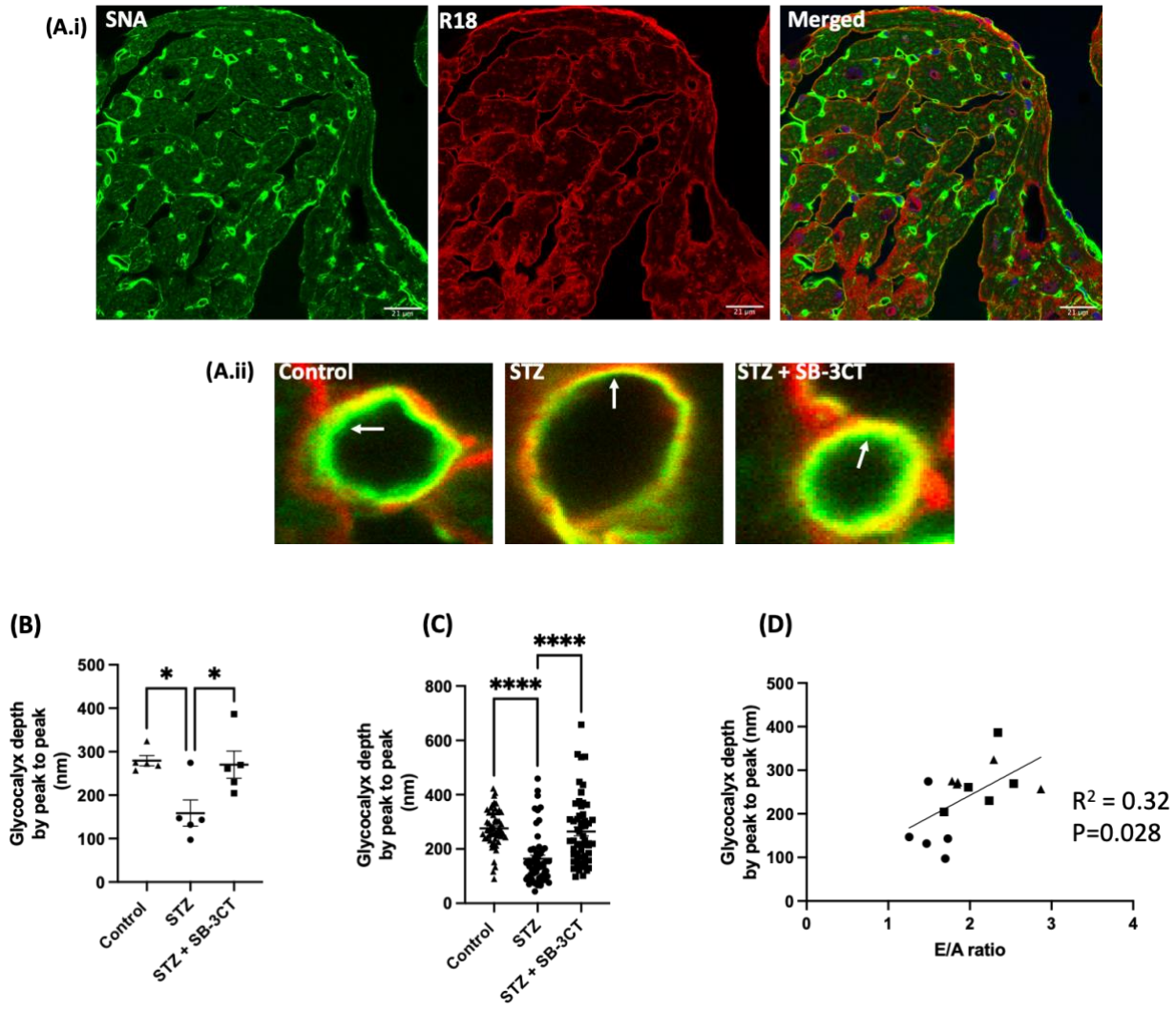

Figure 55. MMP2 and 9 inhibition protects the coronary microvascular EGlx in DCM.

Nine weeks post STZ, mice were cardiac perfused with cadmium chloride to stop the heart at diastole followed by PBS. Paraffin-embedded tissue was sectioned and stained for the EGlx using SNA lectin. ***(A.i)*** *Representative images of heart tissue stained with SNA lectin (green) and the membrane stained with R18 (red). The scale bar is 21 μm.* ***(A.ii)*** *representative image of a vessel stained with SNA lectin and R18. The white arrow points to the EGlx on the luminal side of the vessel.* ***(B)*** *EGlx depth was reduced in diabetic mice compared to controls and this was restored when treated with SB-3CT (n=5 for all groups; *p < 0.05; One-way ANOVA).* ***(C)*** *All the vessels analysed for EGlx depth (****p<0.0001).* ***(D)*** *Coronary microvascular EGlx depth is positively correlated with the E/A ratio (n=15; R^2 = 0.32, *p < 0.05; Pearson r). Triangles represent controls, circles represent STZ, and squares represent STZ + SB-3CT.*

5.4.8 Increased albumin extravasation in diabetic mouse hearts is ameliorated by MMP2 and 9 inhibition

To provide an indication of cardiac microvascular permeability, mouse heart tissue sections were stained for extravasated albumin as described in section 2.4.3. Images of the left ventricle were captured, and the fluorescence intensity was quantified as described in 2.4.3.1. The use of this method provides a non-invasive assessment of cardiac microvascular permeability. Albumin is the most abundant protein in the blood and contributes largely to the plasma oncotic pressure as it does not easily cross the vascular membrane (397,398). Therefore alterations in microvascular protein permeability would cause differences in extravascular albumin content which could be identified by immunofluorescence. Others have shown in the brain and the heart, by immunofluorescence, an increase in albumin extravasation as a result of an alteration in the endothelial tight junction proteins (25,399). In myocardial infarction, an increase in permeability assessed by albumin extravasation is also recognised and correlates with microvessel formation in the infarcted area over time (400). Therefore, this technique is not only a relatively cheap and non-invasive method of assessing changes in microvascular permeability but it can also be applied to disease models. It has previously been shown by electron microscopy, that diabetes causes an increase in capillary permeability to albumin in the diabetic rat myocardium. Therefore I would expect to identify this increase in my diabetic mice.

As expected, in diabetic heart tissue samples, there was an increase in interstitial albumin, indicating increased albumin extravasation due to altered microvascular permeability. This was reduced by SB-3CT treatment. To ensure that the antibody used was specific, sections were stained with goat IgG as a negative control to visually indicate antibody specificity. A vast difference was noticed visually between sections stained with the albumin antibody and sections stained with the matched IgG negative control showing the specificity of the antibody to albumin.

A negative correlation was recognised between the albumin intensity and E/A ratio suggesting increased extravasated albumin is associated with reduced diastolic function. This negative correlation was also found between albumin intensity and EGlx depth suggesting a reduced EGlx depth is associated with increased albumin extravasation (Figure 56).

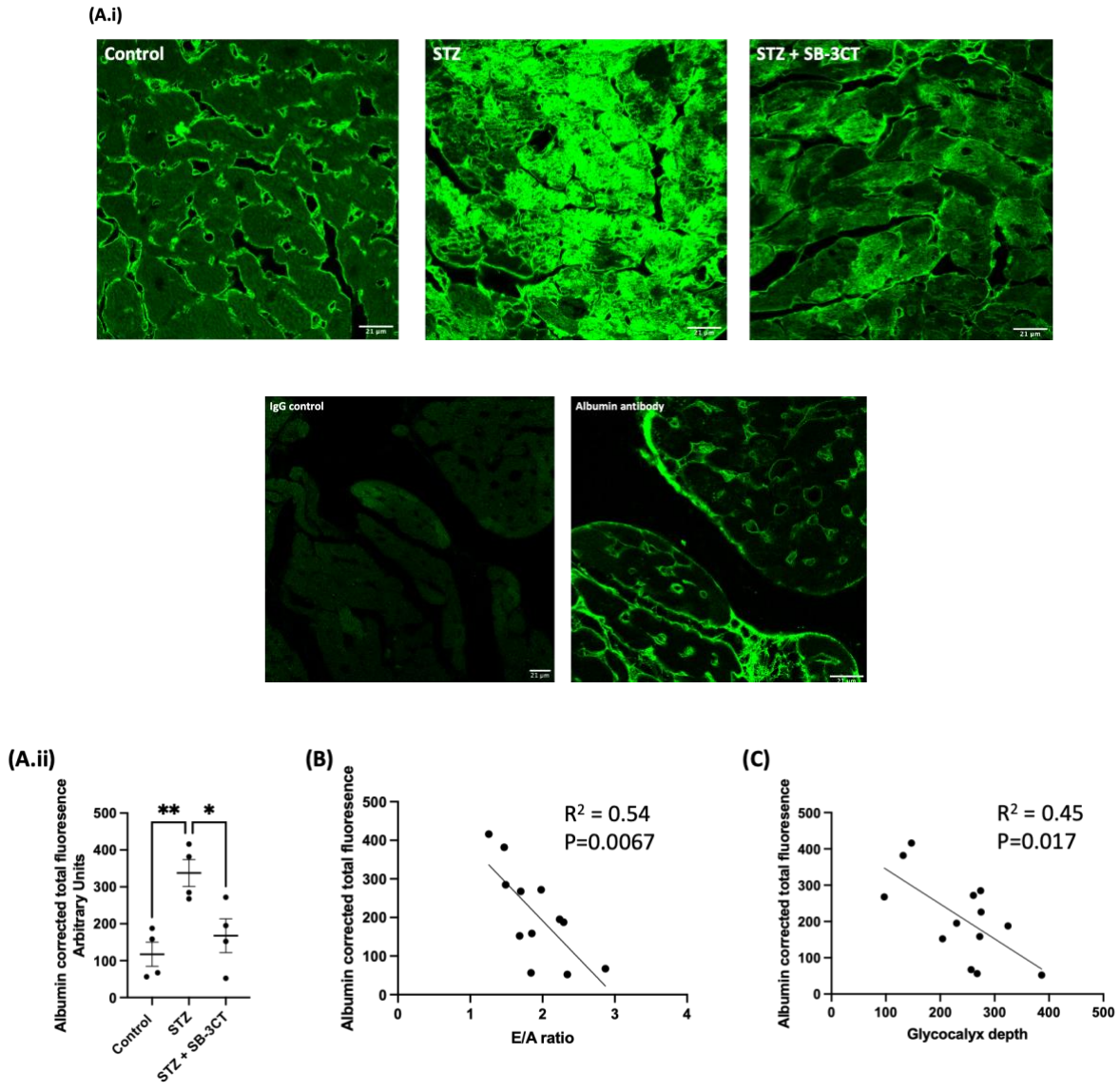

Figure 56. Increased albumin extravasation in diabetic mouse hearts is ameliorated by MMP inhibition.

Immunolabelling for albumin was done in control, STZ and STZ + SB-3CT mouse heart sections. ***(A.i)*** *Representative images of albumin staining in control, STZ and STZ + SB-3CT. The IgG control compared to an albumin-stained section is also shown. Both sections are from the same mouse.* ***(A.ii)*** *Total fluorescence of albumin corrected to the area with the background removed (n=4 for control, STZ and STZ + SB-3CT; Control vs STZ: ** p < 0.01; STZ vs STZ + SB-3CT: *p < 0.05; Ordinary one-way ANOVA).* ***(B)*** *Negative correlation between albumin fluorescent intensity and E/A ratio (n=12; R2=0.54, p**<0.01; Pearson r).* ***(C)*** *Negative correlation between albumin fluorescent intensity and EGlx depth (n=12; R2=0.45, p*<0.05; Pearson r).*

5.4.8 There is no increase in MMP2 activity in FVB diabetic mice

Nine weeks post-STZ, the plasma and left ventricle were collected and MMP activity was assessed. In this study, urine MMP activity was not assessed due to the expense of the kit and time constraints. Despite this, plasma MMP activity is a more suitable representation of circulating MMP activity for this study than urine MMP activity which is largely affected by changes in kidney function (401). No significant difference was found in MMP2 activity between all groups in both the heart tissue and the plasma (Figure 57).

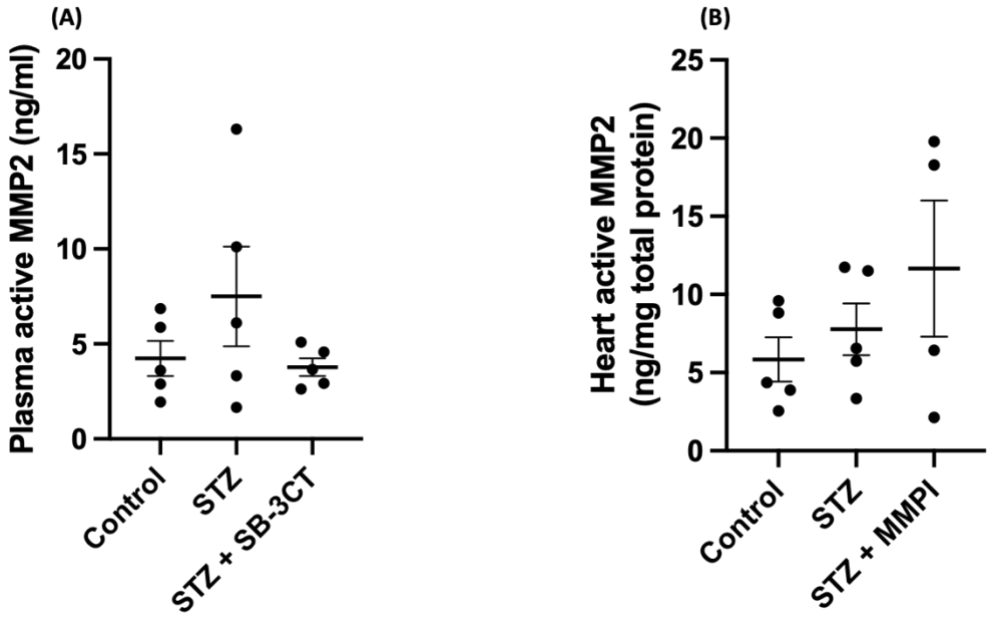

Figure 57. There is no increase in MMP2 activity in FVB diabetic mice.

MMP2 activity was investigated in both the plasma and the heart. ***(A)*** *Plasma MMP2 activity (n=5 for all groups; control vs STZ: p = 0.36; STZ vs STZ + SB-3CT: p = 0.28; One-way ANOVA).* ***(B)*** *Heart MMP2 activity (n=5 for control and STZ and 4 for STZ + SB-3CT; control vs STZ: p = 0.84; STZ vs STZ + SB-3CT: p = 0.55; One-way ANOVA).*

5.4.9 MMP9 activity is increased in diabetes and reduced with SB-3CT

MMP9 activity was also examined in both the plasma and heart tissue. A significant increase in MMP9 activity was found in the heart tissue and plasma and this was reduced when treated with SB-3CT. A negative correlation between both plasma and heart MMP9 activity and EGlx depth was recognized suggesting that increased MMP9 activity is associated with a reduced coronary microvascular EGlx depth. This correlation was also found between MMP9 activity and the E/A ratio showing that increased MMP9 activity is associated with reduced diastolic function (Figure 58).

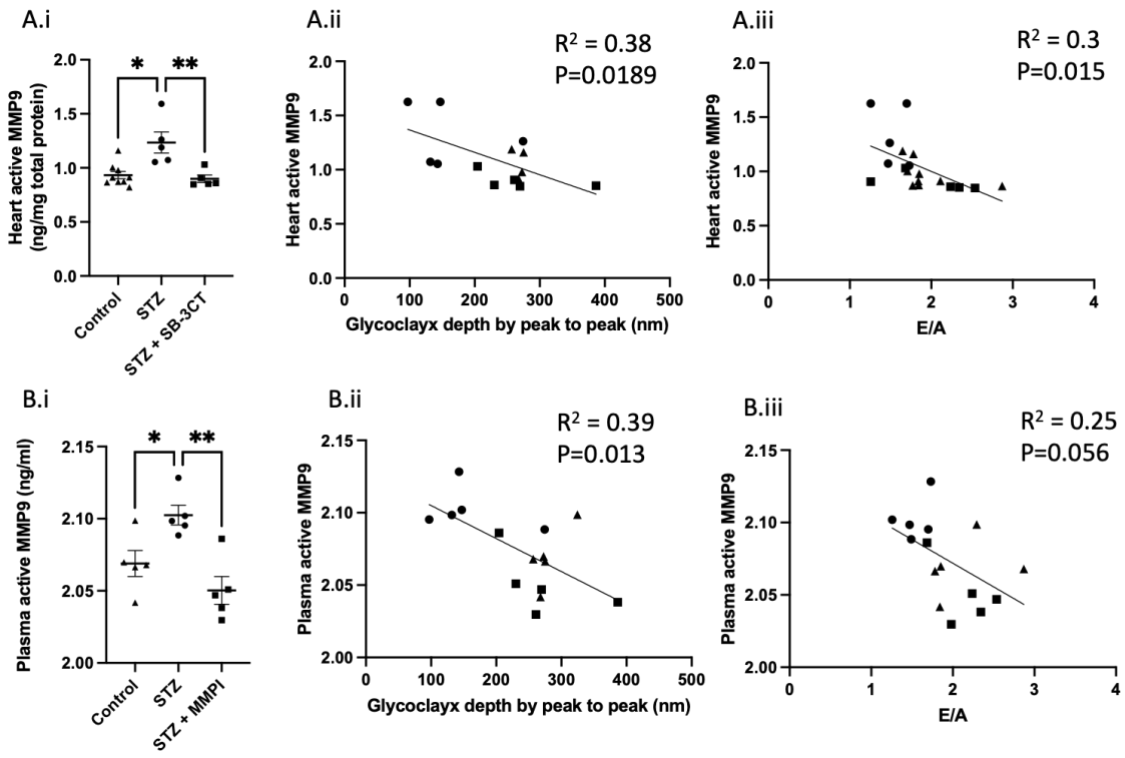

Figure 58. MMP9 activity is increased in diabetes and reduced with SB-3CT.

Nine weeks post STZ, plasma and mouse hearts were collected to assess MMP9 activity. ***(A.i)*** *MMP9 activity in mouse heart tissue 9 weeks post STZ (n=9 for control, 5 for STZ and 5 for STZ + SB-3CT; Control vs STZ, *p<0.05; STZ vs STZ + SB-3CT, **p<0.01; Kruskal-Wallis test).* ***(A.ii)*** *Negative correlation between heart MMP9 activity and heart EGlx depth (n=15; R^2=0.38, p*<0.05; Pearson r).* ***(Aiii)*** *Negative correlation between heart MMP9 activity and E/A ratio (n=19; R^2=0.3, *p<0.05; Pearson r).* ***(B.i)*** *MMP9 activity in mouse plasma 9 weeks post STZ (n=5 for all groups; Control vs STZ, *p<0.05; STZ vs STZ + SB-3CT, **p<0.01; Ordinary one-way ANOVA).* ***(B.ii)*** *Negative correlation between glycocalyx depth and plasma MMP9 activity (n=15; R^2=0.39, *p<0.05; Pearson r).* ***(B.iii)*** *Negative correlation between E/A ratio and MMP9 plasma activity (n=15; R^2=0.33, *p<0.05; Pearson r).*

5.5 Discussion

For the first time, I have shown that the inhibition of MMP2 and 9 protects the coronary microvascular EGlx and restores diastolic function in DCM. This chapter further reinforces that DCM is associated with reduced EGlx depth and increased MMP activity. Similarly, to Chapter 3, an increase in MMP9 activity has specifically been shown in the heart and plasma of diabetic mice. The results of this chapter, highlight the importance of protecting the EGlx in DCM and identify MMP9 as a therapeutic target.

5.5.1 The STZ mouse model of DCM

In Chapter 3, I discussed the value of the STZ mouse model to study DCM (3.4.1) and this chapter provides further support for its use. Similarly to many studies utilising the STZ mouse model of diabetes, hyperglycaemia was recognised 2 weeks post STZ injections which remained for the duration of the study (27,118,126,325,326,361). As well as this a significantly lower mouse body weight was noticed from 1 week post STZ, in diabetic mice compared to controls, a common trait in the human pathology of type 1 diabetes due to insulin resistance. As a model of DCM, both studies have shown consistency in the results demonstrating a reduction in E/A ratio and also a reduction in EGlx depth. This is also consistent with the results of our previous publication (27). Therefore, not only is this model suitable for the investigations of the EGlx and heart function, but I have also demonstrated that the model used in this study is reproducible and reliable.

No change in cardiac function was noticed at 2 weeks post STZ. DCM is a result of prolonged diabetes which leads to various insults to the heart. Therefore, a suitable pre-clinical model must reflect this. As we observe no change in cardiac function at the onset of diabetes, this is more reflective of the human pathology of DCM.

In this model, diastolic dysfunction was present at 6 weeks post STZ with no change in systolic function. In the early phase of DCM (subclinical period), patients present with impaired diastolic function and normal systolic function. As this progresses, patients will eventually develop heart failure with limited ejection fraction (325). The use of echocardiography is widely used clinically to assess diastolic function. Specifically, the E/A ratio and E/E' ratio are used to detect changes in diastolic function. In patients, a reduced E/A ratio is recognised (327,328) along with an increased E/E' ratio before the development of systolic function (331). This is noticed at 6 weeks post STZ and therefore we can be confident that diastolic dysfunction was present in the mice.

Observing diastolic dysfunction before treatment with SB-3CT allows us to identify the inhibition of MMPs as a treatment rather than prevention of DCM. This provides more translatability to this study as clinically patients are diagnosed with DCM before being treated and so this study has therapeutic value. At 9 weeks post STZ, no systolic dysfunction was observed but a reduced E/A ratio along with an increased IVRT was found suggesting diastolic dysfunction. This result is in line with previous studies, which at 10-12 weeks post STZ, do not recognise any changes in systolic function but an increase in IVRT and reduced E/A ratio in diabetes (27,325,326). Therefore, I can be confident in the assessment of heart function due to its consistency between studies. Overall, the results demonstrate that diabetic mice induced by STZ act as a suitable model to study DCM.

5.5.2 Increased MMP9 activity in DCM

I have shown that DCM is associated with an increase in MMP activity. There appears to be a common trend presented throughout this thesis in that an increase in MMP9 is observed. An increase in plasma MMP9 levels has been associated with patients with diastolic dysfunction with a preserved ejection fraction (402). This has also been shown in this study with increased MMP9 activity of both the heart and plasma being correlated with worse diastolic function. A correlation has also been identified between MMP9 activity and EGlx depth suggesting an increase in MMP9 activity is correlated with reduced EGlx depth. Whilst this has previously been identified in the kidney (118), to the best of my knowledge, this is the first time it has been shown in the heart. Thus, specifically targeting MMP9 may be of benefit to protecting cardiac function. From the consistent upregulation of MMP9 in diabetes shown by many studies (117,118,251,251,267,269,403,404) and now its association with DCM, it appears that MMP9 may be a biomarker for cardiac dysfunction. Clinically assessing plasma MMP9 levels may aid in identifying the risk of a patient developing DCM. It may also allow the early identification of those who may be in the subclinical period and ensure early intervention.

No significant difference was found in MMP2 activity in this model of DCM. This is also a trend that appears to be common throughout the thesis. It is important to elucidate the specific role of each MMP to aid in the development of targeted treatments. As MMP2 is constitutively expressed, it may participate in the physiological turnover of the EGlx whilst MMP9 may contribute to the pathological shedding of the EGlx. It is important to recognise that the data presented for MMP2 activity is very spread making it difficult to draw any solid conclusion on changes in MMP2 activity. This may be due to a lack of statistical power due to the sensitivity of the assay in combination with the n used and thus further studies should be done to try and confirm if there are any alterations in MMP2 activity in DCM.

5.5.3 SB-3CT successfully inhibits MMP9

MMP inhibitors tend to fail at clinical trials due to their lack of specificity (279,405). Therefore, it is important for researchers to develop and identify a more targeted approach for specific MMPs to prevent adverse effects. The specificity of SB-3CT is due to the biphenyl moiety fitting in the S1' deep hydrophobic pocket of the gelatinases (283), a region adjacent to the zinc-binding site which shows clear variability among MMPs (288). Inhibition of MMP2 and 9 with SB-3CT occurs in the nanomolar concentrations (Ki = 14 ± 4 nm and Ki = 600 ± 200 nm respectively) and metabolism of SB-3CT in vivo results in a more potent inhibitor, p-hydroxy SB-3CT, (Kis = 6 and 160 nM for MMP2 and MMP9 respectively) (290). A further benefit of SB-3CT is that the reversal of inhibition of MMP2 and 9 occurs slowly with a residence time of 13.4 minutes, which is longer than that of TIMP1 and 2 (7.9 and 6.7 minutes respectively) (406).

In this study, whilst we were unable to see a significant difference in MMP2 activity in diabetes, MMP9 activity was upregulated in both the heart and plasma. This upregulation was reduced back to control levels when treated with SB-3CT suggesting an overall inhibition. In comparison with MMP2/9 inhibitor I, used in Chapter 3, SB-3CT was able to reduce MMP9 activity in the heart tissue which was not observed with the previous inhibitor. The reason for this difference is unclear however a possible explanation is the difference in cell permeability. As the heart is lysed prior to the assessment of MMP activity, both the intracellular and extracellular activity of all cell types of the heart was assessed. I have mentioned in the previous chapters, that intracellular MMP2 and 9 activity has been detected in the cardiomyocytes (349–351). Therefore, as SB-3CT is said to be cell permeable (283), intracellular MMPs could be inhibited by SB-3CT and this would be recognised in the activity assay. Thus, it appears that SB-3CT is an effective inhibitor of MMP9 and may have the potential for clinical use.

However, there are downfalls which may currently limit its progression to clinical trials. SB-3CT is poorly water soluble adding a limitation to its oral use as poorly water-soluble drugs often require high doses to reach therapeutic plasma concentrations after oral administration (407). Other routes can be considered such as subcutaneously, or intramuscularly, however, this may not be a favourable option for patients with diabetes who may already be taking daily insulin injections. Research shows potential in improving the solubility of SB-3CT. Modifications to the SB-3CT compound have been shown to increase its water solubility. These modified compounds become effective inhibitors of MMP9 once hydrolysed in the human blood to a more active form (408). Therefore, there is hope for the future progression of SB-3CT to clinical trials as it has been demonstrated to be effective in inhibiting MMP9 in various preclinical studies (287,290,391,392,408,409) and now I have shown it effective in inhibiting MMP9 in DCM.

5.5.4 Reduced EGlx is associated with increased albumin extravasation

Throughout the thesis, I have reinforced that damage to the coronary microvascular EGlx occurs in DCM and is associated with diastolic dysfunction. We have recently shown that a reduction in the EGlx results in oedema of the heart (27). In this study, an increase in albumin was found in the myocardium suggesting an increase in album extravasation from the blood in diabetes. It is also noted that this increase in albumin was associated with a reduced EGlx depth and diastolic dysfunction. This supports the literature showing that in rats with DCM, enhanced capillary permeability to albumin was found to be markedly increased in the myocardium (410). In the study outlined the heart was perfused with albumin gold complexes in situ and albumin labelling was determined by electron microscopy. However, due to the large dimension of albumin gold complexes, it is not reflective of the monomeric albumin found physiologically in the serum (410). Therefore the changes in the study outlined may not apply to monomeric albumin in diabetes. I have used immunofluorescence for the monomeric

albumin found physiologically and therefore this study provides a more accurate reflection on the changes in albumin permeability in diabetes.

It is not yet clear how exactly the EGlx regulates permeability in the heart. An association has been made previously in patients with elevated plasma levels of syndecan-1 (SDC1) and chondroitin sulfate with severe plasma leakage (411). In this same study, tight junction disruption was also recognised (411). It has been shown that MMP9 causes SDC1 shedding from lung EGlx in mice, resulting in tight junction damage and increased permeability and pulmonary oedema (380). Perhaps this is a mechanism of increased permeability that also occurs in the heart as a result of increased MMP9 activity and EGlx damage. On the other hand, the EGlx is the main determinant of protein permeability and so may not need tight junction damage to result in an increase in permeability. In normal physiology, the EGlx reflects a proportion of albumin molecules back into the vessel lumen ensuring a lower concentration of albumin immediately beneath the EGlx when compared to that of the plasma. An oncotic pressure difference is therefore set up across the EGlx and the interstitium (189). In diabetic rats, an increased binding of albumin to the luminal plasmalemma vesicles was found as well as an increase in the transport of albumin by plasmalemma vesicles across the endothelium of the capillary independently of the intracellular junction (410). It could be that the lack of EGlx in diabetes results in the lack of albumin reflection and so more binding to the plasmalemma vesicles occurs leading to increased transport to the interstitium.

It is important to note that whilst I have shown a correlation between EGlx damage and increased albumin extravasation, I have not directly shown a causal effect. Therefore, with more time, to enhance the results of this chapter I would specifically strip the EGlx of the mouse heart and investigate if there is an increase in albumin leak into the myocardium.

Whilst we focus on the EGlx relationship with altered permeability, shedding of the EGlx may result in various other consequences. In the heart, SDC4 binds to osteopontin protecting it from cleavage. Cleaved osteopontin is known to contribute to fibrotic effects (412,413). Therefore, the shedding of SDC4 removes the protection of osteopontin ultimately enhancing fibrosis. The EGlx has also been associated with microvascular flow; thus, a reduction in EGlx can compromise oxygen delivery and metabolic clearance (343). Therefore, it is clear that the reduced EGlx depth recognised in diabetes, can result in various insults to the heart and so its protection is vital.

5.5.5 Inhibition of MMP9 protects the EGlx in DCM

Complementing the results of the previous chapter, I have shown that SB-3CT can protect the coronary microvascular EGlx in a mouse model of DCM. MMPs are known to cause cleavage of core proteins such as SDC4 from the EGlx, a mechanism of EGlx damage that was highlighted in the previous chapter. Although SDC4 was not directly investigated in this study, it can be inferred that the inhibition of MMPs prevented SDC4 shedding and thus GAG shedding. It is interesting to note that the EGlx was restored to that of the controls similar to what was noticed in vitro. This is despite the expectation that other enzymes that cleave EGlx components should be upregulated as a result of diabetes (203,205,360). Perhaps this is due to the co-regulation of MMPs with other enzymes and thus inhibition could be beneficial for the EGlx both directly and indirectly.

The importance of the EGlx has been identified in its relation to permeability and as mentioned, this chapter shows the correlation between the EGlx and albumin extravasation. The increase in albumin leak was reduced when treated with SB-3CT suggesting protection of coronary microvascular protein permeability. MMP9 is a vital contributor to increased vascular permeability and the benefit of SB-3CT in restoring permeability has been highlighted previously. When immature dendritic cells of

mice were infected with dengue virus, it led to the overproduction of MMP9 from these cells. This resulted in increased endothelial permeability which was reduced by SB-3CT (389). In vitro, endothelial cells overexpressing MMP9 increased endothelial permeability and this effect was diminished when treated with SB-3CT (390). Knowing the suggested impact of MMP9 on the EGlx as highlighted in the kidneys (118) and this study, it is likely that the overexpression of MMP9 resulted in damage to the EGlx and thus contributed to the alteration in permeability. I have provided evidence for the use of SB-3CT to protect the EGlx through the inhibition of MMP9 and supply information on the beneficial effects of inhibiting MMP9 on diastolic function in DCM.

In both this chapter and Chapter 3, I have shown that the EGlx depth correlates with diastolic function and therefore, researchers should no longer ignore the EGlx when investigating the heart but aim to further unravel its role in the heart's physiology.

5.5.6 Inhibition of MMP9 restores diastolic function

The use of the E/A ratio to provide an indication of diastolic function has been widely used in animal models of DCM (27,125,141) and a reduced E/A ratio is recognised in humans with diastolic dysfunction. This has also been shown in this model of DCM. Whilst I was able to detect an increase in the E/E' ratio in the diabetic group at 6 weeks post STZ, unfortunately, I was unable to detect a change at 9 weeks post-STZ. This was because the E' mimicked that of the E wave and thus when the E wave velocity was reduced, the E' also was reduced to a similar degree. Despite this, the evidence for diastolic dysfunction in diabetic mice is strengthened by the increase in IVRT and reduced E'/A' all of which are reversed by the use of SB-3CT. An increased IVRT suggests delayed relaxation of the myocardium and a later valve opening. Combining this measurement with other measurements of diastolic function provides a better understanding of the myocardial relaxation (414). An increased

IVRT has previously been shown in this model of DCM along with a reduced E/A ratio and increased E/E' (27).

The impact of hyperglycaemia on the heart is detrimental resulting in increased ROS, fibrosis, mitochondrial damage and cell death all of which contribute to the pathology of DCM. Treatment with SB-3CT did not impact blood glucose as hyperglycaemia was still observed in the mice. This data, therefore, suggest that the protective effects of SB-3CT on the diabetic heart as well as the EGlx is not dependent on blood glucose but is most likely due to the inhibition of MMPs.

There is therapeutic potential in inhibiting MMPs for the protection of the heart. However, what is not clear is the long-term impact of MMP inhibition as diabetes progresses. Research has shown that DCM is associated with reduced MMP2 activity, contributing to the increase in fibrosis recognised in DCM (112). Therefore, inhibiting MMP2 may have negative effects in the long term and stimulate other pathophysiological mechanisms contributing to DCM. This reinforces the need to identify the roles of each MMP individually and develop more specific inhibitors. It also emphasises the importance of investigating chronic inhibition of MMPs. Regardless, this chapter supplies evidence that MMP9 contributes to diastolic dysfunction and therefore is a therapeutic target for protecting the heart in DCM.

5.6 Conclusion

I have shown that the inhibition of MMP9 with SB-3CT protects the EGlx and restores diastolic function in DCM. MMP9 should now be considered a therapeutic target for DCM. As well as this, evidence has been provided to support the idea that protecting the EGlx is crucial to maintaining normal cardiac function. Research should strive to further unravel how the EGlx regulates permeability in the heart to better understand its functions.

Chapter 6: General Discussion

The role of the EGlx in disease has become of interest to many researchers as it is constantly being revealed to be influential in physiological processes. Similarly, the diverse actions of MMPs have led to them being implicated in many diseases. In this thesis, I aimed to bring together the EGlx and MMPs through the study of DCM. We have previously shown that the EGlx is damaged in DCM and that this contributes to increased coronary microvascular permeability ultimately resulting in oedema and diastolic dysfunction (27). As MMPS are major shedders of the EGlx (specifically MMP2 and 9), my primary aim of this thesis was to inhibit MMP2 and 9 to protect the EGlx in DCM. I can confirm that this aim has been achieved through the studies of the thesis and therefore the conclusion can be drawn that MMPs are a therapeutic target to protect the EGlx in DCM.

6.1 Summary of Objectives and Findings

6.1.1 Main Findings of Chapter 3

In Chapter 3 I reinforced that the coronary microvascular EGlx is damaged in DCM as shown previously in our group (27). Using lectin staining and the peak-to-peak method to quantify EGlx depth, I demonstrated that SNA, MAL-I, and LEL lectins successfully bind to the coronary microvascular EGlx. The results reinforced that the coronary microvascular EGlx depth is reduced in DCM.

Further to this, there was no significant increase in MMP2 activity in the heart, urine and plasma of diabetic mice whilst MMP9 activity was increased. For the first time, I have shown a negative correlation between heart MMP9 activity and coronary microvascular EGlx depth. Therefore, specifically targeting heart MMP9 may be most beneficial to protect the coronary microvascular EGlx.

In this chapter, I investigated the ability of MMP2/9 inhibitor I to protect the coronary microvascular EGlx and improve diastolic function in DCM. Treatment with MMP2/9 inhibitor I did not protect the coronary microvascular EGlx or improve diastolic function in the mouse model of DCM. As well as this, no significant difference in plasma, heart and urine MMP2 activity was found between diabetic mice and diabetic mice treated with MMP2/9 inhibitor I. Surprisingly, the inhibitor was effective in reducing MMP9 activity in the plasma, however, this was not observed in the urine or the heart tissue.

6.1.2 Main Findings of Chapter 4

In Chapter 4, I investigated if inhibition of MMP2 and 9 with SB-3CT would prevent TNF-α induced SDC4 shedding from human CMVEC in vitro. As expected, TNF-α resulted in SDC4 shedding from the CMVEC. As well as this, TNF-α resulted in no significant difference in MMP2 mRNA expression or activity when compared to controls, however, a clear increase in MMP9 mRNA expression and activity was observed supporting the existing literature (213,263,297,299,301). Treatment with SB-3CT inhibited both MMP2 and 9 activity in the conditioned media of the cells and reduced SDC4 and GAG shedding from CMVEC.

To investigate the specific role of MMP9 on SDC4 shedding, MMP9 mRNA expression was knockdown with MMP9 shRNA. This reduced TNF-α induced shedding of SDC4. Further support was supplied by directly treating cells with either MMP2 or 9. It was found that when cells were treated with MMP2, no upregulation in SDC4 mRNA expression was found. However, when treated with MMP9 an increase in SDC4 mRNA expression was identified. This shows that in the absence of TNF-α, MMP9 causes an upregulation in SDC4 mRNA expression. Surprisingly, both MMP2 and 9 caused an increase in GAG shedding. Therefore, chapter 4 not only showed that inhibition of MMP2 and 9 prevents TNF-α induced damaged to the EGlx of CMVEC, but I also began to tease out the individual roles of MMP2 and 9 in damaging the EGlx.

6.1.3 Main Findings of Chapter 5

In Chapter 5, therapeutic application to the use of SB-3CT in DCM was added. Similarly to Chapter 3, an increase in MMP9 activity was observed in both the heart and the plasma of diabetic mice when compared to the controls and this was reduced by SB-3CT. When diabetic mice were treated with SB-3CT, the EGlx was protected and diastolic function was restored as indicated by an increased E/A ratio and reduced IVRT.

Through immunofluorescence for albumin, I have shown that DCM and EGlx damage is correlated with increased albumin extravasation in the hearts suggesting an increase in permeability. SB-3CT reduced albumin extravasation demonstrating a protective effect on vascular permeability. Along with this, I noticed a negative correlation between albumin extravasation and the E/A ratio of the mice suggesting increased albumin extravasation is associated with worse diastolic function.

I can confirm that the aims of this thesis have successfully been achieved and the information presented can be used to enhance the existing knowledge and further the study of the EGlx, MMPs, and DCM.

6.2 Limitations

Whilst this study has successfully explored its aims, there are several limitations that should be noted.

6.2.1 Sex of animals

All animals used in this thesis were male mice. In regard to translatability, gender variations are crucial to consider. There are known gender differences in the diabetic heart such as greater myocardial remodelling in women than in men (415). This has also been shown in the STZ mouse model with a more rapid onset of cardiomyopathy occurring in female mice compared to male mice (416). Therefore, including both males and females in the study would enhance its translatability.

6.2.2 Blood collection from mice

Based upon the boundaries of the animal project licence used in this study, the collection of blood was done as blood flowed out of the mouse's heart. However, this occurred after the heart was perfused with cadmium chloride to stop the heart at diastole. Therefore, the blood sample may not be pure and may have been contaminated with cadmium chloride. Whether cadmium chloride impacts MMP activity has not been tested in this study. However, some studies show that cadmium itself can alter MMP2 and 9 activity (417–419). The blood samples may have also been diluted by the perfusate to varying extents. Therefore, the results of plasma MMP activity should be interpreted with caution.

6.2.3 Measuring MMP activity

In Chapter 3, due to the lack of available MMP2 activity assays, I was unable to increase the n for MMP2 activity. However, with the n used in this study, I was able to detect slight changes in MMP2 activity. Other methods to detect MMP activity are difficult and do not directly show individual MMP activity. A common method utilised in many studies is gelatine zymography (420–423) which identifies MMP activity using sodium dodecyl sulfate (SDS)-polyacrylamide gels co-polymerised with gelatine (424). However various pitfalls arise from gelatine zymography making it difficult sometimes to interpret the results. As the activation of MMPs is a sequential process, it produces inactive intermediate species. Therefore, a lack of good band separation in gelatine zymography can result in the intermediate species being confused for the active species (424). Using a commercially available activity assay kit allowed the direct quantification of specific MMPs by calculating it from the relevant stand curve. This prevents the inclusion of any inactive intermediate MMPs. Also, the use of anti-MMP2 or 9 antibodies in the kits provides further specificity of the assay kits for the MMP of interest.

In Chapter 5, a new MMP2 activity assay kit was used to assess the activity of the heart and plasma. I am not necessarily confident in the sensitivity of the assay due to the wide spread of data within the groups making it difficult to draw any conclusion on changes in MMP2 activity in diabetes and if SB-3CT had any effect. It may be that the antibody used in the kit is not sensitive in detecting mouse MMP2 as it is a human antibody. Unfortunately, the information for the antibody would not be released from the manufacturer but claims that the kit can be used on biological samples in general. Therefore, perhaps a more sensitive assay kit would allow for better conclusions to be drawn on the impact of MMP2.

6.2.4 Lectin staining

As shown in Chapter 4, different lectins produce different information about EGlx depth. This may be due to the chemical configuration of the EGlx with the epitopes for the lectins being at different positions within the EGlx. This in itself could introduce individual bias when deciding which lectin to use to investigate EGlx depth as researchers could proceed with the lectin that shows the greatest difference between experimental groups. Other methods to image the EGlx such as electron microscopy, could be used as supporting data to reinforce what is shown by lectin staining.

Unfortunately, the use of the macro to conduct analysis did not allow the assessment of vessel EGlx coverage but provided an indication of EGlx depth through the peak-peak methods. The coverage and thickness of the EGlx vary between vessels and organs (27,117,118,322,335,425) and so whilst I show a reduced EGlx depth in diabetic mice, whether the effects noticed are due to an altered coverage or strictly due to a change in EGlx depth is not known.

6.2.5 The STZ model of diabetes

Whilst there are benefits to the use of the STZ mouse model such as its reproducibility and disease relevance, there are some limitations to its use. A major pitfall is that it does not accurately represent the insulin-dependent nature of type 1 diabetes in humans. Therefore, it may be difficult to translate the results to patients who take insulin, as the combined effect of both MMP inhibition and insulin therapy is unknown. Another limitation of the STZ mouse model is its rapid onset and severity of disease. Severe hyperglycaemia and beta cell destruction occur relatively rapidly and thus it is difficult to study early-stage disease progression.

6.2.6 Echocardiography

To conduct echocardiography on the mice, they had to be placed under anaesthesia. This is not common for echocardiography in humans as anaesthesia can alter the heart's function (426) and so measurements of heart function do not necessarily show how the heart is behaving in a physiological setting. The mouse's resting heart rate is high (roughly 500 to 700 beats per minute) (427), and measurements of diastolic function are difficult at high heart rates. The use of anaesthesia allowed the slowing of the mouse heart rate which whilst it may not be physiological, allowed certain key diastolic parameters to be assessed such as the E/A ratio. At high heart rates, the E wave and the A wave tend to fuse together and thus gaining an accurate E/A ratio becomes difficult (428).

Other techniques, such as those described in the general introduction, to assess diastolic function should also be considered in research as echocardiography proves to be user dependent, with differences in measurements occurring between researchers. A prime example is shown in this thesis. In Chapter 3, Dr Yan Qiu conducted the echos and was able to show an increase in the E/E' ratio in diabetic mice by the endpoint of the study. However, in Chapter 5, I was unable to identify a significant difference in E/E' ratio between groups. This reinforces the need to use various methods to assess heart function to ensure a more accurate diagnosis. There are other measurements that can be recorded from echocardiography that could provide further confidence in the assessment of diastolic function that was not done in this study. The mitral valve deceleration time is another commonly used parameter to indicate the functioning of the left ventricle. E-wave deceleration time is the rate at which the atrial and ventricular pressures equilibrate. In patients with diastolic dysfunction, the deceleration time is reduced (429).

A further limitation comes from the use of the E/A ratio as the predominant measure of diastolic function. Whilst the assessment of the E/A ratio in cardiology has proven invaluable in diagnosing a range of cardiac conditions and guiding clinical decisions, there are certain limitations and pitfalls associated with this parameter. The E/A ratio can be affected by various factors, including heart rate, loading conditions, and age. As such, it may not always provide a definitive diagnosis on its own. As well as this, identifying pseudonormal filling patterns cannot be distinguished with the E/A ratio. As preload increases, the rise in left atrial pressure can normalise the E velocity, while higher LV end-diastolic pressure tends to expedite the equilibration of the transmitral pressure gradient, thereby shortening the E deceleration time back into the normal range.

Interpreting the E/A ratio also requires careful consideration of the clinical context, as it is just one piece of the puzzle when evaluating diastolic function. Despite these limitations, when used in conjunction with other diagnostic tools and clinical data, the E/A ratio remains a valuable component of the comprehensive evaluation of cardiac function and diastolic performance.

6.2.7 The use of TNF-α in vitro

In my in vitro studies, I investigated the effect of TNF-α on the coronary microvascular EGlx. TNF-α was given for 6 hours and so the results show us the acute effect of TNF-α on the EGlx. However, diabetes results in chronic inflammation (430) and so it would be beneficial to investigate the effect of TNF-α on the EGlx over a longer period.

6.3 Implications of my work

6.3.1 Reducing inflammation to protect the EGlx

In my in vitro study I demonstrated that TNF-α induces SDC4 shedding through the upregulation of MMP9 activity. There are various diseases which are associated with an increase in TNF-α including diabetes (431), rheumatoid arthritis (432), asthma (433) and inflammatory bowel disease (434). Therefore, the EGlx should be assessed in these various conditions and research should strive to understand its role in disease as this reveals further therapeutic targets in inflammatory conditions. Whilst I have not directly shown that TNF-α causes damage to the EGlx specifically in DCM, the implications of the in vitro work suggest that targeting TNF-α directly may have beneficial effects to protect the EGlx and reduce MMP activity. Reducing excessive inflammation should also be a focus of clinicians for patients that present with diabetes through both medication and dietary interventions as this has now been shown to cause damage to the EGlx of several organs (27,213,433,435,436).

6.3.2 Assessing the EGlx in diabetic patients

In this mouse model of DCM, Dr Yan Qiu has shown no fibrosis, a known alteration recognised in DCM, at 10 weeks post STZ (27). It may be that damage to the EGlx is one of the first signs of DCM. Therefore, an assessment of EGlx depth in diabetic patients may identify those that should also be screened for DCM. This may increase patients who are identified in the early phases of DCM, in which symptoms often go unrecognised, ensuring early interventions. A tool used to assess EGlx depth in humans is the GlycoCheck. This non-invasive method estimates the thickness of the EGlx in vessels under the tongue from perfused boundary region (PBR) and microvascular perfusion (red blood cell filling) via a camera and dedicated software (437). However, whether damage to the EGlx occurs at the same time across the body is not known and so this tool may not necessarily suggest

that the coronary microvascular EGlx is damaged. Research should continue to investigate the relationship between the EGlx in different regions of the body to identify a method that can accurately predict EGlx damage in different organs.

6.3.3 Screening for plasma MMPs

Several studies have now shown that MMP9 is upregulated in diabetes and now I have specifically shown that MMP9 is a therapeutic target in DCM. MMP9 screening via a blood test may help to predict the likelihood of certain pathologies such as DCM occurring. However, whilst I have shown an increase in MMP9 activity, I have not shown if this occurs prior to or after the development of DCM. Therefore, research should aim to identify this as it will enhance the likelihood of using circulating MMP activity as a predictor of disease and EGlx damage.

6.3.4 Targeting both heparanase and MMPs at once

I have shown coregulation between heparanase and MMP9 in which reduced MMP9 expression also reduced heparanase expression. Both heparanase and MMP9 are expressed in diabetes and therefore, severe damage to the EGlx can occur. It may be possible to target either MMP9 or heparanase and indirectly target the other. This will prove beneficial not only to protect the EGlx in DCM but also in diseases such as cancer in which both enzymes have been implicated as targets of inhibition (438,439).

6.4 Future work

6.4.1 Investigate if MMP inhibition specifically prevents SDC4 shedding in DCM

In my in vitro work I showed a reduction in CMVEC surface expression of SDC4 as a result of TNF-α and showed that inhibition of MMPs prevented SDC4 shedding. I have therefore identified a mechanism through which the coronary microvascular EGlx is damaged by MMP-mediated SDC4 shedding. We have previously shown in mouse hearts that in DCM, there is a loss of SDC4 at the endothelial cells. Therefore, to enhance the mechanism identified in vitro, the protection of SDC4 as a result of MMP inhibition should be investigated in vivo. This could easily be shown by immunofluorescence for SDC4 on the heart sections from Chapter 5, to identify if there is any protection as a result of MMP inhibition.

6.4.2 Identify how the EGlx contributes to CMVEC barrier properties

As mentioned, whilst I have shown an increase in albumin leak across the CMVEC monolayer as a result of damage to the EGlx, it is not yet understood how this occurs. Research has shown an association between the shedding of syndecans and tight junction disruption (411). Thus, the relationship between the EGlx and tight junctions could therefore be explored further in CMVEC.

6.4.3 The long-term impact of MMP inhibition

The effect of long-term inhibition of MMPs is not yet known. MMPs play a functional role in physiology and are largely involved in the remodelling of the extracellular matrix. In fact, a lack of MMP2 and 9 activities have been implicated in fibrosis of the heart (112). Therefore, longitudinal studies to investigate the impact of MMP inhibition should be conducted as whilst in the short term it may be beneficial, it may have detrimental effects in the long run. As it is difficult to conduct long-

term experiments with the STZ mouse model, due to the severity of the disease, conducting long-term investigations may require the use of a different animal model such as the NOD mouse described in Chapter 1. However, EGlx damage has not yet been characterised in these mice and so this is also required to make an assessment of the impact of long-term MMP inhibition.

6.4.4 Directly assess the role of MMP9 in DCM

MMPs are diverse in action and so the specificity of inhibitors is important. However, to aid in the development of specific treatments, research must continue to unravel the role of each MMP in disease. In this thesis, I have shown that MMP9 appears to play a key role in SDC4 shedding in vitro. To strengthen this, animal models using MMP9 knockdown mice can be used to confirm if MMP9 is a major therapeutic target to protect the EGlx in DCM.

The individual role of MMP2 should also be investigated. Whilst I have initially chosen MMP9 to investigate further as a result of its clear upregulation in diabetes, the specific role of MMP2 on the EGlx is not understood. In vitro, despite no upregulation in MMP2 activity, SB-3CT significantly lowered its activity. This may have been protective for the EGlx. Therefore the exact function of MMP2 in regard to EGlx remodelling should be investigated through knockout mouse models and reduced MMP2 expression in CMVEC as done for MMP9.

6.4.5 Investigate why SB-3CT worked whilst MMP2/9 inhibitor failed to protect the EGlx

Although MMP2/9 inhibitor I was able to inhibit MMPs in the plasma, it did not protect the EGlx. This led to the idea that heart MMP inhibition appeared more important than only inhibiting plasma MMP activity. Future work would aim to explain why SB-3CT was successful whilst MMP 2/9 inhibitor I was not. As mentioned, there are believed to be differences in cell permeability between

the inhibitors in that MMP2/9 inhibitor I is not cell permeable. It is not known if intracellular MMP activity has any effect on damage to the EGlx. Future work would examine if treatment of CMVEC with either inhibitor can inhibit intracellular MMPs or if they only inhibit extracellular MMP activity. It may be that MMP2/9 inhibitor I, inhibits MMP activity in the conditioned media but does not protect the EGlx. This will suggest that inhibition of intracellular MMPs plays a key role in the protection of the CMVEC in which the mechanisms would need to be further explored.

6.4.6 Investigating nonpharmacological methods to inhibit MMPs in diabetes

In diabetes, lifestyle changes play a significant role in preventing disease progression. As I have identified MMP9 as a therapeutic target to protect the coronary microvascular EGlx in DCM, research should now investigate the different ways possible to reduce MMP9 activity in diabetes. Chronic aerobic training has been shown to reduce MMP2 and 9 levels in humans (440) and therefore an exercise programme for patients with diabetes may have protective effects on the EGlx through its ability to reduce MMP activity.

Other investigations include the assessment of the effect of vitamin D on MMP activity. It has been shown in human lung fibroblasts, that vitamin D is able to inhibit MMP9 expression and conversion to its active state. In type 2 diabetic patients, vitamin D deficiency was the sole determinant of circulating MMP9 (inversely). Therefore, the impact of vitamin D on the EGlx should be investigated (441). Exploring these methods would be beneficial as they would provide a relatively cheap option of treatment that can be easily employed by patients.

6.4.7 Progressing SB-3CT to clinical trials

Many inhibitors have progressed to clinical trials and failed, however, there may be hope for the use of SB-3CT due to its success in various preclinical studies (287,290,391,392,408,409). However, it has its downfalls in the fact that it is poorly water soluble (283) limiting its absorption (407) and therefore its progression to clinical trials. Poorly soluble drugs require high doses to reach therapeutic plasma concentrations (407). Therefore, future work should aim to increase its water solubility as this could potentially be a great advancement in MMP inhibitors and stimulate the progression of SB-3CT to clinical trials.

6.4.8 Consideration of tetracyclines

Independent of their antimicrobial actions, tetracyclines are able to inhibit MMP activity of which doxycycline is the most potent inhibitor (292). At sub-antimicrobial doses, tetracyclines are able to chelate the zinc ion altering the activity of MMPs (293,294). Therefore, investigations should occur to determine if doxycycline can protect the EGlx through the inhibition of MMPs. On the other hand, at an antibiotic level doxycycline has been shown to impair mitochondrial function and impaired cardiac contractility in a diabetic mouse model (442). Whilst it is known that tetracyclines can inhibit MMP activity, there is still much to understand in terms of their cellular and molecular effects especially as the effects of the compounds alters drastically with dose. However, as an already clinically licensed drug, it is important that it is tested to protect the EGlx as repurposing the drug makes treatment available faster.

6.5 Conclusion

I hope that throughout this thesis, I have shown that MMPs are a therapeutic target to protect the coronary microvascular EGlx and heart function in DCM. As we learn further about the diverse role of the EGlx we can appreciate its importance more. As well as this, we continue to reveal the role of MMPs in disease and so identifying methods of reducing their activity is of uttermost importance. I hope this study can contribute to advancing research and developing new treatments for DCM.

References

1. Arackal A, Alsayouri K. Histology, Heart. In: StatPearls [Internet]. Treasure Island (FL): StatPearls Publishing; 2022 [cited 2022 Sep 28]. Available from: http://www.ncbi.nlm.nih.gov/books/NBK545143/

2. Rehman I, Nassereddin A, Rehman A. Anatomy, Thorax, Pericardium. In: StatPearls [Internet]. Treasure Island (FL): StatPearls Publishing; 2022 [cited 2022 Sep 28]. Available from: http://www.ncbi.nlm.nih.gov/books/NBK482256/

3. Tran DB, Weber C, Lopez RA. Anatomy, Thorax, Heart Muscles. In: StatPearls [Internet]. Treasure Island (FL): StatPearls Publishing; 2022 [cited 2022 Oct 12]. Available from: http://www.ncbi.nlm.nih.gov/books/NBK545195/

4. Keith A, Flack M. The Form and Nature of the Muscular Connections between the Primary Divisions of the Vertebrate Heart. J Anat Physiol. 1907 Apr;41(Pt 3):172–89.

5. Silverman ME, Hollman A. Discovery of the sinus node by Keith and Flack: on the centennial of their 1907 publication. Heart. 2007 Oct;93(10):1184–7.

6. Padala SK, Cabrera JA, Ellenbogen KA. Anatomy of the cardiac conduction system. Pacing Clin Electrophysiol. 2021;44(1):15–25.

7. Kashou AH, Basit H, Chhabra L. Physiology, Sinoatrial Node. In: StatPearls [Internet]. Treasure Island (FL): StatPearls Publishing; 2022 [cited 2022 Oct 16]. Available from: http://www.ncbi.nlm.nih.gov/books/NBK459238/

8. Heaton J, Goyal A. Atrioventricular Node. In: StatPearls [Internet]. Treasure Island (FL): StatPearls Publishing; 2022 [cited 2022 Oct 31]. Available from: http://www.ncbi.nlm.nih.gov/books/NBK557664/

9. Patra C, Zhang X, Brady MF. Physiology, Bundle of His. In: StatPearls [Internet]. Treasure Island (FL): StatPearls Publishing; 2022 [cited 2023 Mar 8]. Available from: http://www.ncbi.nlm.nih.gov/books/NBK531498/

10. Dun W, Boyden PA. The Purkinje cell; 2008 style. J Mol Cell Cardiol. 2008 Nov;45(5):617–24.

11. Kitmitto A, Baudoin F, Cartwright EJ. Cardiomyocyte damage control in heart failure and the role of the sarcolemma. J Muscle Res Cell Motil. 2019;40(3):319–33.

12. Eisner DA, Caldwell JL, Kistamás K, Trafford AW. Calcium and Excitation-Contraction Coupling in the Heart. Circ Res. 2017 Jul 7;121(2):181–95.

13. Asp ML, Martindale JJ, Heinis FI, Wang W, Metzger JM. Calcium mishandling in diastolic dysfunction: mechanisms and potential therapies. Biochim Biophys Acta. 2013 Apr;1833(4):895–900.

14. Jeong EM, Dudley SC. Diastolic Dysfunction. Circ J Off J Jpn Circ Soc. 2015;79(3):470–7.

15. Oberman R, Bhardwaj A. Physiology, Cardiac. In: StatPearls [Internet]. Treasure Island (FL): StatPearls Publishing; 2022 [cited 2022 Oct 14]. Available from: http://www.ncbi.nlm.nih.gov/books/NBK526089/

16. Pollock JD, Makaryus AN. Physiology, Cardiac Cycle. In: StatPearls [Internet]. Treasure Island (FL): StatPearls Publishing; 2022 [cited 2022 Oct 14]. Available from: http://www.ncbi.nlm.nih.gov/books/NBK459327/

17. Dongaonkar RM, Stewart RH, Geissler HJ, Laine GA. Myocardial microvascular permeability, interstitial oedema, and compromised cardiac function. Cardiovasc Res. 2010 Jul 15;87(2):331–9.

18. Nordick K, Weber C, Singh P. Anatomy, Thorax, Heart Thebesian Veins. In: StatPearls [Internet]. Treasure Island (FL): StatPearls Publishing; 2022 [cited 2022 Jul 17]. Available from: http://www.ncbi.nlm.nih.gov/books/NBK541040/

19. Perea RJ, Ortiz-Perez JT, Sole M, Cibeira MT, de Caralt TM, Prat-Gonzalez S, et al. T1 mapping: characterisation of myocardial interstitial space. Insights Imaging. 2014 Nov 26;6(2):189–202.

20. Goodwill AG, Dick GM, Kiel AM, Tune JD. Regulation of Coronary Blood Flow. Compr Physiol. 2017 Mar 16;7(2):321–82.

21. Rahman M, Siddik AB. Anatomy, Arterioles. In: StatPearls [Internet]. Treasure Island (FL): StatPearls Publishing; 2023 [cited 2023 May 2]. Available from: http://www.ncbi.nlm.nih.gov/books/NBK555921/

22. Tirziu D, Giordano FJ, Simons M. Cell Communications in the Heart. Circulation. 2010 Aug 31;122(9):928–37.

23. Tucker WD, Arora Y, Mahajan K. Anatomy, Blood Vessels. In: StatPearls [Internet]. Treasure Island (FL): StatPearls Publishing; 2023 [cited 2023 May 2]. Available from: http://www.ncbi.nlm.nih.gov/books/NBK470401/

24. Cong X, Kong W. Endothelial tight junctions and their regulatory signaling pathways in vascular homeostasis and disease. Cell Signal. 2020 Feb 1;66:109485.

25. Abelanet A, Camoin M, Rubin S, Bougaran P, Delobel V, Pernot M, et al. Increased Capillary Permeability in Heart Induces Diastolic Dysfunction Independently of Inflammation, Fibrosis, or Cardiomyocyte Dysfunction. Arterioscler Thromb Vasc Biol. 2022 Jun;42(6):745–63.

26. Becker BF, Chappell D, Jacob M. Endothelial glycocalyx and coronary vascular permeability: the fringe benefit. Basic Res Cardiol. 2010 Nov;105(6):687–701.

27. Qiu Y, Buffonge S, Ramnath R, Jenner S, Fawaz S, Arkill KP, et al. Endothelial glycocalyx is damaged in diabetic cardiomyopathy: angiopoietin 1 restores glycocalyx and improves diastolic function in mice. Diabetologia. 2022 May 1;65(5):879–94.

28. Thomsen MS, Routhe LJ, Moos T. The vascular basement membrane in the healthy and pathological brain. J Cereb Blood Flow Metab. 2017 Oct;37(10):3300–17.

29. Shimada T, Noguchi T, Kitamura H, Matsufuji Y, Campbell GR. Structure and distribution of lymphatic capillaries and fenestrated blood capillaries in the conduction system of the rabbit heart. Heart Vessels. 1988;4(3):123–7.

30. Griffin CT, Gao S. Building discontinuous liver sinusoidal vessels. J Clin Invest. 127(3):790–2.

31. Tortora GJ, Derrickson B. Principles of Anatomy & Physiology. 14th ed.

32. Hudson S, Pettit S. What is 'normal' left ventricular ejection fraction? Heart. 2020 Sep 1;106(18):1445–6.

33. Chengode S. Left ventricular global systolic function assessment by echocardiography. Ann Card Anaesth. 2016 Oct;19(Suppl 1):S26–34.

34. Muir WW, Hamlin RL. Myocardial Contractility: Historical and Contemporary Considerations. Front Physiol [Internet]. 2020 [cited 2023 Apr 4];11. Available from: https://www.frontiersin.org/articles/10.3389/fphys.2020.00222

35. Sequeira V, van der Velden J. Historical perspective on heart function: the Frank–Starling Law. Biophys Rev. 2015 Nov 19;7(4):421–47.

36. Delicce AV, Makaryus AN. Physiology, Frank Starling Law. In: StatPearls [Internet]. Treasure Island (FL): StatPearls Publishing; 2023 [cited 2023 Apr 13]. Available from: http://www.ncbi.nlm.nih.gov/books/NBK470295/

37. Vincent JL. Understanding cardiac output. Crit Care. 2008;12(4):174.

38. LaCombe P, Tariq MA, Lappin SL. Physiology, Afterload Reduction. In: StatPearls [Internet]. Treasure Island (FL): StatPearls Publishing; 2023 [cited 2023 Apr 14]. Available from: http://www.ncbi.nlm.nih.gov/books/NBK493174/

39. Nagueh SF, Smiseth OA, Appleton CP, Byrd BF, Dokainish H, Edvardsen T, et al. Recommendations for the Evaluation of Left Ventricular Diastolic Function by Echocardiography: An Update from the American Society of Echocardiography and the European Association of Cardiovascular Imaging. J Am Soc Echocardiogr. 2016 Apr 1;29(4):277–314.

40. Zile MR, Brutsaert DL. New Concepts in Diastolic Dysfunction and Diastolic Heart Failure: Part I. Circulation. 2002 Mar 19;105(11):1387–93.

41. Ribeiro J. Diastolic dysfunction and type 1 diabetes: A sweet link? Rev Port Cardiol Engl Ed. 2021 Oct 1;40(10):767–9.

42. Nagueh SF. Left Ventricular Diastolic Function: Understanding Pathophysiology, Diagnosis, and Prognosis With Echocardiography. JACC Cardiovasc Imaging. 2020 Jan 1;13(1, Part 2):228–44.

43. Redfield MM, Jacobsen SJ, Burnett JC Jr, Mahoney DW, Bailey KR, Rodeheffer RJ. Burden of Systolic and Diastolic Ventricular Dysfunction in the Community: Appreciating the Scope of the Heart Failure Epidemic. JAMA. 2003 Jan 8;289(2):194–202.

44. Parim B, Sathibabu Uddandrao VV, Saravanan G. Diabetic cardiomyopathy: molecular mechanisms, detrimental effects of conventional treatment, and beneficial effects of natural therapy. Heart Fail Rev. 2019 Mar;24(2):279–99.

45. Malik A, Brito D, Vaqar S, Chhabra L. Congestive Heart Failure. In: StatPearls [Internet]. Treasure Island (FL): StatPearls Publishing; 2023 [cited 2023 May 1]. Available from: http://www.ncbi.nlm.nih.gov/books/NBK430873/

46. Hartupee J, Mann DL. Neurohormonal activation in heart failure with reduced ejection fraction. Nat Rev Cardiol. 2017 Jan;14(1):30–8.

47. Savarese G, Stolfo D, Sinagra G, Lund LH. Heart failure with mid-range or mildly reduced ejection fraction. Nat Rev Cardiol. 2022 Feb;19(2):100–16.

48. Redfield MM, Borlaug BA. Heart Failure With Preserved Ejection Fraction: A Review. JAMA. 2023 Mar 14;329(10):827–38.

49. Fagiry MA, Hassan IA, Mahmoud MZ. Two-dimensional echocardiography in the diagnosis of ischemic heart disease. J Radiat Res Appl Sci. 2019 Jan 1;12(1):177–85.

50. Ashley EA, Niebauer J. Understanding the echocardiogram. In: Cardiology Explained [Internet]. Remedica; 2004 [cited 2023 May 1]. Available from: https://www.ncbi.nlm.nih.gov/books/NBK2215/

51. Singh S, Goyal A. The Origin of Echocardiography. Tex Heart Inst J. 2007;34(4):431–8.

52. Omerovic S, Jain A. Echocardiogram. In: StatPearls [Internet]. Treasure Island (FL): StatPearls Publishing; 2023 [cited 2023 May 1]. Available from: http://www.ncbi.nlm.nih.gov/books/NBK558940/

53. Ambrogio S, Ansell J, Gabriel E, Aneju G, Newman B, Negoita M, et al. Pulsed Wave Doppler Measurements of Maximum Velocity: Dependence on Sample Volume Size. Ultrasound Med Biol. 2022 Jan 1;48(1):68–77.

54. Evans DH, Jensen JA, Nielsen MB. Ultrasonic colour Doppler imaging. Interface Focus. 2011 Aug 6;1(4):490–502.

55. Lahoti N, Jabbour RJ, Ariff B, Wang BX. Cardiac MRI in cardiomyopathies. Future Cardiol. 2022 Jan;18(1):51–65.

56. Russo V, Lovato L, Ligabue G. Cardiac MRI: technical basis. Radiol Med (Torino). 2020 Nov 1;125(11):1040–55.

57. Lubien E, DeMaria A, Krishnaswamy P, Clopton P, Koon J, Kazanegra R, et al. Utility of B-Natriuretic Peptide in Detecting Diastolic Dysfunction. Circulation. 2002 Feb 5;105(5):595–601.

58. Troughton RW, Prior DL, Pereira JJ, Martin M, Fogarty A, Morehead A, et al. Plasma B-type natriuretic peptide levels in systolic heart failure: importance of left ventricular diastolic function and right ventricular systolic function. J Am Coll Cardiol. 2004 Feb 4;43(3):416–22.

59. Mottram PM, Marwick TH. Assessment of diastolic function: what the general cardiologist needs to know. Heart. 2005 May;91(5):681–95.

60. Park JH, Marwick TH. Use and Limitations of E/e' to Assess Left Ventricular Filling Pressure by Echocardiography. J Cardiovasc Ultrasound. 2011 Dec;19(4):169–73.

61. Hu M, Li T, Bo Z, Xiang F. The protective role of carnosic acid in ischemic/reperfusion injury through regulation of autophagy under T2DM. Exp Biol Med. 2019 May;244(7):602–11.

62. Tate M, Prakoso D, Willis AM, Peng C, Deo M, Qin CX, et al. Characterising an Alternative Murine Model of Diabetic Cardiomyopathy. Front Physiol [Internet]. 2019 Nov 14 [cited 2020 Sep 3];10. Available from: https://www.ncbi.nlm.nih.gov/pmc/articles/PMC6868003/

63. Ali TM, Abo-Salem OM, El Esawy BH, El Askary A. The Potential Protective Effects of Diosmin on Streptozotocin-Induced Diabetic Cardiomyopathy in Rats. Am J Med Sci. 2020 Jan 1;359(1):32–41.

64. Banday MZ, Sameer AS, Nissar S. Pathophysiology of diabetes: An overview. Avicenna J Med. 2020 Oct 13;10(4):174–88.

65. Kahanovitz L, Sluss PM, Russell SJ. Type 1 Diabetes – A Clinical Perspective. Point Care. 2017 Mar;16(1):37.

66. Fowler MJ. Diabetes: Magnitude and Mechanisms. Clin Diabetes. 2007 Jan 1;25(1):25–8.

67. Katsarou A, Gudbjörnsdottir S, Rawshani A, Dabelea D, Bonifacio E, Anderson BJ, et al. Type 1 diabetes mellitus. Nat Rev Dis Primer. 2017 Mar 30;3(1):1–17.

68. Goyal R, Jialal I. Diabetes Mellitus Type 2. In: StatPearls [Internet]. Treasure Island (FL): StatPearls Publishing; 2020 [cited 2020 Sep 23]. Available from: http://www.ncbi.nlm.nih.gov/books/NBK513253/

69. Ferranti SD de, Boer IH de, Fonseca V, Fox CS, Golden SH, Lavie CJ, et al. Type 1 Diabetes Mellitus and Cardiovascular Disease: A Scientific Statement From the American Heart Association and American Diabetes Association. Diabetes Care. 2014 Oct 1;37(10):2843–63.

70. Nowotny K, Jung T, Höhn A, Weber D, Grune T. Advanced Glycation End Products and Oxidative Stress in Type 2 Diabetes Mellitus. Biomolecules. 2015 Mar 16;5(1):194–222.

71. Sears B, Perry M. The role of fatty acids in insulin resistance. Lipids Health Dis. 2015 Sep 29;14:121.

72. Stumvoll M, Tataranni PA, Bogardus C. The hyperbolic law—a 25-year perspective. Diabetologia. 2005 Feb 1;48(2):207–9.

73. Golay A, Ybarra J. Link between obesity and type 2 diabetes. Best Pract Res Clin Endocrinol Metab. 2005 Dec 1;19(4):649–63.

74. Al-Goblan AS, Al-Alfi MA, Khan MZ. Mechanism linking diabetes mellitus and obesity. Diabetes Metab Syndr Obes Targets Ther. 2014 Dec 4;7:587–91.

75. Jia Guanghong, Hill Michael A., Sowers James R. Diabetic Cardiomyopathy. Circ Res. 2018 Feb 16;122(4):624–38.

76. Rubler S, Dlugash J, Yuceoglu YZ, Kumral T, Branwood AW, Grishman A. New type of cardiomyopathy associated with diabetic glomerulosclerosis. Am J Cardiol. 1972 Nov 8;30(6):595–602.

77. Liu X, Xu Q, Wang X, Zhao Z, Zhang L, Zhong L, et al. Irbesartan ameliorates diabetic cardiomyopathy by regulating protein kinase D and ER stress activation in a type 2 diabetes rat model. Pharmacol Res. 2015 Mar 1;93:43–51.

78. Lorenzo-Almorós A, Tuñón J, Orejas M, Cortés M, Egido J, Lorenzo Ó. Diagnostic approaches for diabetic cardiomyopathy. Cardiovasc Diabetol. 2017 Feb 23;16(1):28.

79. Thomas CM, Yong QC, Seqqat R, Chandel N, Feldman DL, Baker KM, et al. Direct Renin Inhibition Prevents Cardiac Dysfunction in a Diabetic Mouse Model: Comparison with an Angiotensin Receptor Antagonist and Angiotensin Converting Enzyme Inhibitor. Clin Sci Lond Engl 1979. 2013 Apr;124(8):529–41.

80. Ganesan K, Rana MBM, Sultan S. Oral Hypoglycemic Medications. In: StatPearls [Internet]. Treasure Island (FL): StatPearls Publishing; 2021 [cited 2022 Jan 2]. Available from: http://www.ncbi.nlm.nih.gov/books/NBK482386/

81. Palazzuoli A, Ceccarelli E, Ruocco G, Nuti R. Clinical impact of oral antidiabetic medications in heart failure patients. Heart Fail Rev. 2018 May 1;23(3):325–35.

82. Glatz JFC, Nabben M, Young ME, Schulze PC, Taegtmeyer H, Luiken JJFP. Re-balancing cellular energy substrate metabolism to mend the failing heart. Biochim Biophys Acta BBA - Mol Basis Dis. 2020 May 1;1866(5):165579.

83. Borghetti G, von Lewinski D, Eaton DM, Sourij H, Houser SR, Wallner M. Diabetic Cardiomyopathy: Current and Future Therapies. Beyond Glycemic Control. Front Physiol [Internet]. 2018 Oct 30 [cited 2020 Oct 30];9. Available from: https://www.ncbi.nlm.nih.gov/pmc/articles/PMC6218509/

84. Sowton AP, Griffin JL, Murray AJ. Metabolic Profiling of the Diabetic Heart: Toward a Richer Picture. Front Physiol [Internet]. 2019 [cited 2020 Oct 28];10. Available from: https://www.frontiersin.org/articles/10.3389/fphys.2019.00639/full

85. Zheng L, Li B, Lin S, Chen L, Li H. Role and mechanism of cardiac insulin resistance in occurrence of heart failure caused by myocardial hypertrophy. Aging. 2019 Aug 28;11(16):6584–90.

86. Lopaschuk GD. Fatty Acid Oxidation and Its Relation with Insulin Resistance and Associated Disorders. Ann Nutr Metab. 2016;68(Suppl. 3):15–20.

87. Wende AR, Schell JC, Ha CM, Pepin ME, Khalimonchuk O, Schwertz H, et al. Maintaining Myocardial Glucose Utilization in Diabetic Cardiomyopathy Accelerates Mitochondrial Dysfunction. Diabetes. 2020 May 4;69(10):2094–111.

88. Athithan L, Gulsin GS, McCann GP, Levelt E. Diabetic cardiomyopathy: Pathophysiology, theories and evidence to date. World J Diabetes. 2019 Oct 15;10(10):490–510.

89. Nabben M, Luiken JJFP, Glatz JFC. Metabolic remodelling in heart failure revisited. Nat Rev Cardiol. 2018 Dec;15(12):780–780.

90. Zhou YT, Grayburn P, Karim A, Shimabukuro M, Higa M, Baetens D, et al. Lipotoxic heart disease in obese rats: Implications for human obesity. Proc Natl Acad Sci U S A. 2000 Feb 15;97(4):1784–9.

91. Belke DD, Swanson EA, Dillmann WH. Decreased Sarcoplasmic Reticulum Activity and Contractility in Diabetic db/db Mouse Heart. Diabetes. 2004 Dec 1;53(12):3201–8.

92. Dillmann WH. Diabetic Cardiomyopathy. Circ Res. 2019 Apr 12;124(8):1160–2.

93. Trost SU, Belke DD, Bluhm WF, Meyer M, Swanson E, Dillmann WH. Overexpression of the sarcoplasmic reticulum Ca(2+)-ATPase improves myocardial contractility in diabetic cardiomyopathy. Diabetes. 2002 Apr;51(4):1166–71.

94. Montagnani M, Chen H, Barr VA, Quon MJ. Insulin-stimulated Activation of eNOS Is Independent of Ca2+ but Requires Phosphorylation by Akt at Ser1179*. J Biol Chem. 2001 Aug 10;276(32):30392–8.

95. Jubaidi FF, Zainalabidin S, Mariappan V, Budin SB. Mitochondrial Dysfunction in Diabetic Cardiomyopathy: The Possible Therapeutic Roles of Phenolic Acids. Int J Mol Sci [Internet]. 2020 Aug 22 [cited 2021 May 4];21(17). Available from: https://www.ncbi.nlm.nih.gov/pmc/articles/PMC7503847/

96. Lobo V, Patil A, Phatak A, Chandra N. Free radicals, antioxidants and functional foods: Impact on human health. Pharmacogn Rev. 2010;4(8):118–26.

97. Busik JV, Mohr S, Grant MB. Hyperglycemia-Induced Reactive Oxygen Species Toxicity to Endothelial Cells Is Dependent on Paracrine Mediators. Diabetes. 2008 Jul;57(7):1952–65.

98. Kaludercic N, Di Lisa F. Mitochondrial ROS Formation in the Pathogenesis of Diabetic Cardiomyopathy. Front Cardiovasc Med [Internet]. 2020 Feb 18 [cited 2021 Apr 7];7. Available from: https://www.ncbi.nlm.nih.gov/pmc/articles/PMC7040199/

99. Catalá A, Díaz M. Editorial: Impact of Lipid Peroxidation on the Physiology and Pathophysiology of Cell Membranes. Front Physiol [Internet]. 2016 Sep 22 [cited 2021 May 4];7. Available from: https://www.ncbi.nlm.nih.gov/pmc/articles/PMC5031777/

100. Russo I, Frangogiannis NG. Diabetes-associated cardiac fibrosis: cellular effectors, molecular mechanisms and therapeutic opportunities. J Mol Cell Cardiol. 2016 Jan;90:84–93.

101. Jia G, Whaley-Connell A, Sowers JR. Diabetic cardiomyopathy: a hyperglycaemia- and insulin-resistance-induced heart disease. Diabetologia. 2018 Jan 1;61(1):21–8.

102. Goldin Alison, Beckman Joshua A., Schmidt Ann Marie, Creager Mark A. Advanced Glycation End Products. Circulation. 2006 Aug 8;114(6):597–605.

103. Ren X, Ren L, Wei Q, Shao H, Chen L, Liu N. Advanced glycation end-products decreases expression of endothelial nitric oxide synthase through oxidative stress in human coronary artery endothelial cells. Cardiovasc Diabetol [Internet]. 2017 Apr 20 [cited 2021 Apr 7];16. Available from: https://www.ncbi.nlm.nih.gov/pmc/articles/PMC5397770/

104. Ma H, Li S, Xu P, Babcock SA, Dolence EK, Brownlee M, et al. Advanced glycation endproduct (AGE) accumulation and AGE receptor (RAGE) up-regulation contribute to the onset of diabetic cardiomyopathy. J Cell Mol Med. 2009 Aug;13(8b):1751–64.

105. Kaur N, Guan Y, Raja R, Ruiz-Velasco A, Liu W. Mechanisms and Therapeutic Prospects of Diabetic Cardiomyopathy Through the Inflammatory Response. Front Physiol. 2021;12:694864–74.

106. Stentz FB, Umpierrez GE, Cuervo R, Kitabchi AE. Proinflammatory Cytokines, Markers of Cardiovascular Risks, Oxidative Stress, and Lipid Peroxidation in Patients With Hyperglycemic Crises. Diabetes. 2004 Aug 1;53(8):2079–86.

107. Westermann D, Linthout SV, Dhayat S, Dhayat N, Escher F, Bücker-Gärtner C, et al. Cardioprotective and Anti-Inflammatory Effects of Interleukin Converting Enzyme Inhibition in Experimental Diabetic Cardiomyopathy. Diabetes. 2007 Jul 1;56(7):1834–41.

108. Gulsin GS, Swarbrick DJ, Hunt WH, Levelt E, Graham-Brown MPM, Parke KS, et al. Relation of Aortic Stiffness to Left Ventricular Remodeling in Younger Adults With Type 2 Diabetes. Diabetes. 2018 Jul 1;67(7):1395–400.

109. Shang Y, Zhang X, Leng W, Lei X, Chen L, Zhou X, et al. Increased fractal dimension of left ventricular trabeculations is associated with subclinical diastolic dysfunction in patients with type-2 diabetes mellitus. Int J Cardiovasc Imaging. 2019 Apr 1;35(4):665–73.

110. Gulsin GS, Athithan L, McCann GP. Diabetic cardiomyopathy: prevalence, determinants and potential treatments. Ther Adv Endocrinol Metab [Internet]. 2019 Mar 27 [cited 2020 Nov 11];10. Available from: https://www.ncbi.nlm.nih.gov/pmc/articles/PMC6437329/

111. Eguchi K, Boden-Albala B, Jin Z, Rundek T, Sacco RL, Homma S, et al. Association Between Diabetes Mellitus and Left Ventricular Hypertrophy in a Multi-Ethnic Population. Am J Cardiol. 2008 Jun 15;101(12):1787–91.

112. Van Linthout S, Seeland U, Riad A, Eckhardt O, Hohl M, Dhayat N, et al. Reduced MMP-2 activity contributes to cardiac fibrosis in experimental diabetic cardiomyopathy. Basic Res Cardiol. 2008 Jun 1;103(4):319–27.

113. Westermann D, Rutschow S, Jäger S, Linderer A, Anker S, Riad A, et al. Contributions of Inflammation and Cardiac Matrix Metalloproteinase Activity to Cardiac Failure in Diabetic Cardiomyopathy: The Role of Angiotensin Type 1 Receptor Antagonism. Diabetes. 2007 Mar 1;56(3):641–6.

114. van Heerebeek Loek, Hamdani Nazha, Handoko M. Louis, Falcao-Pires Ines, Musters René J., Kupreishvili Koba, et al. Diastolic Stiffness of the Failing Diabetic Heart. Circulation. 2008 Jan 1;117(1):43–51.

115. Verbrugge FH, Bertrand PB, Willems E, Gielen E, Mullens W, Giri S, et al. Global myocardial oedema in advanced decompensated heart failure. Eur Heart J - Cardiovasc Imaging. 2017 Jul 1;18(7):787–94.

116. Nishii T, Kono AK, Shigeru M, Takamine S, Fujiwara S, Kyotani K, et al. Cardiovascular magnetic resonance T2 mapping can detect myocardial edema in idiopathic dilated cardiomyopathy. Int J Cardiovasc Imaging. 2014 Jun 1;30(1):65–72.

117. Crompton M, Ferguson JK, Ramnath R, Onions KL, Ogier AS, Gamez M, et al. Mineralocorticoid receptor antagonism in diabetes reduces albuminuria by preserving the glomerular endothelial glycocalyx. JCI Insight. 2023 Feb 7;8(5):154164–80.

118. Ramnath RD, Butler MJ, Newman G, Desideri S, Russell A, Lay AC, et al. Blocking matrix metalloproteinase-mediated syndecan-4 shedding restores the endothelial glycocalyx and glomerular filtration barrier function in early diabetic kidney disease. Kidney Int. 2020 May;97(5):951–65.

119. Riehle C, Bauersachs J. Of mice and men: models and mechanisms of diabetic cardiomyopathy. Basic Res Cardiol. 2019;112(2).

120. Bugger H, Abel ED. Rodent models of diabetic cardiomyopathy. Dis Model Mech. 2009 Sep 1;2(9–10):454–66.

121. Furman BL. Streptozotocin-Induced Diabetic Models in Mice and Rats. Curr Protoc Pharmacol. 2015;70(1):5.47.1-5.47.20.

122. Marchini GS, Cestari IN, Salemi VMC, Irigoyen MC, Arnold A, Kakoi A, et al. Early changes in myocyte contractility and cardiac function in streptozotocin-induced type 1 diabetes in rats. PLoS ONE [Internet]. 2020 Aug 21 [cited 2020 Nov 24];15(8). Available from: https://www.ncbi.nlm.nih.gov/pmc/articles/PMC7442260/

123. Zhao W, Wang X, Sun KH, Zhou L. α-smooth muscle actin is not a marker of fibrogenic cell activity in skeletal muscle fibrosis. PLoS ONE [Internet]. 2018 Jan 10 [cited 2020 Nov 24];13(1). Available from: https://www.ncbi.nlm.nih.gov/pmc/articles/PMC5761950/

124. Tao H, Tao JY, Song ZY, Shi P, Wang Q, Deng ZY, et al. MeCP2 triggers diabetic cardiomyopathy and cardiac fibroblast proliferation by inhibiting RASSF1A. Cell Signal. 2019 Nov 1;63:109387.

125. De Blasio MJ, Huynh N, Deo M, Dubrana LE, Walsh J, Willis A, et al. Defining the Progression of Diabetic Cardiomyopathy in a Mouse Model of Type 1 Diabetes. Front Physiol. 2020;11:124–39.

126. Chandramouli C, Reichelt ME, Curl CL, Varma U, Bienvenu LA, Koutsifeli P, et al. Diastolic dysfunction is more apparent in STZ-induced diabetic female mice, despite less pronounced hyperglycemia. Sci Rep. 2018 Feb 5;8(1):2346.

127. Wu B, Lin J, Luo J, Han D, Fan M, Guo T, et al. Dihydromyricetin Protects against Diabetic Cardiomyopathy in Streptozotocin-Induced Diabetic Mice. BioMed Res Int [Internet]. 2017 [cited 2020 Dec 9];2017. Available from: https://www.ncbi.nlm.nih.gov/pmc/articles/PMC5379084/

128. Atta MS, El-Far AH, Farrag FA, Abdel-Daim MM, Al Jaouni SK, Mousa SA. Vol. 2018, Oxidative Medicine and Cellular Longevity. Hindawi; 2018 [cited 2020 Dec 10]. p. e7845681 Thymoquinone Attenuates Cardiomyopathy in Streptozotocin-Treated Diabetic Rats. Available from: https://www.hindawi.com/journals/omcl/2018/7845681/

129. Younus H. Therapeutic potentials of superoxide dismutase. Int J Health Sci. 2018;12(3):88–93.

130. Westermann D, Van Linthout S, Dhayat S, Dhayat N, Schmidt A, Noutsias M, et al. Tumor necrosis factor-alpha antagonism protects from myocardial inflammation and fibrosis in experimental diabetic cardiomyopathy. Basic Res Cardiol. 2007 Nov;102(6):500–7.

131. King AJ. The use of animal models in diabetes research. Br J Pharmacol. 2012 Jun;166(3):877–94.

132. Luce S, Guinoiseau S, Gadault A, Letourneur F, Blondeau B, Nitschke P, et al. Humanized Mouse Model to Study Type 1 Diabetes. Diabetes. 2018 Sep 1;67(9):1816–29.

133. Schleier Y, Moreno-Loaiza O, López Alarcón MM, Lopes Martins EG, Braga BC, Ramos IP, et al. NOD Mice Recapitulate the Cardiac Disturbances Observed in Type 1 Diabetes. J Cardiovasc Transl Res. 2021 Apr 1;14(2):271–82.

134. Dong B, Qi D, Yang L, Huang Y, Xiao X, Tai N, et al. TLR4 regulates cardiac lipid accumulation and diabetic heart disease in the nonobese diabetic mouse model of type 1 diabetes. Am J Physiol-Heart Circ Physiol. 2012 Sep 15;303(6):H732–42.

135. Pacher P, Liaudet L, Soriano FG, Mabley JG, Szabó É, Szabó C. The Role of Poly(ADP-Ribose) Polymerase Activation in the Development of Myocardial and Endothelial Dysfunction in Diabetes. Diabetes. 2002 Feb 1;51(2):514–21.

136. Hsueh W, Abel ED, Breslow JL, Maeda N, Davis RC, Fisher EA, et al. Recipes for Creating Animal Models of Diabetic Cardiovascular Disease. Circ Res. 2007 May 25;100(10):1415–27.

137. Basu R, Oudit GY, Wang X, Zhang L, Ussher JR, Lopaschuk GD, et al. Type 1 diabetic cardiomyopathy in the Akita (Ins2WT/C96Y) mouse model is characterized by lipotoxicity and diastolic dysfunction with preserved systolic function. Am J Physiol-Heart Circ Physiol. 2009 Dec 1;297(6):H2096–108.

138. Kambis TN, Shahshahan HR, Kar S, Yadav SK, Mishra PK. Transgenic Expression of miR-133a in the Diabetic Akita Heart Prevents Cardiac Remodeling and Cardiomyopathy. Front Cardiovasc Med. 2019;6:45.

139. Qin F, Siwik DA, Luptak I, Hou X, Wang L, Higuchi A, et al. The Polyphenols Resveratrol and S17834 prevent the Structural and Functional Sequelae of Diet-Induced Metabolic Heart Disease in Mice. Circulation. 2012 Apr 10;125(14):1757–64.

140. Wright JJ, Kim J, Buchanan J, Boudina S, Sena S, Bakirtzi K, et al. Mechanisms for increased myocardial fatty acid utilization following short-term high-fat feeding. Cardiovasc Res. 2009 May 1;82(2):351–60.

141. Fang JY, Lin CH, Huang TH, Chuang SY. In Vivo Rodent Models of Type 2 Diabetes and Their Usefulness for Evaluating Flavonoid Bioactivity. Nutrients. 2019 Feb 28;11(3):530.

142. Buchanan J, Mazumder PK, Hu P, Chakrabarti G, Roberts MW, Yun UJ, et al. Reduced Cardiac Efficiency and Altered Substrate Metabolism Precedes the Onset of Hyperglycemia and Contractile Dysfunction in Two Mouse Models of Insulin Resistance and Obesity. Endocrinology. 2005 Dec 1;146(12):5341–9.

143. Mazumder PK, O'Neill BT, Roberts MW, Buchanan J, Yun UJ, Cooksey RC, et al. Impaired Cardiac Efficiency and Increased Fatty Acid Oxidation in Insulin-Resistant ob/ob Mouse Hearts. Diabetes. 2004 Sep 1;53(9):2366–74.

144. Givre L, Dia M, Leon C, Chouabe C, Chanon S, Rieusset J, et al. Study of the relevance of the ob/ob mouse as a diabetic cardiomyopathy model. Arch Cardiovasc Dis Suppl. 2021 May 1;13(2):220.

145. Wang S, Wang B, Wang Y, Tong Q, Liu Q, Sun J, et al. Zinc Prevents the Development of Diabetic Cardiomyopathy in db/db Mice. Int J Mol Sci. 2017 Mar 7;18(3):580.

146. Aasum E, Hafstad AD, Severson DL, Larsen TS. Age-Dependent Changes in Metabolism, Contractile Function, and Ischemic Sensitivity in Hearts From db/db Mice. Diabetes. 2003 Feb 1;52(2):434–41.

147. Shiota M, Printz RL. Diabetes in Zucker Diabetic Fatty Rat. In: Joost HG, Al-Hasani H, Schürmann A, editors. Animal Models in Diabetes Research [Internet]. Totowa, NJ: Humana Press; 2012 [cited 2021 Dec 20]. p. 103–23. (Methods in Molecular Biology). Available from: https://doi.org/10.1007/978-1-62703-068-7_8

148. van den Brom CE, Bosmans JW, Vlasblom R, Handoko LM, Huisman MC, Lubberink M, et al. Diabetic cardiomyopathy in Zucker diabetic fatty rats: the forgotten right ventricle. Cardiovasc Diabetol. 2010 Jun 15;9(1):25.

149. Golfman LS, Wilson CR, Sharma S, Burgmaier M, Young ME, Guthrie PH, et al. Activation of PPARγ enhances myocardial glucose oxidation and improves contractile function in isolated working hearts of ZDF rats. Am J Physiol-Endocrinol Metab. 2005 Aug 1;289(2):E328–36.

150. Sun G, Zhang G, V. Jackson C, Wang YX (Jim). Zucker Diabetic Sprague Dawley (ZDSD) Rat, A Spontaneously Diabetic Rat Model Develops Cardiac Dysfunction and Compromised Cardiac Reserve. Cardiol Res Cardiovasc Med [Internet]. 2018 Jun 22 [cited 2021 Dec 20];3(1). Available from: https://www.gavinpublishers.com/articles/research-article/Cardiology-Research-and-Cardiovascular-Medicine/zucker-diabetic-sprague-dawley-ZDSD-rat-A-spontaneously-diabetic-rat-model-develops-cardiac-dysfunction-and-compromised-cardiac-reserve

151. Möckl L. The Emerging Role of the Mammalian Glycocalyx in Functional Membrane Organization and Immune System Regulation. Front Cell Dev Biol [Internet]. 2020 [cited 2021 Jan 7];8. Available from: https://www.frontiersin.org/articles/10.3389/fcell.2020.00253/full

152. Ito S. Form and Function of the Glycocalyx on Free Cell Surfaces. Philos Trans R Soc Lond B Biol Sci. 1974;268(891):55–66.

153. BENNETT HS. MORPHOLOGICAL ASPECTS OF EXTRACELLULAR POLYSACCHARIDES. J Histochem Cytochem. 1963 Jan 1;11(1):14–23.

154. Chambers R, Zweifach BW. Intercellular cement and capillary permeability. Physiol Rev. 1947 Jul 1;27(3):436–63.

155. Danielli JF. Capillary permeability and oedema in the perfused frog. J Physiol. 1940;98(1):109–29.

156. Yamada E. THE FINE STRUCTURE OF THE GALL BLADDER EPITHELIUM OF THE MOUSE. J Biophys Biochem Cytol. 1955 Sep 25;1(5):445–58.

157. FAWCETT DW. SURFACE SPECIALIZATIONS OF ABSORBING CELLS. J Histochem Cytochem. 1965 Feb 1;13(2):75–91.

158. Li W, Wang W. Structural alteration of the endothelial glycocalyx: contribution of the actin cytoskeleton. Biomech Model Mechanobiol. 2018;17(1):147–58.

159. Kolářová H, Ambrůzová B, Švihálková Šindlerová L, Klinke A, Kubala L. Vol. 2014, Mediators of Inflammation. Hindawi; 2014 [cited 2021 Feb 5]. p. e694312 Modulation of Endothelial Glycocalyx Structure under Inflammatory Conditions. Available from: https://www.hindawi.com/journals/mi/2014/694312/

160. Yilmaz O, Afsar B, Ortiz A, Kanbay M. The role of endothelial glycocalyx in health and disease. Clin Kidney J. 2019 Oct 1;12(5):611–9.

161. Milford EM, Reade MC. Resuscitation Fluid Choices to Preserve the Endothelial Glycocalyx. Crit Care. 2019 Mar 9;23(1):77.

162. Reitsma S, Slaaf DW, Vink H, van Zandvoort MAMJ, oude Egbrink MGA. The endothelial glycocalyx: composition, functions, and visualization. Pflugers Arch. 2007 Jun;454(3):345–59.

163. Manon-Jensen T, Itoh Y, Couchman JR. Proteoglycans in health and disease: the multiple roles of syndecan shedding. FEBS J. 2010;277(19):3876–89.

164. Szatmári T, Dobra K. The Role of Syndecan-1 in Cellular Signaling and its Effects on Heparan Sulfate Biosynthesis in Mesenchymal Tumors. Front Oncol [Internet]. 2013 [cited 2021 Feb 5];3. Available from: https://www.frontiersin.org/articles/10.3389/fonc.2013.00310/full

165. Pahakis MY, Kosky JR, Dull RO, Tarbell JM. The Role of Endothelial Glycocalyx Components in Mechanotransduction of Fluid Shear Stress. Biochem Biophys Res Commun. 2007 Mar 30;355(1):228–33.

166. Moore KH, Murphy HA, George EM. The glycocalyx: a central regulator of vascular function. Am J Physiol-Regul Integr Comp Physiol. 2021 Apr;320(4):R508–18.

167. Filmus J, Selleck SB. Glypicans: proteoglycans with a surprise. J Clin Invest. 2001 Aug 15;108(4):497–501.

168. Hachim D, Whittaker TE, Kim H, Stevens MM. Glycosaminoglycan-based biomaterials for growth factor and cytokine delivery: Making the right choices. J Controlled Release. 2019 Nov 10;313:131–47.

169. Casale J, Crane JS. Biochemistry, Glycosaminoglycans. In: StatPearls [Internet]. Treasure Island (FL): StatPearls Publishing; 2022 [cited 2022 May 23]. Available from: http://www.ncbi.nlm.nih.gov/books/NBK544295/

170. Uchimido R, Schmidt EP, Shapiro NI. The glycocalyx: a novel diagnostic and therapeutic target in sepsis. Crit Care. 2019 Jan 17;23(1):16.

171. Thorne RF, Legg JW, Isacke CM. The role of the CD44 transmembrane and cytoplasmic domains in co-ordinating adhesive and signalling events. J Cell Sci. 2004 Jan 22;117(3):373–80.

172. Peterson SB, Liu J. Unraveling the Specificity of Heparanase Utilizing Synthetic Substrates. J Biol Chem. 2010 May 7;285(19):14504–13.

173. Simon Davis DA, Parish CR. Heparan Sulfate: A Ubiquitous Glycosaminoglycan with Multiple Roles in Immunity. Front Immunol [Internet]. 2013 [cited 2021 Mar 7];4. Available from: https://www.frontiersin.org/articles/10.3389/fimmu.2013.00470/full

174. Weinbaum S, Tarbell JM, Damiano ER. The Structure and Function of the Endothelial Glycocalyx Layer. Annu Rev Biomed Eng. 2007 Aug 15;9(1):121–67.

175. Hu Z, Cano I, D'Amore PA. Update on the Role of the Endothelial Glycocalyx in Angiogenesis and Vascular Inflammation. Front Cell Dev Biol. 2021 Aug 31;9:734276.

176. Gopal S. Syndecans in Inflammation at a Glance. Front Immunol. 2020 Feb 18;11:227.

177. Qu J, Cheng Y, Wu W, Yuan L, Liu X. Glycocalyx Impairment in Vascular Disease: Focus on Inflammation. Front Cell Dev Biol. 2021 Sep 13;9:730621.

178. Baeyens N. Fluid shear stress sensing in vascular homeostasis and remodeling: Towards the development of innovative pharmacological approaches to treat vascular dysfunction. Biochem Pharmacol. 2018 Dec 1;158:185–91.

179. Lupu F, Kinasewitz G, Dormer K. The role of endothelial shear stress on haemodynamics, inflammation, coagulation and glycocalyx during sepsis. J Cell Mol Med. 2020 Nov;24(21):12258–71.

180. Bartosch AMW, Mathews R, Tarbell JM. Endothelial Glycocalyx-Mediated Nitric Oxide Production in Response to Selective AFM Pulling. Biophys J. 2017 Jul 11;113(1):101–8.

181. Lopez-Quintero SV, Cancel LM, Pierides A, Antonetti D, Spray DC, Tarbell JM. High Glucose Attenuates Shear-Induced Changes in Endothelial Hydraulic Conductivity by Degrading the Glycocalyx. PLOS ONE. 2013 Nov 18;8(11):e78954.

182. Masenga SK, Pilic L, Malumani M, Hamooya BM. Erythrocyte sodium buffering capacity status correlates with self-reported salt intake in a population from Livingstone, Zambia. PLOS ONE. 2022 Mar 2;17(3):e0264650.

183. Sulyok E, Farkas B, Nagy B, Várnagy Á, Kovács K, Bódis J. Tissue Sodium Accumulation: Pathophysiology and Clinical Implications. Antioxidants. 2022 Apr 9;11(4):750.

184. Olde Engberink RHG, Rorije NMG, Homan van der Heide JJ, van den Born BJH, Vogt L. Role of the Vascular Wall in Sodium Homeostasis and Salt Sensitivity. J Am Soc Nephrol JASN. 2015 Apr;26(4):777–83.

185. Oberleithner H, Peters W, Kusche-Vihrog K, Korte S, Schillers H, Kliche K, et al. Salt overload damages the glycocalyx sodium barrier of vascular endothelium. Pflugers Arch. 2011;462(4):519–28.

186. Woodcock TE, Woodcock TM. Revised Starling equation and the glycocalyx model of transvascular fluid exchange: an improved paradigm for prescribing intravenous fluid therapy. Br J Anaesth. 2012 Mar 1;108(3):384–94.

187. Michel CC, Woodcock TE, Curry FRE. Understanding and extending the Starling principle. Acta Anaesthesiol Scand. 2020;64(8):1032–7.

188. Starling EH. On the Absorption of Fluids from the Connective Tissue Spaces. J Physiol. 1896 May 5;19(4):312–26.

189. Salmon AH, Satchell SC. Endothelial glycocalyx dysfunction in disease: albuminuria and increased microvascular permeability. J Pathol. 2012;226(4):562–74.

190. Oltean S, Qiu Y, Ferguson JK, Stevens M, Neal C, Russell A, et al. Vascular Endothelial Growth Factor-A165b Is Protective and Restores Endothelial Glycocalyx in Diabetic Nephropathy. J Am Soc Nephrol JASN. 2015 Aug;26(8):1889–904.

191. Betteridge KB, Arkill KP, Neal CR, Harper SJ, Foster RR, Satchell SC, et al. Sialic acids regulate microvessel permeability, revealed by novel in vivo studies of endothelial glycocalyx structure and function. J Physiol. 2017 Aug 1;595(15):5015–35.

192. Rambourg A, Neutra M, Leblond CP. Presence of a ‘cell coat’ rich in carbohydrate at the surface of cells in the rat. Anat Rec. 1966;154(1):41–71.

193. Luft JH. Fine structures of capillary and endocapillary layer as revealed by ruthenium red. Fed Proc. 1966;25(6):1773–83.

194. Mukai S, Takaki T, Nagumo T, Sano M, Kang D, Takimoto M, et al. Three-dimensional electron microscopy for endothelial glycocalyx observation using Alcian blue with silver enhancement. Med Mol Morphol. 2021;54(2):95–107.

195. Arokiasamy S, King R, Boulaghrasse H, Poston RN, Nourshargh S, Wang W, et al. Heparanase-Dependent Remodeling of Initial Lymphatic Glycocalyx Regulates Tissue-Fluid Drainage During Acute Inflammation in vivo. Front Immunol. 2019;10:2316.

196. Wang G, Tiemeier GL, van den Berg BM, Rabelink TJ. Endothelial Glycocalyx Hyaluronan: Regulation and Role in Prevention of Diabetic Complications. Am J Pathol. 2020 Apr 1;190(4):781–90.

197. Li Z, Wu N, Wang J, Zhang Q. Roles of Endovascular Calyx Related Enzymes in Endothelial Dysfunction and Diabetic Vascular Complications. Front Pharmacol. 2020 Nov 30;11:590614.

198. Dogné S, Flamion B, Caron N. Endothelial Glycocalyx as a Shield Against Diabetic Vascular Complications. Arterioscler Thromb Vasc Biol. 2018 Jul;38(7):1427–39.

199. Frost GI, Csóka TB, Wong T, Stern R. Purification, Cloning, and Expression of Human Plasma Hyaluronidase. Biochem Biophys Res Commun. 1997 Jul 9;236(1):10–5.

200. Dogné S, Rath G, Jouret F, Caron N, Dessy C, Flamion B. Hyaluronidase 1 Deficiency Preserves Endothelial Function and Glycocalyx Integrity in Early Streptozotocin-Induced Diabetes. Diabetes. 2016 May 31;65(9):2742–53.

201. Secchi MF, Crescenzi M, Masola V, Russo FP, Floreani A, Onisto M. Heparanase and macrophage interplay in the onset of liver fibrosis. Sci Rep. 2017 Nov 2;7(1):14956.

202. Vlodavsky I, Ilan N, Naggi A, Casu B. Heparanase: structure, biological functions, and inhibition by heparin-derived mimetics of heparan sulfate. Curr Pharm Des. 2007;13(20):2057–73.

203. Wang F, Wan A, Rodrigues B. The Function of Heparanase in Diabetes and its Complications. Can J Diabetes. 2013 Oct 1;37(5):332–8.

204. Gil N, Goldberg R, Neuman T, Garsen M, Zcharia E, Rubinstein AM, et al. Heparanase Is Essential for the Development of Diabetic Nephropathy in Mice. Diabetes. 2011 Dec 12;61(1):208–16.

205. Goldberg R, Meirovitz A, Abecassis A, Hermano E, Rubinstein AM, Nahmias D, et al. Regulation of Heparanase in Diabetes-Associated Pancreatic Carcinoma. Front Oncol [Internet]. 2019 [cited 2023 Jan 31];9. Available from: https://www.frontiersin.org/articles/10.3389/fonc.2019.01405

206. Wijesekara P, Liu Y, Wang W, Johnston EK, Sullivan MLG, Taylor RE, et al. Accessing and Assessing the Cell-Surface Glycocalyx Using DNA Origami. Nano Lett. 2021 Jun 9;21(11):4765–73.

207. Fougerat A, Pan X, Smutova V, Heveker N, Cairo CW, Issad T, et al. Neuraminidase 1 activates insulin receptor and reverses insulin resistance in obese mice. Mol Metab. 2018 Apr 21;12:76–88.

208. Foote CA, Ghiarone T, Ramirez-Perez FI, Kluser AR, Grunewald ZI, Jurrissen TJ, et al. The targeted inhibition of neuraminidase reverses endothelial glycocalyx degradation and improves endothelial function in type 2 diabetes. FASEB J. 2019;33(S1):527.16-527.16.

209. Laronha H, Caldeira J. Structure and Function of Human Matrix Metalloproteinases. Cells. 2020 Apr 26;9(5):1076.

210. Gersh I, Catchpole HR. The organization of ground substance and basement membrane and its significance in tissue injury disease and growth. Am J Anat. 1949 Nov;85(3):457–521, incl 7 pl.

211. Quiding-Järbrink M, Smith DA, Bancroft GJ. Production of Matrix Metalloproteinases in Response to Mycobacterial Infection. Infect Immun. 2001 Sep;69(9):5661–70.

212. Ali MM, Mahmoud AM, Le Master E, Levitan I, Phillips SA. Role of matrix metalloproteinases and histone deacetylase in oxidative stress-induced degradation of the endothelial glycocalyx. Am J Physiol - Heart Circ Physiol. 2019 Mar 1;316(3):H647–63.

213. Ramnath R, Foster RR, Qiu Y, Cope G, Butler MJ, Salmon AH, et al. Matrix metalloproteinase 9-mediated shedding of syndecan 4 in response to tumor necrosis factor α: a contributor to endothelial cell glycocalyx dysfunction. FASEB J. 2014;28(11):4686–99.

214. Park J, Ha SH, Abekura F, Lim H, Magae J, Ha KT, et al. 4-O-Carboxymethylascochlorin Inhibits Expression Levels of on Inflammation-Related Cytokines and Matrix Metalloproteinase-9 Through NF–κB/MAPK/TLR4 Signaling Pathway in LPS-Activated RAW264.7 Cells. Front Pharmacol [Internet]. 2019 [cited 2023 Jan 31];10. Available from: https://www.frontiersin.org/articles/10.3389/fphar.2019.00304

215. Kothari P, Pestana R, Mesraoua R, Elchaki R, Khan KMF, Dannenberg AJ, et al. IL-6-mediated induction of MMP-9 is modulated by JAK-dependent IL-10 expression in macrophages. J Immunol Baltim Md 1950. 2014 Jan 1;192(1):10.4049/jimmunol.1301906.

216. Gross J, Lapiere CM. COLLAGENOLYTIC ACTIVITY IN AMPHIBIAN TISSUES: A TISSUE CULTURE ASSAY*. Proc Natl Acad Sci U S A. 1962 Jun;48(6):1014–22.

217. Iyer RP, Patterson NL, Fields GB, Lindsey ML. The history of matrix metalloproteinases: milestones, myths, and misperceptions. Am J Physiol - Heart Circ Physiol. 2012 Oct 15;303(8):H919–30.

218. Kar S, Subbaram S, Carrico PM, Melendez JA. Redox-control of Matrix Metalloproteinase-1: A critical link between free radicals, matrix remodeling and degenerative disease. Respir Physiol Neurobiol. 2010 Dec 31;174(3):299–306.

219. Sternlicht MD, Werb Z. HOW MATRIX METALLOPROTEINASES REGULATE CELL BEHAVIOR. Annu Rev Cell Dev Biol. 2001;17:463–516.

220. Nagase H, Visse R, Murphy G. Structure and function of matrix metalloproteinases and TIMPs. Cardiovasc Res. 2006 Feb 15;69(3):562–73.

221. Löffek S, Schilling O, Franzke CW. Biological role of matrix metalloproteinases: a critical balance. Eur Respir J. 2011 Jul 1;38(1):191–208.

222. Marchenko ND, Marchenko GN, Strongin AY. Unconventional Activation Mechanisms of MMP-26, a Human Matrix Metalloproteinase with a Unique PHCG XXD Cysteine-switch Motif*. J Biol Chem. 2002 May 24;277(21):18967–72.

223. Nelson KK, Melendez JA. Mitochondrial redox control of matrix metalloproteinases. Free Radic Biol Med. 2004 Sep 15;37(6):768–84.

224. Tallant C, Marrero A, Gomis-Rüth FX. Matrix metalloproteinases: Fold and function of their catalytic domains. Biochim Biophys Acta BBA - Mol Cell Res. 2010 Jan 1;1803(1):20–8.

225. Sagi I, Gaffney J. Matrix Metalloproteinase Biology [Internet]. New York, UNITED STATES: John Wiley & Sons, Incorporated; 2015 [cited 2021 Oct 19]. Available from: http://ebookcentral.proquest.com/lib/bristol/detail.action?docID=1895594

226. Cui N, Hu M, Khalil RA. Biochemical and Biological Attributes of Matrix Metalloproteinases. Prog Mol Biol Transl Sci. 2017;147:1–73.

227. Ra HJ, Parks WC. Control of Matrix Metalloproteinase Catalytic Activity. Matrix Biol J Int Soc Matrix Biol. 2007 Oct;26(8):587–96.

228. Suenaga N, Mori H, Itoh Y, Seiki M. CD44 binding through the hemopexin-like domain is critical for its shedding by membrane-type 1 matrix metalloproteinase. Oncogene. 2005 Jan;24(5):859–68.

229. Alford VM, Kamath A, Ren X, Kumar K, Gan Q, Awwa M, et al. Targeting the Hemopexin-like Domain of Latent Matrix Metalloproteinase-9 (proMMP-9) with a Small Molecule Inhibitor Prevents the Formation of Focal Adhesion Junctions. ACS Chem Biol. 2017 Nov 17;12(11):2788–803.

230. Yabluchanskiy A, Ma Y, Iyer RP, Hall ME, Lindsey ML. Matrix Metalloproteinase-9: Many Shades of Function in Cardiovascular Disease. Physiology. 2013 Nov;28(6):391–403.

231. Fanjul-Fernández M, Folgueras AR, Cabrera S, López-Otín C. Matrix metalloproteinases: Evolution, gene regulation and functional analysis in mouse models. Biochim Biophys Acta BBA - Mol Cell Res. 2010 Jan 1;1803(1):3–19.

232. Yan C, Boyd DD. Regulation of matrix metalloproteinase gene expression. J Cell Physiol. 2007;211(1):19–26.

233. Mak IWY, Turcotte RE, Popovic S, Singh G, Ghert M. AP-1 as a Regulator of MMP-13 in the Stromal Cell of Giant Cell Tumor of Bone. Biochem Res Int. 2011 Feb 27;2011:e164197.

234. Garces de los Fayos Alonso I, Liang HC, Turner SD, Lagger S, Merkel O, Kenner L. The Role of Activator Protein-1 (AP-1) Family Members in CD30-Positive Lymphomas. Cancers. 2018 Mar 28;10(4):93.

235. Bond M, Chase AJ, Baker AH, Newby AC. Inhibition of transcription factor NF-kappaB reduces matrix metalloproteinase-1, -3 and -9 production by vascular smooth muscle cells. Cardiovasc Res. 2001 Jun;50(3):556–65.

236. Bahar-Shany K, Ravid A, Koren R. Upregulation of MMP-9 production by TNFalpha in keratinocytes and its attenuation by vitamin D. J Cell Physiol. 2010 Mar;222(3):729–37.

237. Cutler SJ, Doecke JD, Ghazawi I, Yang J, Griffiths LR, Spring KJ, et al. Novel STAT binding elements mediate IL-6 regulation of MMP-1 and MMP-3. Sci Rep. 2017 Aug 17;7(1):8526.

238. Keld R, Guo B, Downey P, Cummins R, Gulmann C, Ang YS, et al. PEA3/ETV4-related transcription factors coupled with active ERK signalling are associated with poor prognosis in gastric adenocarcinoma. Br J Cancer. 2011 Jun;105(1):124–30.

239. Lynch CC, Crawford HC, Matrisian LM, McDonnell S. Epidermal growth factor upregulates matrix metalloproteinase-7 expression through activation of PEA3 transcription factors. Int J Oncol. 2004 Jun;24(6):1565–72.

240. Rojas-Quintero J, Owen CA. Matrix metalloproteinases in cystic fibrosis: pathophysiologic and therapeutic perspectives. Met Med. 2016 Aug 22;3:49–62.

241. Klein T, Bischoff R. Physiology and pathophysiology of matrix metalloproteases. Amino Acids. 2011;41(2):271–90.

242. Kuzuya M, Nakamura K, Sasaki T, Wu Cheng X, Itohara S, Iguchi A. Effect of MMP-2 Deficiency on Atherosclerotic Lesion Formation in ApoE-Deficient Mice. Arterioscler Thromb Vasc Biol. 2006 May;26(5):1120–5.

243. Han L, Sheng B, Zeng Q, Yao W, Jiang Q. Correlation between MMP2 expression in lung cancer tissues and clinical parameters: a retrospective clinical analysis. BMC Pulm Med. 2020 Oct 28;20:283.

244. Eshaq RS, Harris NR. The Role of Matrix Metalloproteinase 2 (MMP2) In Diabetes-induced Loss of PECAM-1 in The Retina: Direct and Indirect Mechanisms. FASEB J. 2018;32(S1):706.2-706.2.

245. Kenny HA, Lengyel E. MMP-2 functions as an early response protein in ovarian cancer metastasis. Cell Cycle Georget Tex. 2009 Mar 1;8(5):683–8.

246. Murphy G, Nguyen Q, Cockett MI, Atkinson SJ, Allan JA, Knight CG, et al. Assessment of the role of the fibronectin-like domain of gelatinase A by analysis of a deletion mutant. J Biol Chem. 1994 Mar 4;269(9):6632–6.

247. Sela-Passwell N, Rosenblum G, Shoham T, Sagi I. Structural and functional bases for allosteric control of MMP activities: Can it pave the path for selective inhibition? Biochim Biophys Acta BBA - Mol Cell Res. 2010 Jan 1;1803(1):29–38.

248. Sawicki G. Intracellular Regulation of Matrix Metalloproteinase-2 Activity: New Strategies in Treatment and Protection of Heart Subjected to Oxidative Stress. Scientifica. 2013;2013:130451.

249. Rowsell S, Hawtin P, Minshull CA, Jepson H, Brockbank SMV, Barratt DG, et al. Crystal Structure of Human MMP9 in Complex with a Reverse Hydroxamate Inhibitor. J Mol Biol. 2002 May 24;319(1):173–81.

250. Huang H. Matrix Metalloproteinase-9 (MMP-9) as a Cancer Biomarker and MMP-9 Biosensors: Recent Advances. Sensors. 2018 Sep 27;18(10):3249.

251. Luo S, Li W, Wu W, Shi Q. Elevated expression of MMP8 and MMP9 contributes to diabetic osteoarthritis progression in a rat model. J Orthop Surg. 2021 Jan 19;16(1):64.

252. Li T, Li X, Feng Y, Dong G, Wang Y, Yang J. The Role of Matrix Metalloproteinase-9 in Atherosclerotic Plaque Instability. Mediators Inflamm. 2020 Oct 6;2020:3872367.

253. Christensen J, Shastri VP. Matrix-metalloproteinase-9 is cleaved and activated by Cathepsin K. BMC Res Notes. 2015 Jul 29;8(1):322.

254. Toth M, Chvyrkova I, Bernardo MM, Hernandez-Barrantes S, Fridman R. Pro-MMP-9 activation by the MT1-MMP/MMP-2 axis and MMP-3: role of TIMP-2 and plasma membranes. Biochem Biophys Res Commun. 2003 Aug 22;308(2):386–95.

255. Davis GE, Pintar KA, Salazar A R, Maxwell SA. Matrix metalloproteinase-1 and -9 activation by plasmin regulates a novel endothelial cell-mediated mechanism of collagen gel contraction and capillary tube regression in three-dimensional collagen matrices. J Cell Sci. 2001 Mar 1;114(5):917–30.

256. Flores-Pliego A, Espejel-Nuñez A, Castillo-Castrejon M, Meraz-Cruz N, Beltran-Montoya J, Zaga-Clavellina V, et al. Matrix Metalloproteinase-3 (MMP-3) Is an Endogenous Activator of the MMP-9 Secreted by Placental Leukocytes: Implication in Human Labor. PLOS ONE. 2015 Dec 29;10(12):e0145366.

257. Steenport M, Faisal Khan KM, Du B, Barnhard SE, Dannenberg AJ, Falcone DJ. Matrix metalloproteinase (MMP)-1 and MMP-3 induce macrophage MMP-9: Evidence for the role of TNF-α and cyclooxygenase-2. J Immunol Baltim Md 1950. 2009 Dec 15;183(12):8119–27.

258. Volpe CMO, Villar-Delfino PH, dos Anjos PMF, Nogueira-Machado JA. Cellular death, reactive oxygen species (ROS) and diabetic complications. Cell Death Dis. 2018 Jan 25;9(2):119.

259. Mori K, Uchida T, Yoshie T, Mizote Y, Ishikawa F, Katsuyama M, et al. A mitochondrial ROS pathway controls matrix metalloproteinase 9 levels and invasive properties in RAS-activated cancer cells. Febs J. 2019 Feb;286(3):459–78.

260. Francischetti IMB, Gordon E, Bizzarro B, Gera N, Andrade BB, Oliveira F, et al. Tempol, an Intracellular Antioxidant, Inhibits Tissue Factor Expression, Attenuates Dendritic Cell Function, and Is Partially Protective in a Murine Model of Cerebral Malaria. PLoS ONE. 2014 Feb 28;9(2):e87140.

261. Duansak N, Schmid-Schönbein GW. The oxygen free radicals control MMP-9 and transcription factors expression in the spontaneously hypertensive rat. Microvasc Res. 2013 Nov;90:154–61.

262. Shoshani Y, Pe'er J, Doviner V, Frucht-Pery J, Solomon A. Increased Expression of Inflammatory Cytokines and Matrix Metalloproteinases in Pseudophakic Corneal Edema. Invest Ophthalmol Vis Sci. 2005 Jun 1;46(6):1940–7.

263. Han YP, Tuan TL, Wu H, Hughes M, Garner WL. TNF-α stimulates activation of pro-MMP2 in human skin through NF-κB mediated induction of MT1-MMP. J Cell Sci. 2001 Jan;114(Pt 1):131–9.

264. Ahn SJ, Rhim EM, Kim JY, Kim KH, Lee HW, Kim EC, et al. Tumor Necrosis Factor-α Induces Matrix Metalloproteinases-3, -10, and -13 in Human Periodontal Ligament Cells. J Periodontol. 2014;85(3):490–7.

265. Li DQ, Shang TY, Kim HS, Solomon A, Lokeshwar BL, Pflugfelder SC. Regulated Expression of Collagenases MMP-1, -8, and -13 and Stromelysins MMP-3, -10, and -11 by Human Corneal Epithelial Cells. Invest Ophthalmol Vis Sci. 2003 Jul 1;44(7):2928–36.

266. Cheng CY, Kuo CT, Lin CC, Hsieh HL, Yang CM. IL-1β induces expression of matrix metalloproteinase-9 and cell migration via a c-Src-dependent, growth factor receptor transactivation in A549 cells. Br J Pharmacol. 2010 Aug;160(7):1595–610.

267. Sachwani GR, Jaehne AK, Jayaprakash N, Kuzich M, Onkoba V, Blyden D, et al. The association between blood glucose levels and matrix-metalloproteinase-9 in early severe sepsis and septic shock. J Inflamm Lond Engl. 2016 Apr 22;13:13.

268. Death AK, Fisher EJ, McGrath KCY, Yue DK. High glucose alters matrix metalloproteinase expression in two key vascular cells: potential impact on atherosclerosis in diabetes. Atherosclerosis. 2003 Jun 1;168(2):263–9.

269. Uemura S, Matsushita H, Li W, Glassford AJ, Asagami T, Lee KH, et al. Diabetes Mellitus Enhances Vascular Matrix Metalloproteinase Activity. Circ Res. 2001 Jun 22;88(12):1291–8.

270. Arpino V, Brock M, Gill SE. The role of TIMPs in regulation of extracellular matrix proteolysis. Matrix Biol. 2015 May 1;44–46:247–54.

271. Schulz R. Intracellular Targets of Matrix Metalloproteinase-2 in Cardiac Disease: Rationale and Therapeutic Approaches. Annu Rev Pharmacol Toxicol. 2007;47(1):211–42.

272. Ries C. Cytokine functions of TIMP-1. Cell Mol Life Sci. 2014 Feb 1;71(4):659–72.

273. Li YY, McTiernan CF, Feldman AM. Proinflammatory cytokines regulate tissue inhibitors of metalloproteinases and disintegrin metalloproteinase in cardiac cells. Cardiovasc Res. 1999 Apr 1;42(1):162–72.

274. Fan D, Takawale A, Basu R, Patel V, Lee J, Kandalam V, et al. Differential role of TIMP2 and TIMP3 in cardiac hypertrophy, fibrosis, and diastolic dysfunction. Cardiovasc Res. 2014 Jul 15;103(2):268–80.

275. Kandalam V, Basu R, Moore L, Fan D, Wang X, Jaworski DM, et al. Lack of Tissue Inhibitor of Metalloproteinases 2 Leads to Exacerbated Left Ventricular Dysfunction and Adverse Extracellular Matrix Remodeling in Response to Biomechanical Stress. Circulation. 2011 Nov 8;124(19):2094–105.

276. Hernandez-Barrantes S, Shimura Y, Soloway PD, Sang QA, Fridman R. Differential Roles of TIMP-4 and TIMP-2 in Pro-MMP-2 Activation by MT1-MMP. Biochem Biophys Res Commun. 2001 Feb 16;281(1):126–30.

277. Gao M, Nguyen TT, Suckow MA, Wolter WR, Gooyit M, Mobashery S, et al. Acceleration of diabetic wound healing using a novel protease–anti-protease combination therapy. Proc Natl Acad Sci U S A. 2015 Dec 8;112(49):15226–31.

278. Das N, Benko C, Gill SE, Dufour A. The Pharmacological TAILS of Matrix Metalloproteinases and Their Inhibitors. Pharmaceuticals. 2021 Jan;14(1):31.

279. Fields GB. The Rebirth of Matrix Metalloproteinase Inhibitors: Moving Beyond the Dogma. Cells. 2019 Aug 27;8(9):984.

280. Medeiros NI, Gomes JAS, Fiuza JA, Sousa GR, Almeida EF, Novaes RO, et al. MMP-2 and MMP-9 plasma levels are potential biomarkers for indeterminate and cardiac clinical forms progression in chronic Chagas disease. Sci Rep. 2019 Oct 2;9(1):14170.

281. Vacek TP, Rehman S, Neamtu D, Yu S, Givimani S, Tyagi SC. Matrix metalloproteinases in atherosclerosis: role of nitric oxide, hydrogen sulfide, homocysteine, and polymorphisms. Vasc Health Risk Manag. 2015 Feb 27;11:173–83.

282. Eiden C, Maize KM, Finzel BC, Lipscomb JD, Aldrich CC. Rational Optimization of Mechanism-Based Inhibitors through Determination of the Microscopic Rate Constants of Inactivation. J Am Chem Soc. 2017 May 31;139(21):7132–5.

283. Meisel JE, Chang M. Selective small-molecule inhibitors as chemical tools to define the roles of matrix metalloproteinases in disease. Biochim Biophys Acta BBA - Mol Cell Res. 2017 Nov 1;1864(11, Part A):2001–14.

284. Brown S, Bernardo MM, Li ZH, Kotra LP, Tanaka Y, Fridman R, et al. Potent and Selective Mechanism-Based Inhibition of Gelatinases. J Am Chem Soc. 2000 Jul 1;122(28):6799–800.

285. Solomon A, Rosenblum G, Gonzales PE, Leonard JD, Mobashery S, Milla ME, et al. Pronounced Diversity in Electronic and Chemical Properties between the Catalytic Zinc Sites of Tumor Necrosis Factor-α-converting Enzyme and Matrix Metalloproteinases despite Their High Structural Similarity*. J Biol Chem. 2004 Jul 23;279(30):31646–54.

286. Fields GB. Mechanisms of Action of Novel Drugs Targeting Angiogenesis-Promoting Matrix Metalloproteinases. Front Immunol. 2019 Jun 4;10:1278.

287. Kleifeld O, Kotra LP, Gervasi DC, Brown S, Bernardo MM, Fridman R, et al. X-ray Absorption Studies of Human Matrix Metalloproteinase-2 (MMP-2) Bound to a Highly Selective Mechanism-based Inhibitor: COMPARISON WITH THE LATENT AND ACTIVE FORMS OF THE ENZYME *. J Biol Chem. 2001 May 18;276(20):17125–31.

288. Gimeno A, Beltrán-Debón R, Mulero M, Pujadas G, Garcia-Vallvé S. Understanding the variability of the S1' pocket to improve matrix metalloproteinase inhibitor selectivity profiles. Drug Discov Today. 2020 Jan 1;25(1):38–57.

289. Bernardo MM, Brown S, Li ZH, Fridman R, Mobashery S. Design, Synthesis, and Characterization of Potent, Slow-binding Inhibitors That Are Selective for Gelatinases *. J Biol Chem. 2002 Mar 29;277(13):11201–7.

290. Gooyit M, Suckow MA, Schroeder VA, Wolter WR, Mobashery S, Chang M. Selective Gelatinase Inhibitor Neuroprotective Agents Cross the Blood-Brain Barrier. ACS Chem Neurosci. 2012 Jul 30;3(10):730–6.

291. Tamura Y, Watanabe F, Nakatani T, Yasui K, Fuji M, Komurasaki T, et al. Highly Selective and Orally Active Inhibitors of Type IV Collagenase (MMP-9 and MMP-2): N-Sulfonylamino Acid Derivatives. J Med Chem. 1998 Feb 1;41(4):640–9.

292. Castro MM, Kandasamy AD, Youssef N, Schulz R. Matrix metalloproteinase inhibitor properties of tetracyclines: Therapeutic potential in cardiovascular diseases. Pharmacol Res. 2011 Dec 1;64(6):551–60.

293. Bench TJ, Jeremias A, Brown DL. Matrix metalloproteinase inhibition with tetracyclines for the treatment of coronary artery disease. Pharmacol Res. 2011 Dec;64(6):561–6.

294. Lee HM, Ciancio SG, Tüter G, Ryan ME, Komaroff E, Golub LM. Subantimicrobial dose doxycycline efficacy as a matrix metalloproteinase inhibitor in chronic periodontitis patients is enhanced when combined with a non-steroidal anti-inflammatory drug. J Periodontol. 2004 Mar;75(3):453–63.

295. Samartzis EP, Fink D, Stucki M, Imesch P. Doxycycline reduces MMP-2 activity and inhibits invasion of 12Z epithelial endometriotic cells as well as MMP-2 and -9 activity in primary endometriotic stromal cells in vitro. Reprod Biol Endocrinol. 2019 Apr 13;17(1):38.

296. Layfield HJ, Williams HF, Ravishankar D, Mehmi A, Sonavane M, Salim A, et al. Repurposing Cancer Drugs Batimastat and Marimastat to Inhibit the Activity of a Group I Metalloprotease from the Venom of the Western Diamondback Rattlesnake, Crotalus atrox. Toxins [Internet]. 2020 May [cited 2022 May 31];12(5). Available from: https://www.ncbi.nlm.nih.gov/pmc/articles/PMC7290494/

297. Ding X wei, Sun X, Shen X fang, Lu Y, Wang J qiang, Sun Z rong, et al. Propofol attenuates TNF-α-induced MMP-9 expression in human cerebral microvascular endothelial cells by inhibiting Ca2+/CAMK II/ERK/NF-κB signaling pathway. Acta Pharmacol Sin. 2019 Oct;40(10):1303–13.

298. Tsai CL, Chen WC, Hsieh HL, Chi PL, Hsiao LD, Yang CM. TNF-α induces matrix metalloproteinase-9-dependent soluble intercellular adhesion molecule-1 release via TRAF2-mediated MAPKs and NF-κB activation in osteoblast-like MC3T3-E1 cells. J Biomed Sci. 2014 Feb 5;21(1):12.

299. Shubayev VI, Angert M, Dolkas J, Campana WM, Palenscar K, Myers RR. TNFα-induced MMP-9 promotes macrophage recruitment into injured peripheral nerve. Mol Cell Neurosci. 2006 Mar;31(3):407–15.

300. Satchell SC, Tasman CH, Singh A, Ni L, Geelen J, von Ruhland CJ, et al. Conditionally immortalized human glomerular endothelial cells expressing fenestrations in response to VEGF. Kidney Int. 2006 May 1;69(9):1633–40.

301. Putra A, Ridwan FB, Putridewi AI, Kustiyah AR, Wirastuti K, Sadyah NAC, et al. The Role of TNF-α induced MSCs on Suppressive Inflammation by Increasing TGF-β and IL-10. Open Access Maced J Med Sci. 2018 Oct 4;6(10):1779–83.

302. Li SK lok, Banerjee J, Jang C, Sehgal A, Stone RA, Civan MM. Temperature Oscillations Drive Cycles in the Activity of MMP-2,9 Secreted by a Human Trabecular Meshwork Cell Line. Invest Ophthalmol Vis Sci. 2015 Feb;56(2):1396–405.

303. Wang Y, Chuang CY, Hawkins CL, Davies MJ. Activation and Inhibition of Human Matrix Metalloproteinase-9 (MMP9) by HOCl, Myeloperoxidase and Chloramines. Antioxidants. 2022 Aug 20;11(8):1616.

304. Nagase H, Suzuki K, Morodomi T, Enghild JJ, Salvesen G. Activation mechanisms of the precursors of matrix metalloproteinases 1, 2 and 3. Matrix Stuttg Ger Suppl. 1992;1:237–44.

305. Fernandez-Patron C, Zouki C, Whittal RM, Chan JSD, Davidge ST, Filep JG. Methods for Analysis of Matrix Metalloproteinase Regulation of Neutrophil-Endothelial Cell Adhesion. Biol Proced Online. 2002 Oct 28;4:38–48.

306. Moore CB, Guthrie EH, Huang MTH, Taxman DJ. Short Hairpin RNA (shRNA): Design, Delivery, and Assessment of Gene Knockdown. Methods Mol Biol Clifton NJ. 2010;629:141–58.

307. Elbashir SM, Lendeckel W, Tuschl T. RNA interference is mediated by 21- and 22-nucleotide RNAs. Genes Dev. 2001 Jan 15;15(2):188–200.

308. Vladar EK, Brody SL. Chapter Fourteen - Analysis of Ciliogenesis in Primary Culture Mouse Tracheal Epithelial Cells. In: Marshall WF, editor. Methods in Enzymology [Internet]. Academic Press; 2013 [cited 2023 Jun 21]. p. 285–309. (Cilia, Part B; vol. 525). Available from: https://www.sciencedirect.com/science/article/pii/B9780123979445000146

309. Aviner R. The science of puromycin: From studies of ribosome function to applications in biotechnology. Comput Struct Biotechnol J. 2020 Apr 24;18:1074–83.

310. Smith CJ, Osborn AM. Advantages and limitations of quantitative PCR (Q-PCR)-based approaches in microbial ecology. FEMS Microbiol Ecol. 2009 Jan 1;67(1):6–20.

311. Tajadini M, Panjehpour M, Javanmard SH. Comparison of SYBR Green and TaqMan methods in quantitative real-time polymerase chain reaction analysis of four adenosine receptor subtypes. Adv Biomed Res. 2014 Feb 28;3:85.

312. Jang H. Regulation of Cyclic AMP-Response Element Binding Protein Zhangfei (CREBZF) Expression by Estrogen in Mouse Uterus. Dev Reprod. 2018 Mar;22(1):95–104.

313. Mierzejewski M, Paplinska-Goryca M, Korczynski P, Krenke R. Primary human mesothelial cell culture in the evaluation of the inflammatory response to different sclerosing agents used for pleurodesis. Physiol Rep. 2021 May 1;9(8):e14846–55.

314. Zcharia E, Jia J, Zhang X, Baraz L, Lindahl U, Peretz T, et al. Newly Generated Heparanase Knock-Out Mice Unravel Co-Regulation of Heparanase and Matrix Metalloproteinases. PLoS ONE. 2009 Apr 10;4(4):e5181.

315. Schindelin J, Arganda-Carreras I, Frise E, Kaynig V, Longair M, Pietzsch T, et al. Fiji: an open-source platform for biological-image analysis. Nat Methods. 2012 Jul;9(7):676–82.

316. Konduracka E, Cieslik G, Galicka-Latala D, Rostoff P, Pietrucha A, Latacz P, et al. Myocardial dysfunction and chronic heart failure in patients with long-lasting type 1 diabetes: a 7-year prospective cohort study. Acta Diabetol. 2013 Aug 1;50(4):597–606.

317. Bouthoorn S, Valstar GB, Gohar A, den Ruijter HM, Reitsma HB, Hoes AW, et al. The prevalence of left ventricular diastolic dysfunction and heart failure with preserved ejection fraction in men and women with type 2 diabetes: A systematic review and meta-analysis. Diab Vasc Dis Res. 2018 Nov;15(6):477–93.

318. Li H, Mittal A, Makonchuk DY, Bhatnagar S, Kumar A. Matrix metalloproteinase-9 inhibition ameliorates pathogenesis and improves skeletal muscle regeneration in muscular dystrophy. Hum Mol Genet. 2009 Jul 15;18(14):2584–98.

319. Henein MY. Assessment of Left Ventricular Diastolic Function by Doppler Echocardiography. 2015 Aug 4 [cited 2023 Jun 28]; Available from:

https://www.cfrjournal.com/articles/assessment-left-ventricular-diastolic-function-doppler-echocardiography

320. Lorenzo-Almorós A, Tuñón J, Orejas M, Cortés M, Egido J, Lorenzo Ó. Diagnostic approaches for diabetic cardiomyopathy. Cardiovasc Diabetol. 2017 Feb 23;16:28.

321. Ommen SR, Nishimura RA, Appleton CP, Miller FA, Oh JK, Redfield MM, et al. Clinical Utility of Doppler Echocardiography and Tissue Doppler Imaging in the Estimation of Left Ventricular Filling Pressures. Circulation. 2000 Oct 10;102(15):1788–94.

322. Scruggs AK, Cioffi EA, Cioffi DL, King JAC, Bauer NN. Lectin-Based Characterization of Vascular Cell Microparticle Glycocalyx. PLoS ONE. 2015 Aug 14;10(8):e0135533.

323. Huynh K, McMullen JR, Julius TL, Tan JW, Love JE, Cemerlang N, et al. Cardiac-Specific IGF-1 Receptor Transgenic Expression Protects Against Cardiac Fibrosis and Diastolic Dysfunction in a Mouse Model of Diabetic Cardiomyopathy. Diabetes. 2010 Jun;59(6):1512–20.

324. Pappachan JM, Varughese GI, Sriraman R, Arunagirinathan G. Diabetic cardiomyopathy: Pathophysiology, diagnostic evaluation and management. World J Diabetes. 2013 Oct 15;4(5):177–89.

325. Zhang X, Ke PX, Yuan X, Zhang GP, Chen WL, Zhang GS. Forskolin Protected against Streptozotocin-Induced Diabetic Cardiomyopathy via Inhibition of Oxidative Stress and Cardiac Fibrosis in Mice. BioMed Res Int. 2021 Jan 30;2021:8881843–50.

326. Hou N, Mai Y, Qiu X, Yuan W, Li Y, Luo C, et al. Carvacrol Attenuates Diabetic Cardiomyopathy by Modulating the PI3K/AKT/GLUT4 Pathway in Diabetic Mice. Front Pharmacol. 2019;10:998–1012.

327. Liu JE, Palmieri V, Roman MJ, Bella JN, Fabsitz R, Howard BV, et al. The impact of diabetes on left ventricular filling pattern in normotensive and hypertensive adults: the strong heart study. J Am Coll Cardiol. 2001 Jun 1;37(7):1943–9.

328. Zarich SW, Arbuckle BE, Cohen LR, Roberts M, Nesto RW. Diastolic abnormalities in young asymptomatic diabetic patients assessed by pulsed Doppler echocardiography. J Am Coll Cardiol. 1988 Jul 1;12(1):114–20.

329. Mitter SS, Shah SJ, Thomas JD. A Test in Context: E/A and E/e' to Assess Diastolic Dysfunction and LV Filling Pressure. J Am Coll Cardiol. 2017 Mar 21;69(11):1451–64.

330. Appleton CP. Chapter 10 - Evaluation of Diastolic Function by Two-Dimensional and Doppler Assessment of Left Ventricular Filling Including Pulmonary Venous Flow. In: Klein AL, Garcia MJ, editors. Diastology [Internet]. Philadelphia: W.B. Saunders; 2008 [cited 2023 Jun 29]. p. 115–43. Available from: https://www.sciencedirect.com/science/article/pii/B9781416037545500160

331. From AM, Scott CG, Chen HH. The Development of Heart Failure in Patients with Diabetes Mellitus and Preclinical Diastolic Dysfunction: A Population Based Study. J Am Coll Cardiol. 2010 Jan 26;55(4):10.1016/j.jacc.2009.12.003.

332. Ermert K, Buhl EM, Klinkhammer BM, Floege J, Boor P. Reduction of Endothelial Glycocalyx on Peritubular Capillaries in Chronic Kidney Disease. Am J Pathol. 2023 Feb;193(2):138–47.

333. Maillette de Buy Wenniger LJ, Hohenester S, Maroni L, van Vliet SJ, Oude Elferink RP, Beuers U. The Cholangiocyte Glycocalyx Stabilizes the 'Biliary HCO3- Umbrella': An Integrated Line of Defense against Toxic Bile Acids. Dig Dis. 2015;33(3):397–407.

334. Bojar D, Meche L, Meng G, Eng W, Smith DF, Cummings RD, et al. A Useful Guide to Lectin Binding: Machine-Learning Directed Annotation of 57 Unique Lectin Specificities. ACS Chem Biol. 2022 Nov 18;17(11):2993–3012.

335. Dane MJC, van den Berg BM, Lee DH, Boels MGS, Tiemeier GL, Avramut MC, et al. A microscopic view on the renal endothelial glycocalyx. Am J Physiol-Ren Physiol. 2015 May 1;308(9):F956–66.

336. Edwards JL, Kadav PD, Bandyopadhyay P, Dam TK. Revealing the Identity of Human Galectin-3Galectin-3 (Gal-3)as a Glycosaminoglycan-Binding Protein. In: Stowell SR, Arthur CM, Cummings RD, editors. Galectins: Methods and Protocols [Internet]. New York, NY: Springer US; 2022 [cited 2023 Sep 27]. p. 137–50. (Methods in Molecular Biology). Available from: https://doi.org/10.1007/978-1-0716-2055-7_8

337. Lubec G. [Glycosaminoglycan-glomerular basement membrane interactions revealed by affinity chromatography (author's transl)]. Padiatr Padol. 1982;17(3):591–6.

338. Salamat M, Götz W, Werner J, Herken R. Ultrastructural localization of lectin-binding sites in different basement membranes. Histochem J. 1993 Jun;25(6):464–8.

339. Li Z, Zhang Q, Sun Y yuan, Wu N. Effects of different dehydration methods on the preservation of aortic and renal glycocalyx structures in mice. Heliyon. 2023 Apr 1;9(4):e15197.

340. Nieuwdorp M, Haeften TW van, Gouverneur MCLG, Mooij HL, Lieshout MHP van, Levi M, et al. Loss of Endothelial Glycocalyx During Acute Hyperglycemia Coincides With Endothelial Dysfunction and Coagulation Activation In Vivo. Diabetes. 2006 Feb 1;55(2):480–6.

341. Nieuwdorp M, Mooij HL, Kroon J, Atasever B, Spaan JAE, Ince C, et al. Endothelial Glycocalyx Damage Coincides With Microalbuminuria in Type 1 Diabetes. Diabetes. 2006 Apr 1;55(4):1127–32.

342. van den Berg BM, Vink H, Spaan JAE. The Endothelial Glycocalyx Protects Against Myocardial Edema. Circ Res. 2003 Apr 4;92(6):592–4.

343. McClatchey PM, Schafer M, Hunter KS, Reusch JEB. The endothelial glycocalyx promotes homogenous blood flow distribution within the microvasculature. Am J Physiol - Heart Circ Physiol. 2016 Jul 1;311(1):H168–76.

344. Ebong EE, Macaluso FP, Spray DC, Tarbell JM. Imaging the Endothelial Glycocalyx In Vitro by Rapid Freezing/Freeze Substitution Transmission Electron Microscopy. Arterioscler Thromb Vasc Biol. 2011 Aug;31(8):1908–15.

345. Mohammad G, Kowluru RA. Homocysteine Disrupts Balance between MMP-9 and Its Tissue Inhibitor in Diabetic Retinopathy: The Role of DNA Methylation. Int J Mol Sci. 2020 Mar 5;21(5):1771.

346. Okamoto T, Akaike T, Sawa T, Miyamoto Y, Vliet A van der, Maeda H. Activation of Matrix Metalloproteinases by Peroxynitrite-induced Protein S-Glutathiolation via Disulfide S-Oxide Formation *. J Biol Chem. 2001 Aug 1;276(31):29596–602.

347. Ünal A, Baykal O, Öztürk N. Comparison of matrix metalloproteinase 9 and 14 levels in vitreous samples in diabetic and non-diabetic patients: a case control study. Int J Retina Vitr. 2022 Jun 21;8(1):44.

348. Dede E, Liapis D, Davos C, Katsimpoulas M, Varela A, Mpotis I, et al. The effects of exercise training on cardiac matrix metalloproteinases activity and cardiac function in mice with diabetic cardiomyopathy. Biochem Biophys Res Commun. 2022 Jan 1;586:8–13.

349. DeCoux A, Lindsey ML, Villarreal F, Garcia RA, Schulz R. Myocardial matrix metalloproteinase-2: inside out and upside down. J Mol Cell Cardiol. 2014 Dec;0:64–72.

350. Wang W, Schulze CJ, Suarez-Pinzon WL, Dyck JRB, Sawicki G, Schulz R. Intracellular action of matrix metalloproteinase-2 accounts for acute myocardial ischemia and reperfusion injury. Circulation. 2002 Sep 17;106(12):1543–9.

351. Kwan JA, Schulze CJ, Wang W, Leon H, Sariahmetoglu M, Sung M, et al. Matrix metalloproteinase-2 (MMP-2) is present in the nucleus of cardiac myocytes and is capable of cleaving poly (ADP-ribose) polymerase (PARP) in vitro. FASEB J Off Publ Fed Am Soc Exp Biol. 2004 Apr;18(6):690–2.

352. Lovett DH, Mahimkar R, Raffai RL, Cape L, Maklashina E, Cecchini G, et al. A Novel Intracellular Isoform of Matrix Metalloproteinase-2 Induced by Oxidative Stress Activates Innate Immunity. PLoS ONE. 2012 Apr 3;7(4):e34177.

353. Fitzgerald ML, Wang Z, Park PW, Murphy G, Bernfield M. Shedding of Syndecan-1 and -4 Ectodomains Is Regulated by Multiple Signaling Pathways and Mediated by a Timp-3–Sensitive Metalloproteinase. J Cell Biol. 2000 Feb 21;148(4):811–24.

354. Rouet-Benzineb P, Buhler JM, Dreyfus P, Delcourt A, Dorent R, Perennec J, et al. Altered balance between matrix gelatinases (MMP-2 and MMP-9) and their tissue inhibitors in human dilated cardiomyopathy: potential role of MMP-9 in myosin-heavy chain degradation. Eur J Heart Fail. 1999;1(4):337–52.

355. Yi SJ, Kim K. Histone tail cleavage as a novel epigenetic regulatory mechanism for gene expression. BMB Rep. 2018 May;51(5):211–8.

356. Kim K, Punj V, Kim JM, Lee S, Ulmer TS, Lu W, et al. MMP-9 facilitates selective proteolysis of the histone H3 tail at genes necessary for proficient osteoclastogenesis. Genes Dev. 2016 Jan 15;30(2):208–19.

357. El-Nadi M, Hassan H, Saleh ME, Nassar E, Ismail YM, Amer M, et al. Induction of heparanase via IL-10 correlates with a high infiltration of CD163+ M2-type tumor-associated macrophages in inflammatory breast carcinomas. Matrix Biol Plus. 2020 Feb 29;6–7:100030.

358. Abu El-Asrar AM, Siddiquei MM, Nawaz MI, De Hertogh G, Mohammad G, Alam K, et al. Coexpression of heparanase activity, cathepsin L, tissue factor, tissue factor pathway inhibitor, and MMP-9 in proliferative diabetic retinopathy. Mol Vis. 2016 Apr 30;22:424–35.

359. Masola V, Gambaro G, Tibaldi E, Brunati AM, Gastaldello A, D'Angelo A, et al. Heparanase and Syndecan-1 Interplay Orchestrates Fibroblast Growth Factor-2-induced Epithelial-Mesenchymal Transition in Renal Tubular Cells. J Biol Chem. 2012 Jan 6;287(2):1478–88.

360. Gil N, Goldberg R, Neuman T, Garsen M, Zcharia E, Rubinstein AM, et al. Heparanase Is Essential for the Development of Diabetic Nephropathy in Mice. Diabetes. 2012 Jan;61(1):208–16.

361. Guo Z, Tuo H, Tang N, Liu FY, Ma SQ, An P, et al. Neuraminidase 1 deficiency attenuates cardiac dysfunction, oxidative stress, fibrosis, inflammatory via AMPK-SIRT3 pathway in diabetic cardiomyopathy mice. Int J Biol Sci. 2022 Jan 1;18(2):826–40.

362. Huxley VH, Williams DA. Role of a glycocalyx on coronary arteriole permeability to proteins: evidence from enzyme treatments. Am J Physiol-Heart Circ Physiol. 2000 Apr;278(4):H1177–85.

363. Lipphardt M, Dihazi H, Maas JH, Schäfer AK, Amlaz SI, Ratliff BB, et al. Syndecan-4 as a Marker of Endothelial Dysfunction in Patients with Resistant Hypertension. J Clin Med. 2020 Sep;9(9):3051.

364. Ali MM, Mahmoud AM, Le Master E, Levitan I, Phillips SA. Role of matrix metalloproteinases and histone deacetylase in oxidative stress-induced degradation of the endothelial glycocalyx. Am J Physiol-Heart Circ Physiol. 2019 Mar;316(3):H647–63.

365. Cooper S, Emmott A, McDonald KK, Campeau MA, Leask RL. Increased MMP activity in curved geometries disrupts the endothelial cell glycocalyx creating a proinflammatory environment. PLoS ONE. 2018 Aug 23;13(8):e0202526.

366. Alzamil H. Elevated Serum TNF-α Is Related to Obesity in Type 2 Diabetes Mellitus and Is Associated with Glycemic Control and Insulin Resistance. J Obes. 2020 Jan 31;2020:e5076858.

367. Delgadillo LuisF, Lomakina ElenaB, Kuebel J, Waugh RichardE. Changes in endothelial glycocalyx layer protective ability after inflammatory stimulus. Am J Physiol-Cell Physiol. 2021 Feb;320(2):C216–24.

368. Tao P, Fisher JF, Mobashery S, Bernhard Schlegel H. DFT Studies of the Ring Opening Mechanism of SB-3CT, a Potent Inhibitor of Matrix Metalloproteinase 2. Org Lett. 2009 Jun 18;11(12):2559.

369. Abu El-Asrar AM, Siddiquei MM, Nawaz MI, De Hertogh G, Mohammad G, Alam K, et al. Coexpression of heparanase activity, cathepsin L, tissue factor, tissue factor pathway inhibitor, and MMP-9 in proliferative diabetic retinopathy. Mol Vis. 2016 Apr 30;22:424–35.

370. Chen S, He Y, Hu Z, Lu S, Yin X, Ma X, et al. Heparanase Mediates Intestinal Inflammation and Injury in a Mouse Model of Sepsis. J Histochem Cytochem. 2017 Apr;65(4):241–9.

371. Purushothaman A, Chen L, Yang Y, Sanderson RD. Heparanase Stimulation of Protease Expression Implicates It as a Master Regulator of the Aggressive Tumor Phenotype in Myeloma *. J Biol Chem. 2008 Nov 21;283(47):32628–36.

372. Dinh W, Füth R, Nickl W, Krahn T, Ellinghaus P, Scheffold T, et al. Elevated plasma levels of TNF-alpha and Interleukin-6 in patients with diastolic dysfunction and glucose metabolism disorders. Cardiovasc Diabetol. 2009 Nov 12;8(1):58.

373. Ben-Yosef Y, Lahat N, Shapiro S, Bitterman H, Miller A. Regulation of Endothelial Matrix Metalloproteinase-2 by Hypoxia/Reoxygenation. Circ Res. 2002 Apr 19;90(7):784–91.

374. Sato T, Gotoh M, Kiyohara K, Akashima T, Iwasaki H, Kameyama A, et al. Differential Roles of TwoN-Acetylgalactosaminyltransferases, CSGalNAcT-1, and a Novel Enzyme, CSGalNAcT-2: INITIATION AND ELONGATION IN SYNTHESIS OF CHONDROITIN SULFATE *. J Biol Chem. 2003 Jan 31;278(5):3063–71.

375. Wang J, Markova D, Anderson DG, Zheng Z, Shapiro IM, Risbud MV. TNF-α and IL-1β Promote a Disintegrin-like and Metalloprotease with Thrombospondin Type I Motif-5-mediated Aggrecan Degradation through Syndecan-4 in Intervertebral Disc*. J Biol Chem. 2011 Nov 18;286(46):39738–49.

376. Okuyama E, Suzuki A, Murata M, Ando Y, Kato I, Takagi Y, et al. Molecular mechanisms of syndecan-4 upregulation by TNF-α in the endothelium-like EAhy926 cells. J Biochem (Tokyo). 2013 Jul;154(1):41–50.

377. Bollmann M, Pap T, Lohmann CH, Bertrand J. Matrix metalloproteinase mediated shedding of Syndecan-4 under osteoarthritis conditions. Osteoarthritis Cartilage. 2019 Apr 1;27:S196–7.

378. Zhang D, Zhang J tao, Pan Y, Liu X fei, Xu J wei, Cui W jing, et al. Syndecan-1 Shedding by Matrix Metalloproteinase-9 Signaling Regulates Alveolar Epithelial Tight Junction in

Lipopolysaccharide-Induced Early Acute Lung Injury. J Inflamm Res. 2021 Nov 4;14:5801–16.

379. Bollmann M, Pinno K, Ehnold LI, Märtens N, Märtson A, Pap T, et al. MMP-9 mediated Syndecan-4 shedding correlates with osteoarthritis severity. Osteoarthritis Cartilage. 2021 Feb 1;29(2):280–9.

380. Zhang D, Zhang J tao, Pan Y, Liu X fei, Xu J wei, Cui W jing, et al. Syndecan-1 Shedding by Matrix Metalloproteinase-9 Signaling Regulates Alveolar Epithelial Tight Junction in Lipopolysaccharide-Induced Early Acute Lung Injury. J Inflamm Res. 2021 Nov 4;14:5801–16.

381. Wang Y, Chiu APL, Neumaier K, Wang F, Zhang D, Hussein B, et al. Endothelial Cell Heparanase Taken Up by Cardiomyocytes Regulates Lipoprotein Lipase Transfer to the Coronary Lumen After Diabetes. Diabetes. 2014 Jul 17;63(8):2643–55.

382. Offeddu GS, Haase K, Gillrie MR, Li R, Morozova O, Hickman D, et al. An on-chip model of protein paracellular and transcellular permeability in the microcirculation. Biomaterials. 2019 Aug 1;212:115–25.

383. Fan J, Fu BM. Quantification of Malignant Breast Cancer Cell MDA-MB-231 Transmigration across Brain and Lung Microvascular Endothelium. Ann Biomed Eng. 2016 Jul;44(7):2189–201.

384. Bruhn PJ, Nikolian VC, Halaweish I, Chang Z, Sillesen M, Liu B, et al. Tubastatin A Prevents Hemorrhage-Induced Endothelial Barrier Dysfunction. J Trauma Acute Care Surg. 2018 Feb;84(2):386–92.

385. Araibi H, van der Merwe E, Gwanyanya A, Kelly-Laubscher R. The effect of sphingosine-1-phosphate on the endothelial glycocalyx during ischemia-reperfusion injury in the isolated rat heart. Microcirculation. 2020;27(5):e12612.

386. Kolářová H, Víteček J, Černá A, Černík M, Přibyl J, Skládal P, et al. Myeloperoxidase mediated alteration of endothelial function is dependent on its cationic charge. Free Radic Biol Med. 2021 Jan 1;162:14–26.

387. Xu C, Wu X, Hack BK, Bao L, Cunningham PN. TNF causes changes in glomerular endothelial permeability and morphology through a Rho and myosin light chain kinase-dependent mechanism. Physiol Rep. 2015;3(12):e12636.

388. Aveleira CA, Lin CM, Abcouwer SF, Ambrósio AF, Antonetti DA. TNF-α Signals Through PKCζ/NF-κB to Alter the Tight Junction Complex and Increase Retinal Endothelial Cell Permeability. Diabetes. 2010 Nov;59(11):2872–82.

389. Luplerdlop N, Missé D, Bray D, Deleuze V, Gonzalez JP, Leardkamolkarn V, et al. Dengue-virus-infected dendritic cells trigger vascular leakage through metalloproteinase overproduction. EMBO Rep. 2006 Nov;7(11):1176–81.

390. Chen HR, Chao CH, Liu CC, Ho TS, Tsai HP, Perng GC, et al. Macrophage migration inhibitory factor is critical for dengue NS1-induced endothelial glycocalyx degradation and hyperpermeability. PLOS Pathog. 2018 Apr 27;14(4):e1007033.

391. Zhou P, Yang C, Zhang S, Ke ZX, Chen DX, Li YQ, et al. The Imbalance of MMP-2/TIMP-2 and MMP-9/TIMP-1 Contributes to Collagen Deposition Disorder in Diabetic Non-Injured Skin. Front Endocrinol. 2021 Oct 27;12:734485–95.

392. Wu MY, Gao F, Yang XM, Qin X, Chen GZ, Li D, et al. Matrix metalloproteinase-9 regulates the blood brain barrier via the hedgehog pathway in a rat model of traumatic brain injury. Brain Res. 2020 Jan 15;1727:146553–63.

393. Selective Inhibition of Matrix Metalloproteinase-9 Attenuates Secondary Damage Resulting from Severe Traumatic Brain Injury. PLOS ONE. 2013 Oct 23;8(10):e76904–e16917.

394. Cai H, Ma Y, Jiang L, Mu Z, Jiang Z, Chen X, et al. Hypoxia Response Element-Regulated MMP-9 Promotes Neurological Recovery via Glial Scar Degradation and Angiogenesis in Delayed Stroke. Mol Ther. 2017 Jun 7;25(6):1448–59.

395. Ye Y, Kuang X, Xie Z, Liang L, Zhang Z, Zhang Y, et al. Small-molecule MMP2/MMP9 inhibitor SB-3CT modulates tumor immune surveillance by regulating PD-L1. Genome Med. 2020 Sep 28;12(1):83–101.

396. Petrie MC, Caruana L, Berry C, McMurray JJV. “Diastolic heart failure” or heart failure caused by subtle left ventricular systolic dysfunction? Heart. 2002 Jan;87(1):29–31.

397. van de Wouw J, Joles JA. Albumin is an interface between blood plasma and cell membrane, and not just a sponge. Clin Kidney J. 2021 Oct 5;15(4):624–34.

398. Dvorak HF. Vascular permeability to plasma, plasma proteins, and cells: an update. Curr Opin Hematol. 2010 May;17(3):225–9.

399. Krueger M, Mages B, Hobusch C, Michalski D. Endothelial edema precedes blood-brain barrier breakdown in early time points after experimental focal cerebral ischemia. Acta Neuropathol Commun. 2019 Feb 11;7(1):17.

400. Lavin B, Protti A, Lorrio S, Dong X, Phinikaridou A, Botnar RM, et al. MRI with gadofosveset: A potential marker for permeability in myocardial infarction. Atherosclerosis. 2018 Aug 1;275:400–8.

401. Altemtam N, Nahas ME, Johnson T. Urinary Matrix Metalloproteinase Activity in Diabetic Kidney Disease: A Potential Marker of Disease Progression. Nephron Extra. 2012 Aug 9;2(1):219–32.

402. Chu JW, Jones GT, Tarr GP, Phillips LV, Wilkins GT, van Rij AM, et al. Plasma active matrix metalloproteinase 9 and indices of diastolic function in patients with preserved systolic function. Int J Cardiol. 2013 Aug 20;167(4):1242–6.

403. Jacqueminet S, Ben Abdesselam O, Chapman MJ, Nicolay N, Foglietti MJ, Grimaldi A, et al. Elevated circulating levels of matrix metalloproteinase-9 in type 1 diabetic patients with and without retinopathy. Clin Chim Acta. 2006 May 1;367(1):103–7.

404. Reine TM, Lanzalaco F, Kristiansen O, Enget AR, Satchell S, Jenssen TG, et al. Matrix metalloproteinase-9 mediated shedding of syndecan-4 in glomerular endothelial cells. Microcirculation. 2019;26(4):e12534.

405. Winer A, Adams S, Mignatti P. Matrix Metalloproteinase Inhibitors in Cancer Therapy: Turning Past Failures into Future Successes. Mol Cancer Ther. 2018 Jun;17(6):1147–55.

406. Olson MW, Gervasi DC, Mobashery S, Fridman R. Kinetic Analysis of the Binding of Human Matrix Metalloproteinase-2 and -9 to Tissue Inhibitor of Metalloproteinase (TIMP)-1 and TIMP-2 *. J Biol Chem. 1997 Nov 21;272(47):29975–83.

407. Savjani KT, Gajjar AK, Savjani JK. Drug Solubility: Importance and Enhancement Techniques. ISRN Pharm. 2012 Jul 5;2012:195727.

408. Lee M, Chen Z, Tomlinson BN, Gooyit M, Hesek D, Juárez MR, et al. Water-Soluble MMP-9 Inhibitor Reduces Lesion Volume after Severe Traumatic Brain Injury. ACS Chem Neurosci. 2015 Oct 21;6(10):1658–64.

409. Jia F, Yin YH, Gao GY, Wang Y, Cen L, Jiang J yao. MMP-9 Inhibitor SB-3CT Attenuates Behavioral Impairments and Hippocampal Loss after Traumatic Brain Injury in Rat. J Neurotrauma. 2014 Jul 1;31(13):1225–34.

410. Yamaji T, Fukuhara T, Kinoshita M. Increased capillary permeability to albumin in diabetic rat myocardium. Circ Res. 1993 May;72(5):947–57.

411. Suwarto S, Sasmono RT, Sinto R, Ibrahim E, Suryamin M. Association of Endothelial Glycocalyx and Tight and Adherens Junctions With Severity of Plasma Leakage in Dengue Infection. J Infect Dis. 2017 Mar 3;215(6):992.

412. Herum KM, Romaine A, Wang A, Melleby AO, Strand ME, Pacheco J, et al. Syndecan-4 Protects the Heart From the Profibrotic Effects of Thrombin-Cleaved Osteopontin. J Am Heart Assoc. 2020 Feb 4;9(3):e013518.

413. Abdelaziz Mohamed I, Gadeau AP, Hasan A, Abdulrahman N, Mraiche F. Osteopontin: A Promising Therapeutic Target in Cardiac Fibrosis. Cells. 2019 Dec 3;8(12):1558.

414. Schnelle M, Catibog N, Zhang M, Nabeebaccus AA, Anderson G, Richards DA, et al. Echocardiographic evaluation of diastolic function in mouse models of heart disease. J Mol Cell Cardiol. 2018 Jan;114:20–8.

415. Li Z, Wang Z, Yin Z, Zhang Y, Xue X, Han J, et al. Gender differences in fibrosis remodeling in patients with long-standing persistent atrial fibrillation. Oncotarget. 2017 Mar 17;8(32):53714–29.

416. Moore A, Shindikar A, Fomison-Nurse I, Riu F, Munasinghe PE, Parshu Ram T, et al. Rapid onset of cardiomyopathy in STZ-induced female diabetic mice involves the downregulation of pro-survival Pim-1. Cardiovasc Diabetol. 2014 Apr 1;13(1):68.

417. Lacorte LM, Rinaldi JC, Justulin LA, Delella FK, Moroz A, Felisbino SL. Cadmium exposure inhibits MMP2 and MMP9 activities in the prostate and testis. Biochem Biophys Res Commun. 2015 Feb 20;457(4):538–41.

418. Kundu S, Sengupta S, Chatterjee S, Mitra S, Bhattacharyya A. Cadmium induces lung inflammation independent of lung cell proliferation: a molecular approach. J Inflamm. 2009 Jun 12;6(1):19.

419. Dagouassat M, Lanone S, Boczkowski J. Interaction of matrix metalloproteinases with pulmonary pollutants. Eur Respir J. 2012 Apr 1;39(4):1021–32.

420. Mazzoni A, Mannello F, Tay FR, Tonti GAM, Papa S, Mazzotti G, et al. Zymographic Analysis and Characterization of MMP-2 and -9 Forms in Human Sound Dentin. J Dent Res. 2007 May 1;86(5):436–40.

421. Guo P, Jin Z, Wu H, Li X, Ke J, Zhang Z, et al. Effects of irisin on the dysfunction of blood–brain barrier in rats after focal cerebral ischemia/reperfusion. Brain Behav. 2019 Sep 30;9(10):e01425.

422. Wei P, Wang K, Luo C, Huang Y, Misilimu D, Wen H, et al. Cordycepin confers long-term neuroprotection via inhibiting neutrophil infiltration and neuroinflammation after traumatic brain injury. J Neuroinflammation. 2021 Jun 15;18:137.

423. Arreguin-Cano JA, Ayerdi-Nájera B, Tacuba-Saavedra A, Navarro-Tito N, Dávalos-Martínez A, Emigdio-Vargas A, et al. MMP-2 salivary activity in type 2 diabetes mellitus patients. Diabetol Metab Syndr. 2019 Dec 30;11:113.

424. Toth M, Fridman R. Assessment of Gelatinases (MMP-2 and MMP-9) by Gelatin Zymography. Methods Mol Med. 2001;57:10.1385/1-59259-136-1:163.

425. Choi S, Chung H, Hong H, Kim SY, Kim SE, Seoh JY, et al. Inflammatory hypoxia induces syndecan-2 expression through IL-1b–mediated FOXO3a activation in colonic epithelia. FASEB J. 2017;31(4):1516–30.

426. Constantinides C, Mean R, Janssen BJ. Effects of Isoflurane Anesthesia on the Cardiovascular Function of the C57BL/6 Mouse. ILAR J Natl Res Counc Inst Lab Anim Resour. 2011;52:e21–31.

427. Janssen PML, Biesiadecki BJ, Ziolo MT, Davis JP. The Need for Speed; Mice, Men, and Myocardial Kinetic Reserve. Circ Res. 2016 Jul 22;119(3):418–21.

428. Giannaki CD, Oxborough D, George K. Diastolic Doppler flow and tissue Doppler velocities during, and in recovery from, low-intensity supine exercise. Appl Physiol Nutr Metab Physiol Appl Nutr Metab. 2008 Oct;33(5):896–902.

429. Panesar DK, Burch M. Assessment of Diastolic Function in Congenital Heart Disease. Front Cardiovasc Med. 2017 Feb 15;4:5.

430. Tsalamandris S, Antonopoulos AS, Oikonomou E, Papamikroulis GA, Vogiatzi G, Papaioannou S, et al. The Role of Inflammation in Diabetes: Current Concepts and Future Perspectives. Eur Cardiol Rev. 2019 Apr;14(1):50–9.

431. Swaroop JJ, Rajarajeswari D, Naidu JN. Association of TNF-α with insulin resistance in type 2 diabetes mellitus. Indian J Med Res. 2012 Jan;135(1):127–30.

432. Miyazaki Y, Nakano K, Nakayamada S, Kubo S, Iwata S, Hanami K, et al. Serum TNFα levels at 24 h after certolizumab pegol predict effectiveness at week 12 in patients with rheumatoid arthritis from TSUBAME study. Arthritis Res Ther. 2021 Jun 1;23(1):154.

433. Brightling C, Berry M, Amrani Y. Targeting TNF-α: A novel therapeutic approach for asthma. J Allergy Clin Immunol. 2008 Jan;121(1):5–12.

434. Adegbola SO, Sahnan K, Warusavitarne J, Hart A, Tozer P. Anti-TNF Therapy in Crohn's Disease. Int J Mol Sci. 2018 Jul 31;19(8):2244.

435. Sears B, Saha AK. Dietary Control of Inflammation and Resolution. Front Nutr. 2021 Aug 10;8:709435.

436. Agrawal NK, Kant S. Targeting inflammation in diabetes: Newer therapeutic options. World J Diabetes. 2014 Oct 15;5(5):697–710.

437. Eickhoff MK, Winther SA, Hansen TW, Diaz LJ, Persson F, Rossing P, et al. Assessment of the sublingual microcirculation with the GlycoCheck system: Reproducibility and examination conditions. PLoS ONE. 2020 Dec 23;15(12):e0243737.

438. de Boer C, Armstrong Z, Lit VAJ, Barash U, Ruijgrok G, Boyango I, et al. Mechanism-based heparanase inhibitors reduce cancer metastasis in vivo. Proc Natl Acad Sci. 2022 Aug 2;119(31):e2203167119.

439. Jiang H, Li H. Prognostic values of tumoral MMP2 and MMP9 overexpression in breast cancer: a systematic review and meta-analysis. BMC Cancer. 2021 Feb 10;21(1):149.

440. Nascimento D da C, Durigan R de CM, Tibana RA, Durigan JLQ, Navalta JW, Prestes J. The response of matrix metalloproteinase-9 and -2 to exercise. Sports Med Auckl NZ. 2015 Feb;45(2):269–78.

441. Timms PM, Mannan N, Hitman GA, Noonan K, Mills PG, Syndercombe-Court D, et al. Circulating MMP9, vitamin D and variation in the TIMP-1 response with VDR genotype: mechanisms for inflammatory damage in chronic disorders? QJM Mon J Assoc Physicians. 2002 Dec;95(12):787–96.

442. Wüst RCI, Coolen BF, Held NM, Daal MRR, Alizadeh Tazehkandi V, Baks-te Bulte L, et al. The Antibiotic Doxycycline Impairs Cardiac Mitochondrial and Contractile Function. Int J Mol Sci. 2021 Apr 15;22(8):4100.

Appendix: Publications, awards and extra-curricular during my PhD

Publications/ manuscripts

Amartey J, Okagbue C, Saccoh A, **Buffonge S**, Francois A, Tcheandjieu C, et al. Black In Cardio: promoting diversity and representation in the cardiovascular field. Nat Rev Cardiol. 2022 Nov;19(11):717–8.

Qiu Y, **Buffonge S**, Ramnath R, Jenner S, Fawaz S, Arkill KP, et al. Endothelial glycocalyx is damaged in diabetic cardiomyopathy: angiopoietin 1 restores glycocalyx and improves diastolic function in mice. Diabetologia. 2022 May 1;65(5):879–94.

Buffonge S, Qiu Y, Fawaz S, Gamez M, Crompton M, Satchell S, et al. Inhibition of matrix metalloproteinases 2 & 9 protects the endothelial glycocalyx and improves diastolic function in diabetic cardiomyopathy. Submitted to Cardiovascular Research. 2023

Prizes/Awards

- ***Best Oral Presentation Award*** at the UK Proteoglycan meeting (2023).
- ***Best Oral Presentation Award*** at the Bristol Heart Institute 5th annual Specialists Research Meeting (2021).

Grants

- ***4-year British Heart Foundation studentship*** (2019-2023)
- ***BMVBS travel grant*** to present my research at the Vascular Biology Meeting of the GfMVB and BMVBS in Berlin, Germany (2022)

Conferences

- Oral presentation: European Society for Microcirculation conference 2023, Aarhus, Denmark
- Oral presentation: UK Proteoglycan Meeting 2023, Leeds, United Kingdom
- Poster presentation: Joint Microcirculation and Vascular Biology Meeting of the GfMVB and BMVBS 2022, Berlin, Germany
- Oral Presentation: Bristol Heart Institute 5th annual specialists research meeting 2021, Bristol, United Kindom

Extracurricular

November 2022-June 2023: **Widening participation (WP) tutor, University of Bristol**:

- I designed and delivered seminars, tutorials, and workshops to project participants on the University of Bristol WP programs and summer schools.
- I developed specialist material to deliver to Key Stage 3-Key Stage 5 students (ages 11-18)

Oct 2020 – Present: **Co-founder of Black in Cardio** *(https://blackincardio.com)*

- Initiated and organized Black in Cardio, which highlights Black scientists in cardiovascular science and promotes education about cardiovascular diseases.

- Chaired discussions on diabetes interventions
- Featured in Forbes magazine.
- Interviewed by Nature Medicine journal

- Hosted a Bristol City radio station interview on the importance of representation in science.
- Chaired the DHB seminars